National Library
of Canada

Acquisitions and
Bibliographic Services Branch

395 Wellington Street
Ottawa, Ontario
K1A 0N4

Bibliothèque nationale
du Canada

Direction des acquisitions et
des services bibliographiques

395, rue Wellington
Ottawa (Ontario)
K1A 0N4

Your file Votre référence

Our file Notre référence

NOTICE

The quality of this microform is heavily dependent upon the quality of the original thesis submitted for microfilming. Every effort has been made to ensure the highest quality of reproduction possible.

If pages are missing, contact the university which granted the degree.

Some pages may have indistinct print especially if the original pages were typed with a poor typewriter ribbon or if the university sent us an inferior photocopy.

Reproduction in full or in part of this microform is governed by the Canadian Copyright Act, R.S.C. 1970, c. C-30, and subsequent amendments.

AVIS

La qualité de cette microforme dépend grandement de la qualité de la thèse soumise au microfilmage. Nous avons tout fait pour assurer une qualité supérieure de reproduction.

S'il manque des pages, veuillez communiquer avec l'université qui a conféré le grade.

La qualité d'impression de certaines pages peut laisser à désirer, surtout si les pages originales ont été dactylographiées à l'aide d'un ruban usé ou si l'université nous a fait parvenir une photocopie de qualité inférieure.

La reproduction, même partielle, de cette microforme est soumise à la Loi canadienne sur le droit d'auteur, SRC 1970, c. C-30, et ses amendements subséquents.

Canada

APPLICATION OF ELECTRIC POLARIZATION TO CONTAMINANT DETECTION IN SOILS

by

EDWARD J. HOPPE

Department of Civil Engineering and Applied Mechanics
McGill University
Montreal, Canada

February 1994

A thesis submitted to the Faculty of Graduate Studies
and Research in partial fulfillment of the requirements
for the degree of Doctor of Philosophy

National Library
of Canada

Acquisitions and
Bibliographic Services Branch

395 Wellington Street
Ottawa, Ontario
K1A 0N4

Bibliothèque nationale
du Canada

Direction des acquisitions et
des services bibliographiques

395, rue Wellington
Ottawa (Ontario)
K1A 0N4

Your file Votre référence

Our file Notre référence

THE AUTHOR HAS GRANTED AN IRREVOCABLE NON-EXCLUSIVE LICENCE ALLOWING THE NATIONAL LIBRARY OF CANADA TO REPRODUCE, LOAN, DISTRIBUTE OR SELL COPIES OF HIS/HER THESIS BY ANY MEANS AND IN ANY FORM OR FORMAT, MAKING THIS THESIS AVAILABLE TO INTERESTED PERSONS.

L'AUTEUR A ACCORDE UNE LICENCE IRREVOCABLE ET NON EXCLUSIVE PERMETTANT A LA BIBLIOTHEQUE NATIONALE DU CANADA DE REPRODUIRE, PRETER, DISTRIBUER OU VENDRE DES COPIES DE SA THESE DE QUELQUE MANIERE ET SOUS QUELQUE FORME QUE CE SOIT POUR METTRE DES EXEMPLAIRES DE CETTE THESE A LA DISPOSITION DES PERSONNE INTERESSEES.

THE AUTHOR RETAINS OWNERSHIP OF THE COPYRIGHT IN HIS/HER THESIS. NEITHER THE THESIS NOR SUBSTANTIAL EXTRACTS FROM IT MAY BE PRINTED OR OTHERWISE REPRODUCED WITHOUT HIS/HER PERMISSION.

L'AUTEUR CONSERVE LA PROPRIETE DU DROIT D'AUTEUR QUI PROTEGE SA THESE. NI LA THESE NI DES EXTRAITS SUBSTANTIELS DE CELLE-CI NE DOIVENT ETRE IMPRIMES OU AUTREMENT REPRODUITS SANS SON AUTORISATION.

ISBN 0-612-00098-2

Canadä

ABSTRACT

A new field measurement technique for the determination of the lateral extent of subsurface contamination is proposed. It is applicable to tracing contaminant migration from underground storage tanks and waste disposal sites. The proposed approach involves adaptation of the time-domain reflectometry (TDR) concept and relies on the interaction of matter with an electric field. Analysis of the TDR data collected from soil-contaminant mixtures indicates the feasibility of a subsurface contaminant detection.

The proposed contaminant detection technique relies on matching an unknown TDR waveform with a number of known waveforms stored in a computerized database. The analysis is performed in the frequency-domain through the use of the Fast Fourier Transform (FFT). It is proposed that the matching process utilize the coherence function.

Application of the proposed technique requires a signal generator, a digital waveform recorder, a portable computer, and a coaxial cable terminated with a soil probe. The main advantage of the proposed system is the capability of on site analysis, thus reducing the time and the expense associated with the subsurface contaminant detection and delineation.

RÉSUMÉ

Une nouvelle technique de mesure champêtre pour déterminer l'étendue de contamination latérale souterraine est proposée. Elle est applicable à la migration de contaminants provenant de sources telles que les réservoirs souterrains ainsi que les dépotoirs. L'approche proposée implique l'adaptation du concept du domaine de temps de réflectométrie (DTR) et se fie sur l'interaction de matière avec un champ électrique. L'analyse des données DTR rassemblées provenant de mélanges terre-contaminants démontre que cette méthode de détection est réalisable.

La technique de détection proposée se fie sur la comparaison d'un signal DTR inconnu avec un nombres de signaux connus en réserve dans la base de données d'un ordinateur. L'analyse est accomplie dans le domaine de fréquence. Il est suggéré que la procédure de comparaison implique la fonction de cohérence.

L'application de la technique recommandée requiert un générateur de signaux, un enregistreur de signaux digitaux, un ordinateur portatif, et un cable coaxial muni d'une sonde souterraine. L'avantage principal qu'offre ce système est la capacité d'analyse sur site, donc la réduction de temps et de dépenses associés à la découverte de contaminants.

ACKNOWLEDGMENTS

The author would like to thank Professor Raymond Yong for his support and patience throughout this study. In addition, the author wishes to express his gratitude to Dr. Ryszard Malewski of Hydro-Québec Research Institute (IREQ) for his constructive comments and helpful guidance. The technical assistance of Messr. Jean Douville and Louis Lavallée of IREQ is gratefully acknowledged. Critical comments from Mr. Daniel Tschudi of Asea-Brown Boveri (ABB) are also appreciated. Thanks are extended to Dr. William Cook for his expert computer help in the use of the PC TEX typesetting program and to Mr. Randy Combs of VTRC for his assistance with graphics. This study was supported by Grants from the Québec Ministry of Education (FCAR/MESST) and the Natural Sciences and Engineering Research Council of Canada Grant No. A-882.

TABLE OF CONTENTS

LIST OF FIGURES

LIST OF TABLES

LIST OF SYMBOLS

ϵ'	dielectric constant
ϵ''	dielectric loss
C	capacitance
E	electric field
f	frequency
ω	angular frequency
F_x	Fast Fourier Transform
F_{xx}	power spectrum
F_{xy}	cross spectrum
Γ	coherence function
H	transfer function
I	current
k	Boltzmann constant
R	resistivity
T_r	risetime
μ	magnetic permeabilty
σ	conductivity
τ	relaxation time
V	voltage
Z	impedance

CHAPTER 1

INTRODUCTION

1.1 STATEMENT OF THE PROBLEM

The problem that this study addresses is the detection of a contaminant leakage. Product leakage from underground storage tanks and migration of leachates from waste disposal sites have been known to create acute health risks and require substantial expenditures of funds to clean up. The Environmental Protection Agency (EPA) regulates approximately 2 million underground storage tanks at 750,000 facilities across the United States (Tarrer, 1993). It is estimated that 80 percent of the underground tanks are constructed of bare, unprotected steel, susceptible to corrosion and subsequent leakage. The EPA has identified 175,000 confirmed tank releases that are potential threats to public health and the environment, and that number is expected to rise.

According to the EPA, the American industry produces approximately 35 million metric tons of toxic waste each year. Much of this waste is disposed of in land impoundments. While recently constructed facilities appear to contain the waste in an environmentally sound manner, numerous older disposal sites continue to pollute their surroundings. By some calculations about six billion tons of chemicals have been disposed of since 1950, some in impoundments situated on permeable soils (Boraiko, 1985).

Current detection procedures rely mainly upon monitoring wells, lysimeters, and leachate underdrains. Wells are the most common means of monitoring the groundwater contamination. This approach tends to be expensive and time consuming to implement. Timely detection of the contaminant plume is obviously dependent on the initial layout and a number of monitoring wells. Unfortunately, wells can sample only a small volume of the acquifer. If samples collected from wells are not representative of the area or conditions for which they are intended, misleading and erroneous conclusions may result. Experience has shown that by the time a contaminant becomes detected in a monitoring well, a substantial volume of the surrounding soil and groundwater has already been polluted (Waller and Davis, 1984).

The risk of drilling wells and exploratory holes in unknown hazardous waste sites can be substantial. As the number of holes needed to define a problem area increases, so does the possibility of puncturing buried containers. Toxic fumes and liquids may be released. Explosions and fire may occur in extreme cases.

Lysimeters are commonly installed in the unsaturated zone. They include a ceramic cup into which a pore liquid is drawn. The sample is subsequently forced to the surface for collection and analysis. As in well monitoring, the contaminant plume must intersect the lysimeter. Common problems with lysimeters include clogging and degradation of ceramic cups.

The underdrain system serves to intercept the fluid seeping below an impoundment site. Although this system allows the leak to be detected and managed, it also has some significant drawbacks. It can't be installed at an existing site. It requires daily inspection. Finally, it can't identify the location of a leak.

The limitations associated with present monitoring techniques underscore the need for an alternate approach. Undeniably, early detection and characterization of ensuing subsurface contamination can minimize its negative impact. Therefore, there is a demand for a field diagnostic procedure which allows a rapid determination of the extent of pollutants present in the soil substrate. The method should assist in locating a leak in the impounding boundary so that a corrective action can be taken to alleviate the problem. It should also be adaptable to a wide range of chemicals, as opposed to being ion specific. Currently there are about 60,000 substances classified as hazardous by the EPA (Waller and Davis, 1984).

1.2 OBJECTIVES

The objective of this research is to develop a new field procedure for the detection and delineation of soil contaminants. This study concentrates on a detection method that will improve the efficiency and reduce the costs associated with the current procedures. Both data gathering and data analysis techniques are examined from the standpoint of the applicability to the on-site contaminant characterization and subsurface mapping. The application of digital data acquisition instruments and portable computers to an automated measurement and analysis process is explored. It is envisioned that the proposed contaminant match procedure will minimize the current need to conduct site characterization studies in several stages of monitoring well installation, groundwater sampling, and laboratory analysis.

1.3 APPROACH PURSUED BY THIS STUDY

A study conducted by the U.S. Environmental Protection Agency (EPA) identified a number of existing methodologies that can potentially be applied to subsurface contaminant detection (Waller and Davis, 1984). Most promising candidates include resistivity soundings, electromagnetic (EM) techniques, ground penetrating radar (GPR), time-domain reflectometry (TDR), acoustic emissions (AE) and seismic methods. These approaches typically relate the extent of soil contamination to a change in electrical properties of materials. Seismic techniques may be used to detect a contaminant indirectly by measuring a change in the velocity of sound propagation in a saturated material (Winter, 1973). The propagation velocity of sound in unsaturated soils is about one half the velocity in saturated soils. Therefore, it is theoretically possible to detect a leak that is located in the unsaturated zone.

The approach pursued by this study originates from a measurement method called time-domain reflectometry (TDR). It involves sending a fast risetime electrical impulse into a coaxial cable terminated by a sample material and analyzing the reflected signal. Although this approach necessitates an invasive probing, as opposed to a surface based electromagnetic technique, it is considerably less susceptible to a cultural noise commonly present in the field EM measurements.

The main thrust of this study involves an adaptation of the TDR technology to the in-situ detection of subsurface contaminants by measuring and analyzing the variation of soil-contaminant dielectric properties as a function of frequency. Data gathered by the TDR method is analyzed in the frequency-domain through the use of the Fast Fourier Transform. A contaminant match procedure is developed, whereby a data record obtained from an unknown soil-contaminant system is matched with a computerized database of known records. The matching procedure relies on the coherence function which provides a measure of similarity between the unknown signals. A single parameter match descriptor is proposed. By utilizing a digital recording instrumentation and a portable computer for data acquisition and signal processing this study concentrates on a method which allows an automated measurement and analysis process.

1.4 ORGANIZATION OF THESIS

This thesis contains descriptions of various geophysical techniques that may be adapted to a subsurface contaminant detection. The measurement principles associated with each technique are discussed. The approach selected for subsequent experimental studies is proposed and the background theoretical aspects are elaborated upon. The experimental setup adopted in this study is described and the results from measurements on various soil-contaminant mixtures are presented. A contaminant match procedure based on the coherence function is advanced and tested with the acquired data. The results are analyzed with respect to the applicability of the proposed method to the subsurface contaminant detection.

CHAPTER 2

REVIEW OF PREVIOUS RESEARCH

2.1 APPLICABLE DETECTION TECHNIQUES

A satisfactory contaminant detection system should be capable of pinpointing a leak position and be as nondestructive as possible. The goal set by the U.S. EPA is the ability to pinpoint the leakage in the liner material to within 30 square centimeters (Waller and Davis, 1984). Such accuracy is yet unattainable.

Contaminants propagate through soils principally by advection and dispersion. The advection is a movement with a mean groundwater flow while dispersion refers to spreading through diffusion and mixing. In the unsaturated zone above the water table contaminants percolate downward under the influence of gravity. Accumulation of contaminants typically causes alteration of the transmission, adsorption and diffusion properties of soils (Yong *et al.*, 1992). These processes may in turn affect the electric conductivity, dielectric constant and seismic velocity of the soil. For example, the introduction of an organic liquid into a soil lowers the dielectric constant, increases the resistivity and increases the hydraulic conductivity (Olhoeft, 1986). Thus, a change in soil properties may be exploited to detect contaminants.

The majority of potential detection methodologies represent an outgrowth of the general area of geophysics, as applied to oil, gas, and mineral exploration. Some are extensions of techniques used in the laboratory environment or in agriculture. Typically, a change in electrical properties of a soil is correlated with a potential contamination. Each measurement technique routinely involves two distinct stages: measurement and analysis. An effective in-situ method should perform these tasks quickly and accurately. It should also be relatively easy and economical in implementation. Applicable detection techniques, other than a direct sampling from a monitoring well, are as follows:

2.2 ELECTRICAL RESISTIVITY

This method relies on the fact that any subsurface variation in resistivity alters the form of current flow within the soil. It is therefore possible to obtain some information about subsurface distribution of various bodies from the potential measurements conducted at the surface. The resistivity of soil is influenced by the porosity, moisture content, electrical conductivity of the pore fluid, and the clay content. Typically, the higher the porosity, moisture content, salinity of pore fluid, and clay content, the lower the electrical resistivity of the subsurface soil. The presence of inorganic contaminants generally decreases the resistivity while most organic contaminants cause an increase in resistivity (Olhoeft, 1986). Their influence has not been found equal and opposite. Given the same quantity, most inorganic contaminants exert a much larger effect on resistivity than the organic compounds.

Effective use of the resistivity method can be traced to the pioneering studies of Schlumberger and Wenner in the early 1900's (Schlumberger, 1920). Due to its simplicity and a relatively low cost, a direct current sounding method has become popular in carrying out subsurface studies. Various electrode arrangements are shown in Figure 2.1.

In the Schlumberger method four electrodes are placed along a common line, with the outer two serving as the current electrodes and the inner two as the potential electrodes. The current electrodes are used to provide the input signal while the potential electrodes are used to record the response. In studying the resistivity as a function of

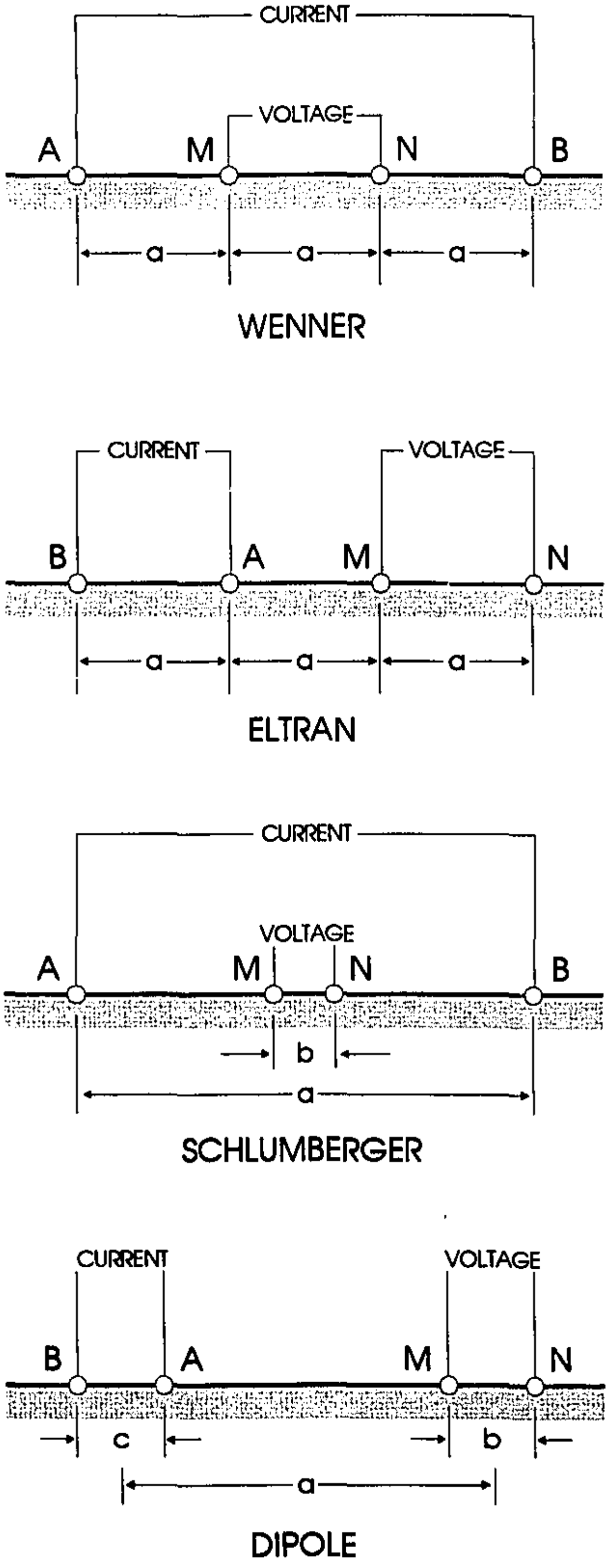

Figure 2.1 Electrical Resistivity Arrays (Wait, 1971).

depth, the current electrode separation is increased in a series of steps while maintaining the spacing on the measuring electrodes. It is assumed that the ratio of the measured voltage to the potential electrode spacing is equal to the gradient of the voltage under the soil surface.

With the Wenner array configuration four equally spaced and colinear electrodes are used. The outer two electrodes are normally used to provide current to the ground, while the inner two are used to measure the voltage drop caused by this current. If the resistivity is being measured as a function of depth, the center point of the array is held fixed and the array spacing is expanded about the midpoint. All four electrodes are separated by an equal distance at all times. The subsurface bulk resistivity R is computed from the measured voltage V, current I and array spacing a:

$$R = \frac{KV}{I} \tag{2-1}$$

where $K = 2\pi a$

A variation of the Wenner array is the Eltran array where the two adjacent electrodes at one end of the line are used to provide current. This array came into widespread use in the 1930's as means for reducing the electromagnetic coupling between the current circuit and the measuring circuit. With the usual Wenner array, the capacitive coupling between the wires leading to the current electrodes and wires leading to measuring electrodes tends to produce larger transient voltages than those produced by the current flow in the ground. In the Eltran array this coupling is reduced by not placing the two circuits adjacent to each other.

Most arrays currently in use belong either to the Wenner class in which the potential difference is measured between two widely spaced electrodes or to the Schlumberger class in which the gradient of the potential is determined from closely spaced measuring electrodes. A third category of arrays is the dipole-dipole class as originally described by Al'pin and Berdichevskii (1966). Four electrodes are used with a dipole array but they do not necessarily occupy positions along a common line. The diagnostic characteristic of a dipole array is the fact that the distance between the center of the current electrode pair and the center of the measuring electrode pair is large compared to the separation within each pair. This condition permits two approximations in the theory of dipole arrays: 1) the ratio of the measured voltage to the potential electrode separation is approximately equal to the the gradient of the voltage, and 2) the voltage field is proportional to the current moment of the current electrode pair, defined as the product of the current and the distance between electrodes.

The resistivity survey is performed at grid points covering the area of interest. The layout of the electrode arrays determines the depth of investigation. Resistivity soundings are used to locate an anomaly in the subsurface resistivity, thus indicating a potential presence of contaminants. Further exploration is usually necessary to confirm that the resistivity contrast is in fact traceable to a contaminant.

2.3 INDUCED POLARIZATION

Induced polarization (IP) is a technique closely related to the resistivity survey. It is sometimes referred to as a complex resistivity since it can measure resistivity both in magnitude and in phase as a function of frequency. A traditional way of measuring IP effects, whether employing frequency-domain or time-domain approach, involves detecting differences in time and/or amplitude between the waveforms of the applied current and the measured (induced) voltage. The actual measurement is conducted with the electrode arrangement similar to that used in the resistivity survey. A predetermined, time-varying current waveform is applied at one set of electrodes and the resultant earth voltage is measured across the other set.

The IP effect is also observed when the current in any of the standard four electrode DC resistivity arrays is suddenly interrupted. The voltage across the potential electrodes is found to decay slowly after an initial rapid drop from the steady state value. The effect was first observed by Schlumberger in 1912 and it was ascribed by him to the polarization of earth material by the current. A comprehensive study of this technique was made by Bleil (1953) who was primarily interested in applying it as a prospecting tool for metallic minerals. The IP method has been actively and successfully applied in mineral explorations since 1948 (Wait, 1959). It is accepted as a basic electrical prospecting method, particularly in the detection of sulphide ore deposits of low conductivity, such as porphyry copper and bedded lead-zinc deposits (Sumner, 1976). Various refinements to the IP method have been studied over the years. The approach pursued by Zonge and Hughes (1980) involved monitoring the phase difference between the applied current and the measured voltage at several distinct frequencies.

The IP effect is due to several sources. Electrode polarization at the boundaries of metallic conductors, such as sulphide ore deposits, is most predominant. The next most important effect is the membrane polarization, resulting from the movement of ions through the pore spaces of the subsurface material. This diffusion phenomenon is most pronounced in the presence of clay minerals, due to the small pore size, large number of ions forming a diffuse double layer and minimal advective forces.

The IP measurement was reported by Olhoeft (1985) as an indicator of the subsurface chemical activity associated with a contaminant presence. Inorganic processes of oxidation-reaction and of cation exchange may be detected. Relatively high IP phase angles were correlated with the presence of active chemical processes. For example, petroleum hydrocarbons are known to react with clays during migration. Baizer and Lund (1983) reported on a variety of organic processes that may be detected with the induced polarization technique.

2.4 TIME-DOMAIN REFLECTOMETRY

Essentially the time-domain reflectometry (TDR) is a technique that measures a reflected voltage as a function of time. Typically a rapid electrical pulse is generated in a coaxial cable and is subsequently reflected from a point of change in the electrical properties along the transmission path. Processing of the acquired data, consisting of the voltage versus time record, is dependent on the physical phenomenon under study.

Originally the TDR was developed for the telecommunications industry. Its major practical application was in locating faults in the underground or undersea cables. This was accomplished by measuring the time that the reflected signal took to travel back to the measurement point. Knowing the velocity of pulse propagation in a cable, the distance to the fault point can be readily established.

A variation of the TDR method is a technique called Corrtex, which stands for continuous reflectometry for radius versus time experiment. The U.S. relies on this technique for monitoring underground nuclear explosions (Adam, 1988). A typical setup includes placement of a cable in drill hole near a nuclear device. When the explosion occurs, the rate at which the cable is crushed by the expanding shock wave is measured by the diminishing time it takes to reflect the pulses from the rapidly dwindling length of cable. That rate of expansion of the shock wave corresponds to the explosion's yield. Corrtex TDR data is typically analyzed from some 4000 electronic pulses after the explosion.

The TDR has also been applied to the measurement of a soil moisture content in the laboratory and field experiments. Laboratory applications of the TDR were reported by Hoekstra and Delaney (1974) and Davis and Annan (1977). Look and Reeves (1992) developed a TDR system to monitor the moisture content of in-situ soils. Satisfactory results were obtained in determining moisture conditions within an expansive clay embankment. In principle, the system relies on the dependence of the static dielectric constant on the moisture content. Since the sand and most aggregates have a dielectric constant of approximately 2 to 4, while the water has a dielectric constant of about 80, the water content essentially dominates the measurement. The test is conducted with a coaxial cable terminated by a soil probe consisting of exposed electrodes of a known length. An electrical pulse is applied to the coaxial cable and recorded on the oscilloscope as it reflects from the soil probe surrounded by a material under study. The time that the pulse travels along the known distance (probe length) determines the propagation velocity and allows the computation of the dielectric constant as follows:

$$K_a = \left(\frac{ct}{L}\right)^2 \tag{2-2}$$

where: K_a = apparent dielectric constant, c = velocity of light, and $\frac{L}{t}$ = propagation velocity.

An empirical relationship between the volumetric moisture content and the apparent dielectric constant was proposed by Topp *et al.* (1980):

$$\theta_v = -5.3 + 2.92K_a - 5.5 \times 10^{-2}K_a^2 + 4.3 \times 10^{-4}K_a^3 \tag{2-3}$$

where: θ_v = volumetric moisture content.

The relationship between the gravimetric and the volumetric moisture contents is obtained from:

$$w = \theta_v * \frac{\gamma_w}{\gamma_d} \tag{2-4}$$

where w = gravimetric moisture content, γ_w = density of water, and γ_d = dry density of soil.

The application of the TDR in physical chemistry was introduced by Fellner-Feldeg (1969), who proposed a laboratory use of the TDR in studying dielectric properties of materials as a function of frequency. This application demands a precise recording of the shape of the reflected pulse. Bose *et al.* (1986) reported measurements on biological substances where the dielectric properties are often masked by the presence of large DC conductivities. The TDR technique allows differentiation of contributions due to a DC conductivity and a complex dielectric constant. Treatment of the transient experimental data obtained by such a method may be divided into two categories: the time-domain analysis and the frequency-domain analysis. The time-domain analysis provides a time dependent polarization response function directly from the TDR data, in contrast to the frequency-domain approach which requires a numerical Fourier transform to obtain dielectric data as a continuous function of frequency.

The underlying link between the TDR and the contaminant detection in soils is the influence of a contaminant on the dielectric constant and the conductivity of a soil-contaminant system. The measurement of these electrical properties as a function of time or frequency may be used to infer the presence and the character of a contaminant.

2.5 ELECTROMAGNETIC TECHNIQUES

Electromagnetic techniques for measuring the electrical parameters of a substrate soil generally involve measurement of a wave propagating through or reflecting from an analyzed material. One of the most commonly used methods is the wave tilt, which involves launching an electromagnetic wave near the earth surface and measuring the tilt of the wavefront at a moderate distance from the transmitter, as shown in Figure 2.2. The wave tilt is defined as the ratio of horizontal to vertical components of the electric field measured at the earth surface (Wait, 1971).

The electric field vector near the earth surface traces an ellipse. The orientation of the major axis of the ellipse and the relation between the major and the minor axis are influenced by the vertical and horizontal components of the electric field. Typically, the ratio of the major to the minor axis is recorded, together with the angle of inclination of the major axis. These measurements allow calculation of a dielectric constant and conductivity of the underlying soil. One approach that offers high vertical

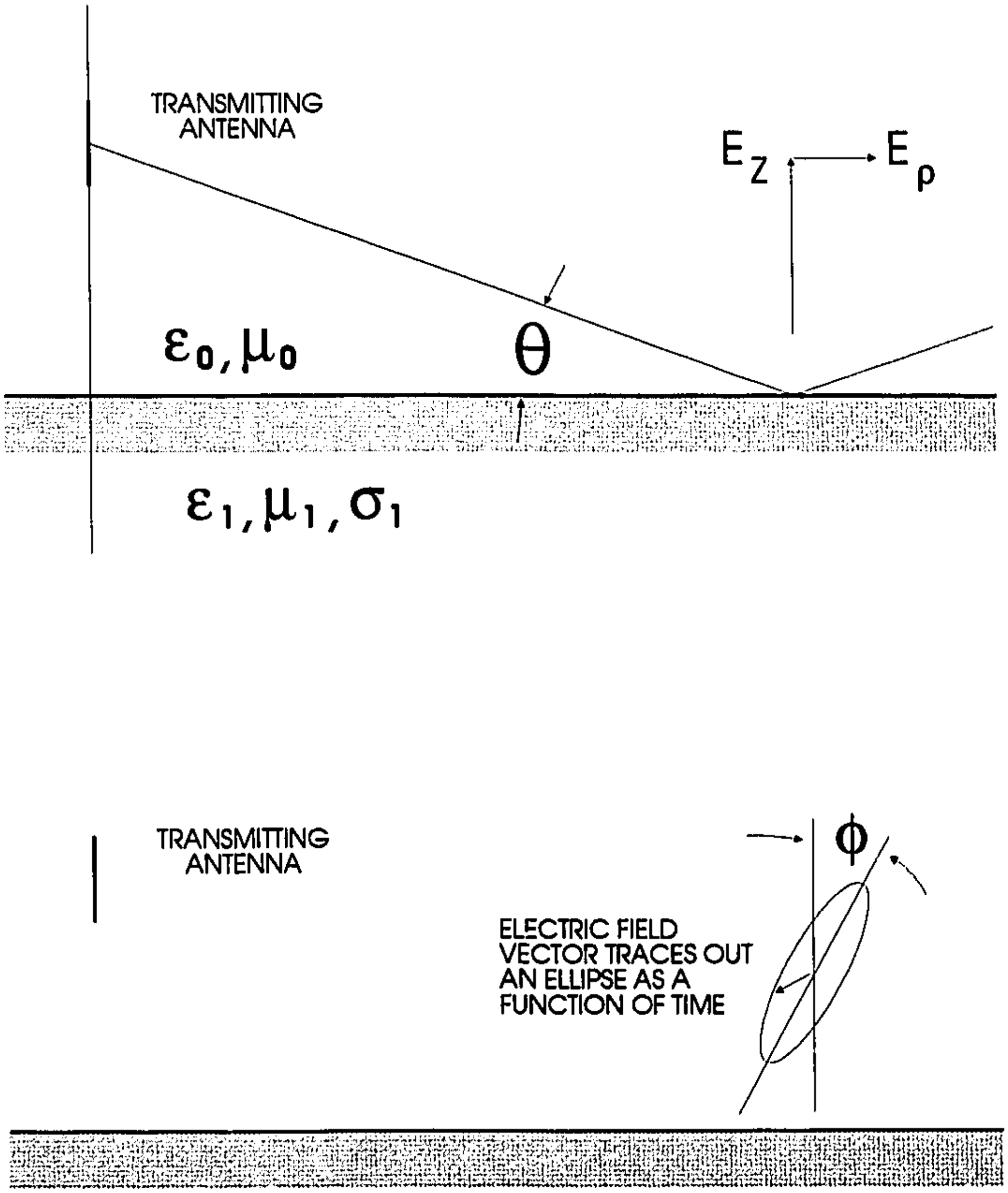

Figure 2.2 Wave Tilt (Wait, 1971).

resolution and deep sounding is the EM method employing a sweep-frequency source. Ryu *et al.* (1972) used 14 discrete frequencies between 200 Hz and 10 kHz to measure tilt angle ellipticity and the modulus of wave tilt to explore for ground water in the Santa Clara Valley, California.

Another commonly used EM technique is the mutual inductance. A terrain conductivity survey is performed by placing a small transmitter coil on or close to the earth's surface. This coil is then energized with an alternating current, typically at the audio frequency. An alternating magnetic field is generated, which, following Faraday's law, causes the electrical current to be induced in the earth. The induced current generates a secondary magnetic field. Both the primary and the secondary fields are detected by receiver coils located at a fixed distance from the transmitter coil. The comparison of the strengths of the primary and secondary fields is used to determine the conductivity of the subsurface. Field surveys are carried out by running the equipment on a grid, with coils at different separations to measure conductivity as a function of depth. A portable instrument can also be used in a preliminary reconnaissance survey.

The subsurface conductivity map that the EM technique generates can be utilized to assess the uniformity of a subsurface soil. The interpretation of data is essentially the same as the one obtained from the resistivity survey (conductivity being the inverse of resistivity). A conductivity variation signifies a potential contaminant location.

2.6 HIGH FREQUENCY PULSE TECHNIQUES

A high frequency pulse technique called ground penetrating radar (GPR) operates by emitting short bursts of radar waves, which are monitored by the receiving antenna. When operated from the ground surface, a radar antenna is manually towed over a site or pulled by a vehicle, to produce a continuous mapping. In the transillumination mode (borehole-to-borehole), the transmitter and the receiver are placed in adjacent boreholes.

This method is similar in principle to the seismic reflection technique, except that it is the electromagnetic waves that are propagated into the soil. Most of the subsurface probing at shallow depths has been based on transmitting pulsed waves in the frequency range of 1 to 900 MHz (Ulriksen, 1982). The transmitted pulse travels through a soil or water until it encounters a material with different electrical characteristics. Part of the pulse is then reflected back to the ground surface where its time of travel is recorded. The depth d at which the interface is located is calculated from:

$$d = \frac{vt}{2} \tag{2-5}$$

where: $v = \frac{c}{\sqrt{\epsilon}}$ = wave velocity $\frac{m}{s}$, c = velocity of light, and ϵ = dielectric constant

GPR measurements are sensitive to the dielectric constant and conductivity. Changes in these electrical properties may be indicative of a contaminant presence. Olhoeft (1986) observed that the conductivity is affected to a large extent by the inorganics, while the dielectric constant is more influenced by the organic contaminants. Since there is a contrast in the dielectric constant of many organics as compared with that of a soil, a contaminant detection is possible. GPR has been found to be most sensitive to changes in the dielectric properties in the unsaturated zone.

Radar measurements conducted by Ulriksen (1982) attest to a fairly high resolution profiling in sandy and gravelly soils. GPR soundings up to approximately 30 meter depth are possible. Excellent radar records are also obtained in a freshwater due to its low conductivity. In contrast, highly conductive, clay rich soils often result in penetrations of less than a meter. The resolution of a sounding depends on the radar operating frequency. A typical radar resolution at 100 MHz is approximately 10 centimeters up to a depth of about 30 meters in a clay-free coarse sand (Olhoeft, 1986).

A variation of a pulsed high frequency technique is the Time-Domain Electromagnetic Sounding (TDEM). Significant advancements in the applicability of the TDEM have been reported by Hoekstra *et al.*, (1988). The TDEM technique employs transmitting and receiving antennas consisting of square loops of insulated wire laid on the ground surface. The receiving coil is placed in the center of the transmitting loop. In the TDEM approach currents are induced by a time varying magnetic field of a transmitter. The current driven through the transmitter loop creates a primary magnetic field. During the rapid current cut-off this primary field varies in time and in accordance with Faraday's Law the resulting electromagnetic induction produces eddy currents in the subsurface soil. The intensity of these currents at a given time and depth is dependent on the subsurface resistivity, hence the TDEM can infer the presence of a contaminant with a sufficient resistivity contrast. The receiver measures the electromotive force (emf) caused by the ground eddy currents. At early times following the primary current shutoff the eddy currents are concentrated near the ground surface. With increasing time, as currents are induced at greater depth the measured emf's are progressively more influenced by the electrical properties of deeper layers.

2.7 SEISMIC TECHNIQUES

Acoustic waves appear to provide a promising approach to the subsurface probing of contaminants. The propagation velocity in unsaturated soils is about half of the velocity in the saturated zone. Moreover, the seismic waves are not as acutely attenuated in a conductive environment as the electromagnetic waves.

Seismic techniques have been employed for a number of years by the petroleum industry. Some applications to map a site stratigraphy have also been made. In a traditional seismic reflection method an impulse (hammer blow, explosion, etc.) is generated in the ground. The elastic waves emanating from the source are picked up by a series of geophones installed on the surface. A characteristic series of return echoes is recorded. The travel time of a wave along with the velocity of propagation through the soil indicates the depth to a dissimilar stratum. This dissimilar stratum may potentially include a contaminant.

In a related method called refraction surveying the time it takes for the echo to reach a transducer is measured for a varying transducer to impact distance. The time is plotted as a function of a distance and if a well defined layer exists below the surface, it results in a characteristic break in the response curve, allowing a determination of the depth of the layer.

2.8 ACOUSTIC EMISSION MONITORING

An entirely different approach to leak detection involves the use of acoustic emission monitoring (AE) techniques. It has been observed that sound emissions occur from a structural distress and from a liquid flow through the porous media. These sounds can be monitored using a microphone or an undamped accelerometer coupled to the ground. Some recent applications relating to leakage detection under existing dams are reported by Koerner *et al.* (1981). It must be realized, however, that certain acoustic emissions, occurring naturally from a decomposition of the waste material or a settlement and deformation of the liner may obscure emissions from liner failures. Fundamentals of the AE process need to further researched before the technique can be optimally applied in the field.

2.9 SOIL GAS SURVEY

The soil gas survey ia a field monitoring technique that has gained an acceptance in site characterization studies. This technique has been applied effectively to detect and define the location and the extent of volatile organic contaminants (VOC) in the soil substrate. Soil gas surveys have been used to estimate the extent of the VOC contamination and to select the optimum locations for groundwater monitoring wells (Karably and Babcock, 1989). The soil gas sampling is typically performed by using driven perforated probes, driven hollow probes, surface static trapping (SST), and augered permanent stations. Probes can be inserted in the ground with a hammer or with a hydraulic ram, reaching depths of tens of meters in some soils. Augered permanent stations offer repeatable sampling locations over an extended period, however, the installation of probes takes a significant amount of time.

The SST sampling technique involves the use of activated carbon which accumulates vapors over a period of time and is subsequently subjected to a chemical analysis. Once the soil gas is extracted, it is analyzed in the field or sent to a laboratory. Analysis methods range from hand held photoionization detectors and organic vapor analyzers to sophisticated field gas chromatographs and mass spectrometers. Sampling depth, soil moisture, permeability, and constituent specific factors commonly influence the results. The real time data analysis in the field allows a more detailed mapping of volatile hydrocarbons.

2.10 ASSESSMENT OF EXISTING TECHNIQUES

Indirect methods of contaminant detection in soils rely on sensing the alterations in soil properties. The properties that easily lend themselves to indirect probing are mainly electrical. The choice of a suitable remote sensing method needs to be evaluated in the context of an initial data collection and a subsequent data analysis. An undue level of complexity at each of these stages can render a particular approach ineffective and impractical.

The introduction of a contaminant into a soil alters its electrical conductivity (or resistivity) if the concentration exceeds certain levels. The degree of that alteration, however, strongly depends on a given soil-contaminant system. Existing studies indicate that the organics tend to increase the resistivity, while the inorganics decrease the resistivity of soils. The impact of inorganics is generally stronger, but on sites where both organic and inorganic contaminants are present the net effect on resistivity may be negligible. A sole reliance on the conductivity survey is further complicated in the areas of a complex lithology where the influence of a soil type needs to be uncoupled from the influence of a contaminant.

Another electrical property which is commonly affected by the introduction of a contaminant into a soil is the dielectric constant. Studies indicate that the organic contaminants exert a substantially greater impact on the dielectric constant than the inorganics, in contrast with the effect on electrical conductivity. It is therefore attractive from the detection point of view to employ a technique which is sensitive to both conductivity and a dielectric constant.

When considering a detection method based on analyzing the electrical properties various measurement approaches are possible. The electrical phenomena occurring in a soil-contaminant system may be studied at a zero frequency (DC), at a particular frequency (f) or at a range of frequencies of the electric or the electromagnetic field. Study of the phenomena occurring at a wide range of frequencies is obviously more technically challenging but it may supply additional valuable data. Some materials may exhibit essentially identical resistivities and/or dielectric constants at a particular frequency but may differ in the distribution of these parameters over a wide frequency range.

DC resistivity methods have been applied in locating leachates from waste impoundments with varying degrees of success. The primary factors influencing their performance are the geology and hydrogeology of the area and the resistivity contrast between the leachate and the host material. Cultural features, such as buried pipes, metal fences, and power lines also play a significant role. Combination of the above factors often limits the resistivity survey to sites with a simple and well defined geologic cross section and a highly conductive leachate. Moreover, at most hazardous sites both organic and inorganic contaminants are present, causing opposite effects on the resistivity. Among the most important constraints in the use of the resistivity techniques are the following:

- complex stratigraphy, making the results ambiguous.
- cultural objects, such as electrical lines, fences, roads, and buried pipes, causing undue conductivity fluctuations.
- insufficient conductivity contrast of the leachate. A ratio of at least 2:1 between conductivities of leachate and groundwater greatly aids in the interpretation of field data.

Similar limitations apply to the electromagnetic techniques. They generally produce a measurement of a bulk electrical conductivity of the subsurface. Data collection is markedly faster with the EM approach as compared to the resistivity survey, however, data processing is significantly more complex and the nearby utilities, power and telephone lines, can greatly interfere with the measurements. A common problem involves masking of conductivity variations at greater depths by the presence of a highly conductive surface layer. Electromagnetic waves attenuate exponentially as they propagate through the earth. The distance that the wave must travel before its amplitude decreases to $\frac{1}{e}$ of its surface amplitude is called the skin depth and represents an effective depth of exploration. The skin depth decreases substantially with increasing conductivity due to the excessive signal attenuation.

Some successful applications of EM techniques have been reported. Greenhouse and Harris (1980) employed the EM conductivity survey to evaluate the leachate flow at the abandoned Bose-Borden waste impoundment in Ontario. Often the interpretation of results is complicated by localized site conditions. Saunders and Germeroth (1986) used a portable EM probe to determine a hydrocarbon thickness under the aprons at Newark International Airport. They concluded that slight variations in the terrain conductivity result in significant changes in the interpreted hydrocarbon thickness.

The sensitivity study of the GPR, conducted by Bowders *et al.* (1982), concluded that a small variation in the soil density will cause a detectable return signal. Since nonhomogeneous situations prevail in the field, and minor density changes abound, it can be concluded the GPR traces will often be cluttered with return signals. Data analysis in such situations becomes complex and requires sophisticated signal enhancement techniques to uncouple the influence of the soil density from the impact of the contaminant. On the other hand, data collection associated with the GPR can be extremely efficient, since the actual measurement is very fast.

Seismic techniques are not as rapid as the EM and the GPR. They work best in very dense materials and perform poorly in loose soils. The problems encountered with the fine detail resolution are similar in nature to those associated with the electromagnetic propagation. As smaller wavelengths are applied for enhanced resolution, excessive scattering and reflections become difficult to uncouple. Typically, in selecting the equipment frequency range a compromise is made between the depth of penetration and the resolution.

Existing acoustic imaging systems typically require that the sound source be separated from the receivers. However, in a layered soil there are many sound paths between any two points in addition to the path due to reflection from the object. The net result is that there will appear to be as many reflectors as there are sound paths. It is a common experience in the seismic field work to observe that a single seismic impulse produces a train of impulses lasting for a number of seconds.

There have been efforts made to develop acoustical imaging systems based on the principle of acoustic holography. It appears that the main obstacles to any kind of sophisticated imaging in soils are severe velocity gradients and multipath conditions (Winter, 1973). The principal factors affecting the velocity are the confining pressure and the water content. The behavior of the acoustic velocity affects any imaging system in three ways. First, it modifies the amount of energy available to illuminate the reflector. Second, it greatly influences refraction. Due to refraction, the ray paths are also irregular and unpredictable. Any imaging system using wavelengths less than a meter which assumes an isotropic medium produces extremely blurred images. The third problem is that as wavelengths get smaller (for enhanced resolution) all of the local variations in velocity become acoustic reflectors, making data analysis extremely complex. Thus, a variation in the seismic velocity due to the contaminant presence may be effectively masked by the site lithology.

In view of the above considerations, remote sensing electromagnetic and seismic methodologies were not pursued in this study. Despite their obvious attractiveness from a data collection point of view it is believed that these techniques do not provide an adequate resolution of a contaminant plume in the heterogeneous environment. In contrast to potential mineral locations, the majority of contaminated sites routinely contain a multitude of cultural features generating a significant level of a background noise. Fences, pipes, underground and overhead power lines typically exert a substantial impact on electromagnetic measurements, often resulting in a low signal to noise ratio. Moreover, remote electromagnetic sensing has met with little success in petroleum exploration mainly because of insufficient resistivity resolution in the oil bearing strata (Keller and Frischknecht, 1966). Yet petroleum products constitute one of the most widespread subsurface pollutants in need of detection. As a result, remote sensing electromagnetic and seismic techniques may be regarded as potentially useful in the initial reconnaissance work, but not very suitable for a detailed exploration.

Techniques based on a soil gas sampling are limited in applicability to the volatile organics. Any permeability variations at the site, such as those stemming from clay layers or fractures, affect the results. Ambient vapors from past operational practices and spills also make this approach difficult to implement. If a laboratory analysis of samples is required, the increased amount of manual handling renders this approach costly and time consuming. Direct probing methods based on the detection of a specific ion, pH or conductivity also suffer from a limited applicability.

Limitations associated with each of the above mentioned methodologies can be mitigated by employing some of these techniques together. Many researchers advocate the use of complementary methodologies in site characterization studies. The selection is obviously dependent on the relative ease of data collection and analysis for the intended application.

The main criteria in pursuing an effective detection methodology adopted by this study were as follows:

- minimization of a site disturbance.
- minimization of the probing and sampling time.
- capability of on-site data analysis.
- capability of an automated measurement and analysis, thus minimizing manual operations.
- capability of a contaminant detection in the unsaturated zone.
- applicability to a wide range of contaminants.

The technique pursued in this study is based on measuring dielectric properties as a function of frequency. Two proven methodologies exploiting this phenomenon are Induced Polarization (IP) and Time-Domain Reflectometry (TDR). Existing studies indicate that the IP method has been used successfully in search of metallic ore bodies (high conductivity) and sulphide ore deposits (low conductivity). The TDR laboratory method, operating at significantly higher frequencies, has been applied to characterize a variety of chemicals, including biological substances, where the dielectric properties are often masked by a high conductivity.

The TDR approach is conceptually attractive as a contaminant detection tool since the influence of an ambient cultural noise on measurements is greatly minimized due to inherent shielding properties of the coaxial transmission line. Although the field application of TDR requires an invasive probing, it allows a measurement at a particular point in the subsurface, with no interference from the adjacent strata (Gajda and Stuchly, 1983). In this respect it differs from EM techniques which tend to measure bulk subsurface properties. The decision to further explore the TDR approach was also motivated by the fact that relatively little research has been conducted to date in adapting this technology to a contaminant detection in soils.

CHAPTER 3

THEORETICAL ASPECTS

In dealing with the subsurface contaminant detection it is informative to relate the level of a soil contamination to the change in electrical properties of the soil. The conductivity and the dielectric constant may be substantially affected by the introduction of a liquid contaminant into the soil pores. In the initial approach to the problem it is common to resort to the DC resistivity survey. This method offers a quick and inexpensive way of locating a subsurface contaminant, provided that the geological cross section is fairly uniform. In areas of a complex lithology, however, this approach cannot readily discern between the resistivity of a particular soil type and that of a pore fluid. In fact, a variety of chemically different materials exhibit essentially similar DC resistivities. To address this lack of selectivity, one may consider monitoring not only the resistivity but also a dielectric constant and to monitor these parameters over a wide frequency range.

Non-conductive materials interacting with the electric field are called dielectrics and their behaviour is governed by the underlying phenomenon of electric polarization. From the measurement point of view most contaminated soils can be regarded as dielectric materials, with their characteristic resistivities and dielectric constants affected by the chemical nature of the contaminant. The problem entails the interaction of these dielectric materials with the electric field.

The mechanics of polarization may be visualized with reference to Figure 3.1 which illustrates a homogeneous non-conducting material placed in the electric field. Although the atomic structure of an insulator is such that it is difficult for electrons to move from one atom to another, the electrons orbiting around each nucleus will be attracted by the (+) plate and repelled by the (-) plate. As a result, the orbits of the electrons in each atom will be displaced. The effect of the positive charge being closer to one side of the atom and the negative charge being closer to the other is called polarization. Because a net movement of electrons in one direction constitutes an electric current, there is a momentary surge of the so-called displacement current, causing increased conductivity in the system while the charges are induced ie. take up their positions (Jackson, 1976). A similar phenomena occurs when the electric field is removed. With some materials a small potential difference momentarily appears between the plates. It indicates that the electron orbits did not instantly return to their original positions. This effect is called dielectric absorption.

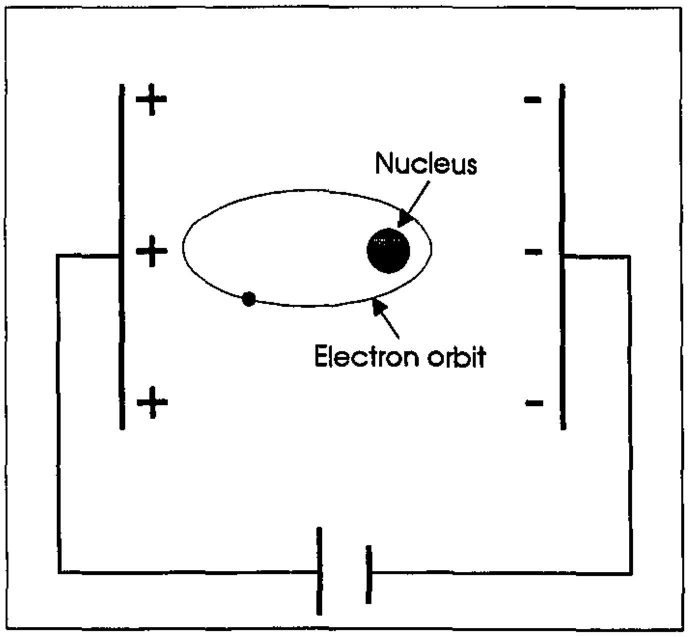

Figure 3.1 Polarization of a Dielectric.

The behavior of a typical dielectric material can be visualized in terms of a molecular dipole aligning or polarizing in the direction of the electric field. The extent of the observed polarization or permittivity is a function of time or frequency of a signal used in the experiments. When the field is reversed, the dipoles tend to realign themselves. As the rate of field reversal becomes faster than the rate of molecular reorientation, rotation of a dipole can no longer occur. At this relaxation frequency the material's dielectric constant drops in value since there are fewer available charges that can be displaced by the electric field. This variability of dielectric constant with frequency is known as "dispersion". In the transition region of dispersion a phenomenon known as "absorption conductivity" takes place and the resulting complex dielectric constant can be expressed by $\epsilon^* = \epsilon' - i\epsilon''$ as shown in Figure 3.2. It is important to note that the Figure 3.2 illustrates the simplest case involving only one type of a dipole. Practical systems containing a collection of various dipoles display a number of step-like transition regions occurring at various characteristic frequencies. The implication of the polarization phenomenon is that as the frequency of electric field increases the material's dielectric constant drops in value and its conductivity increases in a manner characteristic of a given material. This principle forms the cornerstone of this study.

There are several mechanisms of polarization that cause a frequency dependence of electrical properties. Contributions to this polarization arise from the following (Dev *et al.*, 1972):

- displacement of electrons relative to the nucleus of each atom (electronic polarization).
- movement of one nucleus relative to another in the same molecule (atomic polarization).
- rotation of molecular dipoles (orientation polarization).
- migration and piling up of charges within the sample (interfacial polarization).

The electronic polarization is a process requiring about 10^{-15} s, corresponding to

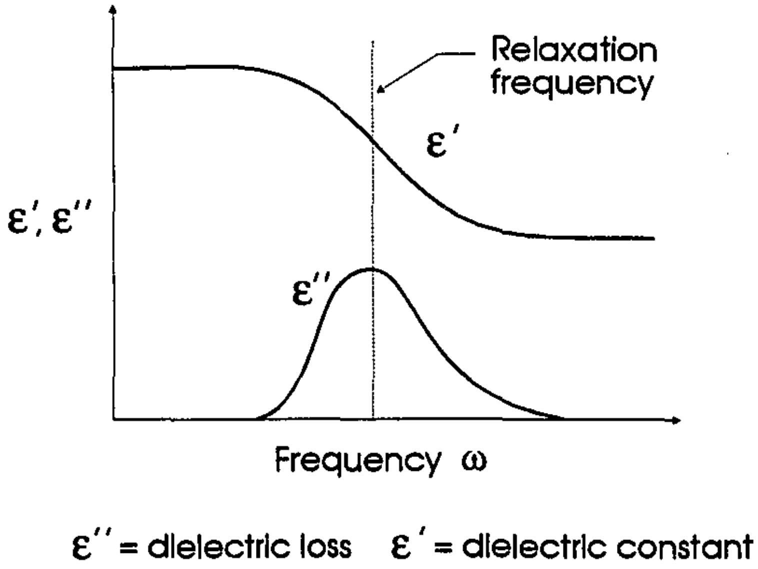

Figure 3.2 Dispersion and Absorption in Dielectrics.

the frequency of ultraviolet light. The atomic polarization takes from 10^{-12} to 10^{-14} s and corresponds to the infrared frequency. The orientation polarization in liquids ranges from 10^{-10} to 10^{-6} s, corresponding to radio and microwave frequencies. In a heterogeneous material the interfacial polarization may require seconds or minutes to complete, a process observed only at very low frequencies.

The classical theory of polarization is commonly associated with Debye (1929). Dielectric properties of materials containing molecules with permanent dipole moments can be described by a modification of the Debye equation due to Cole and Cole (1941). Accordingly:

$$\epsilon^*(\omega) = \epsilon_\infty + \frac{\epsilon_s - \epsilon_\infty}{1 + (i\omega\tau)^{1-\alpha}} \tag{3-1}$$

where ϵ^* is the complex dielectric constant $= \epsilon'(\omega) - i\epsilon''(\omega)$. The real part, ϵ', is the dielectric constant and the imaginary part, ϵ'', is the dielectric loss. ϵ_∞ and ϵ_s are the "infinite frequency" and "static" limits of the dielectric constant, ω is the angular frequency, τ is the relaxation time, and α is the parameter indicating the width of the distribution of relaxation times around τ. For materials with a single relaxation time, such as water, $\alpha = 0$ and the equation 3-1 reduces to the form given by Debye:

$$\epsilon^*(\omega) = \epsilon_\infty + \frac{\epsilon_s - \epsilon_\infty}{1 + i\omega\tau} \tag{3-2}$$

In this case, ϵ^* can be separated into real and imaginary parts as follows:

$$\epsilon' = \epsilon_\infty + \frac{\epsilon_s - \epsilon_\infty}{1 + (\omega\tau)^2} \tag{3-3}$$

$$\epsilon'' = \frac{(\epsilon_s - \epsilon_\infty)\omega\tau}{1 + (\omega\tau)^2} \tag{3-4}$$

The difference between ϵ_s and ϵ_∞ is attributed to dipole polarization. The orientation of polar molecules in an alternating field is opposed by the effects of thermal agitation and molecular interactions. Debye represents the second effect by a picture of viscous damping, the molecules being regarded as spheres in a continuous medium having macroscopic viscosity.

Dispersion and absorption can also occur in nonhomogeneous dielectrics. The possibility of absorption in a double layer dielectric if the ratios of conductivities and dielectric constants are not equal was first pointed out by Maxwell (1854).

Cole and Cole (1941) have shown that a graphical representation of equation 3-2 gives an arc of a semicircle in the complex plane, with the diameter of the semicircle making an angle $\frac{\alpha\pi}{2}$ with the real axis as shown in Figure 3.3.

The complex dielectric constant may be defined in terms of the electric flux density and the intensity of the electric field set up in the dielectric:

$$\epsilon^* = \frac{D}{E} \tag{3-5}$$

where E is the electric field applied to the sample $(\frac{volts}{meter})$ and D is the electric flux density or electric displacement $(\frac{coulombs}{meter^2})$ The magnitude and phase of D is governed

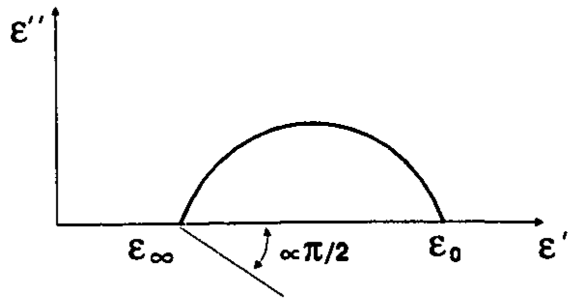

Figure 3.3 Locus of the Dielectric Constant in the Complex Plane.

by the frequency-dependent behavior of the material and is reflected in terms of real and imaginary parts of ϵ^*.

It is possible to perform an alternate class of experiments in which the time dependence between D and E is compared. The quantity D is proportional to charge and E is the voltage gradient across the dielectric. If a step voltage is suddenly applied, the time dependence of D may be used to compute ϵ^*. It is therefore viable to employ either a sinusoidal or a step voltage approach in dielectric measurements. Thus the time or frequency dependence of the dielectric constant can be used to provide information on the chemical composition of a material. The application of the time-domain method offers a faster measurement in comparison to the 'point-by-point' approach required in the frequency-domain. Since a single impulse comprises a large frequency spectrum, transient methods are generally regarded as less time consuming than frequency-domain methods (van Gemert, 1973).

Various researchers have studied the dependence of a dielectric constant on the ionic concentration of a liquid solution. Onsanger (1936) reported that the dielectric constant of dilute solutions forms a linear function of the number of polar molecules per volume of solution. Hedestrand (1929) and Halverstadt and Kumler (1942) examined data for solutions in nonpolar solvents of over fifty polar compounds of widely different nature and have found in every case that the dielectric constant of the solution is a linear function of the weight fraction of a solute. Hasted *et al.* (1948) reported that the dielectric constants of concentrated solutions of a variety of typical electrolytes decrease with increasing concentration. Within the error of measurement, the decrease is linear up to a concentration of about 2 M, above which it becomes gradually less pronounced.

Dielectric constant of liquids is also affected by the type of ion present in the analyzed material. Hasted *et al.* (1948) determined that the static dielectric constant of a solution may be written as:

$$\epsilon = \epsilon_{H_2O} - (\delta^+ + \delta^-)c \tag{3-6}$$

where ϵ_{H_2O} is the static dielectric constant of water, c is the concentration in moles per liter, and δ^+ and δ^- are the contributions of the cation and anion, respectively. Individual ionic contributions to the lowering of dielectric constant per mole of ion per liter of solution are presented in Table 3.1.

Studies of the dielectric constant of soils, conducted by Okrasinski *et al.* (1978) in the frequency range of 0.39 to 1.5 GHz, indicate that:

- dielectric constant decreases linearly as the porosity of the soil increases.
- granular soils show a more linear relationship between the volumetric moisture content and the dielectric constant than clay soils.
- the dependence of the dielectric constant on the temperature in the range from 0 to 25°C is minimal.

It is worth noting that the dielectric constant is proportional to the thickness of the diffuse double layer formed on the colloidal surface. Double layer thickness decreases as the square root of the bulk solution salt concentration and directly with increasing valence of the exchangeable cation (Yong and Warkentin, 1975). The effect of increased

H^+	17	F^-	5
Li^+	11	Cl^-	3
Na^+	8	I^-	7
K^+	8	OH^-	13
Rb^+	7	SO_4^-	7
Mg^{++}	24		
Ba^{++}	22		
La^{+++}	35		

Table 3.1 Ionic Lowering of the Dielectric Constant (Hasted et al., 1948).

salt concentration arises from reduced cation diffusion from the surface toward the bulk solution and increased anion diffusion in the opposite direction. The effect of cation valence stems from the stronger attraction of higher charged cations by the colloid surface.

The theoretical distribution of ions at a negatively charged surface as a result of Coulomb and thermal forces was originally developed by Gouy (1910). The distribution of cations in the electric field at a distance x from the clay surface can be expressed as (Yong and Warkentin, 1975):

$$n_+ = n_o \left(\coth \frac{x}{2} \sqrt{\frac{8\pi^2 z^2 c_o N}{\epsilon k T}} \right)^2 \tag{3-7}$$

where n_+ is the number of cations per unit volume at a distance x from the surface, n_o is the number of cations per unit volume in the pore water away from the influence of the surface, z is the valence of cations, c_o is the concentration of cations in $\frac{moles}{liter}$ away from the influence of the surface, x is the distance from surface in Ångstrom, T is the absolute temperature, k is the Boltzmann constant, and ϵ is the dielectric constant of the solution.

It can be seen from equation 3-7 that if the concentration and/or ionic valence of the pore fluid changes then the dielectric constant changes accordingly, other factors remaining constant. This interdependence may be employed to detect contaminants in soils by means of dielectric measurements. Thus the electric polarization measurements of the double layer may indicate the nature of the pore fluid chemistry.

In measuring the relaxation properties of various materials it is imperative to find a frequency range of interest, where the effects are most observable. As pointed out by Cole, this frequency range is often as awkwardly low for solids as that for liquids is high. The reason for such disparity is that the charge displacement in a solid matrix is much more constrained than in a liquid. For example, water molecules in a liquid state become aligned with an electric field in about 30 nanoseconds (Keller and Frischknecht, 1966). The amount of polarization is fairly large, as water exhibits the dielectric constant of 81.5 at low frequencies. At temperatures below the freezing point these molecules take much longer to align due to the rigid structure of ice.

A study conducted by Hoekstra and Delaney (1974) indicates that in geologic materials the soil type strongly influences dielectric measurements in the frequency range of DC up to about 1 MHz. Olhoeft (1987) reports that in clay-water systems there are significant contributions of the clay type up to 100 MHz. At higher frequencies the influence of the unbound pore fluid becomes dominant. It is also observed that the frequency of maximum dielectric loss in a soil-water mixture is appreciably lower than in a bulk water due to the constraints on charge displacement, characteristic of the double layer. A study by Bockris *et al.*, (1966) indicates that liquid molecules comprising the double layer are severely restricted in their motion, and their relaxation frequency is lowered. Work involving measurements on packed protein powders with adsorbed water, conducted by Harvey and Hoekstra (1972), reports two distinct relaxation frequencies, corresponding to two layers of adsorbed water. Experiments with polyelectrolyte solutions, conducted by Sachs and Spiegler (1964), show that in the range of radio frequencies the dispersion curves are shifted to higher frequencies with increasing concentrations. Studies performed by Arulanandan and Mitchell (1968) conclude that clay-water electrolyte systems behave as anomalous dielectrics in the audio frequency and near radio frequency range.

Based on the above findings, it appears that if the polarization measurements are conducted at sufficiently high frequencies, the results would reflect predominantly pore fluid relaxations, hence a contaminant response. However, even at lower frequencies associated with the interfacial polarization, one should detect the influence of a contaminant on the double layer, although the effect of a soil type needs to be accounted for. The ion concentration in the pore fluid at equilibrium with the adsorbed cations depends on the specific surface area and the cation exchange capacity of clay minerals. The above findings also indicate that in a particular soil type, dielectric constant may be linearly dependent on the contaminant concentration.

The frequency range of interest depends on the composition of a particular soil-contaminant system, hence in the absence of any specific information it is prudent to conduct the measurements over an extensive bandwith. Instead of performing a multitude of point-by-point frequency-domain measurements it is advantageous to employ the time-domain approach using a pulse made up of a wide spectrum of harmonics. It reduces the data collection time and allows a temporary generation of a higher amplitude signal that may otherwise be possible on a continuous basis.

The geophysical technique of Induced Polarization detects mainly interfacial polarization associated with dissimilar materials. However, the traditional four-electrode arrangement used in the IP method is not capable of accurately measuring high frequency relaxations. In order to perform effective high frequency field measurements extending into the MHz range, the monitoring circuit has to be properly shielded from the electromagnetic interference. From a practical point of view it requires the use of a coaxial cable, which is designed to block the outside interference. The electric and magnetic fields are confined between the outer and the inner conductors of a coaxial transmission line.

One technique that lends itself to electric polarization measurements spanning the range covered by IP and extending into the microwave frequencies is the time-domain reflectometry (TDR). In the TDR method the electrical impulse with a fast risetime is sent into a coaxial cable. Upon reaching the end of the cable embedded in the analyzed material the impulse is reflected in a manner indicating the characteristic spectral signature of the sample, as shown in Figure 3.4. The reflected signal can range in magnitude from +100% to -100% of the incident signal. These two extremes correspond to conditions of infinite resistivity and zero resistivity of the sample material. The measurement system is conceptually simple and relatively immune from the electromagnetic interference due to the shielding characteristics of a coaxial cable.

Typical TDR responses to a step function are shown in Figure 3.5 (bold portion), indicating the inherent capability of the TDR method to distinguish between the effects of the resistivity and the dielectric constant. The relationship between the time-domain and the frequency-domain may be regarded as reciprocal, meaning that at small times the waveform is described by the high frequency harmonics, while at later times it is shaped by the low frequencies of the impulse. Purely resistive termination results in the transfer of all frequencies of the input signal equally, both in magnitude and in phase. In the open-circuit termination (infinite resistance) all frequency components of the output signal appear in phase with the spectrum of the incident signal. In the short-circuit termination (zero resistance) the transfer occurs in antiphase. It can be observed that the initial time domain response (high frequency) of the capacitor corresponds to that of a short circuit (R=0), while in the latter stage (low frequency)

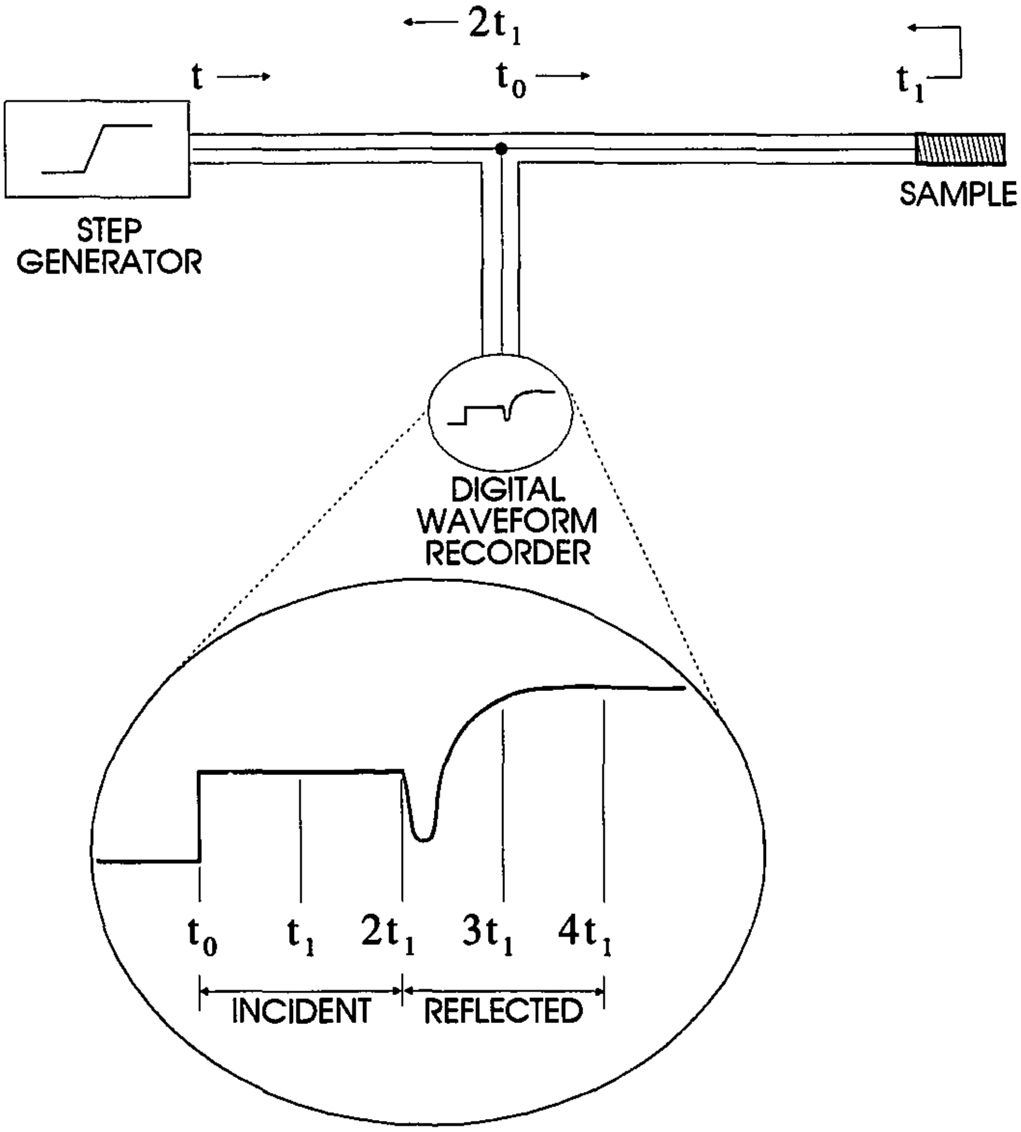

Figure 3.4 Typical Setup for the TDR Method.

it approaches exponentially the behavior of an open circuit (R=∞). The capacitor illustrated in Figure 3.1 would manifest itself in this fashion, indicating the effect of a single polarization. In a heterogeneous dielectric material the reflected signal does not exhibit a purely exponential rise due to multiple polarization phenomena and the resulting dispersion.

The measurements conducted in the time-domain can be transformed into the

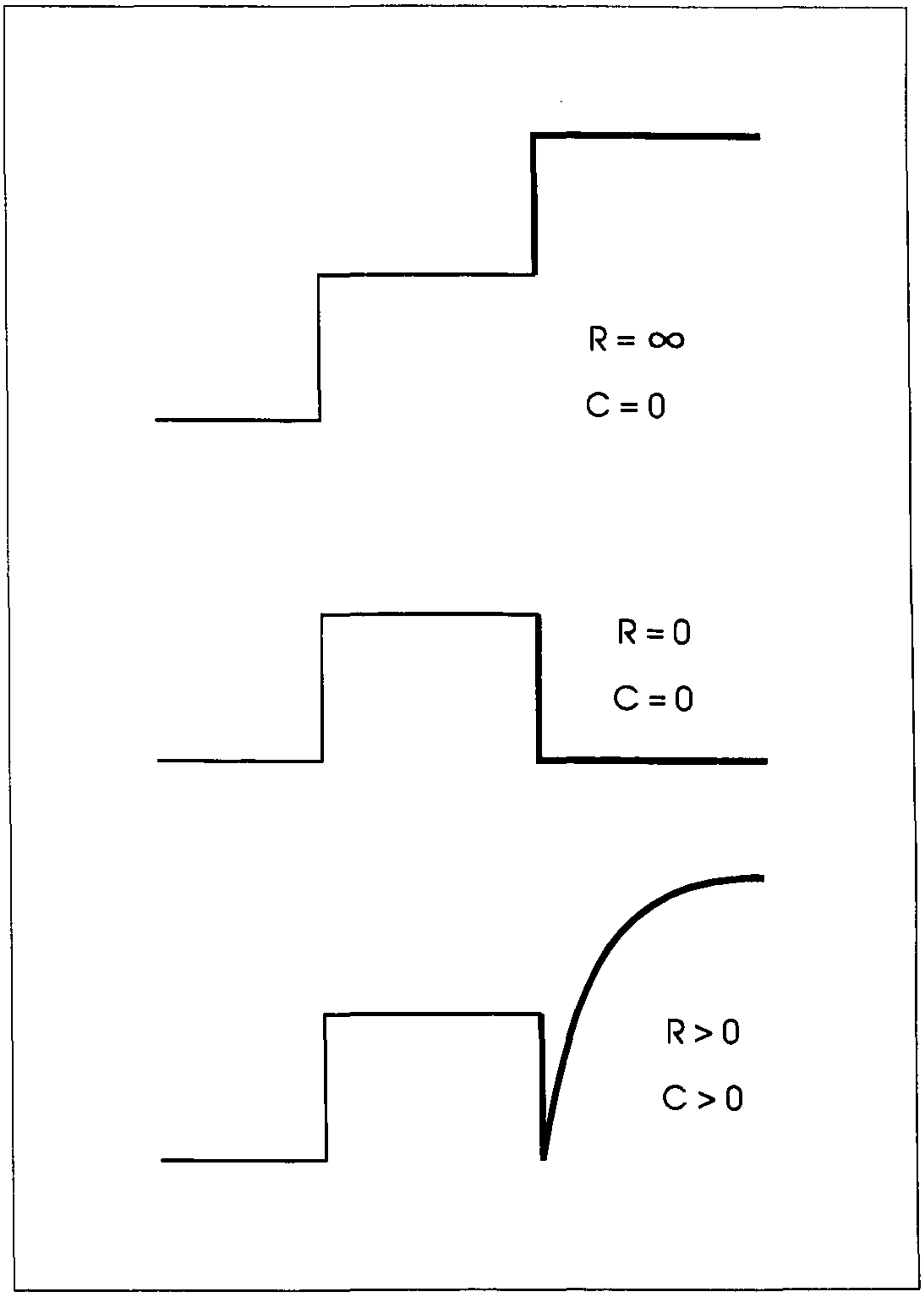

Figure 3.5 Typical TDR Responses.

equivalent information in the frequency-domain through the use of the Fast Fourier transform. The response of a dielectric sample in the frequency-domain may be found by calculating the ratio of Fourier transforms of the reflected and the incident pulses. If $f_i(t)$ and $f_r(t)$ are the incident and the reflected signals in the time-domain then the frequency response or the transfer function $G(\omega)$ of the dielectric system is defined as:

$$G(\omega) = \frac{F_r(\omega)}{F_i(\omega)} = \frac{\int_{-\infty}^{\infty} f_r(t)\exp(-i\omega t)\,dt}{\int_{-\infty}^{\infty} f_i(t)\exp(-i\omega t)\,dt} \tag{3-8}$$

The above deconvolution defines $G(\omega)$ for all frequencies contained in the incident pulse, thus it forms a unique description of the analyzed material regardless of the shape of the applied pulse. The use of a transfer function automatically compensates for an irregularly shaped incident pulse. In a setup involving a relatively long sample terminating the coaxial line, the analysis of direct reflections leads to the computation of the complex dielectric constant as follows:

$$\epsilon^* = \left(\frac{1 - G(\omega)}{1 + G(\omega)}\right)^2 \tag{3-9}$$

This study advocates a practical field implementation of the TDR method for the subsurface contaminant detection. It is proposed that a probe in a coaxial network configuration be inserted into the contaminated soil by pushing or drilling. Following a TDR measurement, a spectral analysis of the collected record would be performed. A broadband measurement of the frequency-dependent electrical properties of a contaminated soil would provide a characteristic "signature", which would be matched with a computerized database of known soil-contaminant "signatures". The mechanics of data analysis associated with this concept is elaborated upon in the experimental section of this study.

CHAPTER 4

EXPERIMENTAL STUDY

4.1 EXPERIMENTAL PROCEDURE

To assess the practicality of applying the TDR method to the contaminant detection in soils, a series of laboratory experiments was conducted. The instrumentation setup employed in this study is shown in Figure 4.1.

The main components include a step function generator, a coaxial transmission cable terminated by a soil probe, a digital waveform recorder and a portable computer to analyze the acquired data. The impulse signal produced by the generator is split as it travels past point A. Half of the amplitude of this voltage signal is recorded by the digitizing oscilloscope, while the other half propagates through the coaxial line and reaches the contaminated soil at point B. Subsequently, a reflection occurs due to a mismatch between the line impedance and some characteristic load impedandce at point B. The reflected impulse passes again through point A, creating a waveform indicative of the material's dielectric response. The role of the matched "T" is to prevent unwanted reflections at point A. Each of the matching resistors has a resistance of $\frac{Z_o}{3}$, where Z_o is the characteristic impedance of the coaxial line. The matched "T" was constructed with three Type N connectors attached to a metallic box (Pomona box), with their center conductors interconnected by three 16.5 ohm resistors.

In order to produce a high frequency polarization the incident signal must exhibit

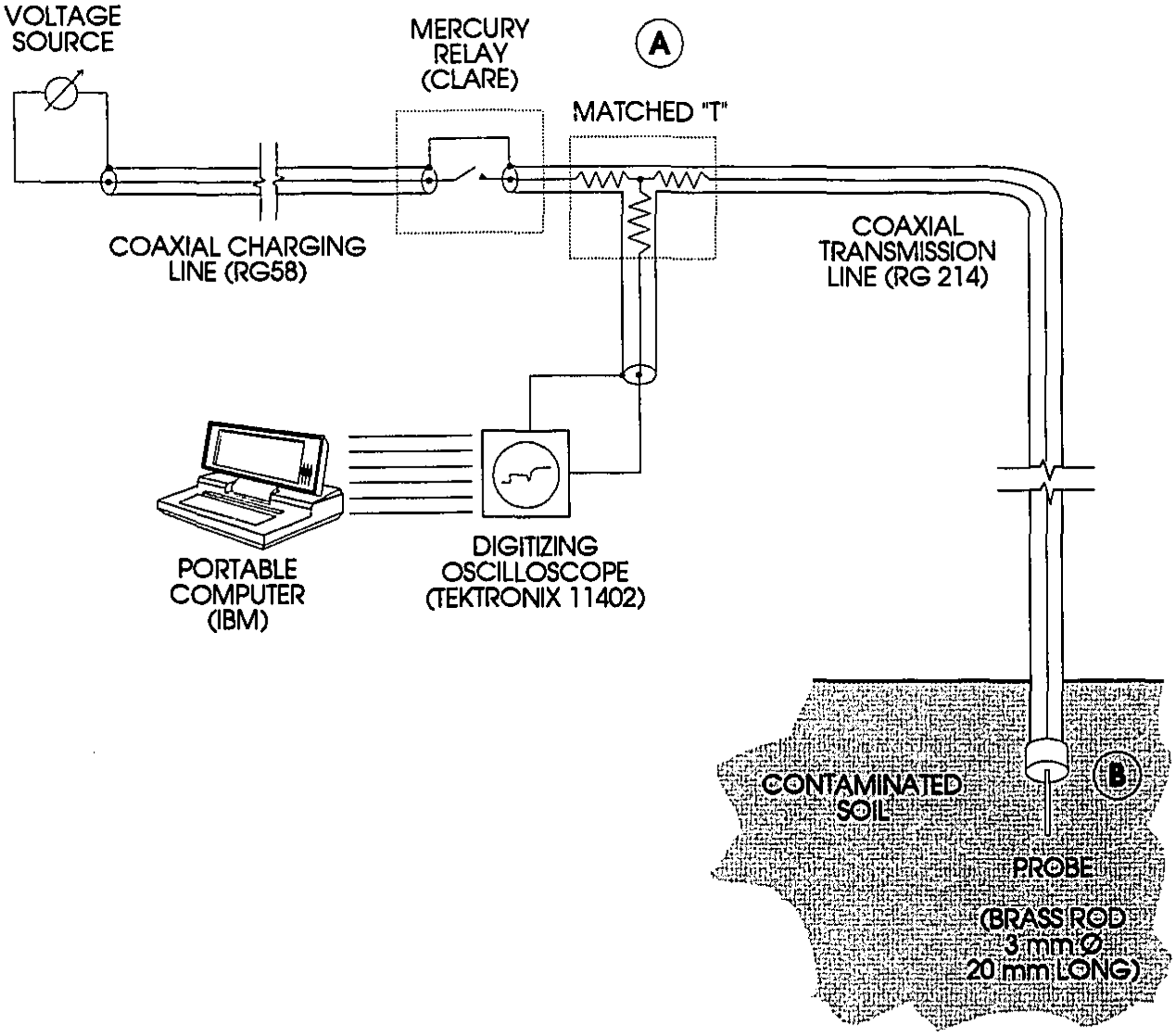

Figure 4.1 Experimental Setup.

a sufficiently fast risetime. The relationship between the signal risetime (T_r) and its frequency bandwidth (BW) may be approximated as follows:

$$BW = \frac{0.35}{T_r} \tag{4-1}$$

Thus, the steeper the pulse risetime the wider its effective frequency spectrum. A simple switch consisting of metal contacts is not satisfactory because the contact bounce during closure may produce an undesirable series of pulses. Brown and Pollard (1947) addressed this problem by developing a relay in which solid platinum contacts are continuously wetted with mercury by means of a capillary connection to a reservoir. The mercury film prevents the contacts from breaking when the armature bounces. Only one pulse is accordingly produced for each relay operation. The mercury relay has been recognized for its ability to deliver reproducible pulses with subnasecond risetimes (Andrews, 1973). Its main advantage is the capability to deliver a fast risetime, high amplitude signal. In contrast, a conventional laboratory TDR setup uses a low amplitude diode for signal generation. Such a signal may not be effective in field applications due to the influence of the ambient noise.

In this study the incident signal was produced with a mercury wetted contact relay manufactured by Clare. The relay was operated at a line frequency of 60 Hz, thus producing recurring waveforms. Each pulse was subsequently acquired by the digital waveform recorder.

The step function generator was created by alternately charging a 10 meter section of RG 58 coaxial cable with a DC voltage source and fast discharging through the mercury relay into the RG 214 coaxial cable. The length of the RG 214 cable was selected at 7 meters to simulate field conditions where the subsurface contaminant occurs at some depth.

It has been observed that a substantial length of the coaxial cable results in a noticeable impulse degradation with a resulting loss of the high frequency components. This is usually not a problem in a typical laboratory TDR setup which includes only about 30 cm of a coaxial line terminating in the sample material. The initial risetime of an impulse and thus its frequency spectrum degrade as the signal travels through a long cable, due to the phenomenon known as the "skin effect". One way of minimizing the pulse distortion is to select a high quality cable with inherently low loss characteristics. For this reason the RG 214 coaxial cable was chosen. It exhibits a maximum attenuation of 1.7 db/100 feet at 50 MHz, increasing to 60 db/100 feet at 11 GHz. The effect of pulse degradation is illustrated in Figure 4.2. The attenuation characteristics of the signal measured directly at the output of the step-function generator are compared with those of the same signal propagated through the coaxial cable, reflected from the short-circuit termination at point B and measured at point A. This comparison shows that a distortion associated with the pulse propagation in the measuring circuit begins to play a significant role only at frequencies above 200 MHz. In the range of 0 - 200 MHz the RG 214 coaxial cable does not exert any appreciable effect on the signal attenuation. Furthermore, it can be seen that the 200 MHz frequency component exhibits about 40 dB attenuation, which translates into the signal strength of 0.01 of the maximum. This signal level is well within the resolution capability of the TEK 11402.

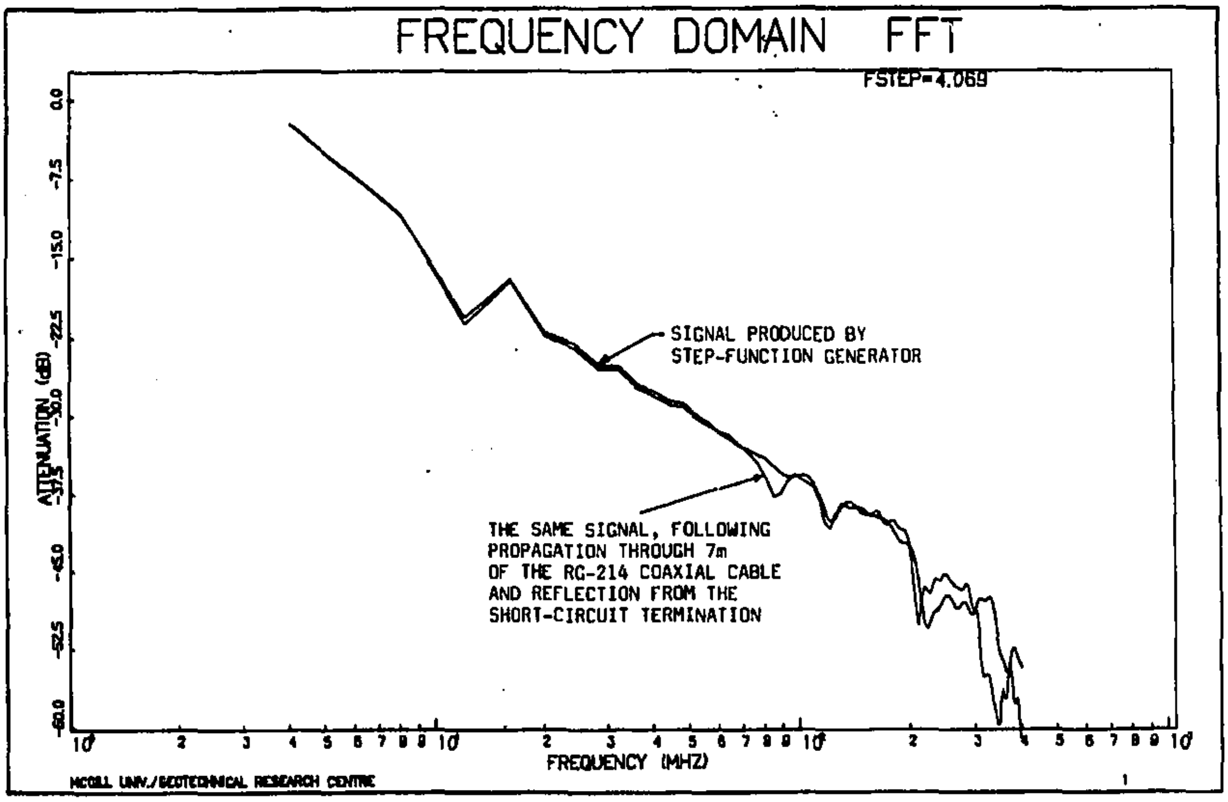

Figure 4.2 Effect of Pulse Propagation Through Coaxial Cable on Attenuation.

It is envisioned that the field probe would be drilled or pushed into the soil, while the recording instruments collect and analyze data at the surface. One potential scenario involves hollow stem auger drilling to a test depth, followed by the probe insertion, TDR measurement and data analysis directly on site. The soil probe used in this study consisted of a modified Type N coaxial connector with an extended center electrode made of a machined brass rod, 3 mm dia. and 20 mm long. The concept of an extended central electrode, surrounded by a dielectric material, was adapted from the in-situ dielectric measurements on oil shales, conducted by Iskander and DuBow (1983). Electrically, at low frequencies the equivalent circuit may be represented by a shunt capacitor terminating the coaxial line. At high frequencies the influence of the fringing field capacitance becomes increasingly dominant. An expression for the input impedance of the dielectric probe which is basically a monopole antenna immersed in the material under test is given by Gooch *et al.* (1963):

$$Z_i^* = \frac{\omega \mu_o}{j2k(S + CU)} \tag{4-2}$$

where the functions k, S, C, and U depend on the measurement frequency, the length and the diameter of the extended soil conductor and on the dielectric properties ϵ' and ϵ''. Due to the complexity of equation 4-2 the derivation of dielectric parameters is typically performed by iterative solutions involving minimization of a two-dimensional error surface, where the minimum indicates the most appropriate values of ϵ' and ϵ'' that satisfy the measured value of the input impedance.

The use of a digital waveform recording instrument provides several advantages, such as capture of transient signals, observation of signals occurring prior to the trigger event, waveform storage, and computer interfacing. The data acquisition equipment used in the study consisted of the Tektronix 11402 Digitizing Oscilloscope. This instrument is characterized by 14-bit vertical resolution with signal averaging and a maximum of 10 ps temporal resolution. The TEK 11402 can acquire up to three channels of data with 1 GHz frequency bandwidth concurrently. Record length is adjustable to 512, 1024, 2048, 4096, 5120, 8192 and 10240 points. Digitized waveforms are transferred for a subsequent data analysis to a portable computer using the IEEE-488 or RS-232 interface. The process of data acquisition lends itself to a full automation. The oscilloscope settings are also saved in a data file, allowing initialization and control of the oscilloscope from the computer.

The operation of the Tektronix 11402 requires a recurrent waveform to enhance its sensitivity and to extend the frequency range. The oscilloscope functions through a random sampling process. The shape of the recurrent waveform is determined by an automatic point-by-point measurement, with each individual data point being determined at a different waveform repetitions. As each recurrent waveform passes the "T" it triggers the automatic signal acquisition based on the predetermined threshold level of the leading edge of the pulse. This approach makes it possible to sample a given waveform with a much greater time resolution that is otherwise available with a single-shot acquisition. Random sampling acquires signals at a random sequence in relation to where they are stored in memory. The points in time at which these samples are acquired are "remembered" in reference to the trigger point.

Rather than computing the absolute values of the complex dielectric constant, the approach pursued in this study involved the material characterization through the use of the Transfer Function, which in turn is a function of ϵ^*. In the time-domain the input signal, the system response and the output signal are related through the Duhamel convolution integral:

$$y(t) = \int_{-\infty}^{\infty} h(\tau)x(t-\tau)\,d\tau \tag{4-3}$$

In the frequency-domain the relationship between the input and the output corresponds to a simple multiplication. The input and the output signals can be transformed into the frequency-domain through the use of the Fast Fourier Transform (FFT). Subsequently, the Transfer Function $H(f)$ of a system may be established by dividing the spectrum of the output by the spectrum of the input waveform.

$$\begin{aligned} Y(f) &= H(f) * X(f) \\ H(f) &= \frac{Y(f)}{X(f)} \end{aligned} \tag{4-4}$$

What usually needs to be established is how a given system responds to each frequency component of an arbitrary input signal. In a linear, time invariant system, such a response offers a complete and unique circuit characterization (Ramirez, 1985). It also represents a characteristic spectral "signature" of a material under test.

4.2 DATA ACQUISITION

Prior to digitizing and processing large quantities of data, a small series of trial tests was conducted with a setup shown in Figure 4.1. The objective was to assess if various "contaminants" produce clearly discernible time-domain responses. Fluids selected for testing included Butyl Alcohol, Methyl Alcohol, Phenol (1000 ppm), and Kerosene. The oscilloscope traces indicating distinctly unique responses are shown in Figures 4.3 through 4.6. It is evident that the shape of the reflected signal is affected by the material examined.

Subsequent tests were conducted using the digital waveform recording capabilities of the TEK 11402. Data acquired and stored by the oscilloscope was transferred to a computer for signal processing. Tests were performed on several arbitrarily chosen "contaminants" and on "soil-contaminant" mixtures. The soil used to create these mixtures consisted of dry portions of 60% Lake Agassiz clay and 40% crushed granodiorite passing sieve #50 and retained on sieve #16. Soil-contaminant mixtures were prepared with 60% and 40% fluid content ("contaminant"), simulating fully saturated

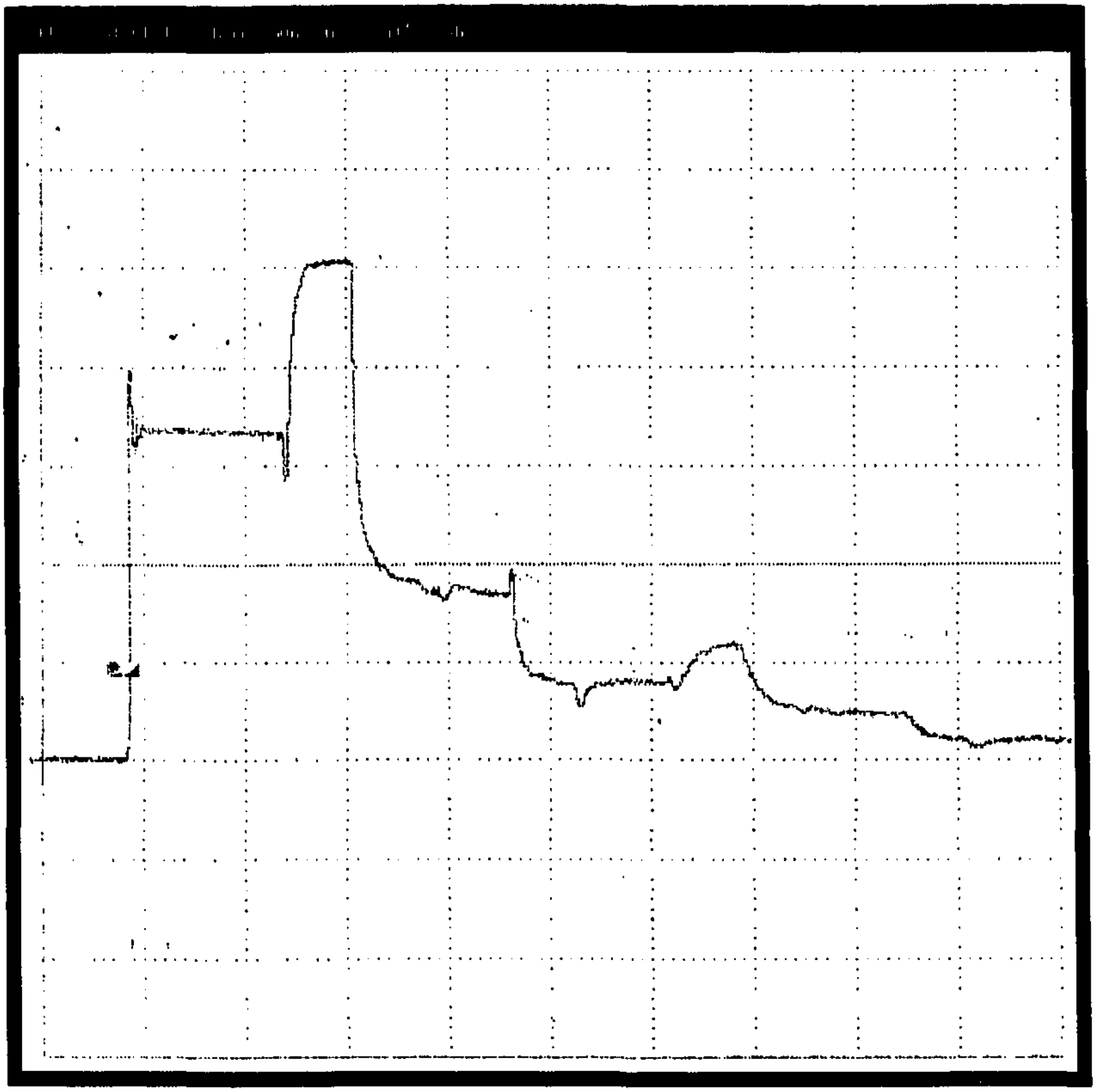

Figure 4.3 Oscilloscope Trace - Butyl Alcohol.

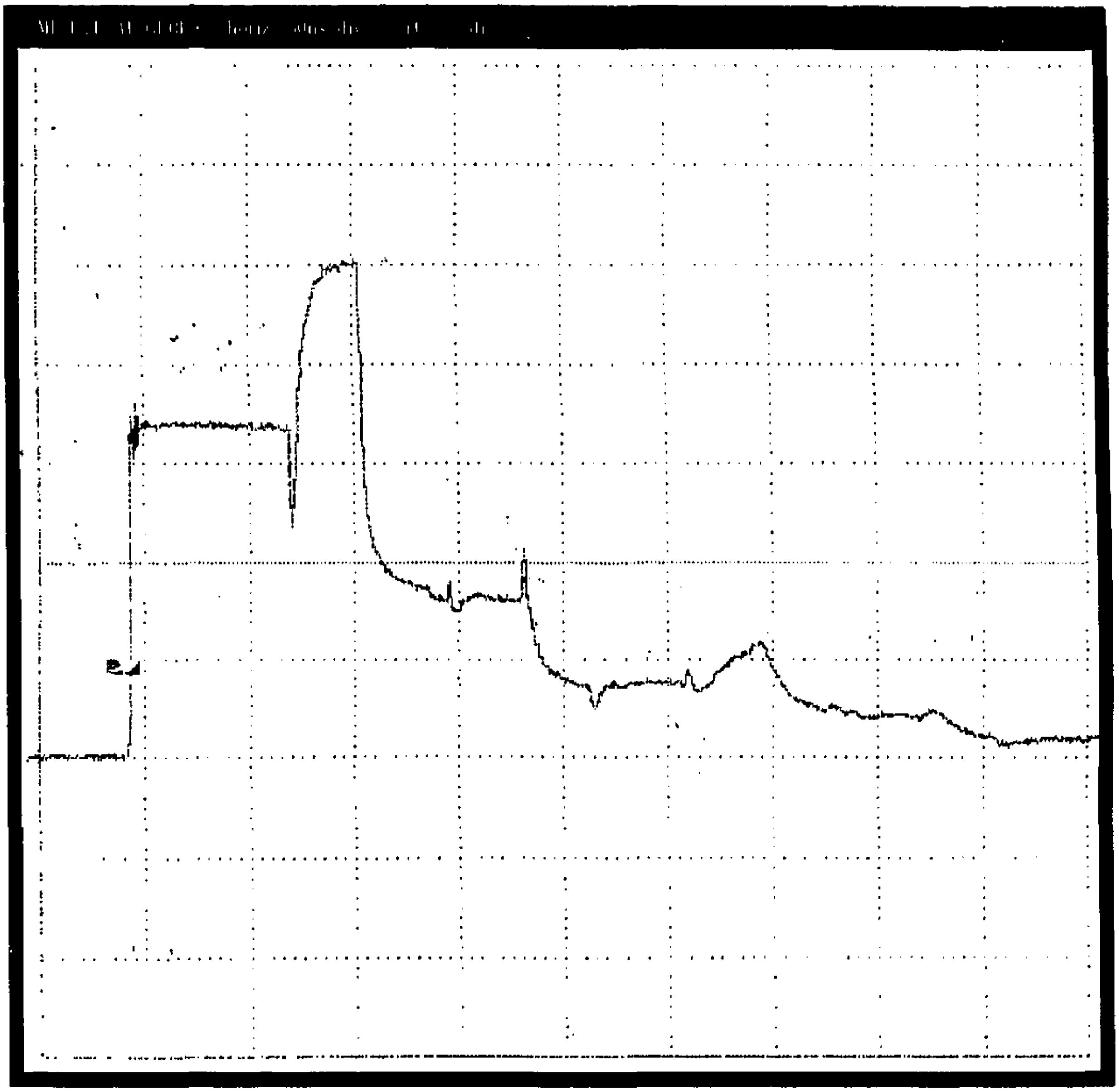

Figure 4.4 Oscilloscope Trace - Methyl Alcohol.

Figure 4.5 Oscilloscope Trace - Phenol (1000 ppm).

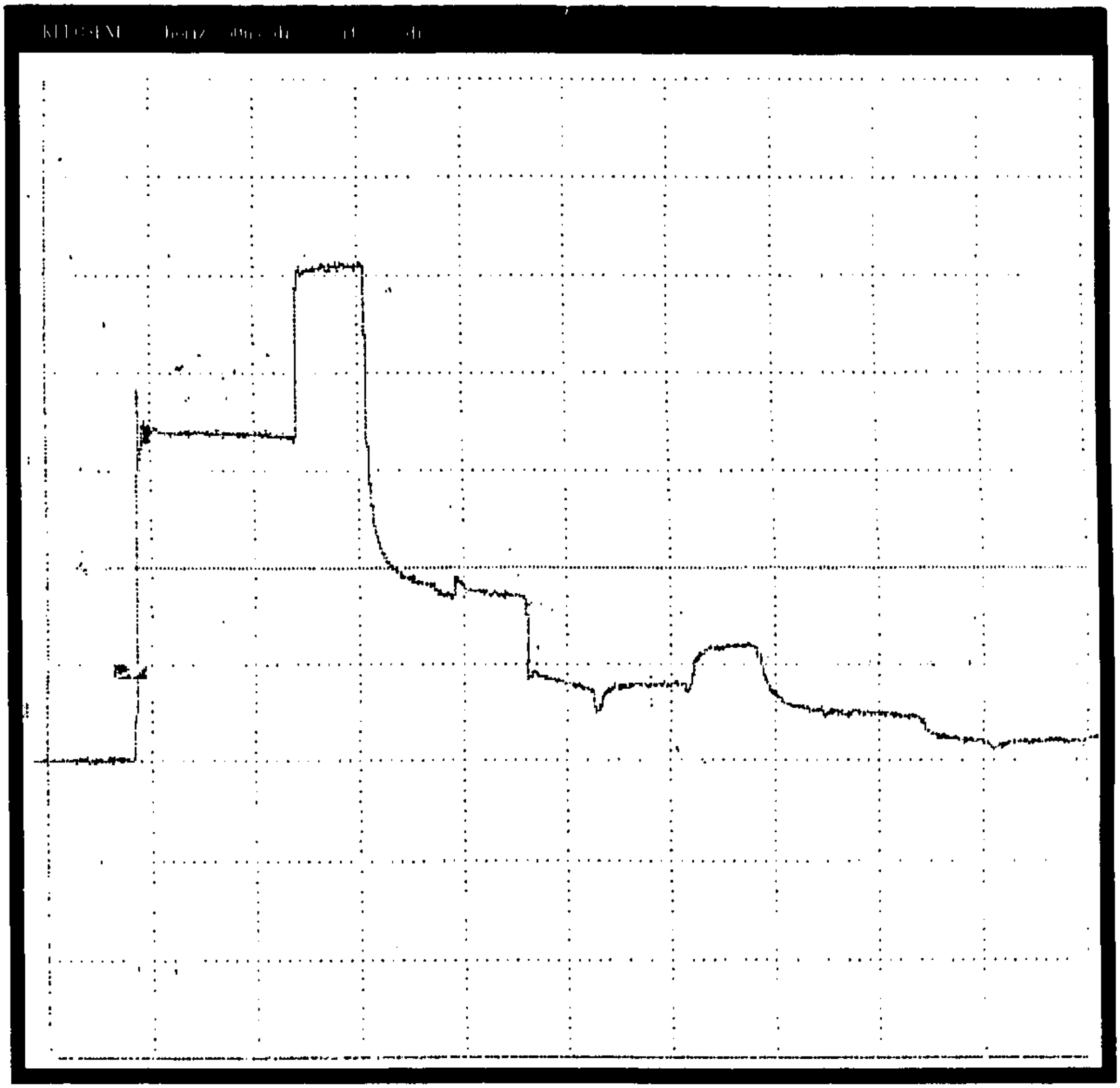

Figure 4.6 Oscilloscope Trace - Kerosene.

Pollutant	pH	*S* (mS/m)	Na (ppm)	Ca (ppm)	K (ppm)	Mg (ppm)	Cl^- (meq/L)	CO_3^{2-} (meq/L)	HCO_3^- (meq/L)
KAH1	7.54	23.0	198	54	103	95	15	0	0
CEZ	2.73	58.7	0	8	2	148	27	0	1.0
PB	2.11	64.7	340	2	1	0	45	0	2.0
H20	5.24	0.3	1	1	0	0	0	0	3.0
LACHENAIE	6.80	2.7	140	180	16	350	5	0	5.0

Pollutant	SO_4^{2-} (meq/L)	Al^{3+} (ppm)	Cd^{2+} (ppm)	Cr^{2+} (ppm)	Cu^{2+} (ppm)	Fe^{2+} (ppm)	Ni^{2+} (ppm)	Pb^{2+} (ppm)	Zn^{2+} (ppm)
KAH1	0.02	0	0	0	0	0	0	0	0
CEZ	107.00	15	17	0	42	47	0	1	2983
PB	0.10	0	0	0	0	0	0	63	0
H20	0.16	0	0	0	0	0	0	0	0
LACHENAIE	--	--	--	--	1.7	5	--	1	2.5

NOTES: S - conductivity;
KAH1 - leachate from Kahnawaki landfill site.
CEZ - waste product from zinc manufacturing facility (diluted to 200 mg/L)

PB - laboratory solution of lead chloride
H2O - distilled water
LACHENAIE - Leachate from Lachenaie landfill site.

Additional materials used in experiments included BENZENE, ETHANOL, 0.01 N $CaCl_2$, and 0.01 N NaCl.

Table 4.1 Chemical Characteristics of "Contaminants".

and unsaturated soil conditions. Table 4.1 summarizes the chemical composition of "contaminants" used in the experiments.

Lake Agassiz clay originated from St. Boniface, Manitoba. Its mineral composition, in a decreasing order of abundance, comprised montmorillonite, illite, quartz, kaolinite, feldspar, and dolomite (Yong *et al.*, 1986). Based on the saturation extract analysis, the main water soluble ions were classified as: Na^+, Ca^{2+}, HCO_3^-. The predominant extractable ion was found to be Ca^{2+} and the cation exchange capacity (CEC) was determined at 71.4 mg/100g. Liquid and plastic limits were 112% and 28%, respectively. The gradation analysis indicated 61% of particles passing the #200 sieve.

The crushed granodiorite originated from Cold Springs Quarry in Lac du Bonnet, Manitoba. Its mineralogical composition included quartz (28%), feldspar plagioclase (35%) and microcline (20%).

Measurements were performed on contaminants and on soil-contaminant mixtures prepared 24 hours prior to testing. All soil specimens were initially air dry. No significant scatter in each material's response was observed during testing. Measurements were performed on the following materials:

- H2O (Distilled water)
- H2O-40 (Soil with 40% H2O)
- H2O-60 (Soil with 60% H2O)
- CACL (0.01 N calcium chloride)
- CACL-40 (Soil with 40% CACL)
- CACL-60 (Soil with 60% CACL)
- PB (Lead chloride)
- PB-40 (Soil with 40% PB)
- PB-60 (Soil with 60% PB)
- CEZ (Waste product from zinc production)
- CEZ-40 (Soil with 40% CEZ)
- CEZ-60 (Soil with 60% CEZ)
- KAH1 (Leachate from Kahnawaki landfill site)
- KAH1-40 (Soil with 40% KAH1)
- KAH1-60 (Soil with 60% KAH1)
- OPEN (Empty probe)

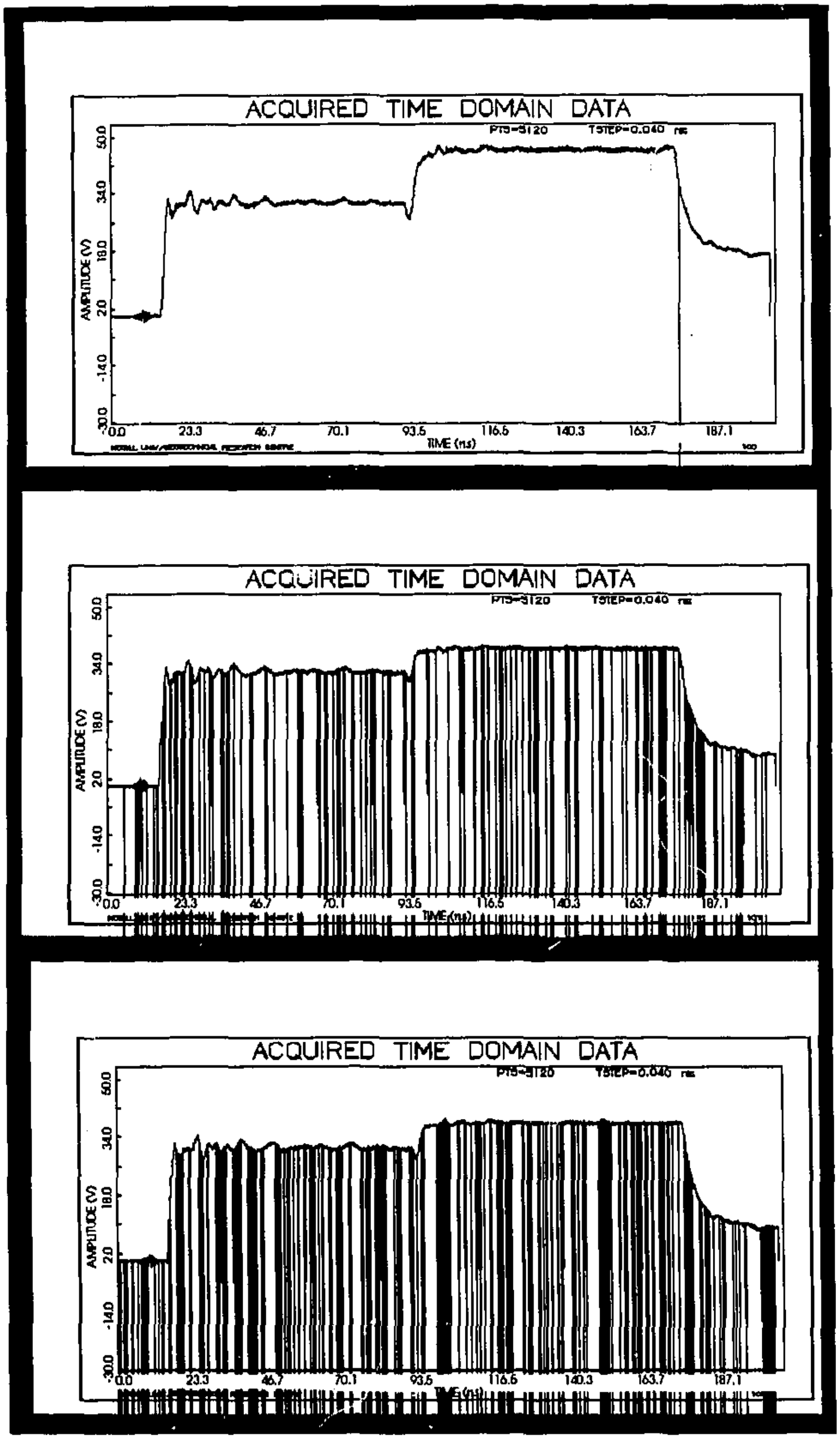

Figure 4.7 Acquired Time-Domain Data : H2O, H2O-40, H2O-60.

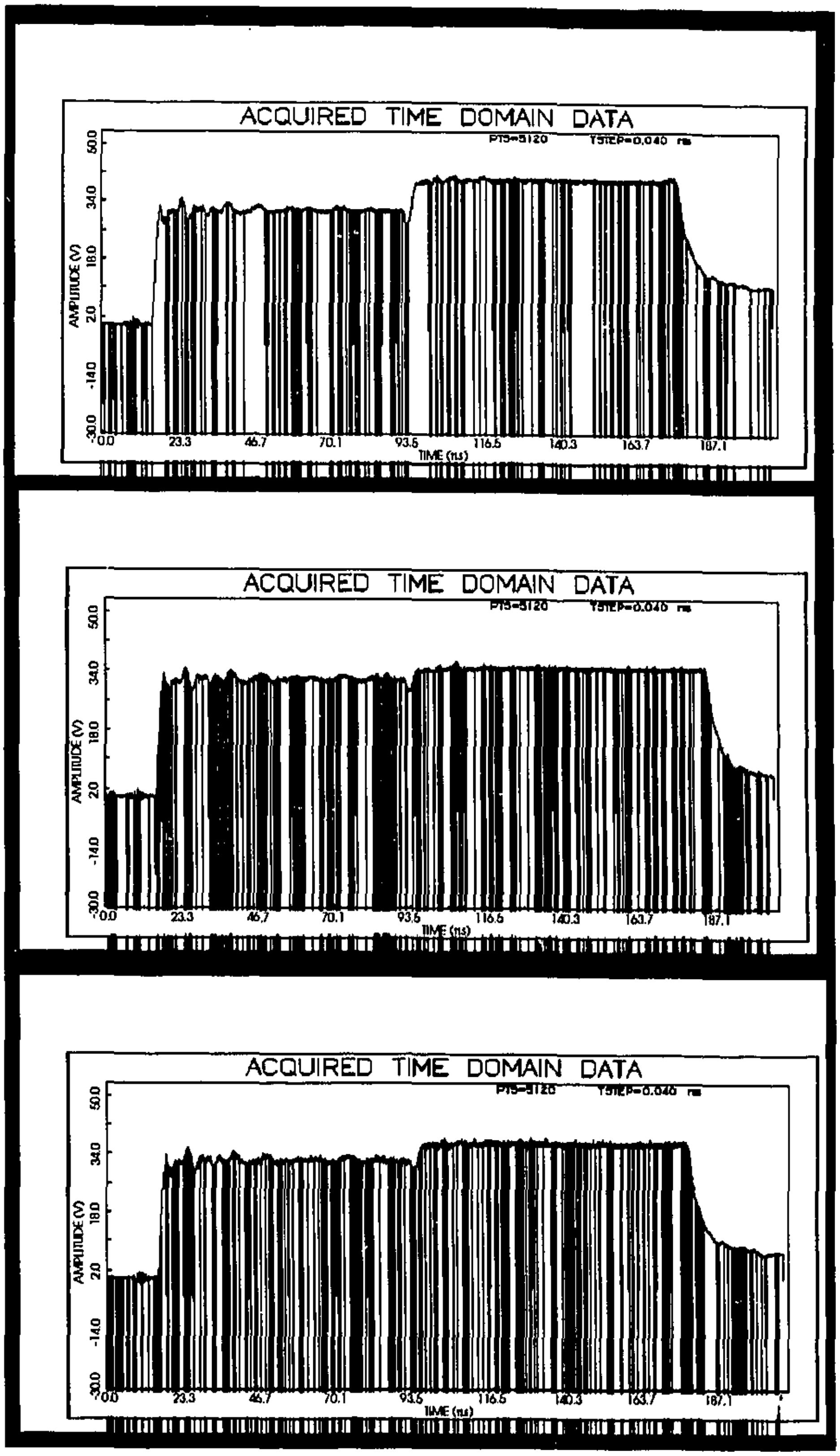

Figure 4.8 Acquired Time-Domain Data : CACL, CACL-40, CACL-60.

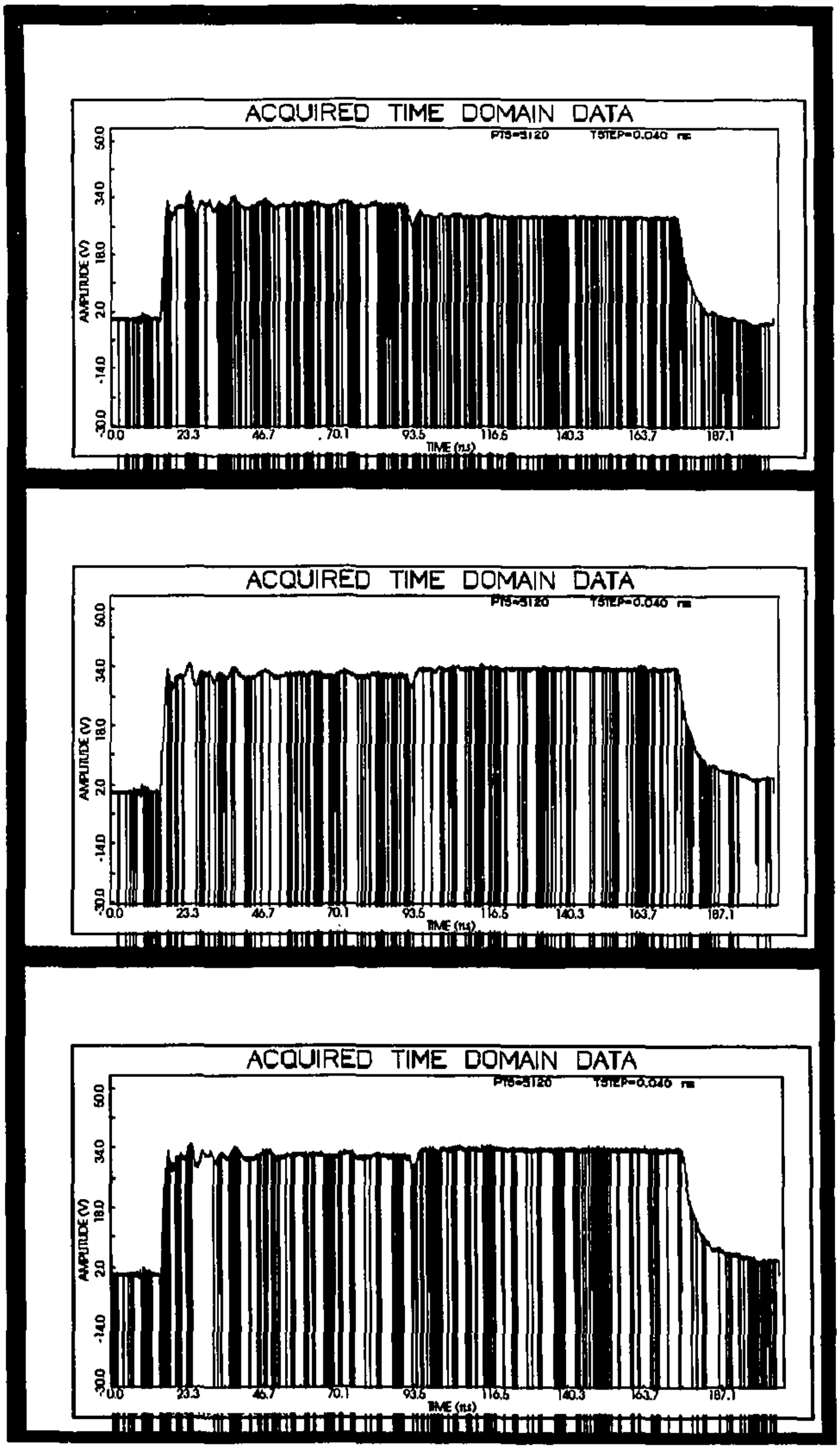

Figure 4.9 Acquired Time-Domain Data : PB, PB-40, PB-60.

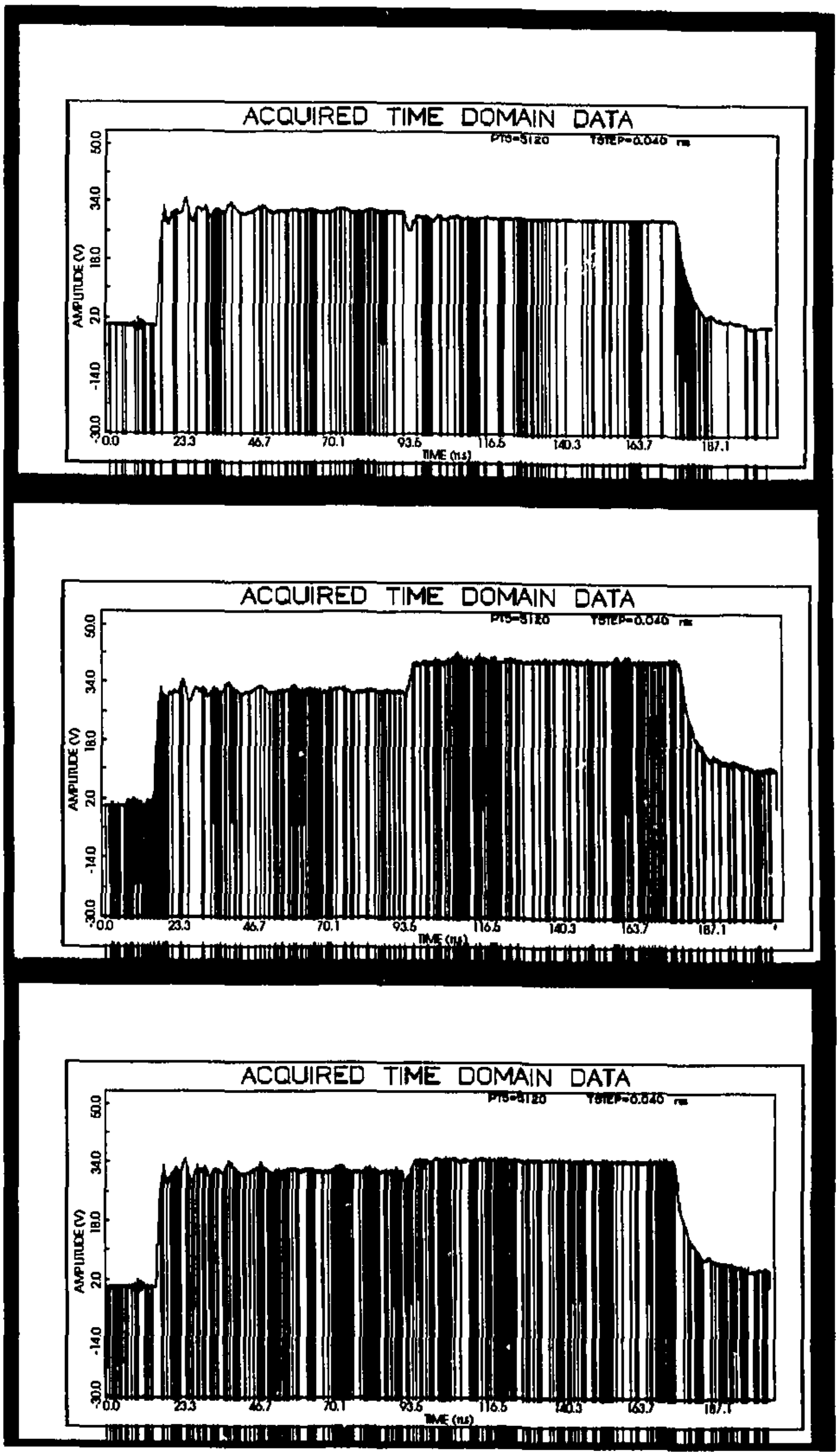

Figure 4.10 Acquired Time-Domain Data : CEZ, CEZ-40, CEZ-60.

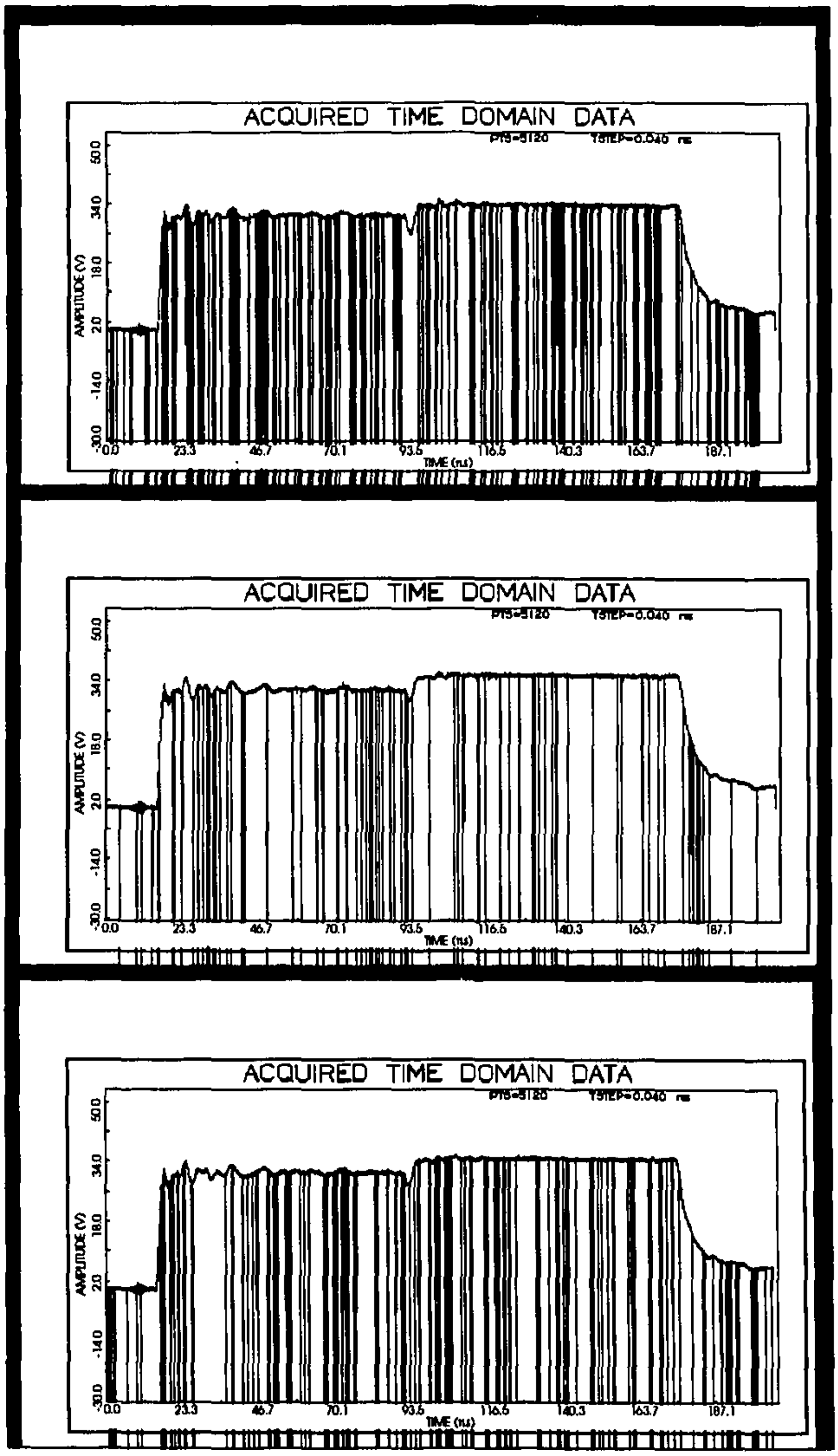

Figure 4.11 Acquired Time-Domain Data : KAH1, KAH1-40, KAH1-60.

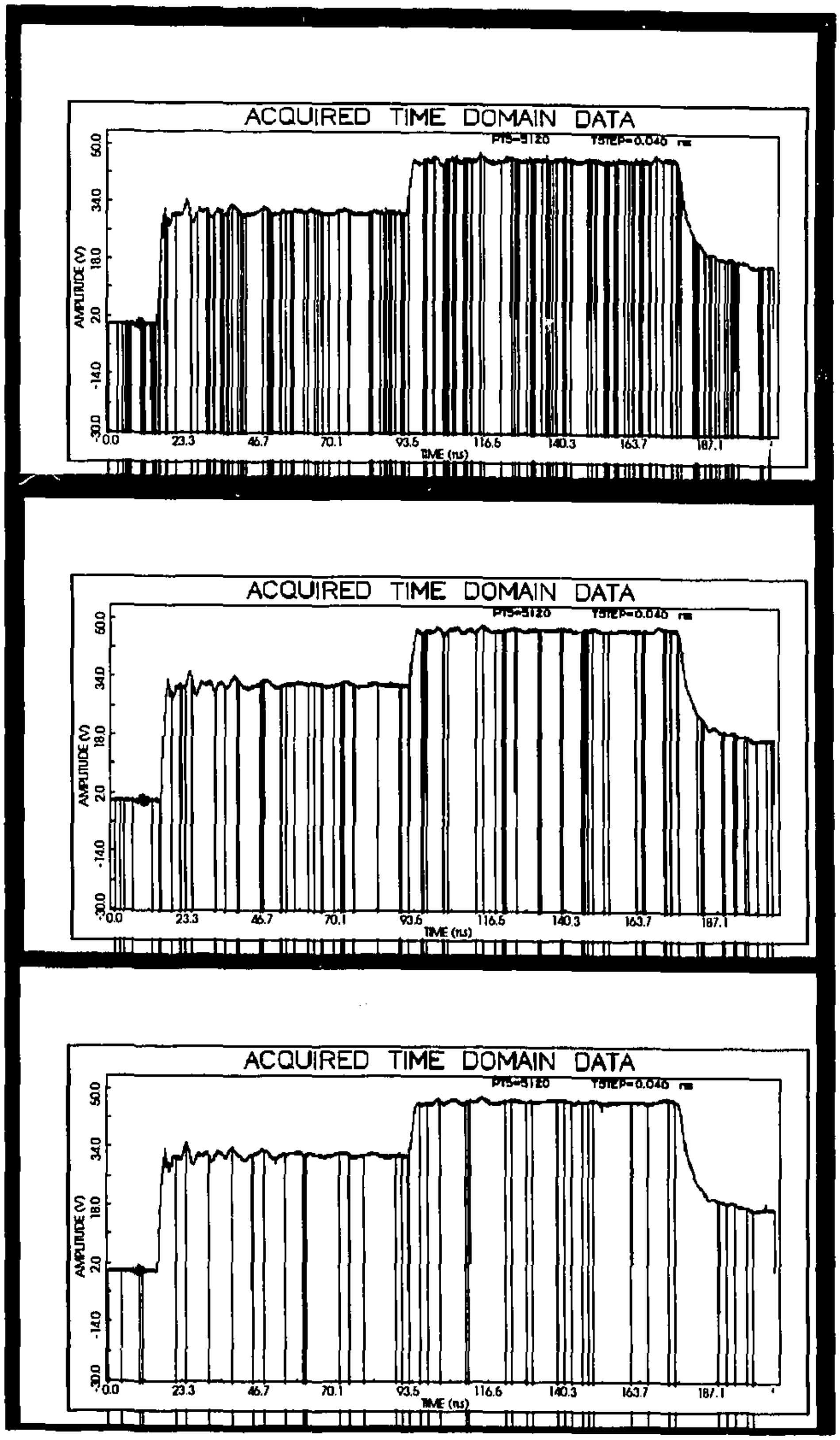

Figure 4.12 Acquired Time-Domain Data : OPEN, BENZENE, ETHANOL.

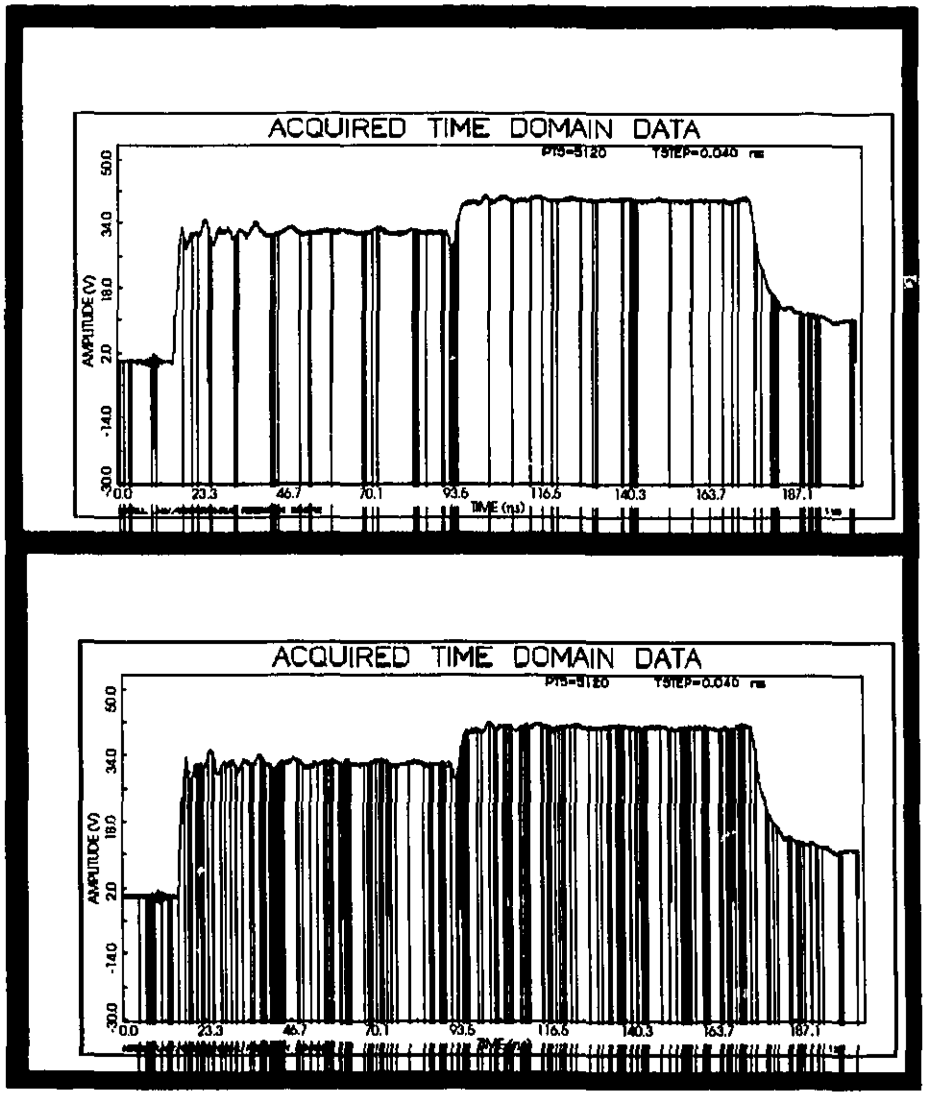

Figure 4.13 Acquired Time-Domain Data : LACHENAIE, NACL.

- BENZENE
- ETHANOL
- LACHEN (Leachate from Lachenaie landfill site)
- NACL (0.01 N sodium chloride)

Figures 4.7 through 4.13 display the experimental data acquired with the measuring circuit shown in Figure 4.1. Each signal, sampled every 40 ps, consists of 5120 data points and indicates the initial voltage step as the impulse reaches the digitizing oscilloscope and a subsequent reflection from the sample material. The time t=0 signifies the triggering point for the waveform acquisition to the digitizer's memory. The negative time range represents pre-trigger events. After about 70 nanoseconds following the start of the incident impulse acquisition, the reflected signal reaches the digitizer. This time lag is governed by the length of the cable between the sampling point and the soil probe. Sporadic vertical spikes corrupting the acquired time-domain data represent points that were missed during the random sampling process. These data points were adjusted at the signal processing stage.

4.3 DATA ANALYSIS

Figures 4.14 through 4.20 display processed time-domain data following splitting the acquired signal into its constituent input $x(t)$ and output $y(t)$ waveforms. Median filtering was used to eliminate the unwanted spikes in data. This method is considered particularly effective when the noise pattern consists of strong, spikelike components, and where the characteristic to be preserved is edge sharpness (Gonzales and Wintz, 1987). The effect of the median filtering operation is the rejection rather than averaging of spikes in data. Each acquired TDR record was successively divided into 25 point data groups, with the 13th largest value being the median of each group. This operation had no appreciable impact on reducing the effective frequency content since the signal was heavily oversampled at the acquisition stage. All output waveforms were also multiplied by 2, to correct for the initial split of the amplitude as the signal passed through the matched "T".

Proper application of the Fast Fourier Transform (FFT) demands that a time-domain waveform begins and terminates at the same amplitude. Step-like waveforms produce a well known truncation error if they are treated by the FFT without any preprocessing. The abrupt data truncation produces a distortion of the true spectrum of the analyzed signal by introducing a series of artificial high frequency components. Several methods addressing this particular problem have been published. Waldmeyer (1980) pointed out that the three widely used techniques of Samulon, Nicolson and Gans, which originate from apparently different ideas lead to the same numerical process. The technique used for preprocessing of the time-domain data in this study involved application of a cosine window to the last 30% of each waveform, thus forming a gradual transition towards the initial amplitude level. Subsequently, a 100% zero padding was applied, so that the analyzed impulse appeared to the FFT algorithm as a repetitive waveform. Additional zeroes were appended to bring each waveform to exactly 4096 data points prior to applying the FFT. All signal processing operations were performed by developing customized programs in Fortran. Applicable source codes are included in the Appendix 1.

The transfer function $H(f)$ was calculated by dividing the FFT of the output waveform by the corresponding FFT of the input. This operation results in a set of complex numbers which may be displayed graphically for ease of interpretation. Representative results are shown in Figures 4.21 though 4.25. Transfer functions for contaminants and soil-contaminant mixtures were computed up to a maximum frequency of 200 MHz. The practical upper frequency limit was imposed by the spectral composition of the generated input signal (function of the risetime). All frequency components above 200 MHz were ignored.

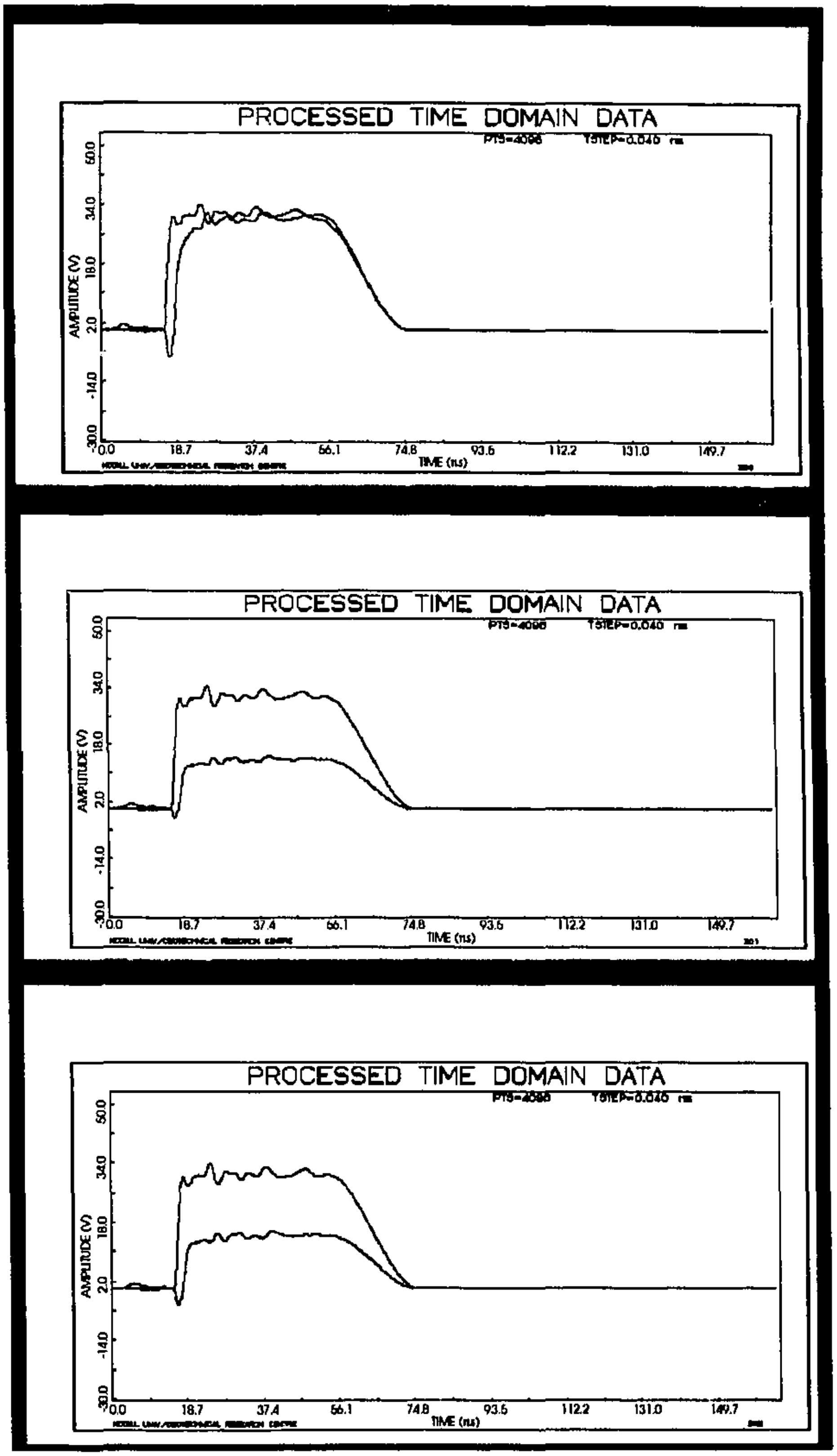

Figure 4.14 Processed Time-Domain Data : H2O, H2O-40, H2O-60.

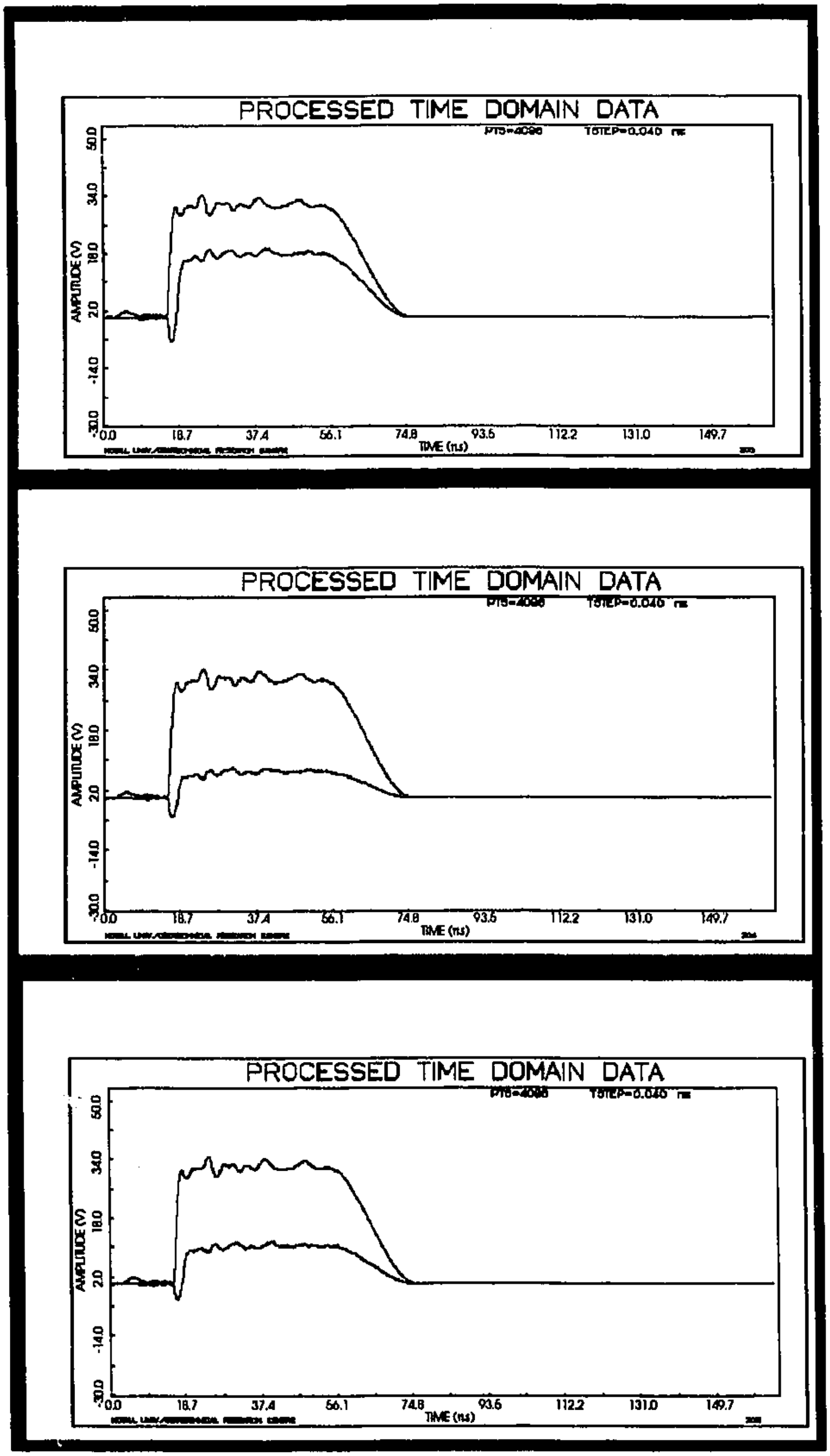

Figure 4.15 Processed Time-Domain Data : CACL, CACL-40, CACL-60.

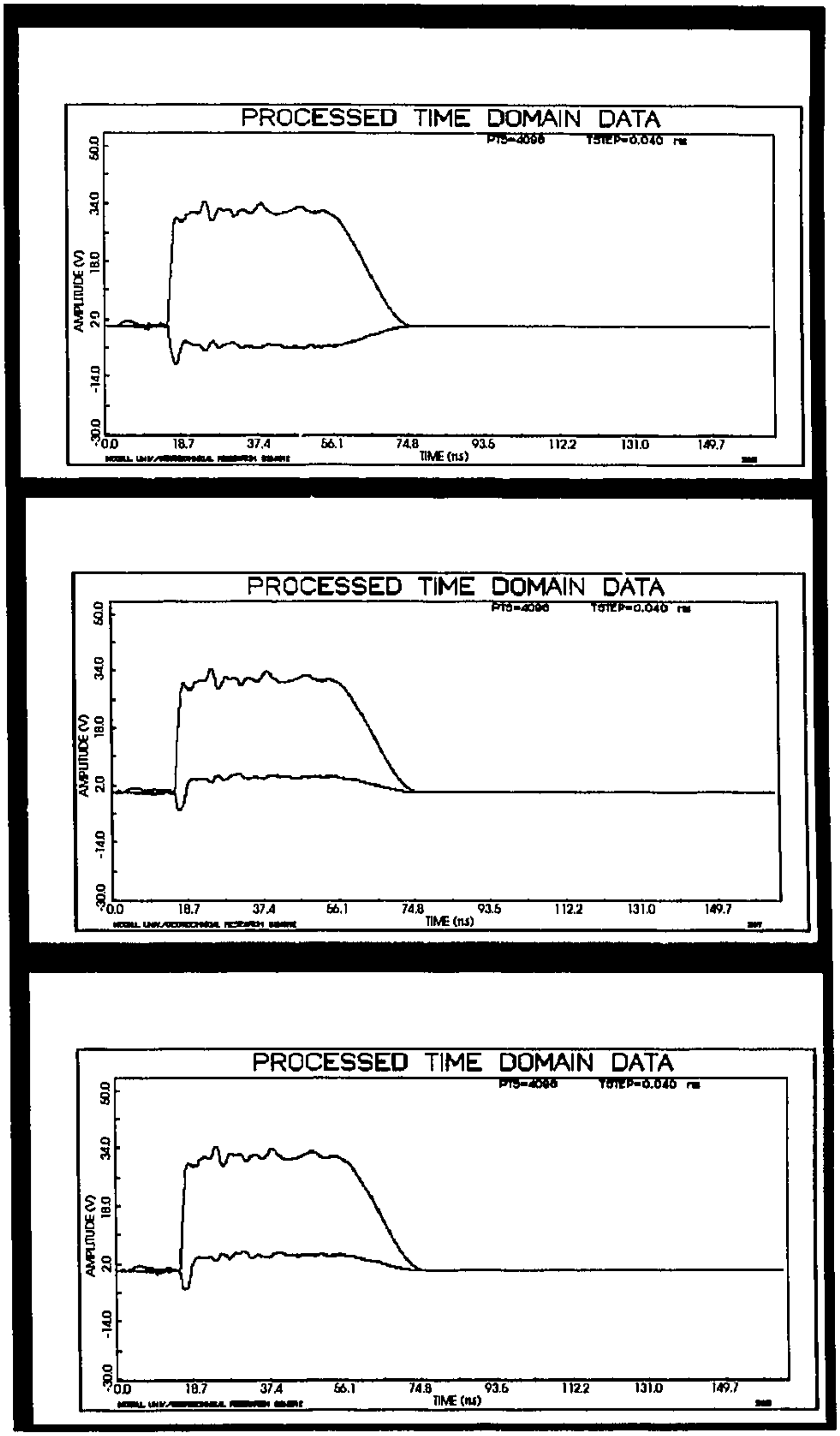

Figure 4.16 Processed Time-Domain Data : PB, PB-40, PB-60.

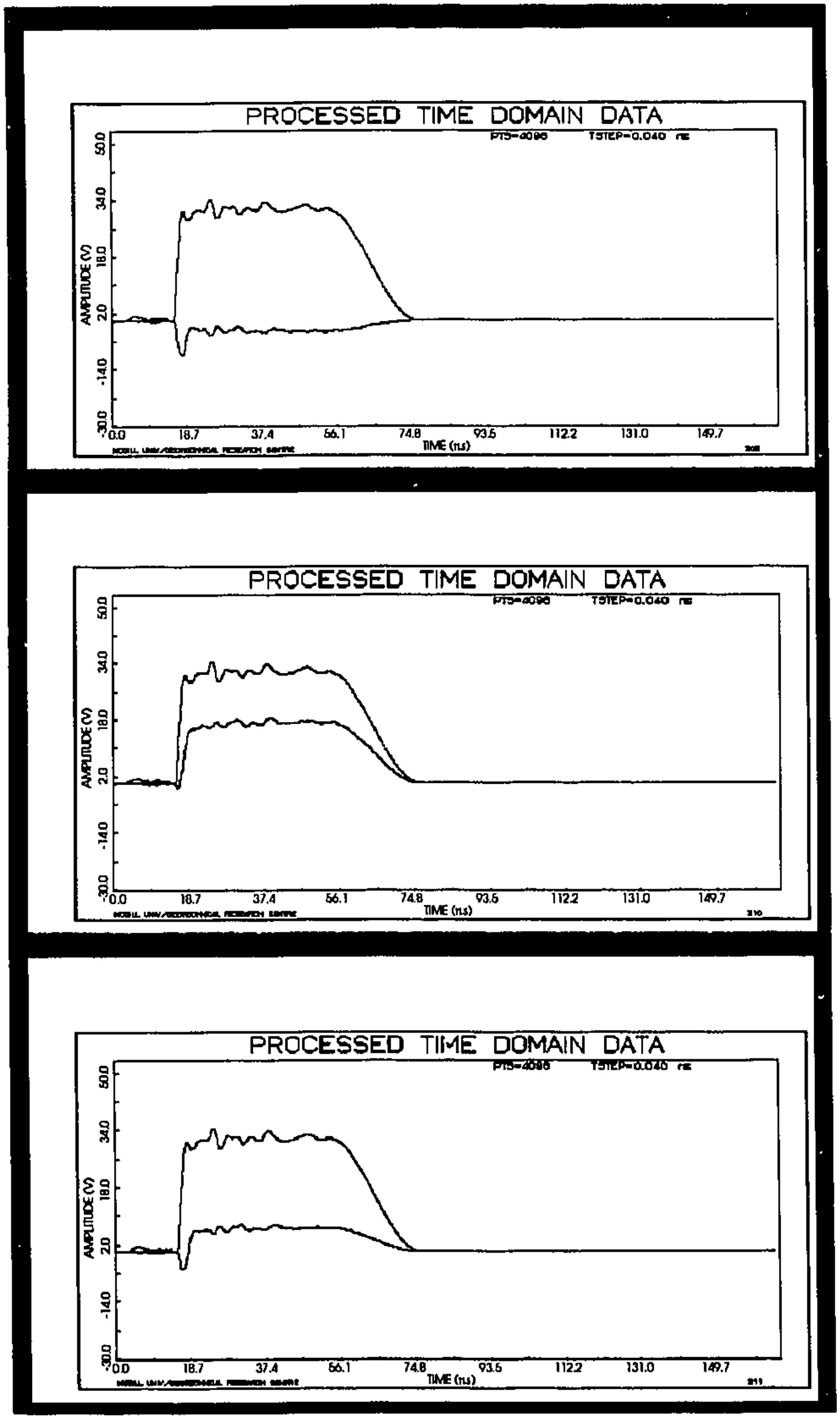

Figure 4.17 Processed Time-Domain Data : CEZ, CEZ-40, CEZ-60.

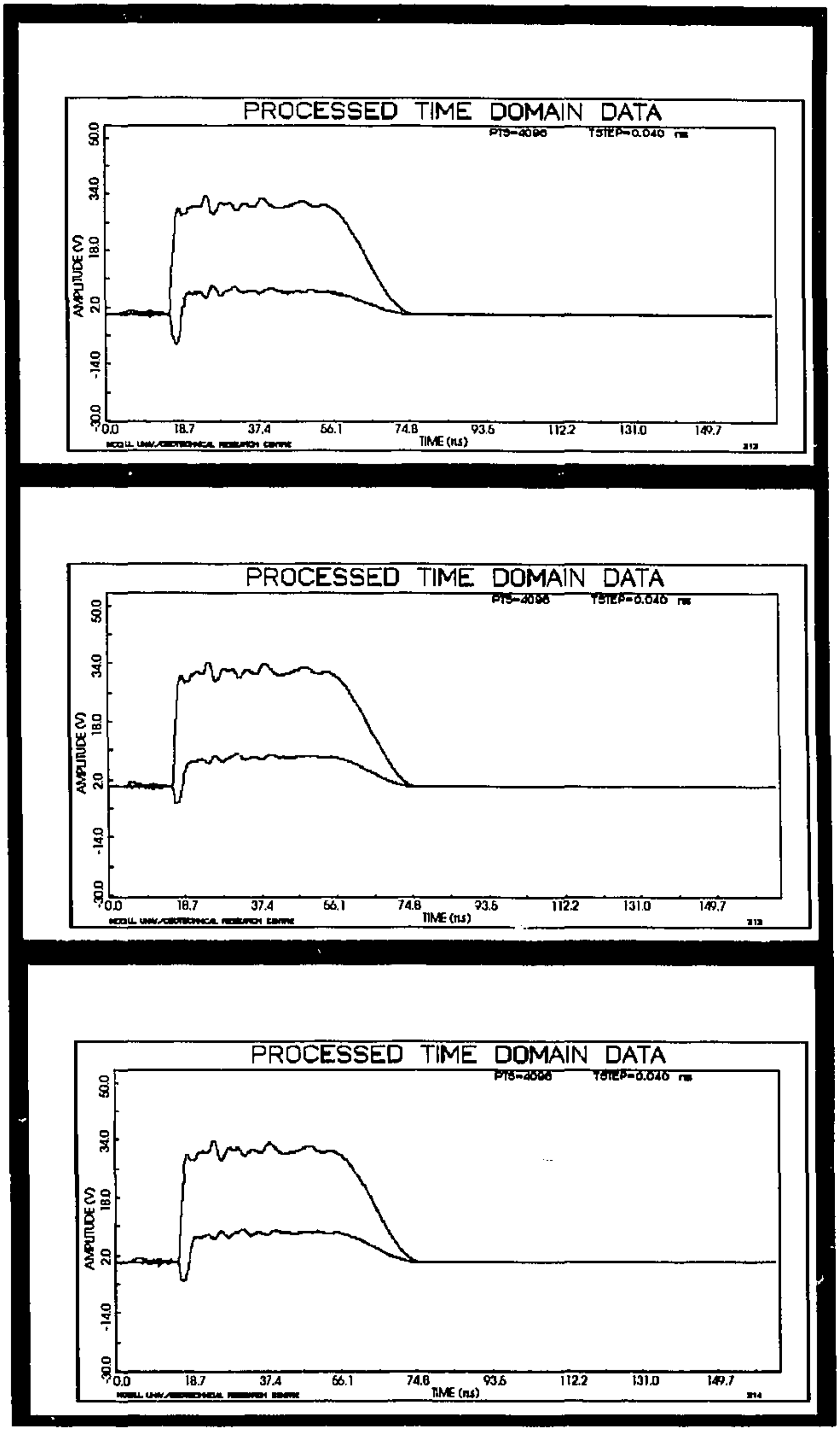

Figure 4.18 Processed Time-Domain Data : KAH1, KAH1-40, KAH1-60.

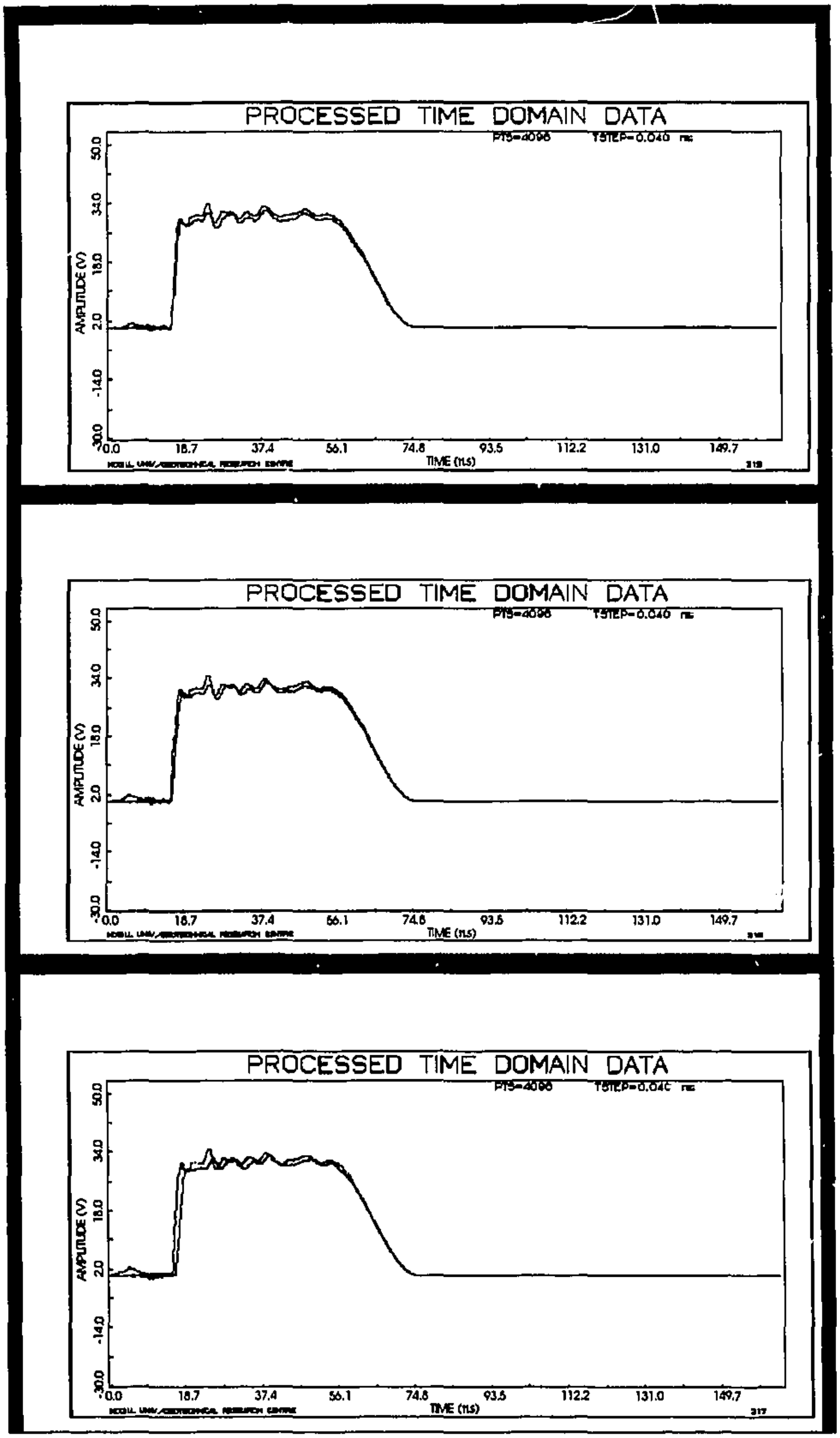

Figure 4.19 Processed Time-Domain Data : OPEN, BENZENE, ETHANOL.

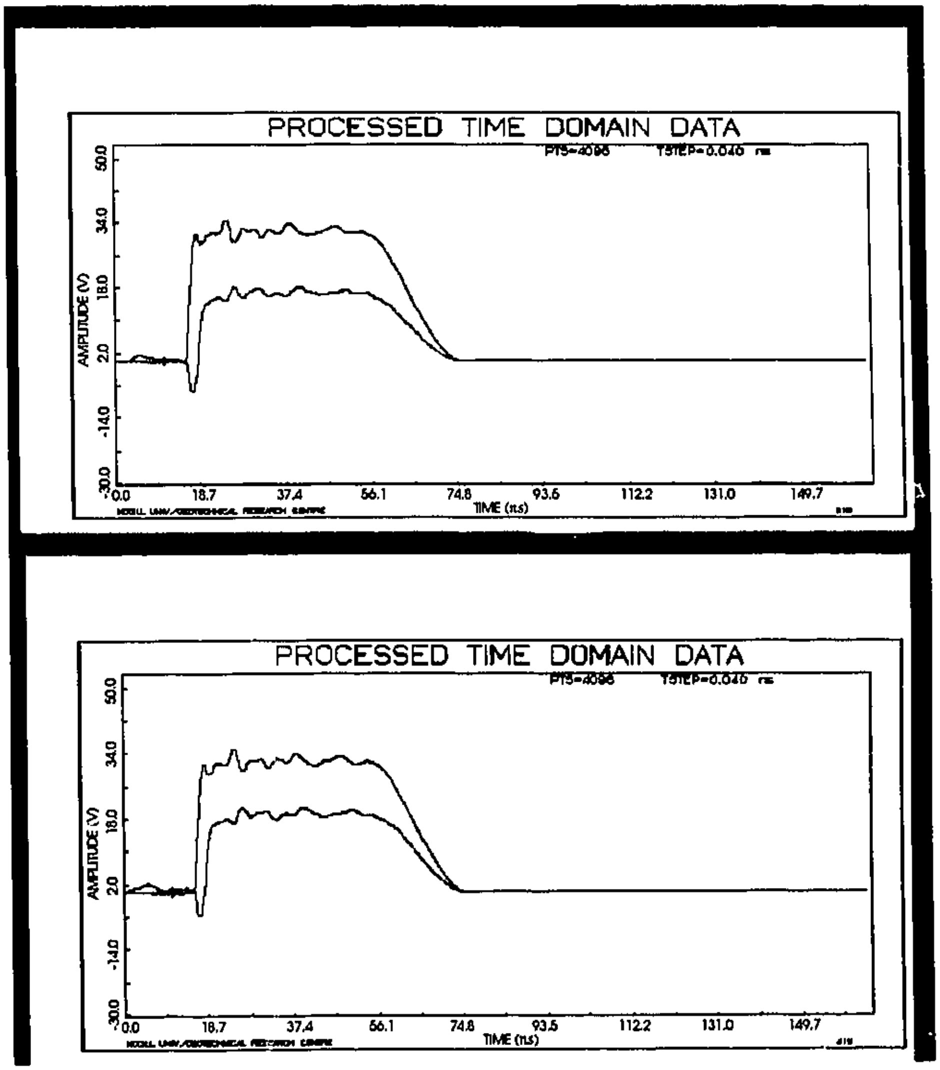

Figure 4.20 Processed Time-Domain Data : LACHENAIE, NACL.

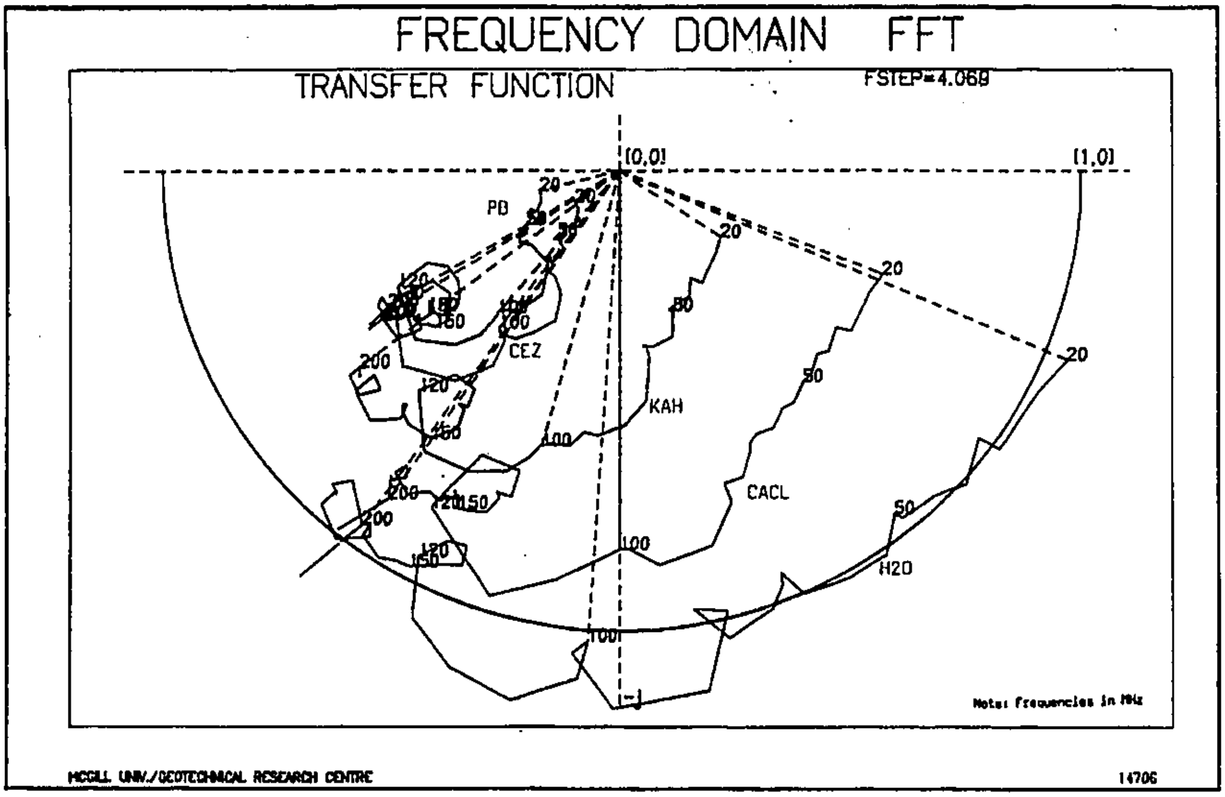

Figure 4.21 Transfer Function : PB, CEZ, KAH, CACL, H2O.

The concept of employing the transfer function in the contaminant detection has been reported by Yong and Hoppe (1989). The previously published material is included in the Appendix 2. It was realized, however, that while a visual presentation in terms of a transfer function expressed by polar coordinates provides a qualitative insight of the polarization phenomenon, it does not render itself well to the task of quantifying numerous test results. It is evident that in polarization measurements both magnitude and phase contain significant information. Much of the useful information is contained in the phase spectrum, yet phase is routinely susceptible to noise, particularly at high frequencies. It leads to a common difficulty in analyzing the polar coordinate transfer function, as manifested by the presence of "loops". Nevertheless, when visually comparing graphs such as Figure 4.23 and Figure 4.24, there appear to be some distinctive

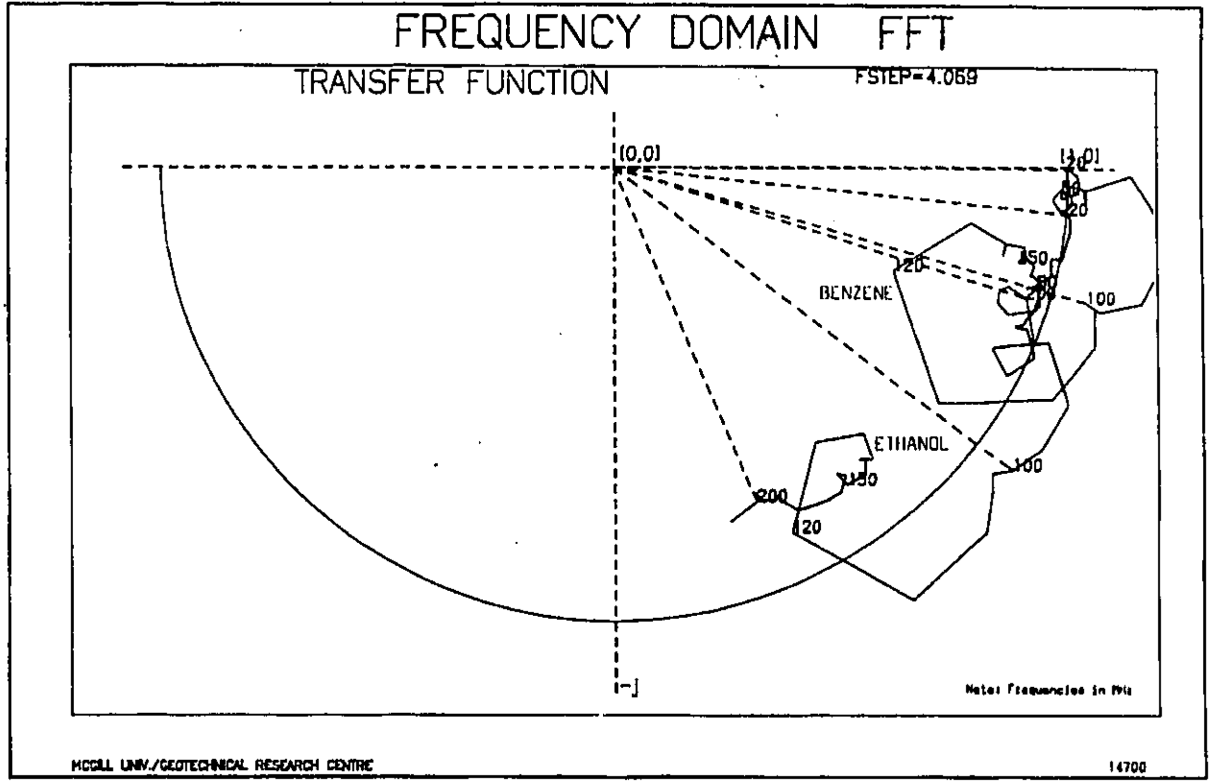

Figure 4.22 Transfer Function : BENZENE, ETHANOL.

similarities amongst each group of "contaminants". Clearly, some systematic approach to quantifying these test results for a subsequent matching of known and unknown responses is needed to facilitate the contaminant detection.

The approach to data analysis proposed in this study involves the application of the coherence function. The complex coherence function is a normalized complex cross power spectral density function (Carter, 1972) given by:

$$\Gamma(f) = \frac{S_{xy}(f)}{\sqrt{S_{xx}(f)\, S_{yy}(f)}} \tag{4-5}$$

where $S_{xx}(f)$ and $S_{yy}(f)$ are the power spectral densities of $s_x(t)$ and $s_y(t)$ respectively and $S_{xy}(f)$ is the cross-power spectral density.

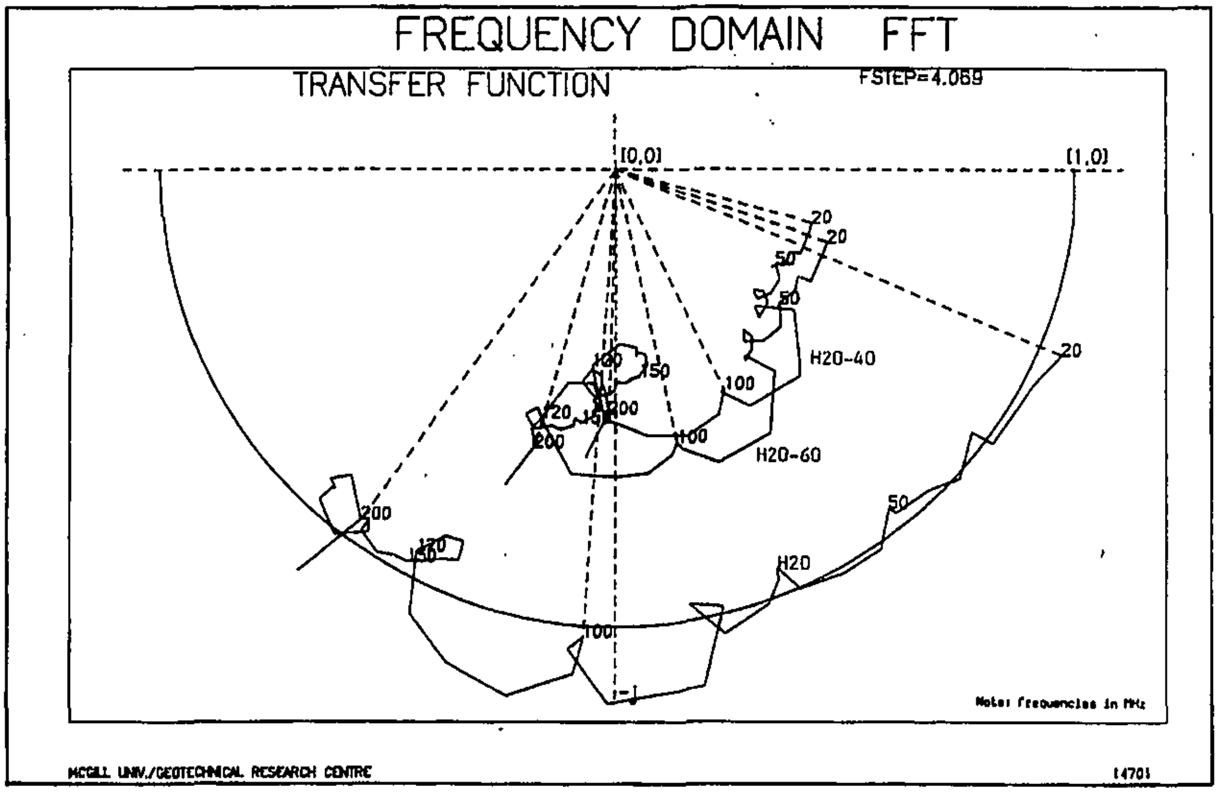

Figure 4.23 Transfer Function : H2O, H2O-40, H2O-60.

The magnitude of the complex coherence function is:

$$|\Gamma(f)| = \frac{|S_{xy}(f)|}{\sqrt{S_{xx}(f)\ S_{yy}(f)}} \tag{4-6}$$

It follows directly that the square of the magnitude of the complex coherence function is:

$$|\Gamma(f)|^2 = \frac{|S_{xy}(f)|^2}{S_{xx}(f)\ S_{yy}(f)} \tag{4-7}$$

The term "coherence" usually refers to equation 4-7. It should be noted that given only one set of waveforms $s_x(t)$ and $s_y(t)$ the magnitude-squared coherence = 1. Consequently, the estimate is biased, depending on the number of sets of waveforms

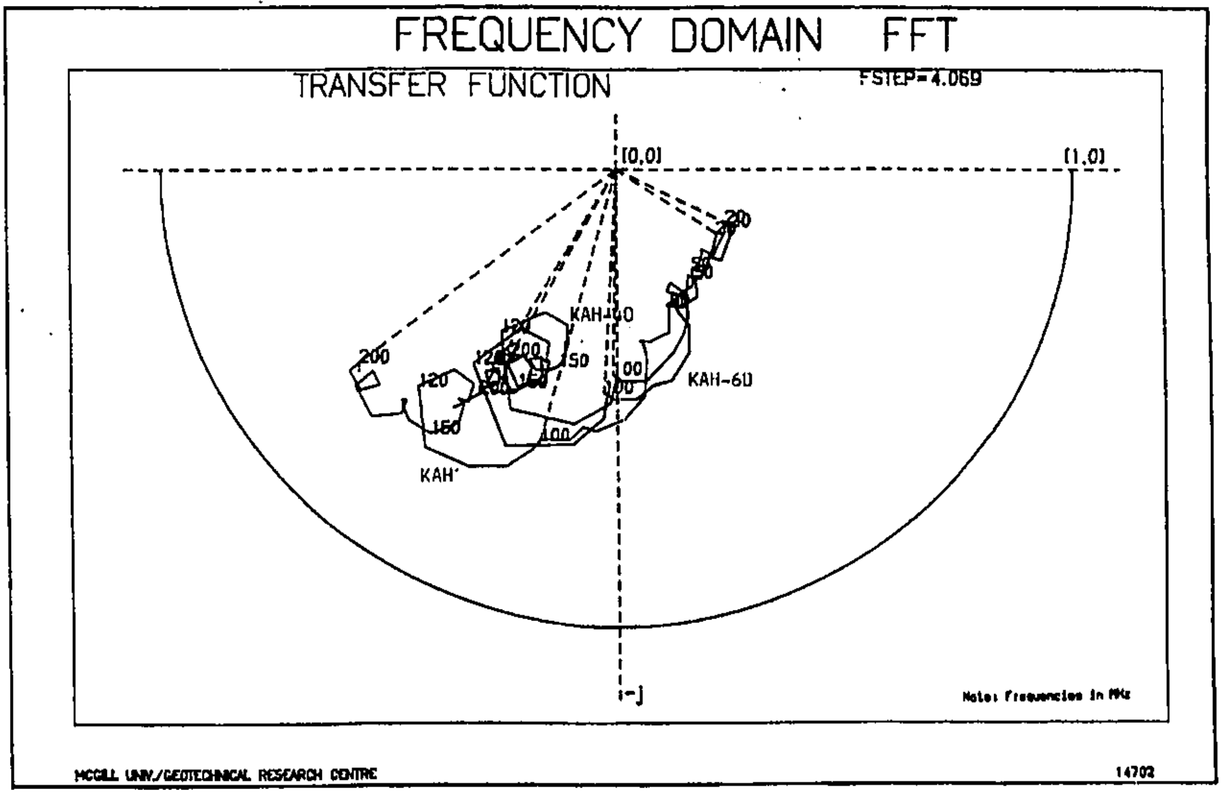

Figure 4.24 Transfer Function : KAH1, KAH1-40, KAH1-60.

that are subsequently averaged. In practice the number of acquisitions of $s_x(t)$ and $s_y(t)$ from a particular measurement setup should be as large as practicable to produce a meaningful estimate of the magnitude-squared coherence. Thus the magnitude-squared coherence function (MSC) of two signals $s_x(t)$ and $s_y(t)$ may be expressed as:

$$\Gamma^2(f) = \frac{| < S_{xy}(f) > |^2}{< S_{xx}(f) > < S_{yy}(f) >} \tag{4-8}$$

where $S_{xx}(f)$, $S_{yy}(f)$, and $S_{xy}(f)$ are each obtained by averaging over a number of data acquisitions.

The MSC always falls between zero and one. It is zero when the waveforms $s_x(t)$ and $s_y(t)$ are uncorrelated. It is equal to unity if and only if there exists a linear relation between $s_x(t)$ and $s_y(t)$. The main applications of the MSC function are as follows:

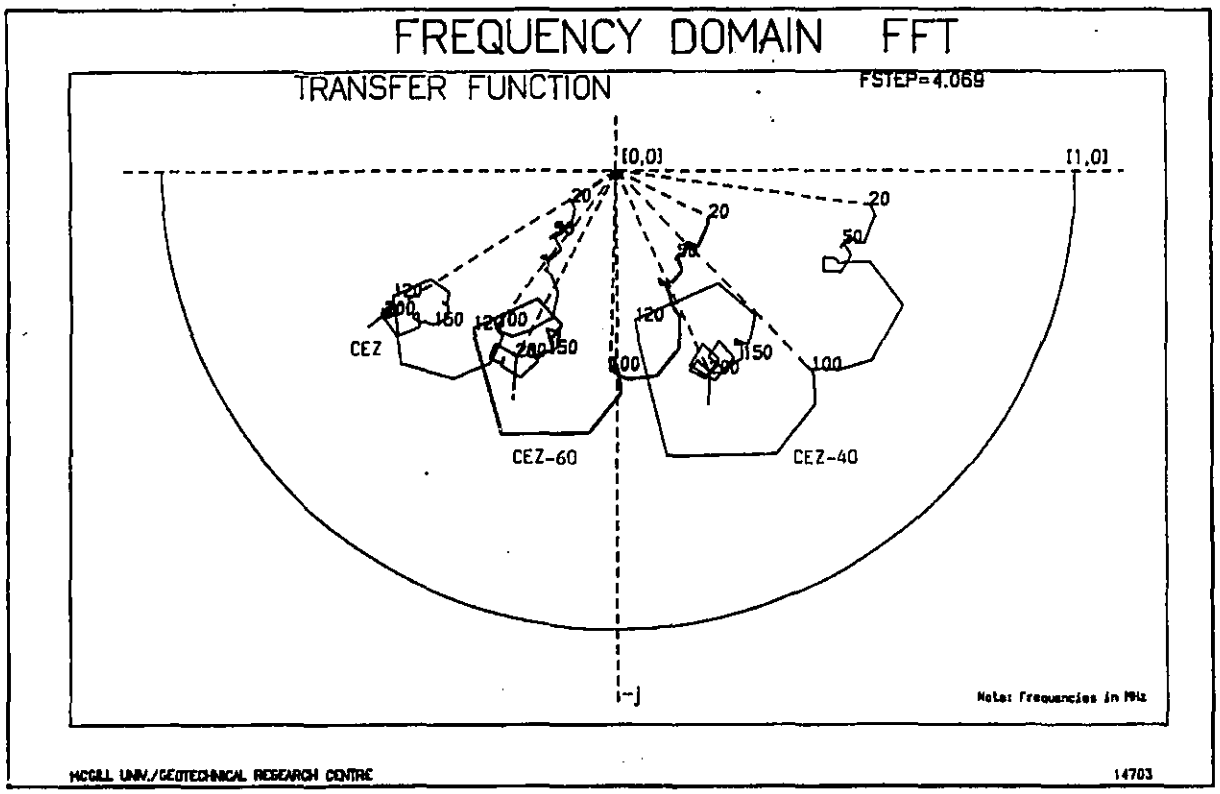

Figure 4.25 Transfer Function : CEZ, CEZ-40, CEZ-60.

- a measure of system linearity.
- a measure of correlation.
- a measure of signal to noise ratio.

The utility of the coherence function is demonstrated in Figures 4.26 and 4.27. It is assumed that a system is subjected to an input signal with a spectral content of $F_x(f)$, resulting in a corresponding output signal $F_y(f)$. Subsequently, another test is performed on the same system using an input signal $G_x(f)$ which results in $G_y(f)$. Nonlinearity and phase distortion are introduced to demonstrate the impact on the coherence. It is evident from the hypothetical example that at a given frequency f it is only when the individual estimates of the cross spectrum $S_{xy}(f)$ have exactly the same phase angle and the system is linear, that the coherence equals to 1. In such a case the vector addition used to form the mean of the cross spectrum gives the same modulus as scalar addition of the power spectrum products, resulting in the Γ of unity. The practical implication of equation 4-8 is that if the signals are statistically same then their coherence equals to 1.

Typical applications of the coherence function in signal processing seek to determine the extent to which the output signal is caused by the input signal, which provides a measure of the validity of the transfer function. The coherence function has been used extensively in the undersea acoustic applications, particularly in situations where a signal source is in motion in a transmission medium (Gerlach, 1980).

A practical linear system is characterized by a coherence function which typically approaches 1 at a wide range of frequencies but eventually departs from unity. This stems from the fact that every practical system exhibits a certain amplitude bandwidth over which all frequency components are amplified or attenuated equally and a certain phase bandwidth over which the phase change is directly proportional to frequency (Lewis and Wells, 1954). Excessive amplitude and phase distortion render the physical interpretation of the measured phenomena unreliable beyond this bandwith.

The application of the coherence function is illustrated in Figures 4.28 through 4.34. Two separate TDR records (Soil 1 and Soil 2), obtained from replicate measurements on a dry soil, are shown and further operations involving preparation of the time-domain data, calculation of the power spectra, cross spectra and transfer functions are illustrated. Figure 4.34 shows the resulting coherence function between the input and the output waveforms (equation 4-8) of both TDR records. The coherence approaches 1 over a frequency range extending from 0 to about 200 MHz, which agrees with the bandwith estimate obtained from the risetime of the incident pulse. It may be concluded that the transfer function of this system is valid in the frequency range of 0 to 200 MHz with a given measurement setup.

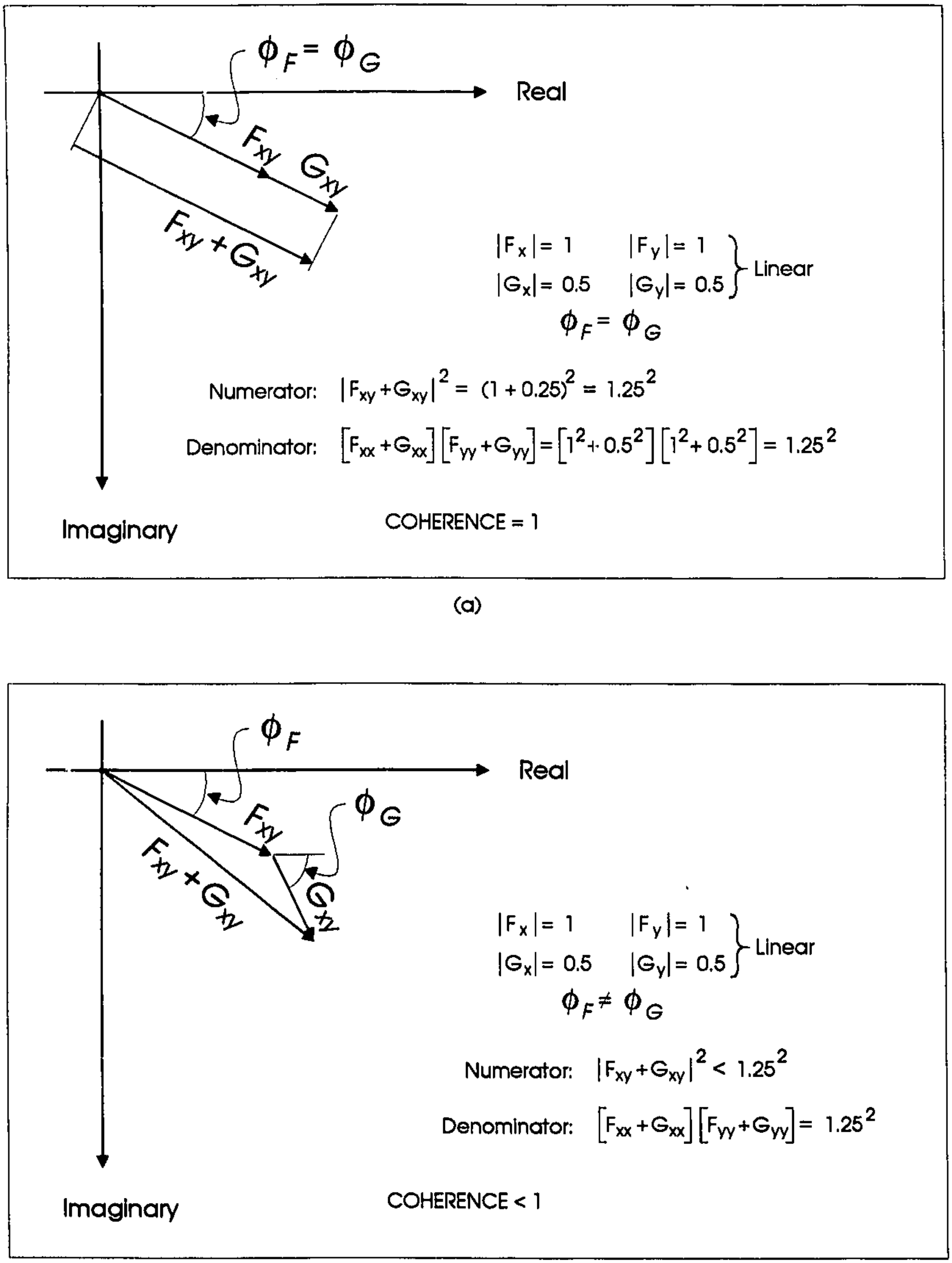

Figure 4.26 The Influence of Phase Angle on Coherence.

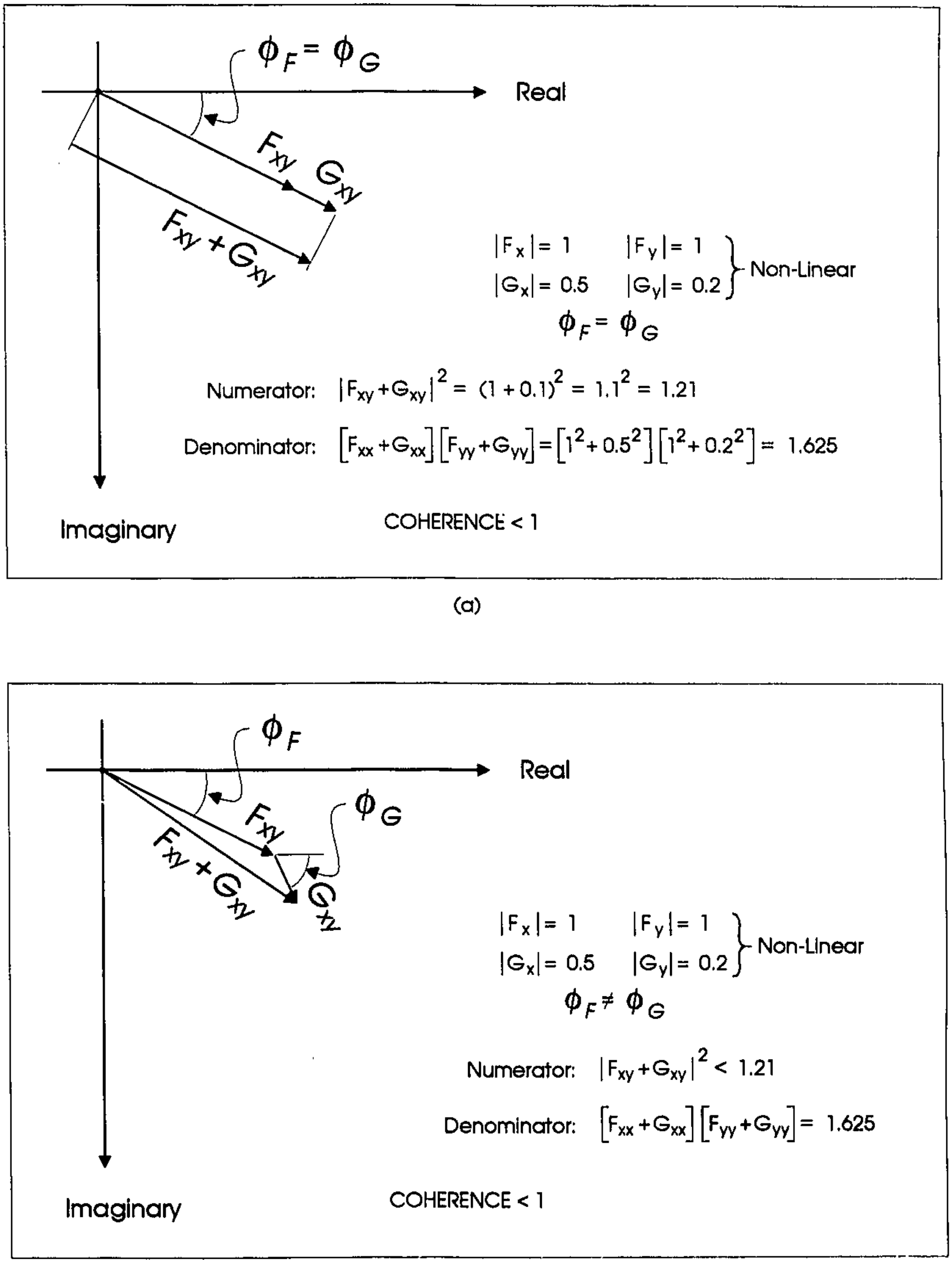

(a)

(b)

Figure 4.27 The Influence of Magnitude on Coherence.

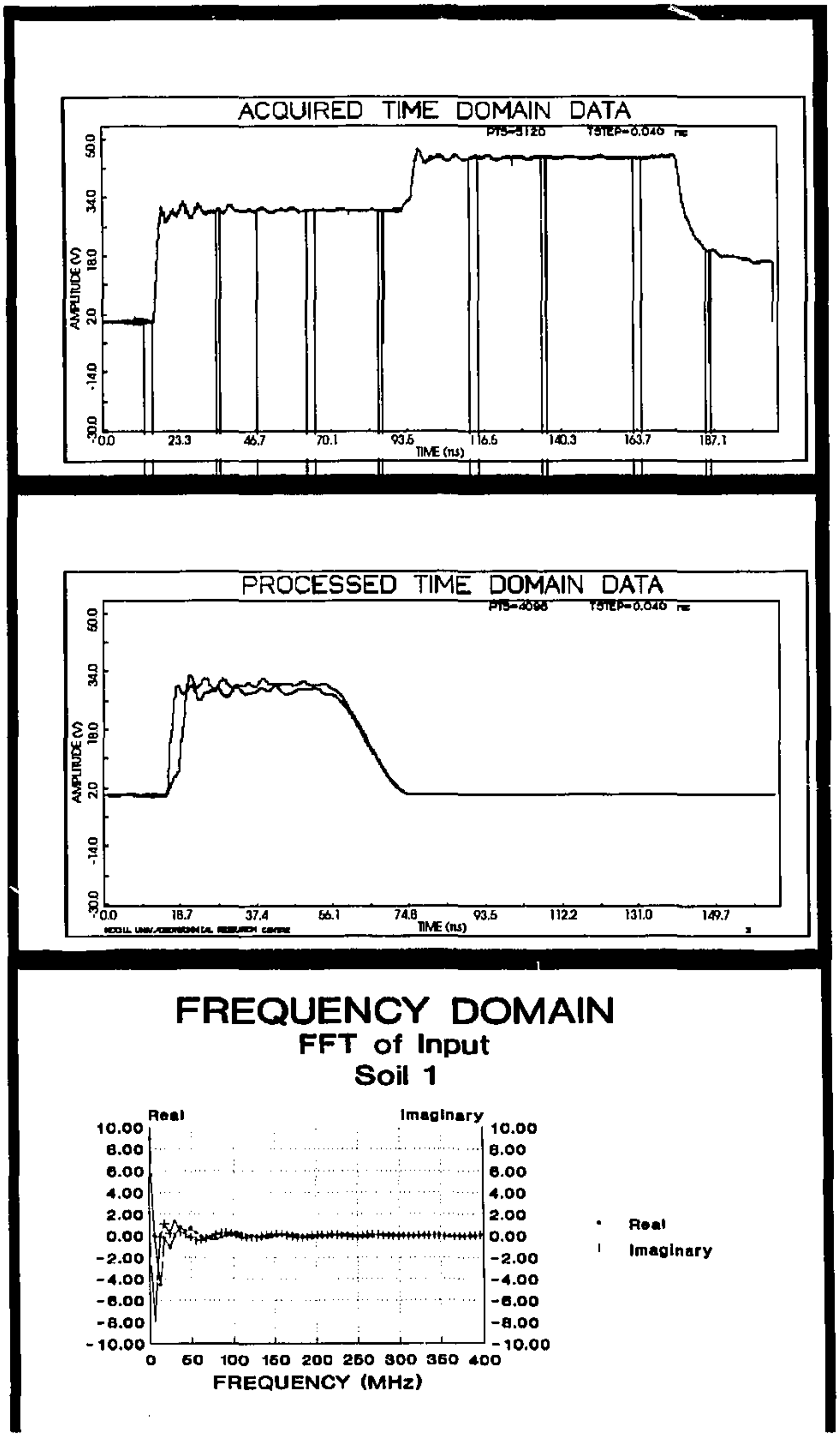

Figure 4.28 Soil 1: Time-Domain Data and FFT of Input.

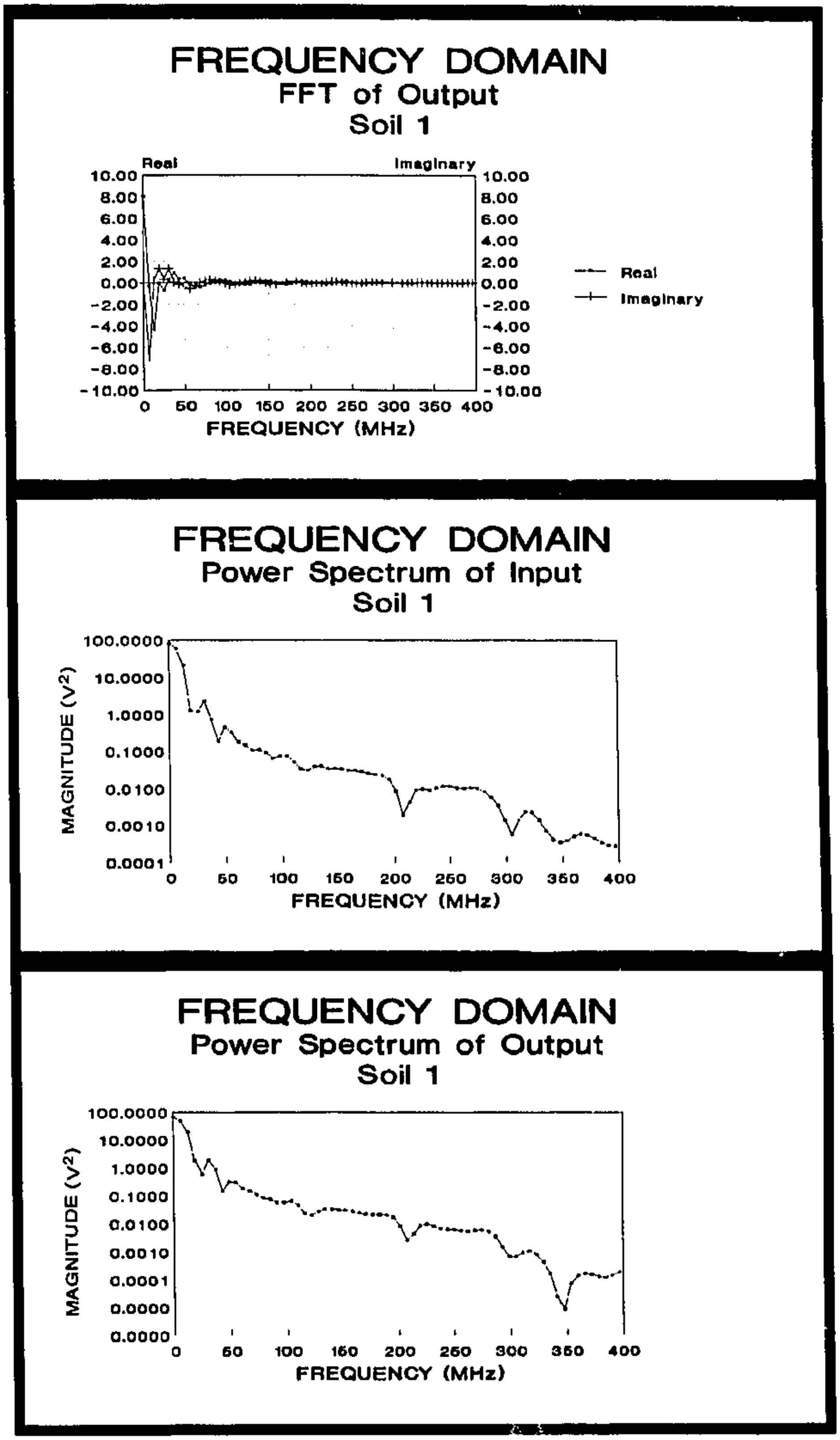

Figure 4.29 Soil 1: FFT of Output and Power Spectra.

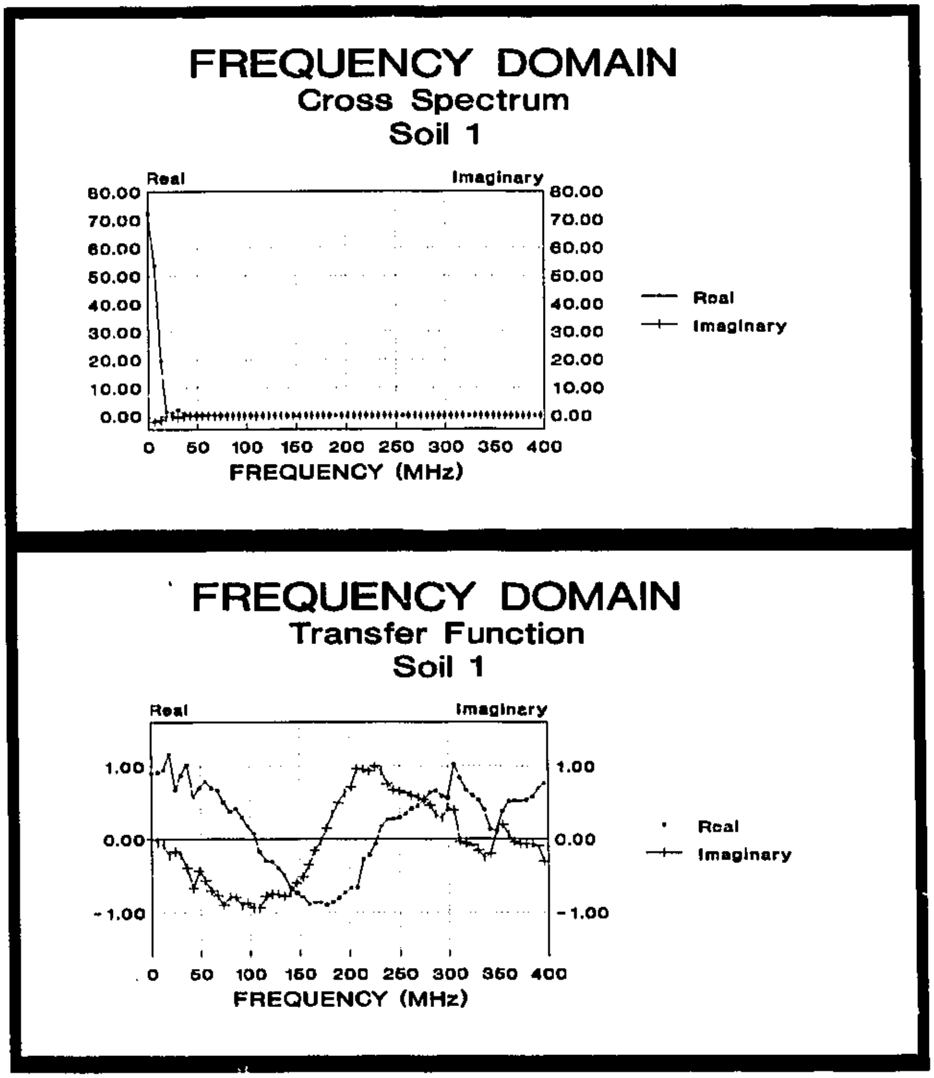

Figure 4.30 Soil 1: Cross Spectrum and Transfer Function.

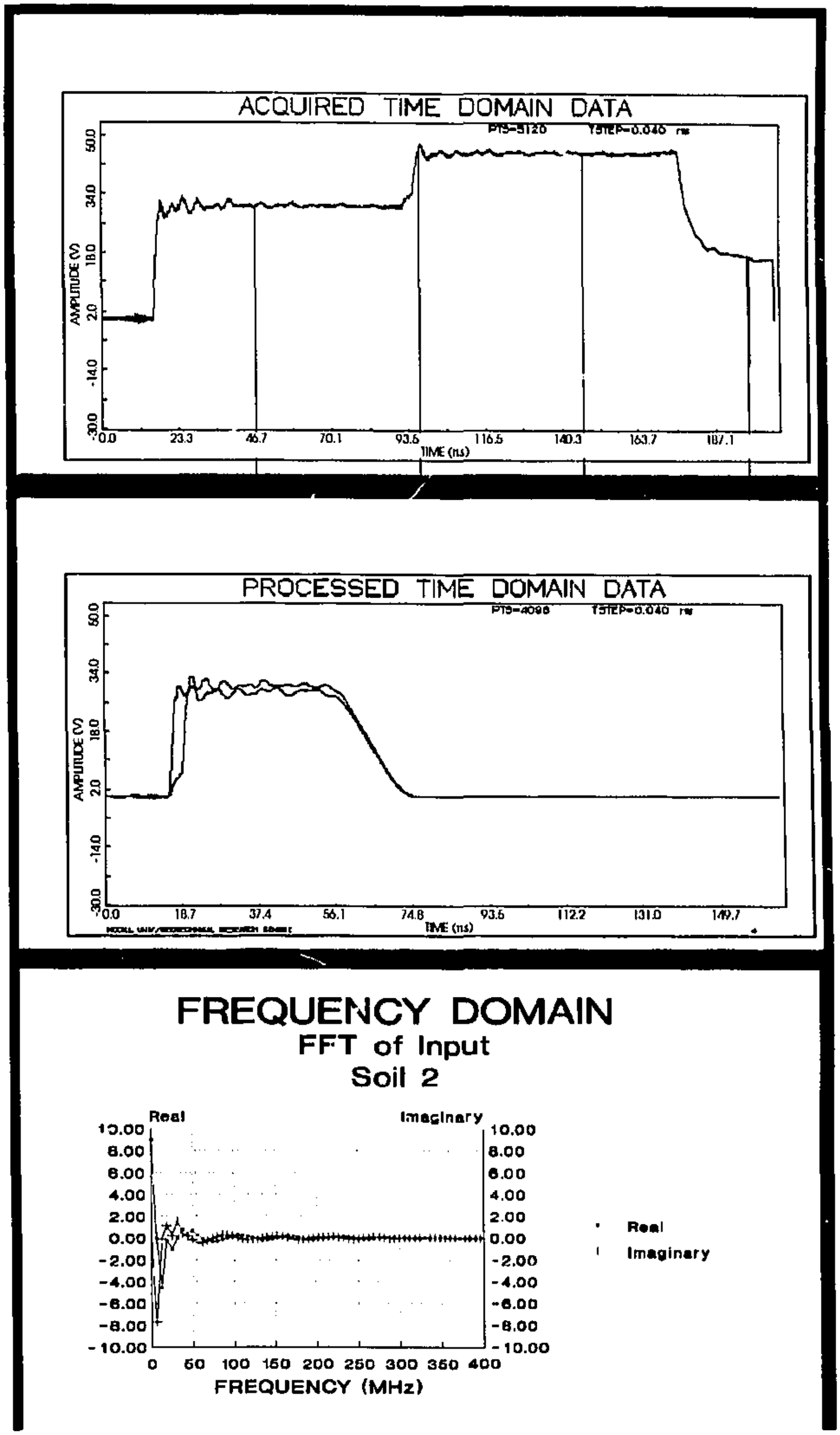

Figure 4.31 Soil 2: Time-Domain Data and FFT of Input.

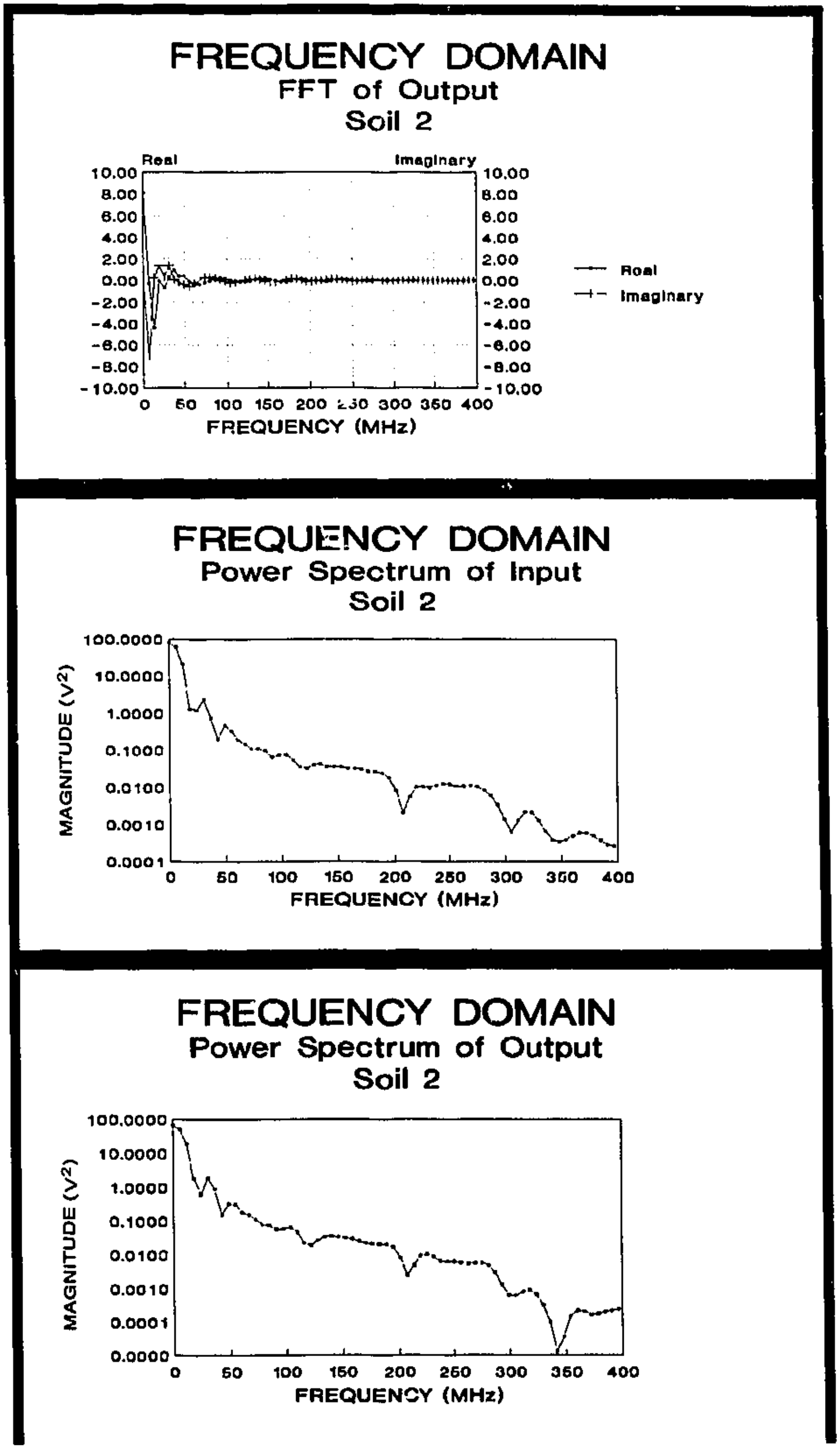

Figure 4.32 Soil 2: FFT of Output and Power Spectra.

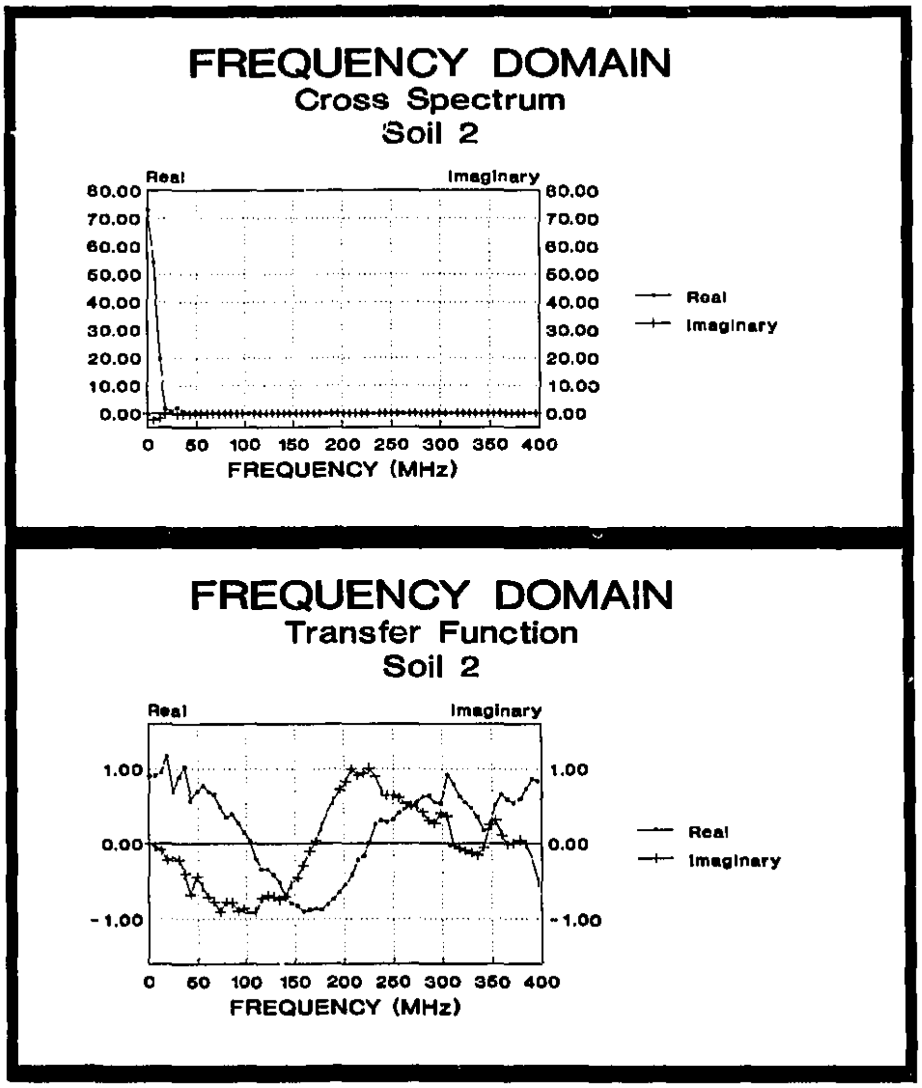

FREQUENCY DOMAIN
Cross Spectrum
Soil 2

FREQUENCY DOMAIN
Transfer Function
Soil 2

Figure 4.33 Soil 2: Cross Spectrum and Transfer Function.

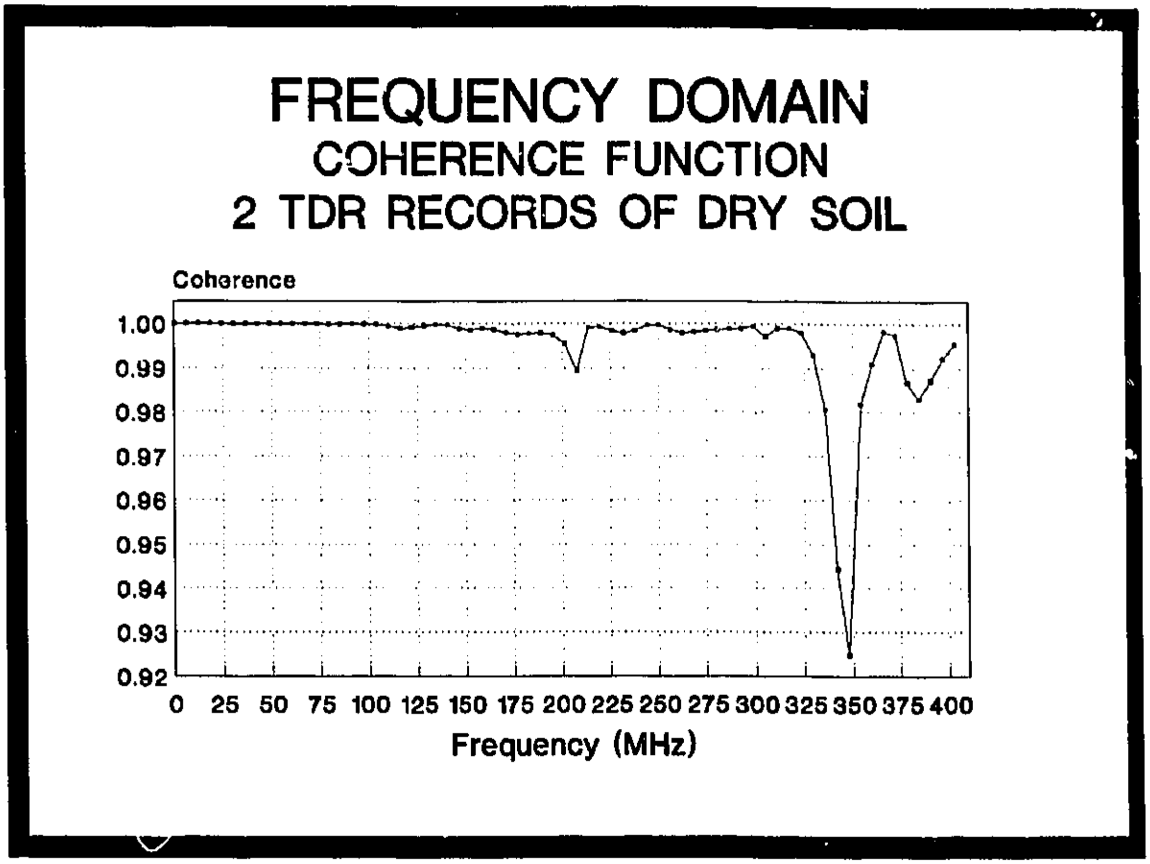

Figure 4.34 Coherence Function Between Dry Soil 1 and Dry Soil 2.

It is also evident that for the coherence to equal unity, the individual transfer functions and hence the systems must have been identical in the corresponding frequency range. Therefore, it follows that a quantitative comparison of transfer functions may be accomplished by computing the coherence between the input and the output waveforms.

In a practical application to a leakage occurring from a point source, a contaminant detection in soil may be achieved as follows:

- obtain representative fluid samples from an underground storage tank or a landfill leachate.

- obtain representative soil samples.
- conduct laboratory TDR measurements on a number of soil-contaminant mixtures and create a database set of known TDR records.
- conduct field TDR measurements by probing areas suspected of contamination and create a test set of unknown TDR records.
- compute the coherence function using unknown and known records. In a perfect match the coherence would equal to 1 over an effective frequency bandwith.

The principal advantage of the above approach is that the entire process of data analysis can be fully automated using a portable computer. It also eliminates the need for a manual handling and the uncertainty of visual comparisons.

In a real life situation no amount of laboratory testing will ever duplicate all the possible permutations encountered in the field. Thus the essence of the matching process is the determination of the most likely association between an unknown TDR "signature" and a waveform traceable to a particular contaminant. Obviously, the closer the match the larger the coherence. The problem entails matching the test signal with a database of signals obtained from known contaminants and soil-contaminant mixtures. Given a field TDR record transformed into its constituent input $G_x(f)$ and output $G_y(f)$ waveforms, and a known TDR record transformed into $F_x(f)$ and $F_y(f)$, a calculation of their coherence indicates if the association is likely.

The frequency range used in the matching procedure needs to be established in advance. This may be accomplished by acquiring a number of TDR records from each test and computing the coherence function as defined in equation 4-8. Obviously, the frequency range used to compare different TDR records must not exceed the range over which the coherence approaches 1 for individual records.

The expected estimation error in coherence is dependent on the number of individual data acquisitions. The relationship for the expected estimation error or bias in computing the MSC was found by Benignus (1969) to be:

$$Bias = \frac{1}{n}(1 - \Gamma^2) \tag{4-9}$$

where n corresponds to a number of records.

It should be noted that:

$$\lim_{n \to \infty} (Bias) = 0 \tag{4-10}$$

The application of the coherence function in this study seeks to answer the question: To what extent does a given test TDR record match a given database TDR record? A flow chart for performing an automated waveform matching based on the above concept is presented in Figure 4.35. The corresponding Fortran computer source code is included in the Appendix 1. In the process of comparing an unknown record ("unknown contaminant") with each database record ("known contaminant") a single parameter descriptor of the fit is introduced. It represents an integration of coherence values substracted from unity, over a frequency range of interest. In a perfect match this descriptor would equal to zero.

The proposed contaminant match procedure addresses a well known TDR problem of identifying an appropriate time reference at which the record is split into its constituent input and output waveforms. This step is essential in accounting for phase differences between various output waveforms. In practical measurements it is often difficult to determine precisely at what point the incident signal ends and the reflected one begins, as illustrated in Figures 4.7 through 4.13. To establish this "cut point", a TDR record of an empty soil probe was analyzed. Since it describes an essentially open circuit termination, involving an infinite resistance and a negligible capacitance, the most appropriate "cut point" is the one that results in a transfer function with minimum phase shifts (all frequencies are transferred in phase in the ideal open circuit termination). After determining this "cut point", it was time referenced to the leading

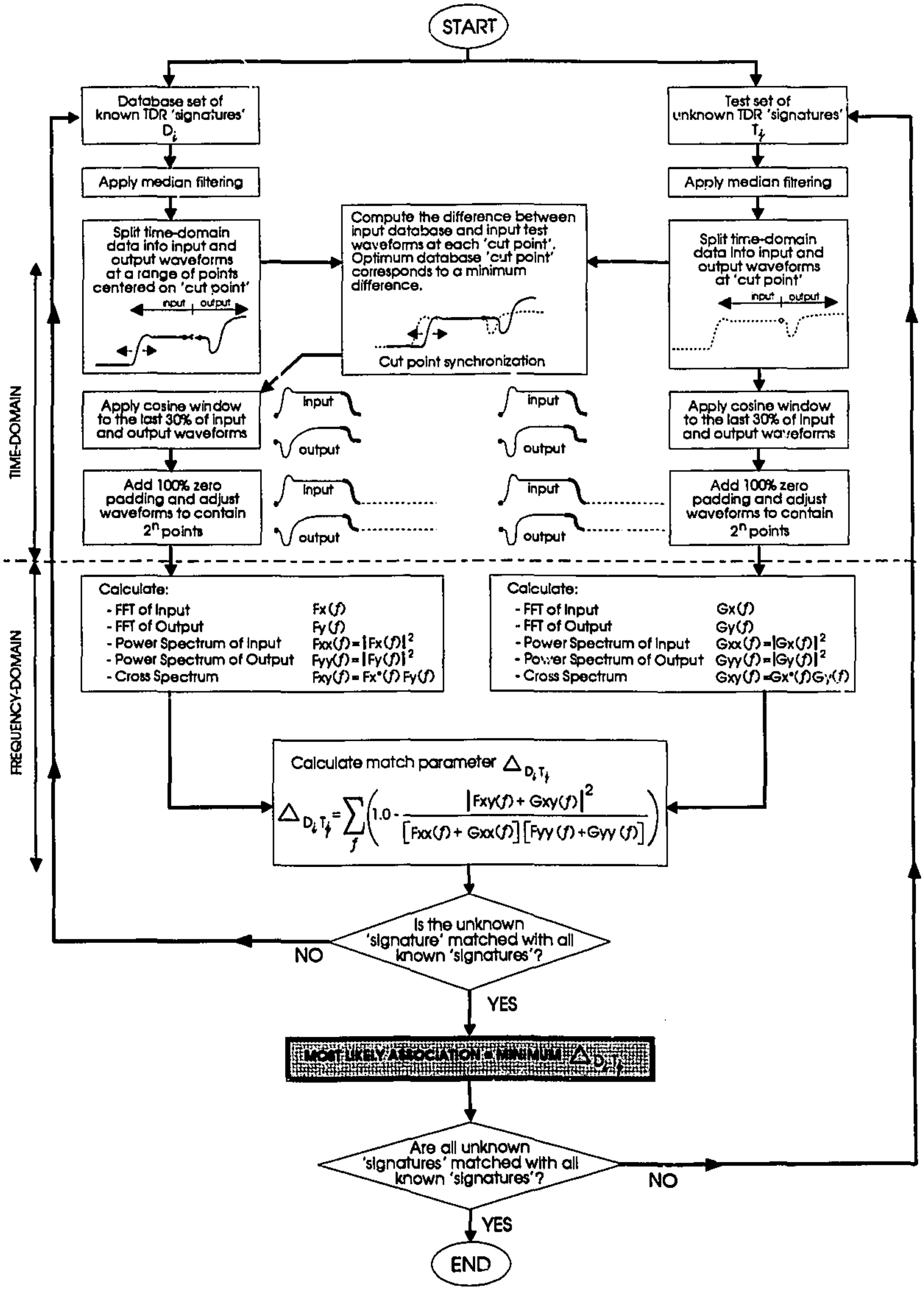

Figure 4.35 Proposed Contaminant Match Procedure.

edge of the incident pulse. As long as the measuring network maintains its geometry, the time between the leading edge of the incident pulse and the "cut point" will always be the same. Thus, if some TDR records are acquired with a different length of the pretrigger data, they can still be time referenced to each other. The approach described in Figure 4.35 involves time-domain matching of the leading edges of incident waveforms. When the leading edges are synchronized so that the difference between the incident waveforms is minimized then their respective "cut points" are also synchronized.

After a TDR record is split at a "cut point", the resulting input and output waveforms are adjusted prior to implementing the Fast Fourier Transform. These adjustments include windowing, zero padding and appending data to obtain 2^n data points (4096 in this study). The reasons for these operations were described previously.

The application of the FFT results in the transformation of data into a set of complex numbers expressed as a function of frequency. Additional operations described in Figure 4.35 include the computation of the power spectrum, which involves a multiplication of the FFT output by its complex conjugate and the cross spectrum, or a conjugate multiplication of input and output spectra. These operations constitute intermediate steps needed to compute the coherence.

The coherence is calculated over a specified frequency range. At each of the specified frequencies the value of coherence is substracted from 1. These values are subsequently integrated to arrive at the single match parameter indicative of the degree of association. The lesser the match parameter the higher the coherence and the closer the association.

To evaluate the concept of coherence matching, two identical sets of data, consisting of the previously acquired TDR records, were created. One set was considered a database of known "signatures" and the other was assumed an "unknown" set. The procedure outlined in Figure 4.35 was subsequently applied. The main objective of this operation was to determine if records from soils containing various concentrations of the same contaminant form the most likely associations. Thus, each element i from the "known" set was matched with each element j from the "unknown" set. The output of the coherence matching program is presented in Tables 4.2 through 4.8. The frequency range of interest is 6.10 MHz (first harmonic) to 201.42 MHz (practical limit of the incident signal bandwidth). In each match the #1 rank corresponds to the simple case of two identical records. Matches ranked #2 and greater correspond to the successively less likely associations.

4.4 DISCUSSION OF RESULTS

The time-domain relationship, shown in Figures 4.7 through 4.13 presents various waveforms acquired by the digitizer. It can be seen that the applied step-function is not perfectly rectangular. The initial stage of the incident impulse is affected by ripples, stemming from imperfections in the impulse generator and unwanted reflections in the measuring circuit. It should be noted, however, that the shape of the incident signal and therefore its spectral composition, remains virtually identical in different tests. This attests to a good reproducibility of pulses produced by the mercury contact relay. The reflected voltage step, commencing after approximately 70 nanoseconds, is characteristic of the material being analyzed. Thus, in non-polar liquids such as benzene or ethanol, the reflected waveform practically mirrors the applied waveform. A substantial signal attenuation occurs in highly conductive liquids, such as in CEZ or PB, which contain ions of heavy metals. The initial dip of the reflected impulse, signifies the capacitive influence. The latter part of each waveform approaches a steady value, indicative of the DC resistivity. This dielectric response appears most predominant in the first 4 ns of the reflected waveform.

After transforming the time-domain data into the frequency-domain, using the Fast Fourier Transform, the transfer function is computed by dividing the spectrum of the reflected signal (Output FFT) by the spectrum of the incident impulse (Input

FFT). The attenuation and phase shift characteristics of individual contaminants and soil-contaminant mixtures are presented in terms of the material transfer function in Figures 4.21 through 4.25. The results are shown in a polar form, with the modulus being the distance from the point of origin to the particular frequency component of the waveform and with the corresponding phase angle measured relative to the positive x-axis. Each transfer function forms a distinctive and unique representation of a particular soil-contaminant system.

The transfer function representation provides a meaningful insight into the material's dielectric behavior. If the charges contained in the material are free to move under the influence of the electric field, the resistance is effectively independent of the frequency of the applied signal, but if these charges are bound, as in oscillating dipoles, the resistance becomes a characteristic function of frequency. This pattern manifests itself readily in the transfer function. It is worth noting the similarity of Figures 4.21 through 4.25 to the general behavior of the dielectric constant illustrated in Figure 3.3.

It can be seen that the transfer function exhibits a different signature for different contaminants. In a practically non-polar material, such as benzene (Figure 4.22), the phase shift and attenuation of different frequency components are minimal. The transfer function reflects the combined influence of the dielectric constant and resistivity of a given material, and thus the response of benzene (ϵ=2.3), ethanol (ϵ=31.2) and distilled water (ϵ=80) illustrate the trend of an increasing dielectric constant and a decreasing resistivity.

Although the polar plot of the transfer function offers a good visual representation of the polarization phenomena, it does not render itself well to an identification of the most likely matches between various signals. It illustrates, however, that both magnitude and phase contain characteristic descriptions of the tested material. The coherence function may be employed to account for both of these descriptors in a numerical fashion, allowing an effective comparison.

The results of the proposed contaminant match procedure are presented in Tables 4.2 through 4.8. The optimum database "cut point" and a match parameter are listed. A perfect match of a test waveform with a database waveform was obtained between the following materials:

- H2O-40 and H2O-60
- H2O-60 and H2O-40
- PB-40 and PB-60
- PB-60 and PB-40
- KAH1-40 and KAH1-60
- KAH1-40 and KAH1
- KAH1-60 and KAH1-40
- KAH1-60 and KAH1

Associations involving BENZENE, ETHANOL, LACHEN, and NACL test waveforms were reasonable given the selection of the database set. BENZENE was matched with OPEN (empty probe), ETHANOL with BENZENE, LACHEN with CACL, and NACL with CACL.

An illustration of the coherence matching concept is presented in Figure 4.36. It demonstrates that a soil contaminated with the leachate collected from the Kahnawaki landfill site exhibits a higher coherence with the Kahnawaki leachate than with the Lachenaie leachate. As Table 4.6 indicates, KAH1-40 matches most closely with KAH1 when only the contaminants and not the soil-contaminant mixtures are considered in the database set. Relatively poor match results were obtained with soils contaminated by CACL and CEZ. CACL-40 was matched with CEZ-60 and CACL-60 was paired with KAH1-40. A common element in these matches appears to be the Ca ion in KAH1 and CEZ. Also CEZ-40 was matched with H2O-40 and CEZ-60 with CACL-40. Again, the most common element is the Ca ion which is the most predominant extractable ion in the soil (see soil description).

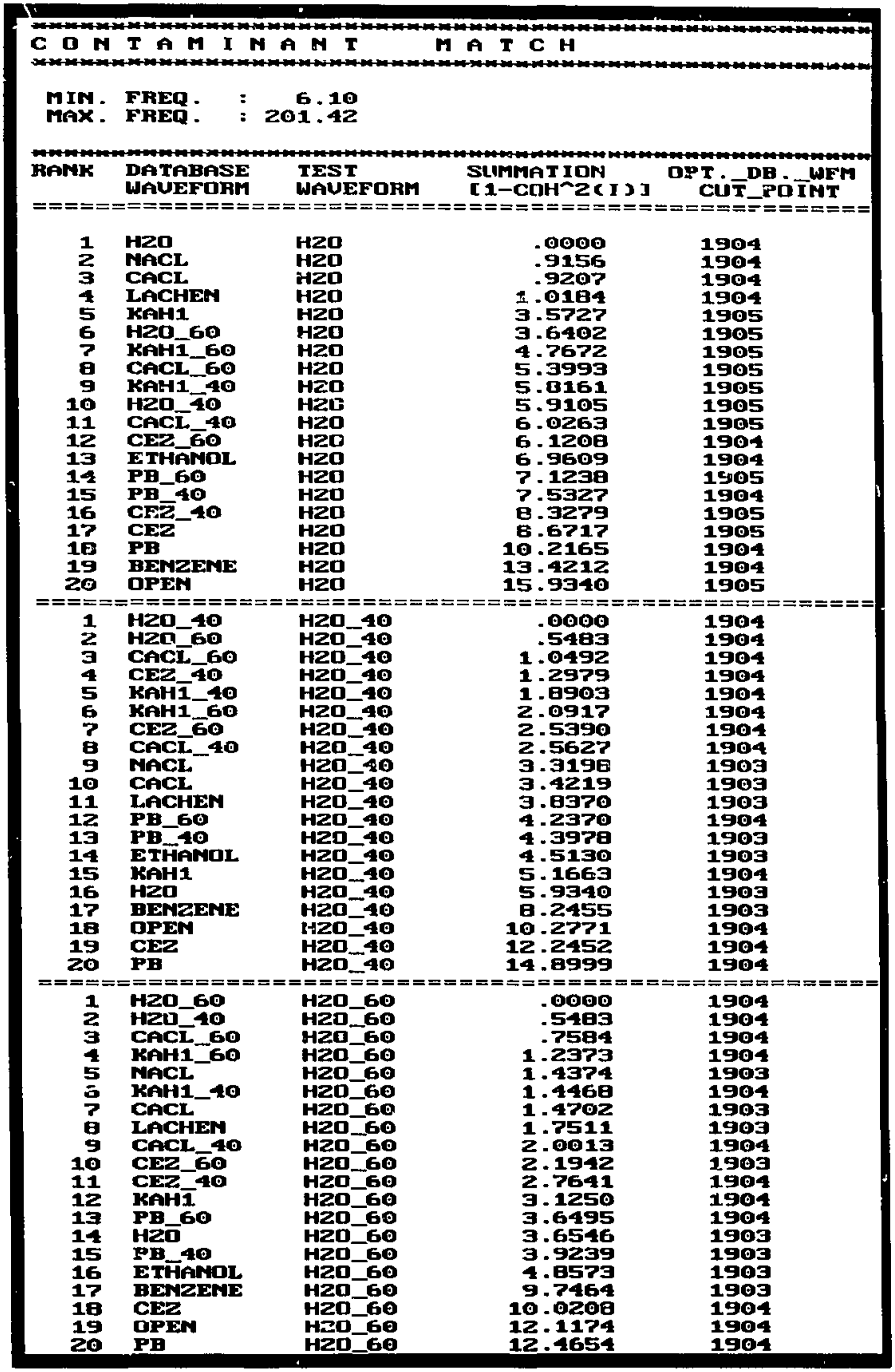

```
******************************************************************
C O N T A M I N A N T     M A T C H
******************************************************************

 MIN. FREQ.  :   6.10
 MAX. FREQ.  : 201.42

******************************************************************
RANK  DATABASE    TEST        SUMMATION      OPT._DB._WFM
      WAVEFORM    WAVEFORM    [1-COH^2(I)]    CUT_POINT
==================================================================

   1  H20         H20                .0000      1904
   2  NACL        H20                .9156      1904
   3  CACL        H20                .9207      1904
   4  LACHEN      H20               1.0184      1904
   5  KAH1        H20               3.5727      1905
   6  H20_60      H20               3.6402      1905
   7  KAH1_60     H20               4.7672      1905
   8  CACL_60     H20               5.3993      1905
   9  KAH1_40     H20               5.8161      1905
  10  H20_40      H20               5.9105      1905
  11  CACL_40     H20               6.0263      1905
  12  CEZ_60      H20               6.1208      1904
  13  ETHANOL     H20               6.9609      1904
  14  PB_60       H20               7.1238      1905
  15  PB_40       H20               7.5327      1904
  16  CEZ_40      H20               8.3279      1905
  17  CEZ         H20               8.6717      1905
  18  PB          H20              10.2165      1904
  19  BENZENE     H20              13.4212      1904
  20  OPEN        H20              15.9340      1905
==================================================================
   1  H20_40      H20_40             .0000      1904
   2  H20_60      H20_40             .5483      1904
   3  CACL_60     H20_40            1.0492      1904
   4  CEZ_40      H20_40            1.2979      1904
   5  KAH1_40     H20_40            1.8903      1904
   6  KAH1_60     H20_40            2.0917      1904
   7  CEZ_60      H20_40            2.5390      1904
   8  CACL_40     H20_40            2.5627      1904
   9  NACL        H20_40            3.3198      1903
  10  CACL        H20_40            3.4219      1903
  11  LACHEN      H20_40            3.8370      1903
  12  PB_60       H20_40            4.2370      1904
  13  PB_40       H20_40            4.3978      1903
  14  ETHANOL     H20_40            4.5130      1903
  15  KAH1        H20_40            5.1663      1904
  16  H20         H20_40            5.9340      1903
  17  BENZENE     H20_40            8.2455      1903
  18  OPEN        H20_40           10.2771      1904
  19  CEZ         H20_40           12.2452      1904
  20  PB          H20_40           14.8999      1904
==================================================================
   1  H20_60      H20_60             .0000      1904
   2  H20_40      H20_60             .5483      1904
   3  CACL_60     H20_60             .7584      1904
   4  KAH1_60     H20_60            1.2373      1904
   5  NACL        H20_60            1.4374      1903
   6  KAH1_40     H20_60            1.4468      1904
   7  CACL        H20_60            1.4702      1903
   8  LACHEN      H20_60            1.7511      1903
   9  CACL_40     H20_60            2.0013      1904
  10  CEZ_60      H20_60            2.1942      1903
  11  CEZ_40      H20_60            2.7641      1904
  12  KAH1        H20_60            3.1250      1904
  13  PB_60       H20_60            3.6495      1904
  14  H20         H20_60            3.6546      1903
  15  PB_40       H20_60            3.9239      1903
  16  ETHANOL     H20_60            4.8573      1903
  17  BENZENE     H20_60            9.7464      1903
  18  CEZ         H20_60           10.0208      1904
  19  OPEN        H20_60           12.1174      1904
  20  PB          H20_60           12.4654      1904
```

Table 4.2 Contaminant Match Results : H2O, H2O-40, H2O-60.

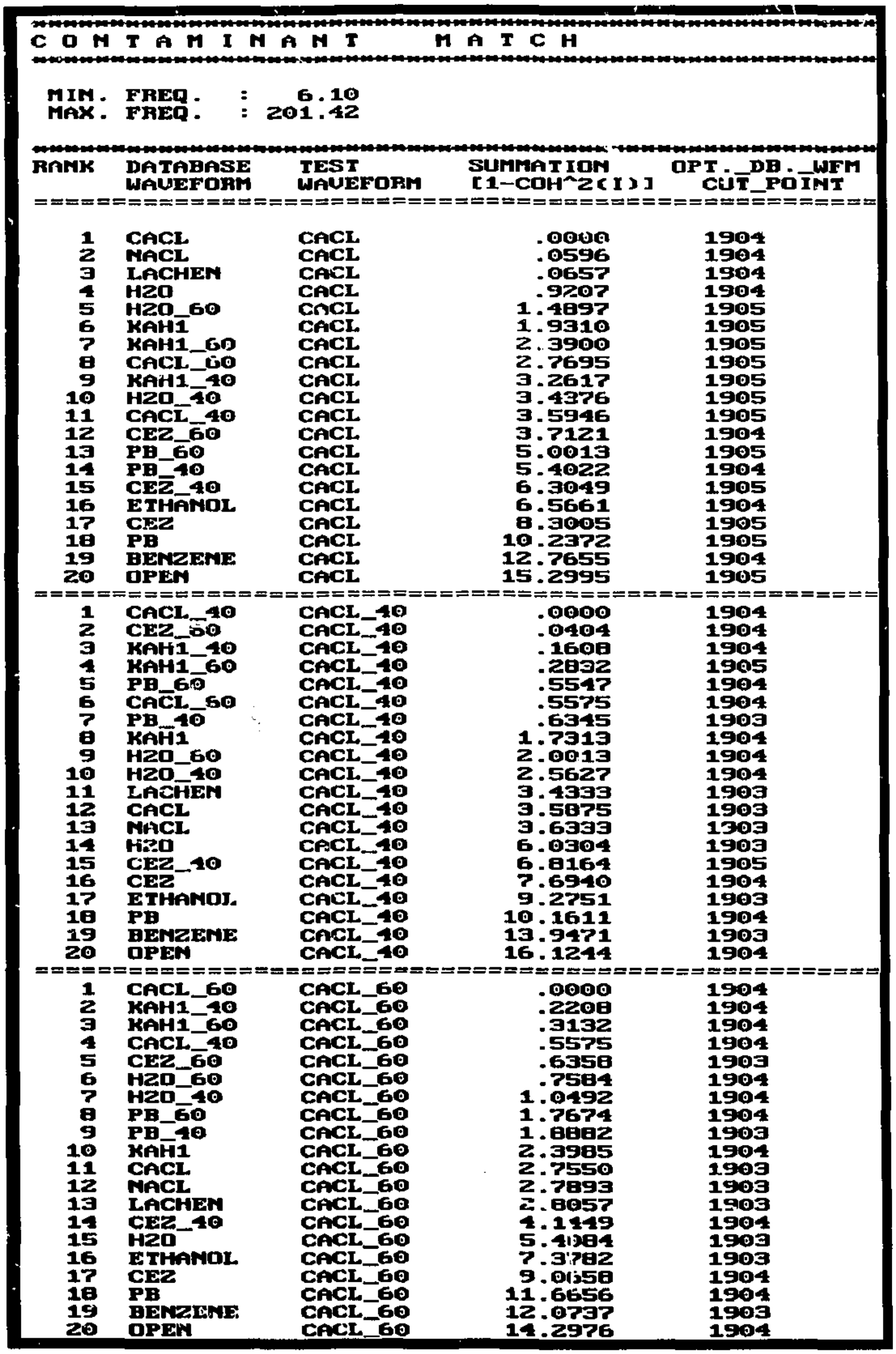

```
*****************************************************************
C O N T A M I N A N T     M A T C H
*****************************************************************

 MIN. FREQ.  :   6.10
 MAX. FREQ.  : 201.42

*****************************************************************
RANK  DATABASE     TEST         SUMMATION      OPT._DB._WFM
      WAVEFORM     WAVEFORM     [1-COH^2(I)]    CUT_POINT
=================================================================

  1   CACL         CACL               .0000        1904
  2   NACL         CACL               .0596        1904
  3   LACHEN       CACL               .0657        1904
  4   H2O          CACL               .9207        1904
  5   H2O_60       CACL              1.4897        1905
  6   KAH1         CACL              1.9310        1905
  7   KAH1_60      CACL              2.3900        1905
  8   CACL_60      CACL              2.7695        1905
  9   KAH1_40      CACL              3.2617        1905
 10   H2O_40       CACL              3.4376        1905
 11   CACL_40      CACL              3.5946        1905
 12   CEZ_60       CACL              3.7121        1904
 13   PB_60        CACL              5.0013        1905
 14   PB_40        CACL              5.4022        1904
 15   CEZ_40       CACL              6.3049        1905
 16   ETHANOL      CACL              6.5661        1904
 17   CEZ          CACL              8.3005        1905
 18   PB           CACL             10.2372        1905
 19   BENZENE      CACL             12.7655        1904
 20   OPEN         CACL             15.2995        1905
=================================================================
  1   CACL_40      CACL_40            .0000        1904
  2   CEZ_60       CACL_40            .0404        1904
  3   KAH1_40      CACL_40            .1608        1904
  4   KAH1_60      CACL_40            .2832        1905
  5   PB_60        CACL_40            .5547        1904
  6   CACL_60      CACL_40            .5575        1904
  7   PB_40        CACL_40            .6345        1903
  8   KAH1         CACL_40           1.7313        1904
  9   H2O_60       CACL_40           2.0013        1904
 10   H2O_40       CACL_40           2.5627        1904
 11   LACHEN       CACL_40           3.4333        1903
 12   CACL         CACL_40           3.5875        1903
 13   NACL         CACL_40           3.6333        1303
 14   H2O          CACL_40           6.0304        1903
 15   CEZ_40       CACL_40           6.8164        1905
 16   CEZ          CACL_40           7.6940        1904
 17   ETHANOL      CACL_40           9.2751        1903
 18   PB           CACL_40          10.1611        1904
 19   BENZENE      CACL_40          13.9471        1903
 20   OPEN         CACL_40          16.1244        1904
=================================================================
  1   CACL_60      CACL_60            .0000        1904
  2   KAH1_40      CACL_60            .2208        1904
  3   KAH1_60      CACL_60            .3132        1904
  4   CACL_40      CACL_60            .5575        1904
  5   CEZ_60       CACL_60            .6358        1903
  6   H2O_60       CACL_60            .7584        1904
  7   H2O_40       CACL_60           1.0492        1904
  8   PB_60        CACL_60           1.7674        1904
  9   PB_40        CACL_60           1.8882        1903
 10   KAH1         CACL_60           2.3985        1904
 11   CACL         CACL_60           2.7550        1903
 12   NACL         CACL_60           2.7893        1903
 13   LACHEN       CACL_60           2.8057        1903
 14   CEZ_40       CACL_60           4.1149        1904
 15   H2O          CACL_60           5.4084        1903
 16   ETHANOL      CACL_60           7.3782        1903
 17   CEZ          CACL_60           9.0658        1904
 18   PB           CACL_60          11.6656        1904
 19   BENZENE      CACL_60          12.0737        1903
 20   OPEN         CACL_60          14.2976        1904
```

Table 4.3 Contaminant Match Results : CACL, CACL-40, CACL-60.

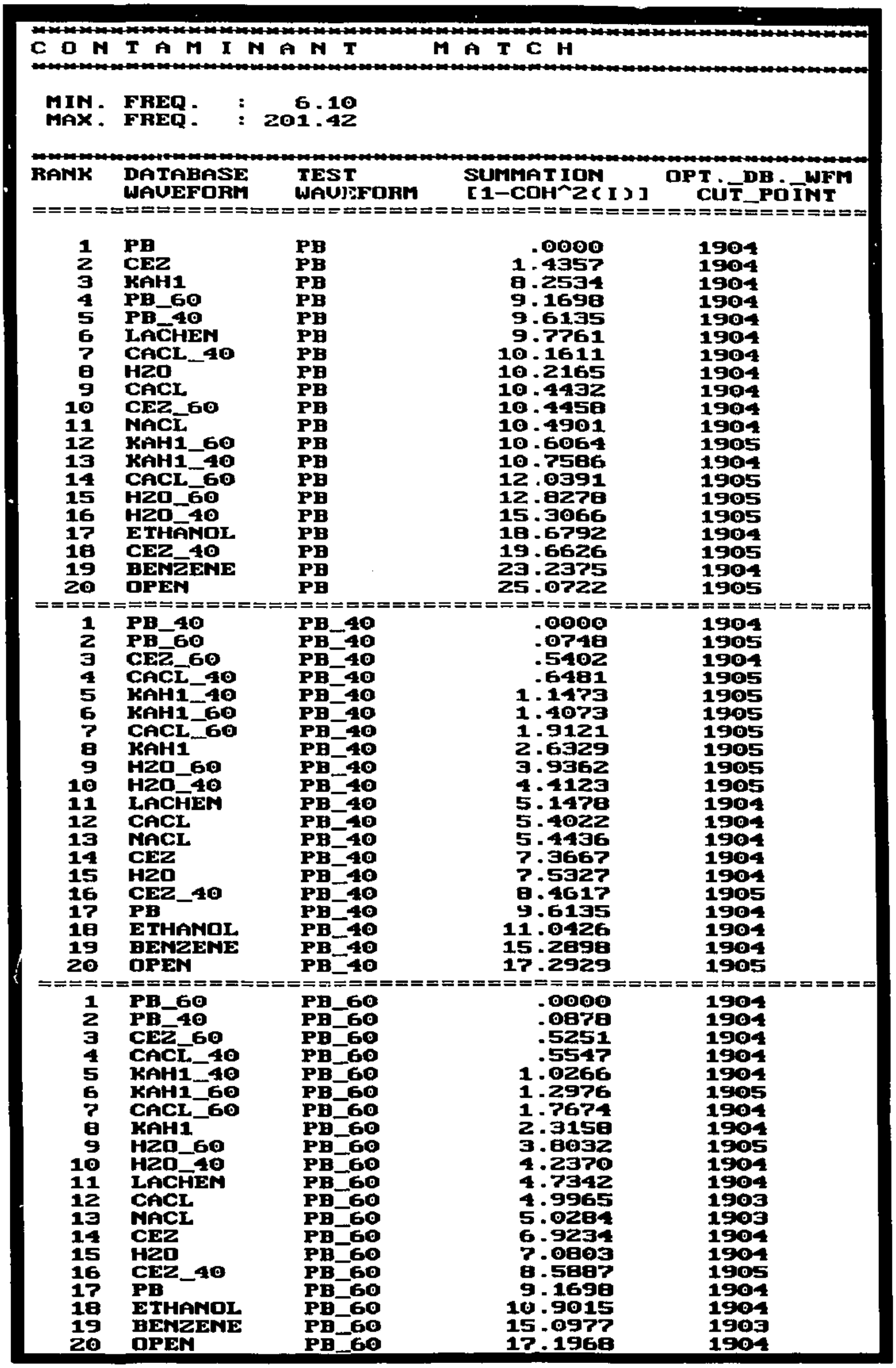

```
*************************************************************************
C O N T A M I N A N T     M A T C H
*************************************************************************

 MIN. FREQ.  :   6.10
 MAX. FREQ.  : 201.42

*************************************************************************
RANK  DATABASE     TEST         SUMMATION       OPT._DB._WFM
      WAVEFORM     WAVEFORM     [1-COH^2(I)]     CUT_POINT
=========================================================================

  1   PB           PB                 .0000        1904
  2   CEZ          PB                1.4357        1904
  3   KAH1         PB                8.2534        1904
  4   PB_60        PB                9.1698        1904
  5   PB_40        PB                9.6135        1904
  6   LACHEN       PB                9.7761        1904
  7   CACL_40      PB               10.1611        1904
  8   H2O          PB               10.2165        1904
  9   CACL         PB               10.4432        1904
 10   CEZ_60       PB               10.4458        1904
 11   NACL         PB               10.4901        1904
 12   KAH1_60      PB               10.6064        1905
 13   KAH1_40      PB               10.7586        1904
 14   CACL_60      PB               12.0391        1905
 15   H2O_60       PB               12.8278        1905
 16   H2O_40       PB               15.3066        1905
 17   ETHANOL      PB               18.6792        1904
 18   CEZ_40       PB               19.6626        1905
 19   BENZENE      PB               23.2375        1904
 20   OPEN         PB               25.0722        1905
=========================================================================
  1   PB_40        PB_40              .0000        1904
  2   PB_60        PB_40              .0748        1905
  3   CEZ_60       PB_40              .5402        1904
  4   CACL_40      PB_40              .6481        1905
  5   KAH1_40      PB_40             1.1473        1905
  6   KAH1_60      PB_40             1.4073        1905
  7   CACL_60      PB_40             1.9121        1905
  8   KAH1         PB_40             2.6329        1905
  9   H2O_60       PB_40             3.9362        1905
 10   H2O_40       PB_40             4.4123        1905
 11   LACHEN       PB_40             5.1478        1904
 12   CACL         PB_40             5.4022        1904
 13   NACL         PB_40             5.4436        1904
 14   CEZ          PB_40             7.3667        1904
 15   H2O          PB_40             7.5327        1904
 16   CEZ_40       PB_40             8.4617        1905
 17   PB           PB_40             9.6135        1904
 18   ETHANOL      PB_40            11.0426        1904
 19   BENZENE      PB_40            15.2898        1904
 20   OPEN         PB_40            17.2929        1905
=========================================================================
  1   PB_60        PB_60              .0000        1904
  2   PB_40        PB_60              .0878        1904
  3   CEZ_60       PB_60              .5251        1904
  4   CACL_40      PB_60              .5547        1904
  5   KAH1_40      PB_60             1.0266        1904
  6   KAH1_60      PB_60             1.2976        1905
  7   CACL_60      PB_60             1.7674        1904
  8   KAH1         PB_60             2.3158        1904
  9   H2O_60       PB_60             3.8032        1905
 10   H2O_40       PB_60             4.2370        1904
 11   LACHEN       PB_60             4.7342        1904
 12   CACL         PB_60             4.9965        1903
 13   NACL         PB_60             5.0284        1903
 14   CEZ          PB_60             6.9234        1904
 15   H2O          PB_60             7.0803        1904
 16   CEZ_40       PB_60             8.5887        1905
 17   PB           PB_60             9.1698        1904
 18   ETHANOL      PB_60            10.9015        1904
 19   BENZENE      PB_60            15.0977        1903
 20   OPEN         PB_60            17.1968        1904
```

Table 4.4 Contaminant Match Results : PB, PB-40, PB-60.

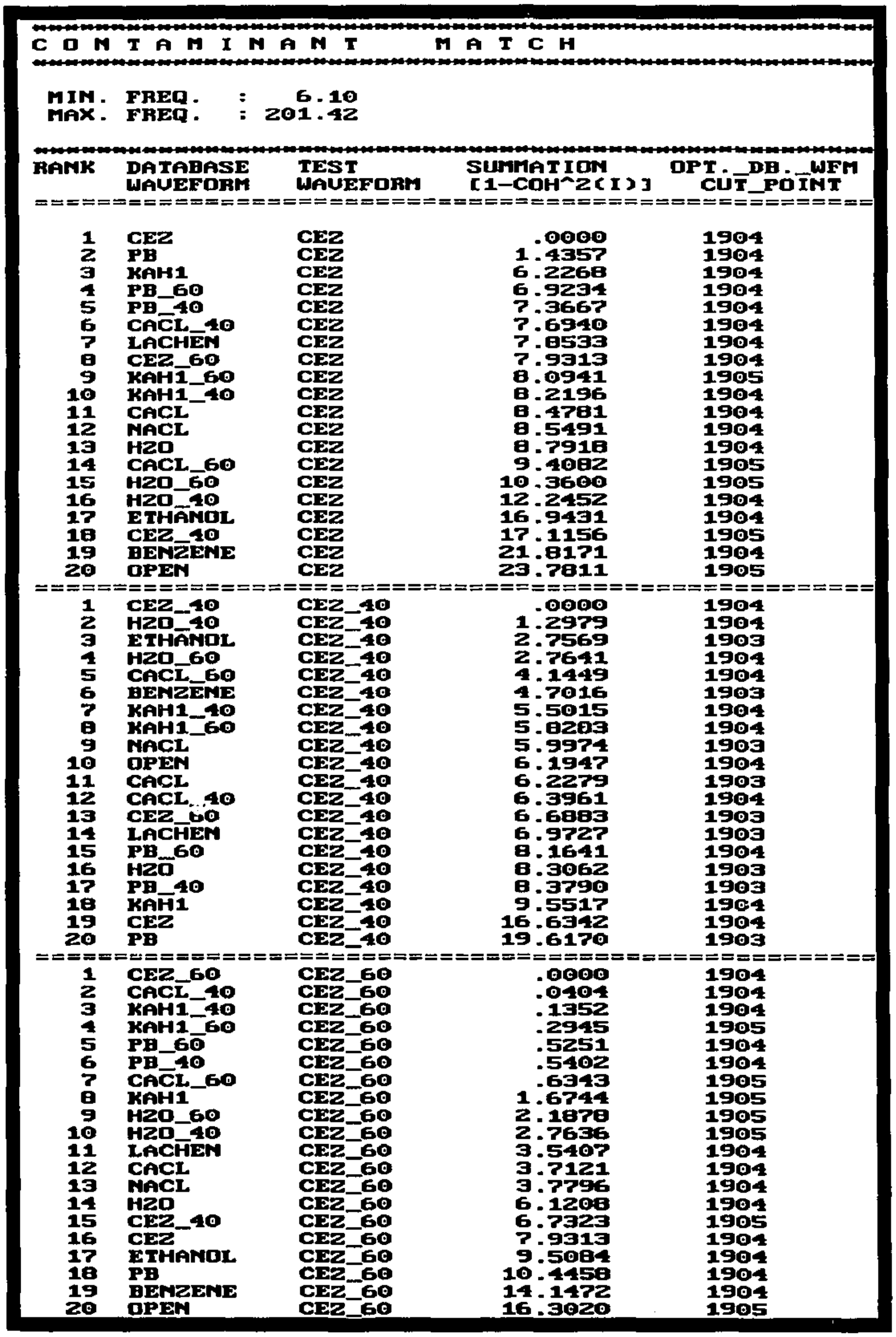

```
****************************************************************
C O N T A M I N A N T     M A T C H
****************************************************************

 MIN. FREQ.  :   6.10
 MAX. FREQ.  : 201.42

****************************************************************
RANK  DATABASE    TEST        SUMMATION      OPT._DB._WFM
      WAVEFORM    WAVEFORM    [1-COH^2(I)]    CUT_POINT
================================================================

   1  CEZ         CEZ              .0000       1904
   2  PB          CEZ             1.4357       1904
   3  KAH1        CEZ             6.2268       1904
   4  PB_60       CEZ             6.9234       1904
   5  PB_40       CEZ             7.3667       1904
   6  CACL_40     CEZ             7.6940       1904
   7  LACHEN      CEZ             7.8533       1904
   8  CEZ_60      CEZ             7.9313       1904
   9  KAH1_60     CEZ             8.0941       1905
  10  KAH1_40     CEZ             8.2196       1904
  11  CACL        CEZ             8.4781       1904
  12  NACL        CEZ             8.5491       1904
  13  H2O         CEZ             8.7918       1904
  14  CACL_60     CEZ             9.4082       1905
  15  H2O_60      CEZ            10.3600       1905
  16  H2O_40      CEZ            12.2452       1904
  17  ETHANOL     CEZ            16.9431       1904
  18  CEZ_40      CEZ            17.1156       1905
  19  BENZENE     CEZ            21.8171       1904
  20  OPEN        CEZ            23.7811       1905
================================================================
   1  CEZ_40      CEZ_40           .0000       1904
   2  H2O_40      CEZ_40          1.2979       1904
   3  ETHANOL     CEZ_40          2.7569       1903
   4  H2O_60      CEZ_40          2.7641       1904
   5  CACL_60     CEZ_40          4.1449       1904
   6  BENZENE     CEZ_40          4.7016       1903
   7  KAH1_40     CEZ_40          5.5015       1904
   8  KAH1_60     CEZ_40          5.8283       1904
   9  NACL        CEZ_40          5.9974       1903
  10  OPEN        CEZ_40          6.1947       1904
  11  CACL        CEZ_40          6.2279       1903
  12  CACL_40     CEZ_40          6.3961       1904
  13  CEZ_60      CEZ_40          6.6883       1903
  14  LACHEN      CEZ_40          6.9727       1903
  15  PB_60       CEZ_40          8.1641       1904
  16  H2O         CEZ_40          8.3062       1903
  17  PB_40       CEZ_40          8.3790       1903
  18  KAH1        CEZ_40          9.5517       1904
  19  CEZ         CEZ_40         16.6342       1904
  20  PB          CEZ_40         19.6170       1903
================================================================
   1  CEZ_60      CEZ_60           .0000       1904
   2  CACL_40     CEZ_60           .0404       1904
   3  KAH1_40     CEZ_60           .1352       1904
   4  KAH1_60     CEZ_60           .2945       1905
   5  PB_60       CEZ_60           .5251       1904
   6  PB_40       CEZ_60           .5402       1904
   7  CACL_60     CEZ_60           .6343       1905
   8  KAH1        CEZ_60          1.6744       1905
   9  H2O_60      CEZ_60          2.1878       1905
  10  H2O_40      CEZ_60          2.7636       1905
  11  LACHEN      CEZ_60          3.5407       1904
  12  CACL        CEZ_60          3.7121       1904
  13  NACL        CEZ_60          3.7796       1904
  14  H2O         CEZ_60          6.1208       1904
  15  CEZ_40      CEZ_60          6.7323       1905
  16  CEZ         CEZ_60          7.9313       1904
  17  ETHANOL     CEZ_60          9.5084       1904
  18  PB          CEZ_60         10.4458       1904
  19  BENZENE     CEZ_60         14.1472       1904
  20  OPEN        CEZ_60         16.3020       1905
```

Table 4.5 Contaminant Match Results : CEZ, CEZ-40, CEZ-60.

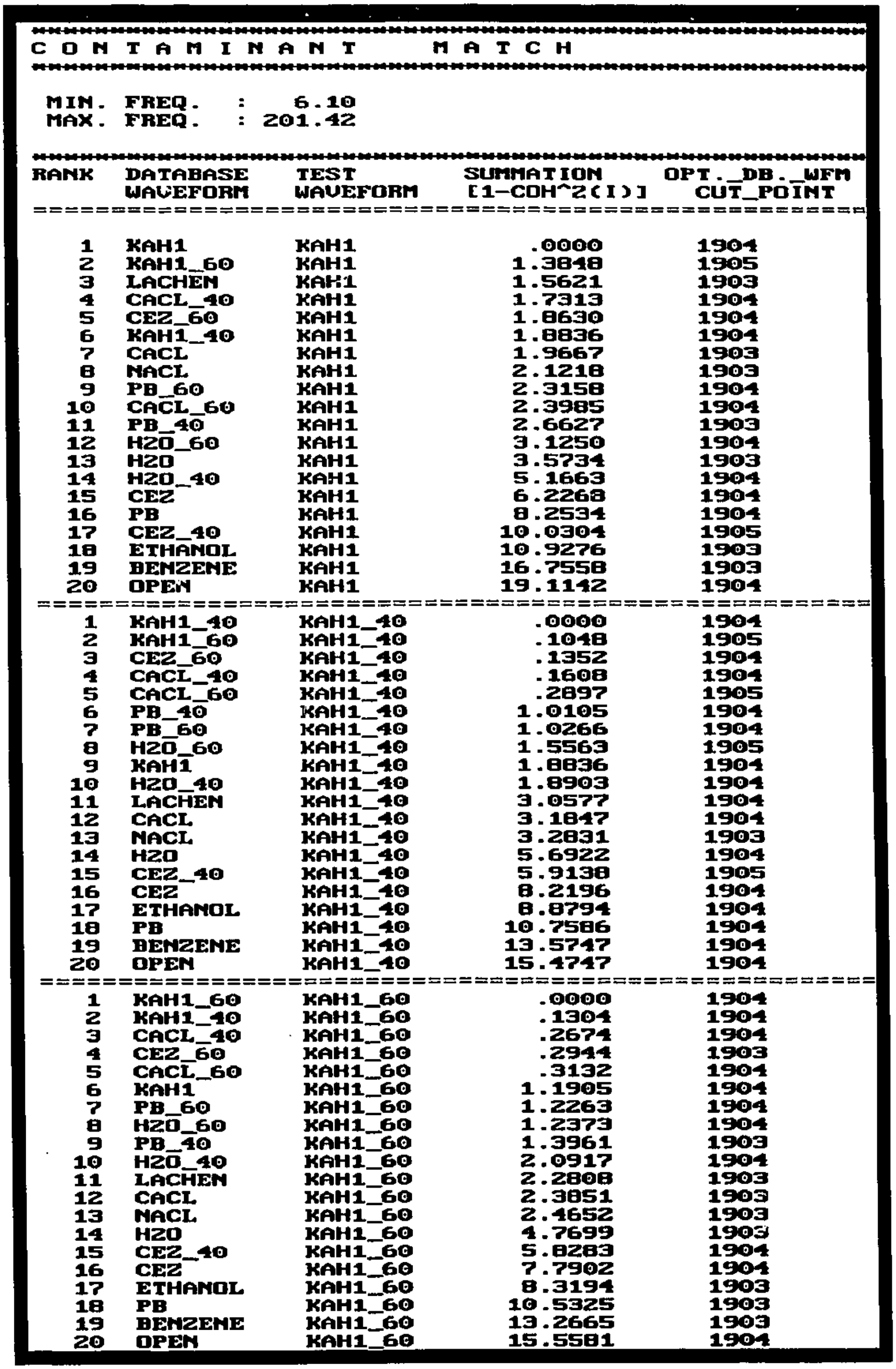

```
**************************************************************
C O N T A M I N A N T     M A T C H
**************************************************************

 MIN. FREQ.  :   6.10
 MAX. FREQ.  : 201.42

**************************************************************
RANK   DATABASE     TEST         SUMMATION      OPT._DB._WFM
       WAVEFORM     WAVEFORM     [1-COH^2(I)]    CUT_POINT
==============================================================

   1   KAH1         KAH1              .0000        1904
   2   KAH1_60      KAH1             1.3848        1905
   3   LACHEN       KAH1             1.5621        1903
   4   CACL_40      KAH1             1.7313        1904
   5   CEZ_60       KAH1             1.8630        1904
   6   KAH1_40      KAH1             1.8836        1904
   7   CACL         KAH1             1.9667        1903
   8   NACL         KAH1             2.1218        1903
   9   PB_60        KAH1             2.3158        1904
  10   CACL_60      KAH1             2.3985        1904
  11   PB_40        KAH1             2.6627        1903
  12   H2O_60       KAH1             3.1250        1904
  13   H2O          KAH1             3.5734        1903
  14   H2O_40       KAH1             5.1663        1904
  15   CEZ          KAH1             6.2268        1904
  16   PB           KAH1             8.2534        1904
  17   CEZ_40       KAH1            10.0304        1905
  18   ETHANOL      KAH1            10.9276        1903
  19   BENZENE      KAH1            16.7558        1903
  20   OPEN         KAH1            19.1142        1904
==============================================================
   1   KAH1_40      KAH1_40           .0000        1904
   2   KAH1_60      KAH1_40           .1048        1905
   3   CEZ_60       KAH1_40           .1352        1904
   4   CACL_40      KAH1_40           .1608        1904
   5   CACL_60      KAH1_40           .2897        1905
   6   PB_40        KAH1_40          1.0105        1904
   7   PB_60        KAH1_40          1.0266        1904
   8   H2O_60       KAH1_40          1.5563        1905
   9   KAH1         KAH1_40          1.8836        1904
  10   H2O_40       KAH1_40          1.8903        1904
  11   LACHEN       KAH1_40          3.0577        1904
  12   CACL         KAH1_40          3.1847        1904
  13   NACL         KAH1_40          3.2831        1903
  14   H2O          KAH1_40          5.6922        1904
  15   CEZ_40       KAH1_40          5.9138        1905
  16   CEZ          KAH1_40          8.2196        1904
  17   ETHANOL      KAH1_40          8.8794        1904
  18   PB           KAH1_40         10.7586        1904
  19   BENZENE      KAH1_40         13.5747        1904
  20   OPEN         KAH1_40         15.4747        1904
==============================================================
   1   KAH1_60      KAH1_60           .0000        1904
   2   KAH1_40      KAH1_60           .1304        1904
   3   CACL_40      KAH1_60           .2674        1904
   4   CEZ_60       KAH1_60           .2944        1903
   5   CACL_60      KAH1_60           .3132        1904
   6   KAH1         KAH1_60          1.1905        1904
   7   PB_60        KAH1_60          1.2263        1904
   8   H2O_60       KAH1_60          1.2373        1904
   9   PB_40        KAH1_60          1.3961        1903
  10   H2O_40       KAH1_60          2.0917        1904
  11   LACHEN       KAH1_60          2.2808        1903
  12   CACL         KAH1_60          2.3851        1903
  13   NACL         KAH1_60          2.4652        1903
  14   H2O          KAH1_60          4.7699        1903
  15   CEZ_40       KAH1_60          5.8283        1904
  16   CEZ          KAH1_60          7.7902        1904
  17   ETHANOL      KAH1_60          8.3194        1903
  18   PB           KAH1_60         10.5325        1903
  19   BENZENE      KAH1_60         13.2665        1903
  20   OPEN         KAH1_60         15.5581        1904
```

Table 4.6 Contaminant Match Results : KAH1, KAH1-40, KAH1-60.

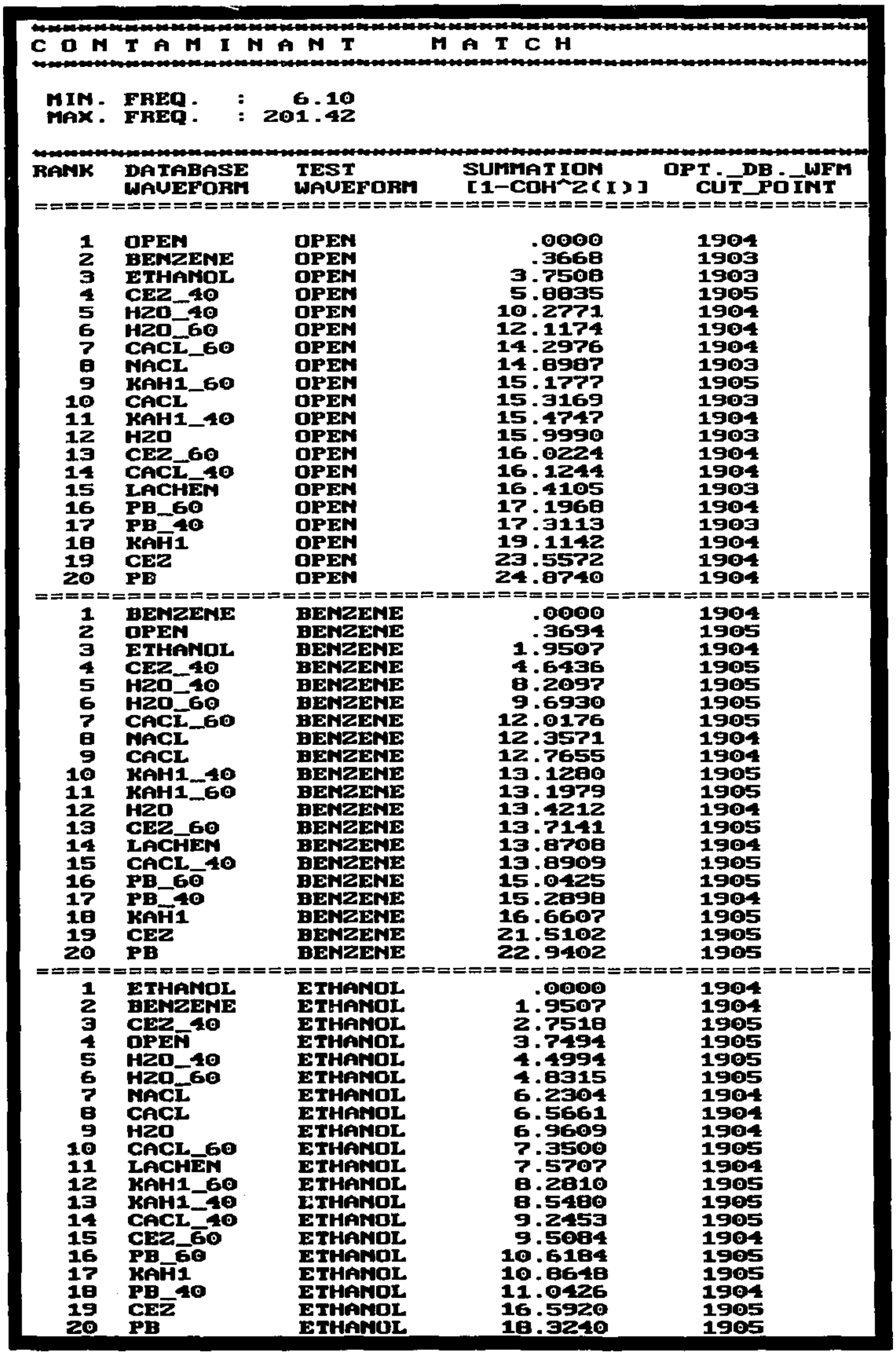

```
****************************************************************
C O N T A M I N A N T     M A T C H
****************************************************************

 MIN. FREQ.   :    6.10
 MAX. FREQ.   :  201.42

****************************************************************
RANK   DATABASE     TEST          SUMMATION       OPT._DB._WFM
       WAVEFORM     WAVEFORM      [1-COH^2(I)]     CUT_POINT
================================================================

   1   OPEN         OPEN                .0000         1904
   2   BENZENE      OPEN                .3668         1903
   3   ETHANOL      OPEN               3.7508         1903
   4   CEZ_40       OPEN               5.8835         1905
   5   H2O_40       OPEN              10.2771         1904
   6   H2O_60       OPEN              12.1174         1904
   7   CACL_60      OPEN              14.2976         1904
   8   NACL         OPEN              14.8987         1903
   9   KAH1_60      OPEN              15.1777         1905
  10   CACL         OPEN              15.3169         1903
  11   KAH1_40      OPEN              15.4747         1904
  12   H2O          OPEN              15.9990         1903
  13   CEZ_60       OPEN              16.0224         1904
  14   CACL_40      OPEN              16.1244         1904
  15   LACHEN       OPEN              16.4105         1903
  16   PB_60        OPEN              17.1968         1904
  17   PB_40        OPEN              17.3113         1903
  18   KAH1         OPEN              19.1142         1904
  19   CEZ          OPEN              23.5572         1904
  20   PB           OPEN              24.8740         1904
================================================================
   1   BENZENE      BENZENE             .0000         1904
   2   OPEN         BENZENE             .3694         1905
   3   ETHANOL      BENZENE            1.9507         1904
   4   CEZ_40       BENZENE            4.6436         1905
   5   H2O_40       BENZENE            8.2097         1905
   6   H2O_60       BENZENE            9.6930         1905
   7   CACL_60      BENZENE           12.0176         1905
   8   NACL         BENZENE           12.3571         1904
   9   CACL         BENZENE           12.7655         1904
  10   KAH1_40      BENZENE           13.1280         1905
  11   KAH1_60      BENZENE           13.1979         1905
  12   H2O          BENZENE           13.4212         1904
  13   CEZ_60       BENZENE           13.7141         1905
  14   LACHEN       BENZENE           13.8708         1904
  15   CACL_40      BENZENE           13.8909         1905
  16   PB_60        BENZENE           15.0425         1905
  17   PB_40        BENZENE           15.2898         1904
  18   KAH1         BENZENE           16.6607         1905
  19   CEZ          BENZENE           21.5102         1905
  20   PB           BENZENE           22.9402         1905
================================================================
   1   ETHANOL      ETHANOL             .0000         1904
   2   BENZENE      ETHANOL            1.9507         1904
   3   CEZ_40       ETHANOL            2.7518         1905
   4   OPEN         ETHANOL            3.7494         1905
   5   H2O_40       ETHANOL            4.4994         1905
   6   H2O_60       ETHANOL            4.8315         1905
   7   NACL         ETHANOL            6.2304         1904
   8   CACL         ETHANOL            6.5661         1904
   9   H2O          ETHANOL            6.9609         1904
  10   CACL_60      ETHANOL            7.3500         1905
  11   LACHEN       ETHANOL            7.5707         1904
  12   KAH1_60      ETHANOL            8.2810         1905
  13   KAH1_40      ETHANOL            8.5480         1905
  14   CACL_40      ETHANOL            9.2453         1905
  15   CEZ_60       ETHANOL            9.5084         1904
  16   PB_60        ETHANOL           10.6184         1905
  17   KAH1         ETHANOL           10.8648         1905
  18   PB_40        ETHANOL           11.0426         1904
  19   CEZ          ETHANOL           16.5920         1905
  20   PB           ETHANOL           18.3240         1905
```

Table 4.7 Contaminant Match Results : OPEN, BENZENE, ETHANOL.

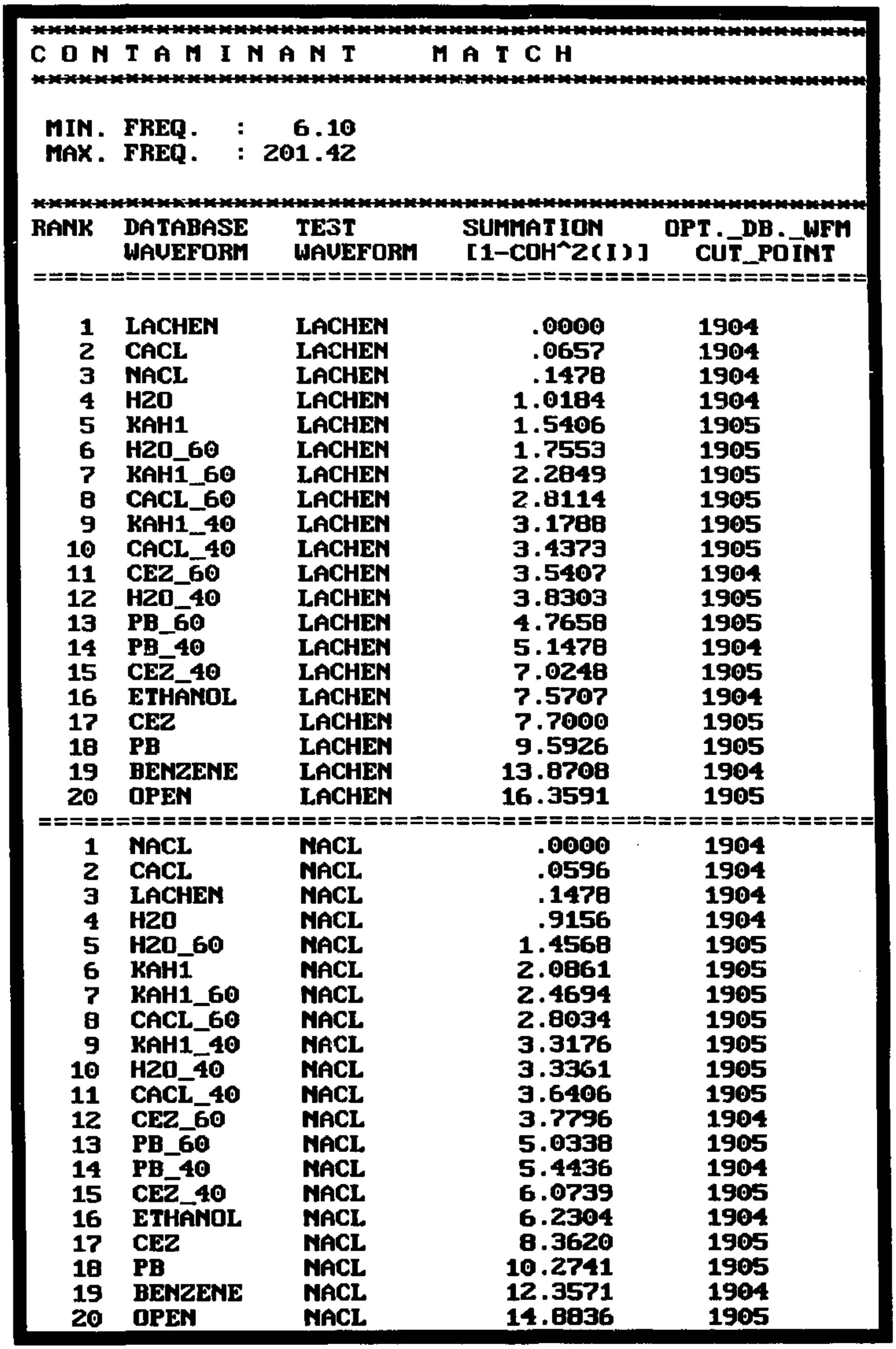

```
**********************************************************
C O N T A M I N A N T     M A T C H
**********************************************************

 MIN. FREQ.  :   6.10
 MAX. FREQ.  : 201.42

**********************************************************
RANK  DATABASE    TEST        SUMMATION      OPT._DB._WFM
      WAVEFORM    WAVEFORM    [1-COH^2(I)]    CUT_POINT
==========================================================

   1  LACHEN      LACHEN           .0000        1904
   2  CACL        LACHEN           .0657        1904
   3  NACL        LACHEN           .1478        1904
   4  H2O         LACHEN          1.0184        1904
   5  KAH1        LACHEN          1.5406        1905
   6  H2O_60      LACHEN          1.7553        1905
   7  KAH1_60     LACHEN          2.2849        1905
   8  CACL_60     LACHEN          2.8114        1905
   9  KAH1_40     LACHEN          3.1788        1905
  10  CACL_40     LACHEN          3.4373        1905
  11  CEZ_60      LACHEN          3.5407        1904
  12  H2O_40      LACHEN          3.8303        1905
  13  PB_60       LACHEN          4.7658        1905
  14  PB_40       LACHEN          5.1478        1904
  15  CEZ_40      LACHEN          7.0248        1905
  16  ETHANOL     LACHEN          7.5707        1904
  17  CEZ         LACHEN          7.7000        1905
  18  PB          LACHEN          9.5926        1905
  19  BENZENE     LACHEN         13.8708        1904
  20  OPEN        LACHEN         16.3591        1905
==========================================================
   1  NACL        NACL             .0000        1904
   2  CACL        NACL             .0596        1904
   3  LACHEN      NACL             .1478        1904
   4  H2O         NACL             .9156        1904
   5  H2O_60      NACL            1.4568        1905
   6  KAH1        NACL            2.0861        1905
   7  KAH1_60     NACL            2.4694        1905
   8  CACL_60     NACL            2.8034        1905
   9  KAH1_40     NACL            3.3176        1905
  10  H2O_40      NACL            3.3361        1905
  11  CACL_40     NACL            3.6406        1905
  12  CEZ_60      NACL            3.7796        1904
  13  PB_60       NACL            5.0338        1905
  14  PB_40       NACL            5.4436        1904
  15  CEZ_40      NACL            6.0739        1905
  16  ETHANOL     NACL            6.2304        1904
  17  CEZ         NACL            8.3620        1905
  18  PB          NACL           10.2741        1905
  19  BENZENE     NACL           12.3571        1904
  20  OPEN        NACL           14.8836        1905
```

Table 4.8   Contaminant Match Results : LACHENAIE, NACL.

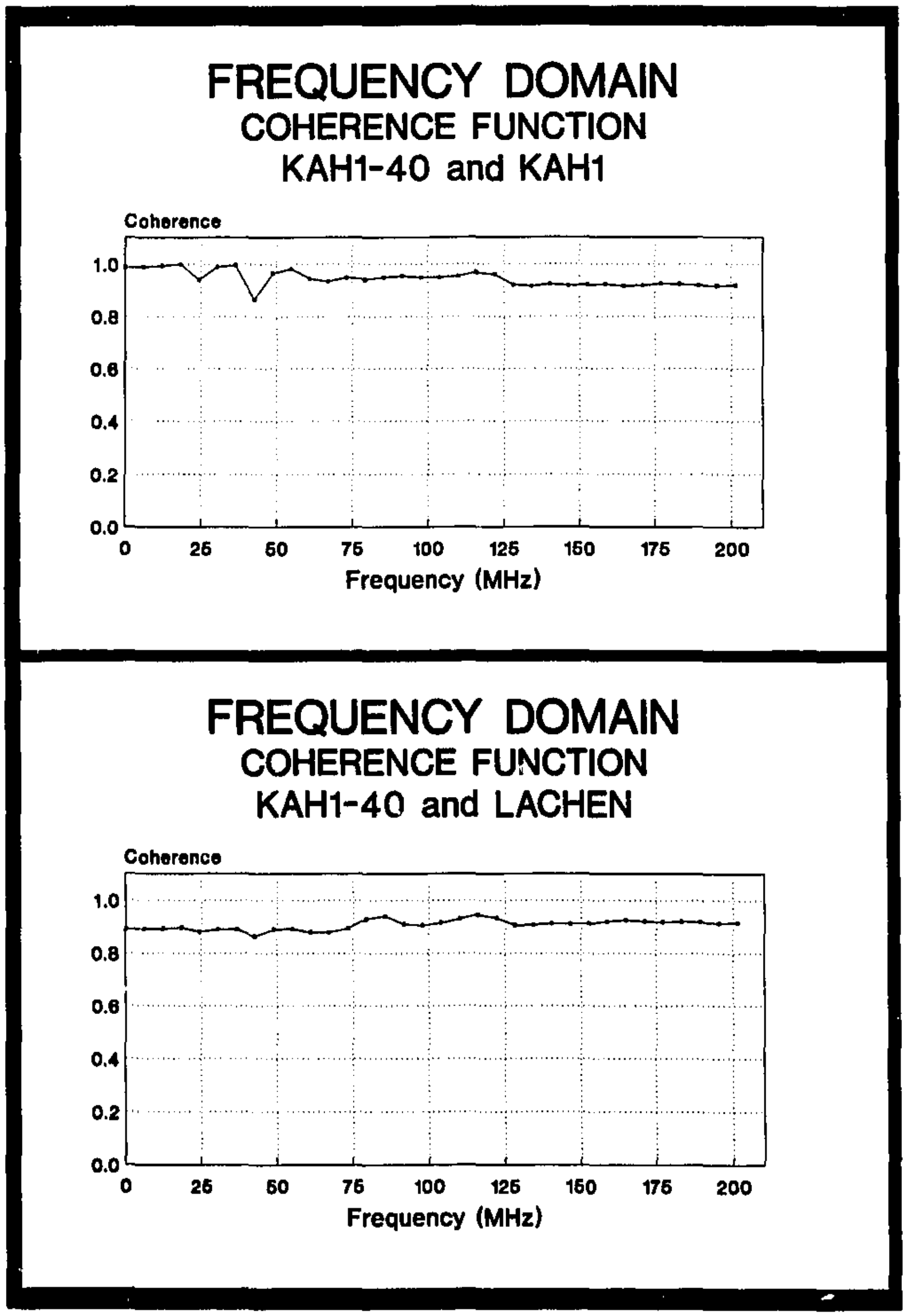

FREQUENCY DOMAIN
COHERENCE FUNCTION
KAH1-40 and KAH1

FREQUENCY DOMAIN
COHERENCE FUNCTION
KAH1-40 and LACHEN

Figure 4.36 Coherence Function Between KAH1-40, KAH1 and LACHEN.

The results indicate that an unknown, contaminated soil may be matched with a known (database) soil-contaminant mixture through a signal processing of TDR records. A direct match involving a contaminated soil and a database contaminant appears to be more challenging. The only direct association was obtained for KAH1. This may suggest that measurements conducted up to a maximum frequency of 200 MHz reflect mainly the influence of the interfacial polarization occurring in the double layer of the colloidal material. It is worth noting that the PB-contaminated soils were matched with each other despite almost identical conductivity of the CEZ-contaminated soils (Table 4.1). This demonstrates the principal advantage of the polarization versus the conductivity measurement. A number of materials display similar conductivities but contain different ionic compositions.

Poor matching of CACL and CEZ contaminated soils may be explained by the excessive conductivity of the analyzed material, masking or short-circuiting the polarization phenomena. However, highly conductive contaminants such as CEZ can be easily traced with a conventional resistivity survey. Conversely, low conductivity contaminants such as petroleum by-products are well suited to electric polarization measurements but are difficult to detect with the resistivity survey.

It should be noted that the degree of success in waveform matching is directly proportional to the amount of laboratory work involved in generating a database set of known "signatures". The laboratory testing program may also be used to determine quantitatively what influence a set change in a contaminant concentration exerts on a coherence function of a particular soil-contaminant system. This information may be subsequently used to estimate the contaminant concentration in the field.

4.5 PRACTICAL IMPLEMENTATION

Obviously, technical problems and refinements associated with the digital signal processing need to explored further. Continuous advances in the microcomputer technology and the measurement instrumentation make it increasingly feasible. Extensive experimentation with various soil probes to enhance the measurement sensitivity is also warranted. Additional studies are also needed to explore various low loss coaxial transmission lines and high bandwidth step function generators. The optimal measuring network should cause a negligible degradation of the incident pulse, hence low loss of bandwidth, as the signal propagates through the transmission line.

Much work remains to be done to sort out the specific effects of contaminant-soil interactions, particularly in situations involving multi-component contaminants. It is proposed that further research include "calibration" experiments, seeking to identify before and after contamination scenarios. These are required for classifying various "signatures", especially with reference to a soil type, soil density, moisture content, porosity, contaminant species and ionic concentrations. Efforts need to be directed at uncoupling the effects of a soil from those of a contaminant on the frequency dependent dielectric properties. Existing studies indicate that these effects manifest themselves at different frequency ranges (solids at low frequencies and liquids at high frequencies), but it is conceivable that they may interact in some cases. Also, the interference effects and other possible causes of spectral differences between the incident and the reflected pulses might exist without being indicative of the contaminant presence. Further understanding of the polarization phenomena in contaminated soils may be enhanced by a numerical modeling of the measuring network.

CHAPTER 5

CONCLUSIONS

This study demonstrates the feasibility of an effective subsurface contaminant detection method based on the phenomenon of electric polarization in soils. Technically, the instrumentation set-up is relatively simple and borrows from the well established TDR method. Waveform acquisition by a digitizer and its processing by a portable computer can be performed directly on site, with the aid of database of "signatures" generated through the laboratory testing. The spatial extent of an underground contamination can be determined by probing the affected area and analyzing the incident and the reflected signals in the frequency-domain. Currently available test instruments and portable computers are suited for a practical implementation of this task.

The results of this study indicate promising means of identifying contaminants through the application of the coherence function to data analysis. The proposed approach involves utilization of the coherence function in two phases. First, it would be applied to individual measurements in order to check the validity of the transfer function within a set frequency range. Second, it would be applied to establish a degree of association between known and unknown records. It is envisioned that through the systematic means of creating a database of "signatures", an automated measurement and analysis process can be applied to the detection of subsurface contaminants.

The primary task of an in-situ contaminant detection technique is a determination of the lateral extent of a contaminant. The approach presented in this study indicates the feasibility of performing this task. The secondary task involves a detailed chemical characterization of a suspected contaminant. It is expected that with a greater variety of test situations a series of "signatures" can be cataloged to permit an effective characterization.

The effectiveness of the subsurface contaminant detection method proposed in this study can be enhanced if it is used in conjunction with other measurement techniques. Thus, an initial site reconnaissance can be rapidly performed with a portable electromagnetic conductivity probe. The area of interest can be subsequently analyzed with the TDR method. Further refinement, if required, can be achieved by a direct sampling from a monitoring well, which at this stage can be judiciously located.

STATEMENT OF ORIGINALITY

A technique for a rapid detection and delineation of contaminants in soils is presented. The proposed methodology is based on the principles of electric polarization and the interaction of matter with the electric field. The technique employs time-domain reflectometry (TDR) measurements using a digital oscilloscope for signal recording and a microcomputer for data analysis.

Test results indicate that it is feasible to detect a particular contaminant in a subsurface soil through the observation of its characteristic dielectric response. The proposed contaminant detection procedure employs the coherence function to match an unknown TDR "signature" with a set of database "signatures" and establish the most likely association. The author is not aware of any previous studies involving the application of both the TDR and the coherence function to a subsurface contaminant detection.

APPENDIX 1

Computer Source Code Listings

1.1 Data Transfer from TEK 11402 to IBM PC

```
10 DIM CURVE% (10240)
20 CLS
30 PRINT "                W A V E F O R M   T R A N S F E R"
40 INPUT "FILE NAME :";F$
50 OPEN F$ FOR OUTPUT AS #2
60 OPEN "COM1:9600,N,8,1" AS #1
70 PRINT #1,"LONGFORM ON;SELECT?"
80 LINE INPUT #1,TRACE$
81 PRINT TRACE$
83 PRINT #1,"WFMPRE?"
84 LINE INPUT #1,WFMPRE$
85 PRINT WFMPRE$
90 PRINT #1,"ENCDG WAV:BIN;BYT.OR LSB;OUTPUT "+MID$(TRACE$,8)
100 PRINT #1,"CURVE?"
110 HEADER$ = INPUT$(7,#1)
120 HIGH$ = INPUT$(1,#1) : LOW$ = INPUT$(1,#1)
130 BYTCNT = CVI(LOW$+HIGH$)
140 NRPT = (BYTCNT-1)/2
150 FOR I=0 TO NRPT-1
160 CURVE%(I) = CVI(INPUT$(2,#1))
170 PRINT CURVE%(I);
180 PRINT #2,CURVE%(I);
190 NEXT I
200 LINE INPUT #1,CKSUM$
210 CLOSE
220 END
```

1.2 Processing of Acquired Waveforms

```
      DIMENSION F(2049),A(5200),V(5200),MA(200)
      COMPLEX*8 IN(4096),OU(4096),Z(4096)
      CHARACTER*10 KNOWN,FNAME
C     **********************************************
C     THIS PROGRAM OPERATES ON THE ACQUIRED TIME DOMAIN
C     DATA FILES AND
C     PRODUCES PROCESSED TIME DOMAIN DATA AND
C     PROVIDES CONVERSION TO FREQUENCY DOMAIN
C     USING THE FFT ALGORITHM
C     ARRAY DEFINITIONS:
C     F()=FREQUENCY
C     A()=PROCESSED TIME DOMAIN OUTPUT
C     V()=PROCESSED TIME DOMAIN INPUT
C     MA()=MAGNITUDE OF TRANSFER FUNCTION
C     Z()=COMPLEX TRANSFER FUNCTION
C     IN()=INPUT FFT
C     OU()=OUTPUT FFT
C     COMPILE WITH MICROSOFT FORTRAN v.4.01
C     LAST REVISION 09/22/94  @ EDWARD J. HOPPE
C     **********************************************
      ND=-1
      WRITE(*,*)
C     ** ASK FOR A FILENAME
      WRITE(*,890)
      READ(*,891) KNOWN
890   FORMAT(' NAME OF FILE SET: '\)
891   FORMAT(A)
      OPEN(9,FILE=KNOWN)
C         READ(9,*) FMIN,FMAX
C     ** MINIMUM FREQUENCY=0, MAXIMUM=200 MHz
      FMIN=0.0
      FMAX=200.0
C     ** DATA SET WITH 2 TO THE POWER OF 12 (FOR FFT)
1     LN=12
      N=2**LN
      ND2P1=N/2+1
      PI=3.141593
      DEG=180.0/PI
      READ(9,'(A)') FNAME
      IF(FNAME.EQ.'FIN') GOTO 999
      WRITE(*,*) FNAME
C          READ(9,*) J
C     ** DEFINE OPTIMUM CUT POINT
      J=1904
C          WRITE(*,*) ' OPTIMUM CUT_POINT '
           WRITE(*,*) J
C     ** READ AND SCALE INPUT DATA
      OPEN(4,FILE=FNAME)
C     ** NPT=NUMBER OF POINTS
C     ** TSTEP=SAMPLING INTERVAL
C     ** XZERO=INITIAL TIME
      READ(4,*) NPT,TSTEP,XZERO
      TSTEP=(TSTEP/1.333)*1.0E9
      XZERO=(XZERO/1.333)*1.0E9
      READ(4,*) A(1)
      IF(A(1).LT.-1.0) A(1)=0.0
      DO 2 L=2,NPT
      READ(4,*) A(L)
C      IF(A(L).LE.-50.0) A(L)=A(L-1)
2     CONTINUE
```

```
      CLOSE(4,STATUS='KEEP')
      WRITE(*,*) 'FILE ACCESSED'
C     ** APPLY MEDIAN FILTERING
      CALL MEDIAN(A,NPT)
      WRITE(*,*)
      DO 115 L=1,J
      V(L)=A(L)
115   CONTINUE
      N1=J+J
C     ** MULTIPLY REFLECTED SIGNAL BY 2
      DO 117 L=J+1,N1
      A(L-J)=2.0*A(L)
117   CONTINUE
      DO 120 L=2,J
      A(L)=A(L)-A(1)
      V(L)=V(L)-V(1)
120   CONTINUE
      A(1)=0.0
      V(1)=0.0
C     ** APPLY COSINE TAIL TO LAST 30% OF DATA POINTS
      CALL TAIL(A,J,PI,N)
      CALL TAIL(V,J,PI,N)
C     ** RECORD INPUT (V) AND OUTPUT (A)
C     ** PROCESSED TIME DOMAIN DATA
      OPEN(1,FILE=FNAME//'.IN',STATUS='UNKNOWN')
      OPEN(2,FILE=FNAME//'.OUT',STATUS='UNKNOWN')
      WRITE(1,*) N,TSTEP
      WRITE(2,*) N,TSTEP
      DO 121 L=1,N
      WRITE (1,902) V(L)
      WRITE (2,902) A(L)
121   CONTINUE
      CLOSE(1,STATUS='KEEP')
      CLOSE(2,STATUS='KEEP')
      GOTO 1
C     ** PERFORM FFT: IN=INPUT SIGNAL FFT ; OU=OUTPUT SIGNAL FFT
      DO 125 L=1,N
      IN(L)=CMPLX(V(L))
      OU(L)=CMPLX(A(L))
125   CONTINUE
C     ** COMPUTE FREQUENCY STEP
      FSTEP=(1.0/(FLOAT(N)*TSTEP*1.0E-9))/1.0E6
      F(1)=0.0
      IF(FMIN.EQ.0.0) ND=1
      DO 25 L=2,ND2P1
      F(L)=F(L-1)+FSTEP
      IF (F(L).GT.FMAX) GOTO 26
      IF(ND.EQ.-1.AND.F(L).GE.FMIN) THEN
      ND=L
      FN=F(L)
C      WRITE(*,920) ' NORM. FREQ. : ',FN
C      WRITE(*,*)
      ENDIF
25    CONTINUE
C     ** PERFORM FAST FOURIER TRANSFORM
26    CALL FFT(IN,LN,PI)
      CALL FFT(OU,LN,PI)
C     ** CREATE FREQUENCY DOMAIN DATA FILES
      OPEN(1,FILE=FNAME//'.FIN',STATUS='UNKNOWN')
      OPEN(2,FILE=FNAME//'.FOT',STATUS='UNKNOWN')
```

```
        DO 127 L=1,ND2P1
        IF (F(L).GT.FMAX) GOTO 128
        WRITE(1,901) F(L),IN(L)
        WRITE(2,901) F(L),OU(L)
127     CONTINUE
128     CLOSE(1,STATUS='KEEP')
        CLOSE(2,STATUS='KEEP')
        DO 130 L=1,ND2P1
        IF (F(L).GT.FMAX) GOTO 135
C       ** COMPUTE TRANSFER FUNCTION
        Z(L)=OU(L)/IN(L)
C        Z(L)=CMPLX(1.0,0.0)+Z(L)/(CMPLX(1.0,0.0)-Z(L))
C        MA(L)=ABS(Z(L))
C        MA(L)=ATAN2(IMAG(Z(L)),REAL(Z(L)))
130     CONTINUE
C       ** RECORD TRANSFER FUNCTION DATA
135     OPEN(1,FILE=FNAME//'.FFT',STATUS='UNKNOWN')
        DO 136 L=1,ND2P1
        IF (F(L).GT.FMAX) GOTO 137
        WRITE(1,901) F(L),Z(L)
136     CONTINUE
137     CLOSE(1,STATUS='KEEP')
        GOTO 1
C
C        DIV=MA(ND)
        SUM=0.0
        I=0
        DO 140 L=ND,ND2P1
        IF (F(L).GT.FMAX) GOTO 145
C        MA(L)=MA(L)/DIV
        SUM=SUM+MA(L)
        I=I+1
140     CONTINUE
145     DIV=SUM/FLOAT(I)
        OPEN(1,FILE=FNAME//'.NFT',STATUS='UNKNOWN')
        DO 150 L=1,ND2P1
        IF (F(L).GT.FMAX) GOTO 155
         MA(L)=MA(L)/DIV
        WRITE(1,901) F(L),MA(L)
150     CONTINUE
155     CLOSE(1,STATUS='KEEP')
        GOTO 1
901     FORMAT(1F25.15,3X,2(1F25.15,3X))
902     FORMAT(1F25.10)
920     FORMAT(1X,A15,1F6.2)
999     END
C       ****************************************************
C       ** SUBROUTINE FOR ADDING COSINE TAIL TO ACQUIRED
C       ** TIME DOMAIN DATA
        SUBROUTINE TAIL (F,NX,PI,N)
        REAL*4 F(4096),A,PI
        M=INT(0.70*NX)
        I=(NX-M)*2
        K=(NX-M)-1
        DO 10 L=M,NX
        K=K+1
        A=0.5*(1.0-COS(2.0*PI*FLOAT(K)/FLOAT(I)))
        F(L)=F(L)*A
10      CONTINUE
        DO 20 L=NX+1,N
```

```
      F(L)=F(NX)
20    CONTINUE
      RETURN
      END
C     ****************************************
C     ** FAST FOURIER TRANSFORM ALGORITHM
      SUBROUTINE FFT (F,LN,PI)
      REAL*4 PI,X
      COMPLEX*8 F(4096),U,W,T
      N=2**LN
      NV2=N/2
      NM1=N-1
      J=1
      DO 3 I=1,NM1
         IF(I.GE.J) GOTO 1
         T=F(J)
         F(J)=F(I)
         F(I)=T
1        K=NV2
2        IF(K.GE.J) GOTO 3
         J=J-K
         K=K/2
         GOTO 2
3        J=J+K
      DO 5 L=1,LN
         LE=2**L
         LE1=LE/2
         U=CMPLX(1.0,0.0)
         X=PI/FLOAT(LE1)
         W=CMPLX(COS(X),-SIN(X))
         DO 5 J=1,LE1
            DO 4 I=J,N,LE
               IP=I+LE1
               T=F(IP)*U
               F(IP)=F(I)-T
4              F(I)=F(I)+T
5           U=U*W
      DO 6 I=1,N
      F(I)=F(I)/FLOAT(N)
6     CONTINUE
      RETURN
      END
C     ****************************************
C     ** MEDIAN FILTERING OF ACQUIRED
C     ** TIME DOMAIN DATA
      SUBROUTINE MEDIAN(A,NPT)
      REAL*4 A(5200),D(25),SMALL
      REAL*4 B(5200)
      DO 10 L=13,NPT-12
      M=1
      DO 15 I=L-12,L+12
      D(M)=A(I)
      M=M+1
15    CONTINUE
      DO 20 K=1,13
      SMALL=1.0E10
      DO 30 M=1,25
      SMALL=AMIN1(SMALL,D(M))
30    CONTINUE
      DO 17 M=1,25
```

```
          IF(D(M).EQ.SMALL) THEN
          D(M)=1.0E10
          GOTO 20
          ENDIF
17        CONTINUE
20        CONTINUE
          B(L)=SMALL
10        CONTINUE
          DO 50 L=1,12
          B(L)=B(13)
50        CONTINUE
          DO 55 L=NPT-11,NPT
          B(L)=B(NPT-12)
55        CONTINUE
          DO 60 L=1,NPT
          A(L)=B(L)
60        CONTINUE
          RETURN
          END
```

1.3 Display of Time-Domain Waveforms

```
      DIMENSION TA(6000),A(6000),V(6000)
      CHARACTER*30 FNAME,ARG
      INTEGER DEV
C     ******************************************
C     THIS PROGRAM PRODUCES A SCREEN DISPLAY
C     OF TIME DOMAIN DATA USING McGILL FORTRAN
C     PLOTTING SUBROUTINES
C     ARRAY DEFINITIONS:
C     TA()=TIME
C     V()=FIRST DATA FILE
C     A()=SECOND DATA FILE
C     COMPILE WITH MICROSOFT FORTRAN v.4.01
C     AND McGILL PLOTTING SUBROUTINES
C     LAST REVISION 9/22/94  @ EDWARD J. HOPPE
C     ******************************************
C     ### TAG MARKS EACH PLOT
      WRITE(*,*) 'PLOT ID NUMBER'
      READ(*,*) TAG
      WRITE(*,'(A\)') ' VIEW OR FILE ? ( 1 or 2 ): '
      READ(*,*) NDEV
      IF (NDEV.EQ.2) THEN
        WRITE(*,'(A\)') ' OUTPUT FILE NAME ?  '
        READ(*,'(A)') ARG
      ENDIF
      WRITE(*,'(A\)') ' NUMBER OF WAVEFORMS (1 or 2) : '
      READ(*,*) NFILES
      WRITE(*,'(A\)') ' NUMBER OF POINTS TO DISCARD (TAIL) : '
      READ(*,*) NDISC
      WRITE(*,'(A\)') ' WAVEFORM PLOT ONLY (1=YES) : '
      READ(*,*) NPLOT
      XZERO=0.0
      DO 13 I=1,NFILES
      WRITE(*,'(A\)') ' TIME DOMAIN FILE : '
C     ** READ TIME DOMAIN FILE
      READ(*,'(A)') FNAME
      OPEN(4,FILE=FNAME)
      READ(4,*) NPT,TSTEP,XZERO
      IF(XZERO.EQ.0.0) GOTO 1
      TSTEP=(TSTEP/1.333)*1.0E9
      XZERO=(XZERO/1.333)*1.0E9
1     NPT=NPT-NDISC
      WRITE(*,*)
      WRITE(*,*) '       NPT      TSTEP (ns)  '
      WRITE(*,*) NPT,TSTEP
      WRITE(*,*)
      TA(1)=0.0
      DO 7 L=1,NPT-1
      READ(4,*) A(L)
      TA(L+1)=TA(L)+TSTEP
7     CONTINUE
      CLOSE(4,STATUS='KEEP')
      WRITE(*,*) 'FILE ACCESSED'
C     ************************************************
      IF(I.EQ.2) GOTO 19
       DO 250 L=1,NPT
       V(L)=A(L)
250    CONTINUE
18    CONTINUE
C     *******************************************************************
19    IF (NDEV.EQ.1) CALL PLOTON(9,'8')
```

```
       IF (NDEV.EQ.2) CALL PLOTON(3,ARG)
       CALL FACTOR(0.6,0.6)
       TFIRST=TA(1)
       TDELTA=(TA(NPT)-TA(1))/14.0
       CALL SCALE(V,8.0,NPT,-1)
C         VLAST=V(NPT+1)
        VLAST=50.0
       CALL SCALE(V,8.0,NPT,1)
C         VFIRST=V(NPT+1)
        VFIRST=-30.0
       IF (NFILES.EQ.2) THEN
        CALL SCALE(A,8.0,NPT,-1)
C         ALAST=A(NPT+1)
        ALAST=VLAST
        CALL SCALE(A,8.0,NPT,1)
C         AFIRST=A(NPT+1)
        AFIRST=VFIRST
        IF (ALAST.GT.VLAST) VLAST=ALAST
        IF (AFIRST.LT.VFIRST) VFIRST=AFIRST
       ENDIF
       VDELTA=(VLAST-VFIRST)/8.0
C      ***************************
       V(NPT+1)=VFIRST
       A(NPT+1)=VFIRST
       V(NPT+2)=VDELTA
       A(NPT+2)=VDELTA
       TA(NPT+1)=TFIRST
       TA(NPT+2)=TDELTA
C      ^^^^^^^^^^^^^^^^^^^^^^^^^^
       IF (NPLOT.EQ.1) THEN
           CALL PLOT(1.8,1.25,-3)
           GOTO 88
       ENDIF
C      ** DRAW RECTANGLE AND SYMBOLS
       CALL RECT(1.,0.4,10.,15.5,0.,3)
       CALL RECT(1.01,0.41,9.98,15.48,0.,3)
       CALL SYMBOL(1.8,0.5,0.1,
     + 'MCGILL UNIV./GEOTECHNICAL RESEARCH CENTRE',0.,41)
       CALL NUMBER(15.2,0.5,0.1,TAG,0.,-1)
       IF(XZERO.NE.0.0) GOTO 50
       CALL SYMBOL(4.7,9.84,0.35,'PROCESSED TIME DOMAIN DATA',0.,26)
       CALL SYMBOL(4.69,9.83,0.35,'PROCESSED TIME DOMAIN DATA',0.,26)
       GOTO 55
50     CALL SYMBOL(4.7,9.84,0.35,'ACQUIRED TIME DOMAIN DATA',0.,25)
       CALL SYMBOL(4.69,9.83,0.35,'ACQUIRED TIME DOMAIN DATA',0.,25)
C                         CALL SYMBOL(12.5,8.75,0.25,'INPUT (V)',0.,9)
C                         CALL SYMBOL(12.5,4.35,0.25,'OUTPUT (V)',0.,10)
55     CALL SYMBOL(9.9,9.35,0.15,'PTS=',0.,4)
       PTS=FLOAT(NPT)
       CALL NUMBER(10.5,9.35,0.15,PTS,0.,-1)
       CALL SYMBOL(12.,9.35,0.15,'TSTEP=      ns',0.,14)
       CALL NUMBER(12.9,9.35,0.15,TSTEP,0.,3)
       CALL RECT(1.8,1.2,8.40,14.1,0.,3)
C      ^^^^^^^^^^^^^^^^^^^^^^^^^^^^^^^^^^^^^^^^^^^^^^
C      ** DRAW AXES
       CALL PLOT(1.8,1.2,-3)
       CALL AXS(0.,0.,'TIME (NANOSEC)',-14,-14.01,0.,
     + TFIRST,TDELTA*0.8,1,0.,0.8)
       EX=0.0
C      ** LABEL AXES
```

```
      IF (VDELTA.LT.1.0) EX=-1.0
      IF (VDELTA.LT.0.1) EX=-2.0
      IF (VDELTA.LT.0.01) EX=-3.0
      IF (VDELTA.LT.0.001) EX=-4.0
      IF (VDELTA.LT.0.0001) EX=-5.0
      IF (VDELTA.LT.0.00001) EX=-6.0
      IF (VDELTA.LT.0.000001) EX=-7.0
      IF (VDELTA.LT.0.0000001) EX=-8.0
      IF (VDELTA.LT.0.00000001) EX=-9.0
      IF (VDELTA.LT.0.000000001) EX=-10.0
      IF (VDELTA.GT.100.0) EX=2.0
      IF (VDELTA.GT.1000.0) EX=3.0
      IF (VDELTA.GT.10000.0) EX=4.0
      IF (VDELTA.GT.100000.0) EX=5.0
      IF (VDELTA.GT.1000000.0) EX=6.0
      IF (VDELTA.GT.10000000.0) EX=7.0
      IF (VDELTA.GT.100000000.0) EX=8.0
      IF (VDELTA.GT.1000000000.0) EX=9.0
      IF (VDELTA.GT.10000000000.0) EX=10.0
      CALL AXS(0.,0.05,'AMPLITUDE (VOLTS)',17,-8.01,90.,
     + VFIRST,VDELTA*0.8,1,EX,0.8)
C     ** PLOT WAVEFORM 1
      CALL PLOT(0.,0.05,-3)
C        88     CALL NEWPEN(2)
88    CALL FLINE(TA,V,NPT,1,0,3)
      IF (NFILES.EQ.2) THEN
C     ** PLOT WAVEFORM 2
      CALL PLOT(0.,0.05,3)
C               CALL NEWPEN(1)
        CALL FLINE(TA,A,NPT,1,0,3)
      ENDIF
C     ** TERMINATE PLOTTING
      CALL ENDPLT
      END
```

```
      DIMENSION F(500),OX(500),PH(500),A(180),R(180)
      DIMENSION O1(500),PH1(500)
      DIMENSION O2(500),PH2(500)
      DIMENSION O3(500),PH3(500)
      DIMENSION O4(500),PH4(500)
      COMPLEX*8 Z(500)
      CHARACTER*30 FNAME,ARG
      PI=3.141593
      DEG=180.0/PI
C     ******************************************
C     THIS PROGRAM PRODUCES A POLAR PLOT
C     OF THE TRANSFER FUNCTION
C     ARRAY DEFINITIONS:
C     A()=MAGNITUDE OF THE SEMICIRCLE ON THE PLOT
C     R()=PHASE ANGLE OF EACH POINT ON THE SEMICIRCLE
C     O1() THROUGH O4()= MAGNITUDE OF TRANSFER FUNCTION
C     PH1() THROUGH PH4()= PHASE OF TRANSFER FUNCTION
C     Z()= TRANSFER FUNCTION (MAGNITUDE, PHASE)
C     F()=FREQUENCY
C     OX()=INTERMEDIATE MAGNITUDE OF TRANSFER FUNCTION
C     PH()=INTERMEDIATE PHASE OF TRANSFER FUNCTION
C     COMPILE WITH MICROSOFT FORTRAN VERSION 4.01
C     AND McGILL FORTRAN PLOTTING SUBROUTINES
C     LAST REVISION 09/22/94 @ EDWARD J. HOPPE
C     ******************************************
C     *** TAG NUMBER WILL MARK THE PLOT ***
      WRITE(*,*) '*******************************************'
      WRITE(*,*) 'ID NUMBER'
      READ(*,*) TAG
C     ** CHOICE OF SCREEN DISPLAY, DRAWING FILE OR HP PLOT FILE
      WRITE(*,'(A)') ' VIEW, FILE OR HPFILE ? ( 1, 2 OR 3 ): '
      READ(*,*) NDEV
      WRITE(*,'(A)') ' FUNCTION PLOT ONLY ? (1=YES): '
      READ(*,*) NDPL
      IF (NDEV.NE.1) THEN
      WRITE(*,'(A)') ' OUTPUT FILENAME ? : '
      READ(*,'(A)') ARG
      ENDIF
      WRITE(*,850)
      READ(*,*) NFILES
850   FORMAT(' NO. OF INPUT FILES (Max.= 4) :'\)
      WRITE(*,*) 'NO. OF POINTS TO DISCARD (Start,End)'
      READ(*,*) NSTRT,NEND
855   DO 18 I=1,NFILES
      WRITE(*,900)
      READ(*,910) FNAME
900   FORMAT(' INPUT FILENAME :'\)
910   FORMAT(A)
C      WRITE(*,920)
C      READ(*,*) XO,XB,XA
C920   FORMAT(' AMPL. MULTIPLIER :'\)
C      WRITE(*,922)
C      READ(*,*) XP
C922   FORMAT(' PHASE SHIFT :'\)
C     ********************************************
C     ** DEFINE THE SEMICIRCLE
      DO 60 J=1,180
      A(J)=1.0
      R(J)=-FLOAT(J)*0.017453293
60    CONTINUE
```

```
        LIMIT=42
        LIMIT=LIMIT-NEND
        OPEN(5,FILE=FNAME)
        DO 25 J=1,LIMIT
        READ(5,901) F(J),Z(J)
25      CONTINUE
901     FORMAT(1F25.15,3X,2(1F25.15,3X))
252     CLOSE(5,STATUS='KEEP')
C       ** DEFINE FREQUENCY STEP AND MAX. FREQUENCY
        FSTEP=F(2)
        FMAX=250.0
C       ** CONVERT TRANSFER FUNCTION
C       ** INTO MAGNITUDE AND PHASE
        CALL MAGPHASE (Z,PI,LIMIT)
        DO 27 J=1,LIMIT
        OX(J)=REAL(Z(J))
        PH(J)=IMAG(Z(J))
C           OX(J)=XO+XB*OX(J)*EXP(XA*FLOAT(J-1))
C             OX(J)=OX(J)*EXP(XP*FLOAT(J-1))
C               PH(J)=PH(J)*EXP(XP*FLOAT(J-1))
27      CONTINUE
2       IF (NSTRT.EQ.0) GOTO 51
        LIMIT=LIMIT-NSTRT
        DO 50 J=1,LIMIT
        F(J)=F(J+NSTRT)
        OX(J)=OX(J+NSTRT)
        PH(J)=PH(J+NSTRT)
50      CONTINUE
          OX(LIMIT+1)=0.0
          OX(LIMIT+2)=1.0
          PH(LIMIT+1)=0.0
          PH(LIMIT+2)=1.0
51      IF (I.EQ.1) GOTO 10
        IF (I.EQ.2) GOTO 12
        IF (I.EQ.3) GOTO 14
        IF (I.EQ.4) GOTO 16
10      DO 11 L=1,LIMIT
        O1(L)=OX(L)
        PH1(L)=PH(L)
11      CONTINUE
        GOTO 18
12      DO 13 L=1,LIMIT
        O2(L)=OX(L)
        PH2(L)=PH(L)
13      CONTINUE
        GOTO 18
14      DO 15 L=1,LIMIT
        O3(L)=OX(L)
        PH3(L)=PH(L)
15      CONTINUE
        GOTO 18
16      DO 17 L=1,LIMIT
        O4(L)=OX(L)
        PH4(L)=PH(L)
17      CONTINUE
18      CONTINUE
C       *****************************************************
        IF (NDEV.EQ.1) CALL PLOTON(9,'8')
        IF (NDEV.EQ.2) CALL PLOTON(3,ARG)
        IF (NDEV.EQ.3) CALL PLOTON(1,ARG)
```

```
C     *******************************************************
      CALL FACTOR(0.6,0.6)
C     ** PLOT THE RECTANGLE AND SYMBOLS
      CALL RECT(1.,0.4,10.,15.5,0.,3)
      IF (NDPL.EQ.1) GOTO 44
      CALL RECT(1.01,0.41,9.98,15.48,0.,3)
      CALL SYMBOL(1.8,0.5,0.1,
     + 'MCGILL UNIV./GEOTECHNICAL RESEARCH CENTRE',0.,41)
      CALL NUMBER(15.2,0.5,0.1,TAG,0.,-1)
      CALL SYMBOL(6.,9.85,0.35,'FREQUENCY DOMAIN  FFT',0.,21)
      CALL SYMBOL(5.99,9.84,0.35,'FREQUENCY DOMAIN  FFT',0.,21)
      CALL SYMBOL(4.7,9.25,0.25,'TRANSFER FUNCTION',0.,17)
C                      CALL SYMBOL(12.,9.4,0.15,'FSTEP=      MHz',0.,15)
C                              CALL NUMBER(12.9,9.4,0.15,FSTEP,0.,3)
C                    CALL SYMBOL(12.,8.4,0.15,'FMAX =      MHz',0.,15)
C                    CALL NUMBER(12.9,8.4,0.15,FMAX,0.,3)
      CALL RECT(1.8,1.2,8.40,14.1,0.,3)
      CALL DASH(2.50,8.3,15.35,8.3,0.5)
      CALL DASH(8.85,9.0,8.85,1.5,0.5)
      CALL SYMBOL(8.9,8.4,0.15,'[0,0]',0.,5)
      CALL SYMBOL(14.6,8.4,0.15,'[1,0]',0.,5)
      CALL SYMBOL(2.5,8.4,0.15,'[-1,0]',0.,6)
      CALL SYMBOL(8.9,1.5,0.15,'-j',0.,2)
44    CALL PLOT(8.85,8.3,-3)
C           CALL GETWDW(XMIN,XMAX,YMIN,YMAX)
C                 YMAX=8.3
      CALL PLTSZE(7.0,7.0,1E6)
      LIM=179
C     ** PLOT TRANSFER FUNCTIONS
      CALL POLAR(A,R,LIM,1,0,3,0.0,0.17)
      CALL NEWPEN(1)
      CALL POLAR(O1,PH1,LIMIT,1,5,0,0.0,0.17)
C      CALL PLOT(-8.5,-6.0,-3)
C      CALL POLAR(O1,PH1,LIMIT,1,0,03,0.0,0.17)
C       CALL FLINE(O1,PH1,-LIMIT,1,0)
      GOTO 800
C     ** COMPUTE LOCATIONS OF VARIOUS
C     ** FREQUENCY COMPONENTS
C               F12X=O1(1)*COS(PH1(1))*5.882352941
C               F12Y=O1(1)*SIN(PH1(1))*5.882352941
C               CALL SYMBOL(F12X,F12Y,0.13,'12',0.,2)
      F20X=O1(1)*COS(PH1(1))*5.882352941
      F20Y=O1(1)*SIN(PH1(1))*5.882352941
      CALL DASH(0.0,0.0,F20X,F20Y,0.5)
      CALL SYMBOL(F20X,F20Y,0.13,'20',0.,2)
      F50X=O1(8)*COS(PH1(8))*5.882352941
      F50Y=O1(8)*SIN(PH1(8))*5.882352941
      CALL SYMBOL(F50X,F50Y,0.13,'50',0.,2)
      F100X=O1(21)*COS(PH1(21))*5.882352941
      F100Y=O1(21)*SIN(PH1(21))*5.882352941
      CALL DASH(0.0,0.0,F100X,F100Y,0.5)
      CALL SYMBOL(F100X,F100Y,0.13,'100',0.,3)
      F120X=O1(26)*COS(PH1(26))*5.882352941
      F120Y=O1(26)*SIN(PH1(26))*5.882352941
      CALL SYMBOL(F120X,F120Y,0.13,'120',0.,3)
      F150X=O1(33)*COS(PH1(33))*5.882352941
      F150Y=O1(33)*SIN(PH1(33))*5.882352941
      CALL SYMBOL(F150X,F150Y,0.13,'150',0.,3)
      IF (F(LIMIT+NSTRT).GT.200.0) THEN
      F200X=O1(45)*COS(PH1(45))*5.882352941
```

```
      F200Y=O1(45)*SIN(PH1(45))*5.882352941
      CALL DASH(0.0,0.0,F200X,F200Y,0.5)
      CALL SYMBOL(F200X,F200Y,0.13,'200',0.,3)
      ENDIF
C      IF (F(LIMIT+NSTRT).GT.500.0) THEN
C      F500X=O1(121)*COS(PH1(121))*5.882352941
C      F500Y=O1(121)*SIN(PH1(121))*5.882352941
C      CALL DASH(0.0,0.0,F500X,F500Y,0.5)
C      CALL SYMBOL(F500X,F500Y,0.13,'500',0.,3)
C      ENDIF
800   IF (NFILES.EQ.1) GOTO 30
      CALL NEWPEN(2)
      N=1
C     ** PLOT SECOND TRANSFER FUNCTION
700   CALL POLAR(O2,PH2,LIMIT,1,0,3,0.0,0.17)
      GOTO 701
C                 F12X=O2(1)*COS(PH2(1))*5.882352941
C                 F12Y=O2(1)*SIN(PH2(1))*5.882352941
C                 CALL SYMBOL(F12X,F12Y,0.13,'12',0.,2)
      F20X=O2(1)*COS(PH2(1))*5.882352941
      F20Y=O2(1)*SIN(PH2(1))*5.882352941
      CALL DASH(0.0,0.0,F20X,F20Y,0.5)
      CALL SYMBOL(F20X,F20Y,0.13,'20',0.,2)
      F50X=O2(8)*COS(PH2(8))*5.882352941
      F50Y=O2(8)*SIN(PH2(8))*5.882352941
      CALL SYMBOL(F50X,F50Y,0.13,'50',0.,2)
      F100X=O2(21)*COS(PH2(21))*5.882352941
      F100Y=O2(21)*SIN(PH2(21))*5.882352941
      CALL DASH(0.0,0.0,F100X,F100Y,0.5)
      CALL SYMBOL(F100X,F100Y,0.13,'100',0.,3)
      F120X=O2(26)*COS(PH2(26))*5.882352941
      F120Y=O2(26)*SIN(PH2(26))*5.882352941
      CALL SYMBOL(F120X,F120Y,0.13,'120',0.,3)
      F150X=O2(33)*COS(PH2(33))*5.882352941
      F150Y=O2(33)*SIN(PH2(33))*5.882352941
      CALL SYMBOL(F150X,F150Y,0.13,'150',0.,3)
      IF (F(LIMIT+NSTRT).GT.200.0) THEN
      F200X=O2(45)*COS(PH2(45))*5.882352941
      F200Y=O2(45)*SIN(PH2(45))*5.882352941
      CALL DASH(0.0,0.0,F200X,F200Y,0.5)
      CALL SYMBOL(F200X,F200Y,0.13,'200',0.,3)
      ENDIF
C      IF (F(LIMIT+NSTRT).GT.500.0) THEN
C      F500X=O2(121)*COS(PH2(121))*5.882352941
C      F500Y=O2(121)*SIN(PH2(121))*5.882352941
C      CALL DASH(0.0,0.0,F500X,F500Y,0.5)
C      CALL SYMBOL(F500X,F500Y,0.13,'500',0.,3)
C      ENDIF
      IF (N.EQ.3) GOTO 701
      N=N+1
      GOTO 700
701   IF (NFILES.EQ.2) GOTO 30
      CALL NEWPEN(5)
C     ** PLOT THIRD TRANSFER FUNCTION
      CALL POLAR(O3,PH3,LIMIT,1,0,3,0.0,0.17)
      GOTO 702
C                   F12X=O3(1)*COS(PH3(1))*5.882352941
C                   F12Y=O3(1)*SIN(PH3(1))*5.882352941
C                   CALL SYMBOL(F12X,F12Y,0.13,'12',0.,2)
      F20X=O3(1)*COS(PH3(1))*5.882352941
```

```
      F20Y=O3(1)*SIN(PH3(1))*5.882352941
      CALL DASH(0.0,0.0,F20X,F20Y,0.5)
      CALL SYMBOL(F20X,F20Y,0.13,'20',0.,2)
      F50X=O3(8)*COS(PH3(8))*5.882352941
      F50Y=O3(8)*SIN(PH3(8))*5.882352941
      CALL SYMBOL(F50X,F50Y,0.13,'50',0.,2)
      F100X=O3(21)*COS(PH3(21))*5.882352941
      F100Y=O3(21)*SIN(PH3(21))*5.882352941
      CALL DASH(0.0,0.0,F100X,F100Y,0.5)
      CALL SYMBOL(F100X,F100Y,0.13,'100',0.,3)
      F120X=O3(26)*COS(PH3(26))*5.882352941
      F120Y=O3(26)*SIN(PH3(26))*5.882352941
      CALL SYMBOL(F120X,F120Y,0.13,'120',0.,3)
      F150X=O3(33)*COS(PH3(33))*5.882352941
      F150Y=O3(33)*SIN(PH3(33))*5.882352941
      CALL SYMBOL(F150X,F150Y,0.13,'150',0.,3)
      IF (F(LIMIT+NSTRT).GT.200.0) THEN
      F200X=O3(45)*COS(PH3(45))*5.882352941
      F200Y=O3(45)*SIN(PH3(45))*5.882352941
      CALL DASH(0.0,0.0,F200X,F200Y,0.5)
      CALL SYMBOL(F200X,F200Y,0.13,'200',0.,3)
      ENDIF
C      IF (F(LIMIT+NSTRT).GT.500.0) THEN
C      F500X=O3(121)*COS(PH3(121))*5.882352941
C      F500Y=O3(121)*SIN(PH3(121))*5.882352941
C      CALL DASH(0.0,0.0,F500X,F500Y,0.5)
C      CALL SYMBOL(F500X,F500Y,0.13,'500',0.,3)
C      ENDIF
702   IF (NFILES.EQ.3) GOTO 30
      CALL NEWPEN(6)
      N=1
C     ** PLOT FOURTH TRANSFER FUNCTION
705   CALL POLAR(O4,PH4,LIMIT,1,0,3,0.0,0.17)
C                    F12X=O4(1)*COS(PH4(1))*5.882352941
C                    F12Y=O4(1)*SIN(PH4(1))*5.882352941
C                    CALL SYMBOL(F12X,F12Y,0.13,'12',0.,2)
       GOTO 30
      F20X=O4(1)*COS(PH4(1))*5.882352941
      F20Y=O4(1)*SIN(PH4(1))*5.882352941
      CALL DASH(0.0,0.0,F20X,F20Y,0.5)
      CALL SYMBOL(F20X,F20Y,0.13,'20',0.,2)
      F50X=O4(8)*COS(PH4(8))*5.882352941
      F50Y=O4(8)*SIN(PH4(8))*5.882352941
      CALL SYMBOL(F50X,F50Y,0.13,'50',0.,2)
      F100X=O4(21)*COS(PH4(21))*5.882352941
      F100Y=O4(21)*SIN(PH4(21))*5.882352941
      CALL DASH(0.0,0.0,F100X,F100Y,0.5)
      CALL SYMBOL(F100X,F100Y,0.13,'100',0.,3)
      F120X=O4(26)*COS(PH4(26))*5.882352941
      F120Y=O4(26)*SIN(PH4(26))*5.882352941
      CALL SYMBOL(F120X,F120Y,0.13,'120',0.,3)
      F150X=O4(33)*COS(PH4(33))*5.882352941
      F150Y=O4(33)*SIN(PH4(33))*5.882352941
      CALL SYMBOL(F150X,F150Y,0.13,'150',0.,3)
      IF (F(LIMIT+NSTRT).GT.200.0) THEN
      F200X=O4(45)*COS(PH4(45))*5.882352941
      F200Y=O4(45)*SIN(PH4(45))*5.882352941
      CALL DASH(0.0,0.0,F200X,F200Y,0.5)
      CALL SYMBOL(F200X,F200Y,0.13,'200',0.,3)
      ENDIF
```

```
C        IF (F(LIMIT+NSTRT).GT.500.0) THEN
C        F500X=O4(121)*COS(PH4(121))*5.882352941
C        F500Y=O4(121)*SIN(PH4(121))*5.882352941
C        CALL DASH(0.0,0.0,F500X,F500Y,0.5)
C        CALL SYMBOL(F500X,F500Y,0.13,'500',0.,3)
C        ENDIF
        IF (N.EQ.3) GOTO 30
        N=N+1
        GOTO 705
30      CALL ENDPLT
        GOTO  855
        END
C       ******************************************
C       ** CONVERT TRANSFER FUNCTION TO MAGNITUDE AND PHASE
        SUBROUTINE MAGPHASE (A,PI,LIMIT)
        COMPLEX*8 A(500)
        REAL*4 M(500),P(500)
        DEG=180.0/PI
        DO 5 K=1,LIMIT
        DBLA=IMAG(A(K))
        DBLB=REAL(A(K))
C       ** MAGNITUDE **
        M(K)=ABS(A(K))
C       ** PHASE **
        IF(DBLA.EQ.0.0.AND.DBLB.EQ.0.0) THEN
        P(K)=0.0
        GOTO 10
        ENDIF
        P(K)=ATAN2(DBLA,DBLB)
C         P(K)=P(K)*DEG
        IF(K.EQ.1) P(K)=0.0
10      A(K)=CMPLX(M(K),P(K))
5       CONTINUE
        RETURN
        END
```

1.5 Matching of Database and Test Waveforms

```
      DIMENSION F(2049),A(5200),B(5200),V(5200),MA(200)
      DIMENSION X(5200),DIFF(200),D(20),DS(200)
      COMPLEX*8 IN(4096),OU(4096),Z(4096)
      COMPLEX*8 FXX(4096),FYY(4096),FXY(4096)
      COMPLEX*8 GXX(4096),GYY(4096),GXY(4096)
      INTEGER*2 NDB(200),JC(200),JCL(200)
      CHARACTER*10 PARAM,KNOWN,ANAME,UNKNOWN,BNAME
      CHARACTER*6 FL
C     ***********************************************
C     THIS PROGRAM MATCHES TEST AND DATABASE WAVEFORMS
C     AS PER FIGURE 4.35
C     ARRAY DEFINITIONS:
C     F()=FREQUENCY
C     A()=INPUT DATABASE FILE
C     B()=INPUT TEST FILE
C     V()=INPUT TEST FILE
C     MA()=MAGNITUDE OF TRANSFER FUNCTION
C     X()=INPUT DATABSE FILE
C     DIFF()=DIFFERENCE BETWEEN 1 AND ACTUAL COHERENCE
C     D()=SUM OF 1-COH
C     DS()=NUMERICAL SORT OF 1-COH VALUES
C     IN()=TIME DOMAIN DATA
C     OU()=TIME DOMAIN DATA
C     Z()= TRANSFER FUNCTION
C     FXX()=DATABASE INPUT POWER SPECTRUM
C     FYY()=DATABASE OUTPUT POWER PECTRUM
C     FXY()=DATABASE CROSS SPECTRUM
C     GXX()=TEST INPUT POWER SPECTRUM
C     GYY()=TEST OUTPUT POWER SPECTRUM
C     GXY()=TEST CROSS SPECTRUM
C     NDB()=NUMERICAL SORTING
C     JC()=NUMERICAL SORTING
C     JCL()=NUMERICAL SORTING
C     COMPILE WITH MICROSOFT FORTRAN v.4.01
C     LAST REVISION 09/22/94  @ EDWARD J. HOPPE
C     ***********************************************
      ITF=0
      WRITE(*,*)
      WRITE(*,890)
890   FORMAT(' NAME OF DATABASE SET: '\)
      READ(*,891) KNOWN
891   FORMAT(A)
      WRITE(*,892)
892   FORMAT(' NAME OF TEST SET: '\)
      READ(*,891) UNKNOWN
      WRITE(*,894)
894   FORMAT(' NAME OF PARAMETER FILE: '\)
      READ(*,891) PARAM
      WRITE(*,*)
      OPEN(7,FILE='MATCH',STATUS='UNKNOWN')
C      ** OPEN INPUT SET **
      OPEN(4,FILE=UNKNOWN,STATUS='OLD')
2     OPEN(3,FILE=PARAM)
C     -- INPUT CUT_POINT, +/-CUT, TRIM --
      READ(3,*) NX,IPM,ITM
C     -- INPUT FREQUENCY RANGE
      READ(3,*) FST,FSP
      CLOSE(3,STATUS='KEEP')
      PI=3.141593
      DEG=180.0/PI
```

```
      LN=12
      N=2**LN
      ND2P1=N/2+1
      IDB=0
      INP=0
C       ** READ INPUT FILENAME **
      READ(4,'(A)') BNAME
      IF(BNAME.EQ.'FIN') THEN
      CLOSE(4,STATUS='KEEP')
      CLOSE(7,STATUS='KEEP')
      GOTO 999
      ENDIF
C       ** OPEN INPUT FILE **
      OPEN(2,FILE=BNAME,STATUS='OLD')
      INP=INP+1
      READ(2,*) NPT,TSTEP,XZERO
      TSTEP=(TSTEP/1.333)*1.0E9
      XZERO=(XZERO/1.333)*1.0E9
      READ(2,*) B(1)
      IF(B(1).LT.-1.0) B(1)=0.0
      DO 11 L=2,NPT
      READ(2,*) B(L)
C       IF(B(L).LE.-50.0) B(L)=B(L-1)
11    CONTINUE
      CLOSE(2,STATUS='KEEP')
      CALL MEDIAN(B,NPT)
      WRITE(*,*)
      DO 12 L=1,NX
      V(L)=B(L)
12    CONTINUE
      N1=NX+ITM
      N2=NX+NX
      N3=NX-ITM
      DO 15 L=N1+1,N2
      B(L-N1)=2.0*B(L)
15    CONTINUE
      DO 16 L=ITM+1,NX
      V(L-ITM)=V(L)
16    CONTINUE
      DO 17 L=2,N3
      B(L)=B(L)-B(1)
      V(L)=V(L)-V(1)
17    CONTINUE
      B(1)=0.0
      V(1)=0.0
      DO 171 L=1,N3
      X(L)=V(L)
171   CONTINUE
      CALL TAIL(B,NX,ITM,PI,N)
      CALL TAIL(V,NX,ITM,PI,N)
C     ** V=INPUT ; B=OUTPUT **
      DO 22 L=1,N
      IN(L)=CMPLX(V(L))
      OU(L)=CMPLX(B(L))
22    CONTINUE
      FSTEP=(1.0/(FLOAT(N)*TSTEP*1.0E-9))/1.0E6
      IST=-1
      ISP=-1
      IF(FST.EQ.0.0) IST=1
      F(1)=0.0
```

```
      DO 25 L=2,ND2P1
      F(L)=F(L-1)+FSTEP
      IF(IST.EQ.-1.AND.F(L).GE.FST) THEN
      IST=L
      FST=F(L)
      ENDIF
      IF(ISP.EQ.-1.AND.F(L).GE.FSP) THEN
      ISP=L
      FSP=F(L)
      ENDIF
25    CONTINUE
      CALL FFT(IN,LN,PI)
      CALL FFT(OU,LN,PI)
      DO 30 L=1,ND2P1
      IF (F(L).GT.FSP) GOTO 45
      Z(L)=OU(L)/IN(L)
      GXX(L)=CONJG(IN(L))*IN(L)
      GYY(L)=CONJG(OU(L))*OU(L)
      GXY(L)=CONJG(IN(L))*OU(L)
30    CONTINUE
C      ** OPEN DATABASE SET **
45    OPEN(5,FILE=KNOWN,STATUS='OLD')
1     IDB=IDB+1
      OPEN(10,FILE='TMP',STATUS='UNKNOWN')
      IF=100+IDB
      JF=200+INP
      WRITE(10,903) IF,JF
      CLOSE(10,STATUS='KEEP')
C      ** READ DATABASE FILENAME **
      READ(5,'(A)') ANAME
      IF(ANAME.EQ.'FIN') GOTO 200
C      ** OPEN DATABASE FILE **
      OPEN(1,FILE=ANAME,STATUS='OLD')
      WRITE(*,*) ANAME,BNAME
      READ(1,*) NPT,TSTEP,XZERO
      TSTEP=(TSTEP/1.333)*1.0E9
      XZERO=(XZERO/1.333)*1.0E9
      READ(1,*) A(1)
      IF(A(1).LT.-1.0) A(1)=0.0
      DO 10 L=2,NPT
      READ(1,*) A(L)
C      IF(A(L).LE.-50.0) A(L)=A(L-1)
10    CONTINUE
      CLOSE(1,STATUS='KEEP')
      CALL MEDIAN(A,NPT)
      IK=0
      DO 100 K=ITM-IPM,ITM+IPM
      IK=IK+1
      DO 50 L=1+K,N3+K
      V(L-K)=A(L)
50    CONTINUE
      SUM=0.0
      DO 55 L=1,N3
      SUM=SUM+(V(L)-X(L))**2
55    CONTINUE
      DIFF(IK)=SUM
100   CONTINUE
      SMALL=1.0E6
      DO 110 L=1,IK
      SMALL=MIN(SMALL,DIFF(L))
```

```
110     CONTINUE
        DO 112 L=1,IK
        IF(SMALL.EQ.DIFF(L)) THEN
        J=NX-IPM+L-1
        ITJ=ITM+(J-NX)
        GOTO 114
        ENDIF
112     CONTINUE
114     WRITE(*,*) ' OPTIMUM DATABASE WAVEFORM CUT_POINT '
        WRITE(*,*) J
        WRITE(*,*) ' OPTIMUM DATABASE WAVEFORM PRETRIGGER TRIM '
        WRITE(*,*) ITJ
        WRITE(*,*)
        DO 115 L=1,J
        V(L)=A(L)
115     CONTINUE
        N1=J+ITJ
        N2=J+J
        DO 56 L=N1+1,N2
        B(L-N1)=2.0*A(L)
56      CONTINUE
        DO 57 L=ITJ+1,J
        V(L-ITJ)=V(L)
57      CONTINUE
        DO 58 L=2,J-ITJ
        B(L)=B(L)-B(1)
        V(L)=V(L)-V(1)
58      CONTINUE
        B(1)=0.0
        V(1)=0.0
        CALL TAIL(B,J,ITJ,PI,N)
        CALL TAIL(V,J,ITJ,PI,N)
C       PERFORM FFT: IN=INPUT_FFT ; OU=OUTPUT_FFT
        DO 60 L=1,N
        IN(L)=CMPLX(V(L))
        OU(L)=CMPLX(B(L))
60      CONTINUE
        CALL FFT(IN,LN,PI)
        CALL FFT(OU,LN,PI)
        OPEN(10,FILE='TMP',STATUS='OLD')
        READ(10,891) FL
        CLOSE(10,STATUS='DELETE')
C       ** .TF = TRANSFER FUNCTIOM
C       ** .PS = POWER SPECTRUM
C       ** .CS = CROSS SPECTRUM
C       ** .COH = COHERENCE
        OPEN(10,FILE=FL//'.TF',STATUS='UNKNOWN')
        OPEN(11,FILE=FL//'.PS',STATUS='UNKNOWN')
        OPEN(12,FILE=FL//'.CS',STATUS='UNKNOWN')
        OPEN(13,FILE=FL//'.COH',STATUS='UNKNOWN')
        DO 62 L=1,ND2P1
        IF (F(L).GT.FSP) GOTO 70
        ZIN=Z(L)
        Z(L)=OU(L)/IN(L)
C        Z(L)=(CMPLX(1.0,0.0)+Z(L))/(CMPLX(1.0,0.0)-Z(L))
C        MA(L)=ABS(Z(L))
        FXX(L)=GXX(L)+CONJG(IN(L))*IN(L)
        FYY(L)=GYY(L)+CONJG(OU(L))*OU(L)
        FXY(L)=GXY(L)+CONJG(IN(L))*OU(L)
        MA(L)=REAL(ABS(FXY(L))**2/(FXX(L)*FYY(L)))
```

```
      WRITE(10,902) F(L),ABS(Z(L)),ATAN2(IMAG(Z(L)),
     + REAL(Z(L))),ABS(ZIN),ATAN2(IMAG(ZIN),REAL(ZIN))
      WRITE(11,901) F(L),REAL(FXX(L)),REAL(FYY(L))
      WRITE(12,901) F(L),FXY(L)
      WRITE(13,901) F(L),MA(L)
62    CONTINUE
70    CLOSE(10,STATUS='KEEP')
      CLOSE(11,STATUS='KEEP')
      CLOSE(12,STATUS='KEEP')
      CLOSE(13,STATUS='KEEP')
      SUM=0.0
      DO 575 L=IST,ISP
      SUM=SUM+(1.0-MA(L))
575   CONTINUE
      WRITE(*,*) ' SUM [1-COH(I)]'
      WRITE(*,*) SUM
      WRITE(*,*)
      D(IDB)=SUM
      JC(IDB)=J
      GOTO 1
200   CLOSE(5,STATUS='KEEP')
      IF(ITF.EQ.1) GOTO 202
      WRITE(7,915)
      WRITE(7,917)
917   FORMAT(' C O N T A M I N A N T    M A T C H')
      WRITE(7,915)
      WRITE(7,*)
      WRITE(7,920) ' MIN. FREQ.  : ',FST
      WRITE(7,920) ' MAX. FREQ.  : ',FSP
      WRITE(7,*)
      WRITE(7,915)
      WRITE(7,918)
      WRITE(7,919)
918   FORMAT(' RANK  DATABASE  TEST      SUMMATION    OPT._DB._WFM')
919   FORMAT('       WAVEFORM  WAVEFORM  [1-COH^2(I)]   CUT_POINT')
      WRITE(7,916)
      WRITE(7,*)
      ITF=1
202   WRITE(*,915)
      WRITE(*,917)
      WRITE(*,915)
      WRITE(*,*)
      WRITE(*,920) ' MIN. FREQ.  : ',FST
      WRITE(*,920) ' MAX. FREQ.  : ',FSP
      WRITE(*,*)
      WRITE(*,915)
      WRITE(*,918)
      WRITE(*,919)
      WRITE(*,916)
      WRITE(*,*)
      DO 161 N=1,IDB-1
      SMALL=1.0E6
      DO 163 L=1,IDB-1
      SMALL=MIN(SMALL,D(L))
163   CONTINUE
      DS(N)=SMALL
      DO 165 L=1,IDB-1
      IF(D(L).EQ.SMALL) THEN
      NDB(N)=L
      JCL(N)=JC(L)
```

```
      D(L)=1.0E6
      ENDIF
165   CONTINUE
161   CONTINUE
      DO 175 N=1,IDB-1
      OPEN(5,FILE=KNOWN,STATUS='OLD')
      DO 170 L=1,IDB-1
      READ(5,'(A)') ANAME
      IF(NDB(N).EQ.L) THEN
      WRITE(*,908) N,ANAME,BNAME,DS(N),JCL(N)
      WRITE(7,908) N,ANAME,BNAME,DS(N),JCL(N)
      ENDIF
170   CONTINUE
      CLOSE(5,STATUS='KEEP')
175   CONTINUE
      WRITE(7,916)
      WRITE(*,915)
      WRITE(*,*)
      GOTO 2
901   FORMAT(1F25.15,3X,2(1F25.15,3X))
902   FORMAT(1F10.2,2X,6(1F8.5,2X))
903   FORMAT(2(I3))
908   FORMAT(1X,I4,2X,A10,1X,A10,1F10.4,4X,I6)
915   FORMAT(' ******************************************************')
916   FORMAT(' ======================================================')
920   FORMAT(1X,A15,1F6.2)
999   END
C     ****************************************************
C     ****************************************************
C     ** COSINE TAIL APPLICATION
      SUBROUTINE TAIL (F,NX,ITM,PI,N)
      REAL*4 F(4096),A,PI
      IX=NX-ITM
      M=INT(0.70*IX)
      I=(IX-M)*2
      K=(IX-M)-1
      DO 10 L=M,IX
      K=K+1
      A=0.5*(1.0-COS(2.0*PI*FLOAT(K)/FLOAT(I)))
      F(L)=F(L)*A
10    CONTINUE
      DO 20 L=IX+1,N
      F(L)=F(IX)
20    CONTINUE
      RETURN
      END
C     *****************************************
C     ** FAST FOURIER TRANSFORM
      SUBROUTINE FFT (F,LN,PI)
      REAL*4 PI,X
      COMPLEX*8 F(4096),U,W,T
      N=2**LN
      NV2=N/2
      NM1=N-1
      J=1
      DO 3 I=1,NM1
         IF(I.GE.J) GOTO 1
         T=F(J)
         F(J)=F(I)
         F(I)=T
```

```
1          K=NV2
2          IF(K.GE.J) GOTO 3
           J=J-K
           K=K/2
           GOTO 2
3          J=J+K
       DO 5 L=1,LN
          LE=2**L
          LE1=LE/2
          U=CMPLX(1.0,0.0)
          X=PI/FLOAT(LE1)
          W=CMPLX(COS(X),-SIN(X))
          DO 5 J=1,LE1
             DO 4 I=J,N,LE
                IP=I+LE1
                T=F(IP)*U
                F(IP)=F(I)-T
4               F(I)=F(I)+T
5            U=U*W
       DO 6 I=1,N
       F(I)=F(I)/FLOAT(N)
6      CONTINUE
       RETURN
       END
C      *****************************************
C      ** MEDIAN FILTERING
       SUBROUTINE MEDIAN(A,NPT)
       REAL*4 A(5200),D(25),SMALL
       REAL*4 B(5200)
       DO 10 L=13,NPT-12
       M=1
       DO 15 I=L-12,L+12
       D(M)=A(I)
       M=M+1
15     CONTINUE
       DO 20 K=1,13
       SMALL=1.0E10
       DO 30 M=1,25
       SMALL=AMIN1(SMALL,D(M))
30     CONTINUE
       DO 17 M=1,25
       IF(D(M).EQ.SMALL) THEN
       D(M)=1.0E10
       GOTO 20
       ENDIF
17     CONTINUE
20     CONTINUE
       B(L)=SMALL
10     CONTINUE
       DO 50 L=1,12
       B(L)=B(13)
50     CONTINUE
       DO 655 L=NPT-11,NPT
       B(L)=B(NPT-12)
655     CONTINUE
       DO 60 L=1,NPT
       A(L)=B(L)
60     CONTINUE
       RETURN
       END
```

APPENDIX 2

Previously Published Material

National Research Council Canada
Conseil national de recherches Canada

Canada

Reprinted from

Réimpression de la

Canadian Geotechnical Journal

Revue canadienne de géotechnique

Application of electric polarization to contaminant detection in soils

RAYMOND N. YONG AND EDWARD J. HOPPE

Volume 26 • Number 4 • 1989

Pages 536–550

Printed in Canada / Imprimé au Canada

Application of electric polarization to contaminant detection in soils

RAYMOND N. YONG AND EDWARD J. HOPPE
Geotechnical Research Centre, McGill University, Montréal, Que., Canada H3A 2K6

Received November 24, 1988
Accepted April 18, 1989

Preliminary experiments indicate the feasibility of constructing for field use a contaminant-detection instrumentation based on dielectric measurements. This study applies the technique of time-domain reflectometry to assess characteristic "signatures" of some selected contaminants and soil-contaminant mixtures. The results imply that a proper differentiation between various signatures can be attained, allowing an assessment in regard to soil-contaminant status. The proposed technique is similar in principle to the induced-polarization method applied in mineral exploration.

Key words: electric polarization, contaminant transport, dielectrics, induced polarization, nonpolar liquids, time-domain reflectometry, relaxation, contaminant-soil interaction.

Des expériences préliminaires indiquent la faisabilité de la construction d'une instrumentation pour la détection de contaminants sur le terrain basée sur les mesures diélectriques. Cette étude utilise la technique de reflectométrie à plage temporelle pour évaluer les « signatures » caractéristiques de contaminants sélectionnés et de mélanges sol-contaminant. Les résultats impliquent que l'on peut obtenir une différentiation entre les diverses signatures suffisante pour permettre une évaluation quant à l'état du sol-contaminant. La technique suggérée est en principe semblable à la méthode de polarisation induite utilisée pour l'exploration minière.

Mots clés : polarisation électrique, transport de contaminant, diélectriques, polarisation induite, liquides non polaires, réflectométrie à plage temporelle, relaxation, interaction sol-contaminant.

[Traduit par la revue]

Can. Geotech. J. 26, 536-550 (1989)

Introduction

In the last decade, mounting environmental concerns have forced governments of the United States and Canada to pass a series of regulatory legislations, aimed at protecting the groundwater supply. These actions have resulted in a substantial decrease of waste water discharges into lakes and streams, but the use of land as a major repository of hazardous waste still continues. According to the United States Environmental Protection Agency, American industry produces approximately 35 million metric tons of toxic waste each year (Waller and Davis 1984). Much of this waste is disposed in land impoundments contained within man-made or natural materials, such as synthetic and clay liners. The single, most important requirement for these liners is that they act as barriers to fully contain hazardous wastes or leachates within the disposal site. In many instances, as for example in the Province of Quebec, Canada, the use of clay liners as barriers has become a mandatory requirement on all newly constructed landfill sites (ministère de l'Environnement du Québec 1987*a*, *b*).

The use of low-permeability lining materials has been proven an effective method for containment of many types of waste leachates and could benefit from the use of an *in situ* detection technique to monitor the performance of these liners. Current monitoring procedures, which generally rely upon groundwater-quality monitoring or use of suction lysimeters, are not totally satisfactory in pinpointing the location of a liner failure or in evaluating the extent of movement of a contaminant plume in the liner or in the subsurface. Obviously, detection of a plume advance between wells can pose a serious challenge, particularly if the wells are not "properly" placed.

The aim of this study centers on the development of a viable field monitoring technique capable of detecting the advance of a contaminant plume in the substrate soil material. The proposed method involves an application of phenomena associated with the electrical polarization of dielectrics. The measurement of frequency-dependent electrical properties of a contaminated soil can provide a characteristic "signature" sufficiently different from that of an uncontaminated soil to permit detection of a plume advance.

Before providing an accounting of the development of the technique and of the obtained results, it is useful to review the dielectric behaviour of materials and stress its relevance to the problem at hand.

Theory

In dealing with subsurface contamination, it is informative to relate the level of soil contamination to the change in electrical properties of the soil. These properties may be substantially affected by the introduction of liquid contaminant into the soil pores. In the initial approach to the problem, it is common to resort to a dc resistivity survey *in situ*. This method can provide a quick and inexpensive way of locating a subsurface contamination, provided that the geological cross section is fairly uniform. In areas of complex lithology, however, such an approach cannot readily discern between the resistivity of a particular soil type and that of a pore fluid. In fact, a variety of chemically different materials exhibit essentially similar dc resistivities. To address this lack of selectivity, one may consider monitoring the resistivity not only at zero frequency (dc) but also over a very wide range of electrical frequencies. From the measurement standpoint, contaminated soils can be regarded as dielectric materials, with characteristic resistivities and dielectric constants influenced by the chemical nature of the contaminant. The problem entails the interaction of these dielectric materials with an electric or a magnetic field.

When a time-dependent voltage $V(t)$ is applied to the dielectric, it causes a charge Q to vary with time, resulting in a flow of current I. Dielectric relaxation concerns the tim-

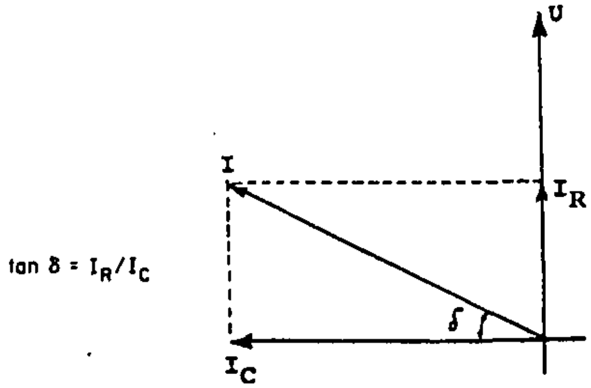

FIG. 1. Phase relationship between voltage (U) and current (I) in a real dielectric. I_R, resistive component of current; I_C, capacitive component of current.

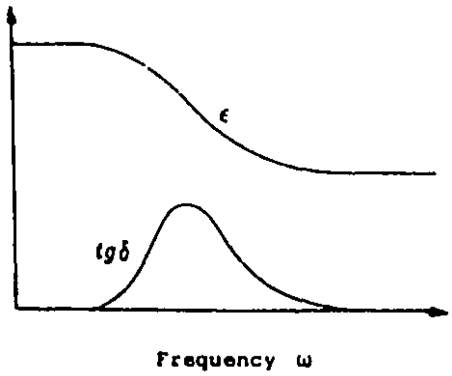

FIG. 2. Idealized frequency dependence of dielectric constant and loss angle (after Gemant 1933).

ing of this electrical response, which reflects the specific relationship between $V(t)$, $Q(t)$, and $I(t)$ for various materials. This relationship applies to a linear system, where a response and a stimulus are proportional to each other. Relaxation constitutes a delayed response to a changing stimulus. The stimulus is usually an electrical field, while $Q(t)$ and $I(t)$ (Daniel 1967) form the response.

The relationship of $V(t)$, $Q(t)$, and $I(t)$ can be considered by an analogy to an electrical circuit consisting of a capacitance C and a resistance R. When a step-function voltage is applied to a capacitor (connected in series with a resistor), the charge rises exponentially form $Q = 0$ at $t = 0$ to a fraction $1/e$ of its final value at a time $\tau = RC$:

$$[1] \quad Q = CV(1 - e^{-t/\tau})$$

The delay time τ is called a "time constant" in electrical engineering and a "relaxation time" in physics and chemistry. The capacitance of the dielectric is equal to the product of the geometrical component C_0 and the dielectric constant ϵ. Dielectric relaxation is the manifestation of a phenomenon whereby the material constant ϵ is variable over a wide range of frequencies. Therefore, the capacitance of a real capacitor actually varies as the time-dependent voltage is imposed on its terminals.

When the excitation voltage is sinusoidal, with a given frequency f, and the recorded response forms a current I, then the phase relationship between these quantities reflects the dielectric properties of the material. In a textbook example of a perfect dielectric placed in an electric field, the current leads the voltage by 90° and no power is being dissipated. At the other extreme, in a conductor, the drift of free electrons forms a conduction current in phase with the applied voltage. It has been documented that in practical dielectric materials there is always a detectable conduction current, which in the case of a good insulator has a very small value (von Hippel 1954). Thus, in real dielectrics the resultant current no longer leads the voltage by 90° but by $(90 - \delta)$, where δ may be called a "loss angle." The greater the value of δ, the greater the power loss in the dielectric (Fig. 1).

There are several mechanisms of polarization that cause a frequency dependence of electrical properties. Contributions to this polarization arise from the displacement of electrons relative to the nucleus of an atom (electronic polarization), the movement of one atomic nucleus relative to another in the same molecule (atomic polarization), the alignment of molecular dipoles in the direction of applied electric field (orientational polarization), and the accumulation of charges at interfaces between materials with different electrical properties.

It has been observed that, due to polarization phenomena, δ is not a constant for a particular material but varies with the frequency. The behaviour of the material can be visualized in terms of a molecular dipole rotating into the direction of the electric field. When the speed of field reversal becomes faster than the rate of dipolar reorientation, rotation of the molecules cannot occur. At this relaxation frequency the material's dielectric constant drops in value, since there are fewer available charges that can be displaced by the electric field. Simultaneously, the loss angle δ increases markedly, signifying a substantial rise in energy dissipation (Fig. 2). The variability of dielectric constant with frequency is known as dispersion. Thus, the time or frequency dependence of the dielectric constant can be used to provide information on the rate of dipolar reorientation in the material. The relaxation frequency is found to be characteristic of the particular polar molecule.

The geophysical technique of induced polarization (IP) detects phenomena primarily associated with interfacial polarization. Recent work suggests that organic chemicals can interfere with the exchange process in clays, permitting direct detection of these organics (Olhoeft 1986). This mechanism has been a subject of particular interest to chemists and molecular physicists performing laboratory studies on material properties.

Generally, polarization can be attributed to a motion of ions, a motion of molecular dipoles, or a motion of electrons in a molecule. The first group of causes occurs at the low end of the spectrum, typically at so-called power frequencies. A dipole action is commonly observable at microwave frequencies, whereas a motion of electrons is associated with optical frequencies. The polarization phenomenon due to ionic displacement was investigated extensively by Maxwell (1854) and Wagner (1913). Credit belongs to Debye (1929) for exploring the mechanism of dipole polarization and to Lorentz (1915) for work on electronic polarization.

In studying the relaxation properties of various materials it is imperative to find a frequency range of interest where the effects are most pronounced. As pointed out by Cole,

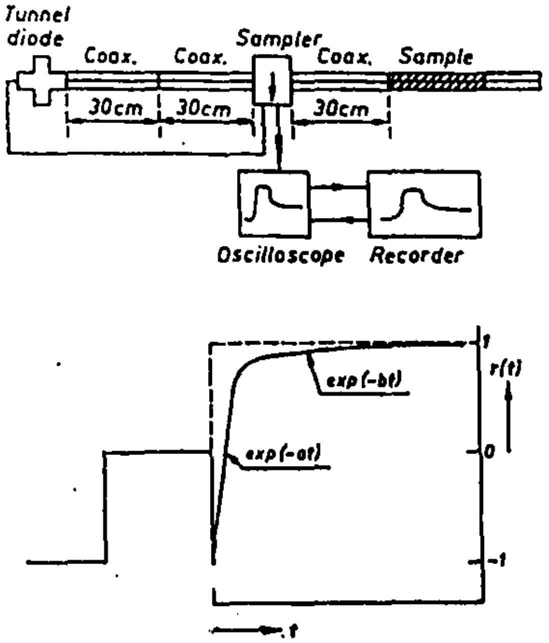

FIG. 3. Typical setup for the TDR method and a schematic form of the step response for a Debye relation; the tunnel diode produces a step impulse (after van Gemert 1973).

this frequency range is often as awkwardly low for solids as it is awkwardly high for liquids. The reason for such disparity is that the charge displacement is much more constrained in a solid matrix than in a liquid. For example, water molecules in a liquid state become aligned with an electric field in about 30 ns (Keller and Frischknecht 1966). The amount of polarization is fairly large, as water exhibits the dielectric constant of 81.5 at low frequencies.

A study conducted by Hoekstra and Delaney (1974) indicates that in geological materials the relationship between water content, conductivity, and dielectric constant is a strong function of the soil type from dc levels up to about 1 MHz. Olhoeft (1987) shows that in clay-water systems, there are significant effects of the clay up to 100 MHz. At higher frequencies the influence of the pore fluid becomes dominant. It is also observed that the frequency of maximum dielectric loss is appreciably lower in a soil-water mixture than in bulk water because of the constraints on charge displacement, attributable to the double layer. It is envisaged that the problem might become more significant in active clay soils where double-layer effects and influences are more pronounced. A study by Bockris *et al.* (1966) indicates that liquid molecules of the double layer are severely restricted in their motion, and their relaxation frequency is lowered. Work involving measurements on packed protein powders with adsorbed water, conducted by Harvey and Hoekstra (1972), reports two distinct relaxation frequencies, corresponding to two layers of adsorbed water.

Available measurement techniques

The traditional four-electrode arrangement used in the IP method is capable of detecting low-frequency relaxations, which are commonly associated with the interfacial polarization. While effective for mineral exploration, this setup is not designed to detect relaxations of orientational polarization occurring in pore fluid. A majority of high-frequency dielectric measurements have been confined to a laboratory environment; however, as with the IP *in situ* technique, the objective of each method of measurement was detection of the electric polarization phenomena. To perform high-frequency measurements, the monitoring circuit must be properly shielded from, for example, inductive coupling in IP between the transmitter and receiver.

To investigate the relaxation pattern of an analyzed material, the dispersion of electric properties of dielectrics is usually evaluated over several decades of frequency. Since the transient technique covers a broad frequency spectrum with a single impulse, it is often judged more expedient than the alternative of performing a multitude of frequency-domain measurements. Many researchers favour the application of a transient method over the "point-by-point" approach required in the frequency domain. A Fourier spectrum of such an impulse contains a wide range of frequencies. A single impulse, applied to a dielectric material, yields a time-domain response. When the Fourier spectra of the input and the response signal are calculated, it is possible to arrive at the same outcome as obtained with the frequency-domain approach. The experimental results are often displayed in the form of a Cole–Cole plot (Cole and Cole 1941).

Following the work of Fellner-Feldegg (1969), pulse transient methods have found a widespread use in the study of fast relaxation processes appearing at microwave frequencies. These methods commonly originate from the field of study called time-domain reflectometry (TDR), developed in electrical engineering. Typically, an electrical impulse with a fast rise time is sent into a coaxial cable. Upon reaching the end of the cable embedded in the analyzed material, the impulse is reflected in a manner indicating the characteristic spectral signature of the sample material (Fig. 3). The reflected signal can range in magnitude from +100% to −100% of the incident signal. These two extremes correspond to conditions of open-circuit and short-circuit resistivity of the sample material. The shape of the wave form at early times is indicative of capacitive properties of the material. In the case of an ideal capacitor terminating the coaxial cable, the reflected wave form drops rapidly to zero potential, before increasing exponentially towards the level of twice the amplitude of the incident wave form. This type of behaviour represents the capacitor's property of being a virtual conductor at high frequencies and behaving like an insulator at a dc level. In the case of a practical dielectric material, the reflected signal does not exhibit a purely exponential rise, because of polarization phenomena and variation in dielectric constant and capacitance. A good review of the application of TDR techniques to soils can be found in Davis *et al.* (1977).

Dielectric relaxation has long been recognized as a powerful tool for analyzing the physical state of a system containing polar molecules or groups. Historically, one of the methods for studying the behaviour of polar molecules has been by measuring the complex dielectric constant $\epsilon(i\omega) = \epsilon'(\omega) - i\epsilon''(\omega)$ over the frequency range of interest. The results are commonly expressed either as a dielectric constant versus frequency graph or as a Cole–Cole plot of a dielectric loss versus dielectric constant. Dielectric spectroscopy covers an unusually wide range of frequencies, from the 10^{-4} Hz to the high GHz region, with geologial materials typically analyzed in the lower end of this spectrum.

Experimental study

In the present study, both time-domain and the frequency-domain approaches were evaluated and the time-domain technique was selected. In time-domain measurement the distribution of high-frequency components of an impulse is dependent on the signal's rise time. Thus, a steeply rising impulse exhibits a wide spectrum.

To assess the practicality of applying a TDR method to contaminant detection, a series of laboratory experiments was conducted. The instrumentation setup is shown in Fig. 4. The main components include the step-function generator, coaxial cable terminated by a probe, digital waveform recorder, and portable computer to analyze the acquired data. The recording device selected was a Tektronix 11402 digitizing oscilloscope that has a bandwidth of 1 GHz. The impulse signal transmitted by the generator is split as it travels past point A. Half of this signal is detected by the digitizing oscilloscope, while the other half reaches the dielectric material at point B, where it is reflected. Because the return signal is also split in half at point A, its amplitude ranges from −50% to +50% of the incident signal.

The step-function generator uses a mercury-wetted contact relay, which delivers reproducible pulses with subnanosecond rise times (Andrews 1973). The step-function generator charges a section of RG 58 coaxial cable, acting as a capacitor, and discharges it through the mercury switch to a low-loss RG 214 cable, where it propagates with minimum distortion.

To simulate field conditions, the length of the RG 214 cable was selected as 7 m. In the field, a probe would be drilled or pushed into the soil and the recording instruments placed at the surface. A substantial length of coaxial cable results in impulse deterioration. The effect of pulse degradation is illustrated in Fig. 5. The attenuation characteristics of the initial signal are compared with those of the signal reflected from point B, measured at point A. In the range of 0–200 MHz the RG 214 coaxial cable does not significantly attenuate the signal. Furthermore, it can be seen that the 200 MHz frequency component exhibits about 40 dB attenuation, which translates into a signal strength of 0.01 of the dc component. This signal level is well within the resolution capability of Tektronix 11402.

The concept of an extended central electrode, surrounded by a dielectric material, borrows from the lumped capacitance method of Iskander and Stuchly (1972). Electrically, the equivalent circuit may be represented by a shunt capacitor terminating the coaxial line. The reflection coefficient Γ for a transmission line of impendance Z_0 terminated by the load impedance Z_l can be expressed as

$$[2]\quad \Gamma = \frac{Z_l - Z_0}{Z_l + Z_0} = \frac{V_{\text{refl}}}{V_{\text{inc}}}$$

In the time domain, the input signal, system response, and output signal are related through the Duhamel convolution integral:

$$[3]\quad y(t) = \int_{-\infty}^{\infty} h(\tau)x(t - \tau)\mathrm{d}\tau$$

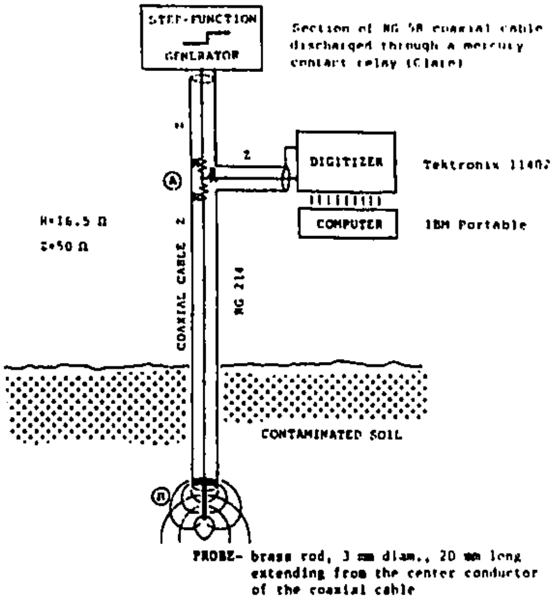

FIG. 4. Experimental setup employed in this study.

In principle, the convolution may be seen as a process of correlating one time series with another that has been reversed in time. The input and the output signals can be transformed into the frequency domain through the use of fast fourier transform (FFT). Subsequently, the transfer function $H(f)$ of a system may be deconvolved by dividing the spectrum of the output by the spectrum of the input waveform:

$$[4]\quad \begin{aligned} Y(f) &= H(f)\cdot X(f) \\ H(f) &= \frac{Y(f)}{X(f)} \end{aligned}$$

What usually needs to be established is how a given system responds to each frequency component of an arbitrary input signal. In a linear, time-invariant system, such a response, referred to as a transfer function, offers a complete circuit characterization (Ramirez 1985). Proper application of the spectral analysis demands that a wave form to be transformed begins and ends at the same amplitude. Steplike wave forms produce a well-known truncation error, if they are directly treated by the FFT algorithm. Several methods addressing this particular problem have been published (e.g., Waldemeyer 1980).

Tests were performed on several arbitrarily chosen "contaminants" and on soil–contaminant mixtures. The soil used to create these mixtures (simulating a typical sandy clay) consisted of 60% Lake Agassiz clay and 40% crushed granodiorite passing sieve No. 50 and retained on sieve No. 16. Samples were prepared with 60 and 40% fluid content, representing fully saturated and unsaturated soil conditions. Table 1 summarizes the chemical composition of fluids used in the experiments.

Lake Agassiz clay was collected from St. Boniface, Manitoba. Its mineral composition, in decreasing order of abundance, is montmorillonite, illite, quartz, kaolinite, feldspar, and dolomite (Yong *et al.* 1986). Based on the saturation extract analysis, the main water-soluble ions were classified as Na^+, Ca^{2+}, HCO_3^-. The predominant extract-

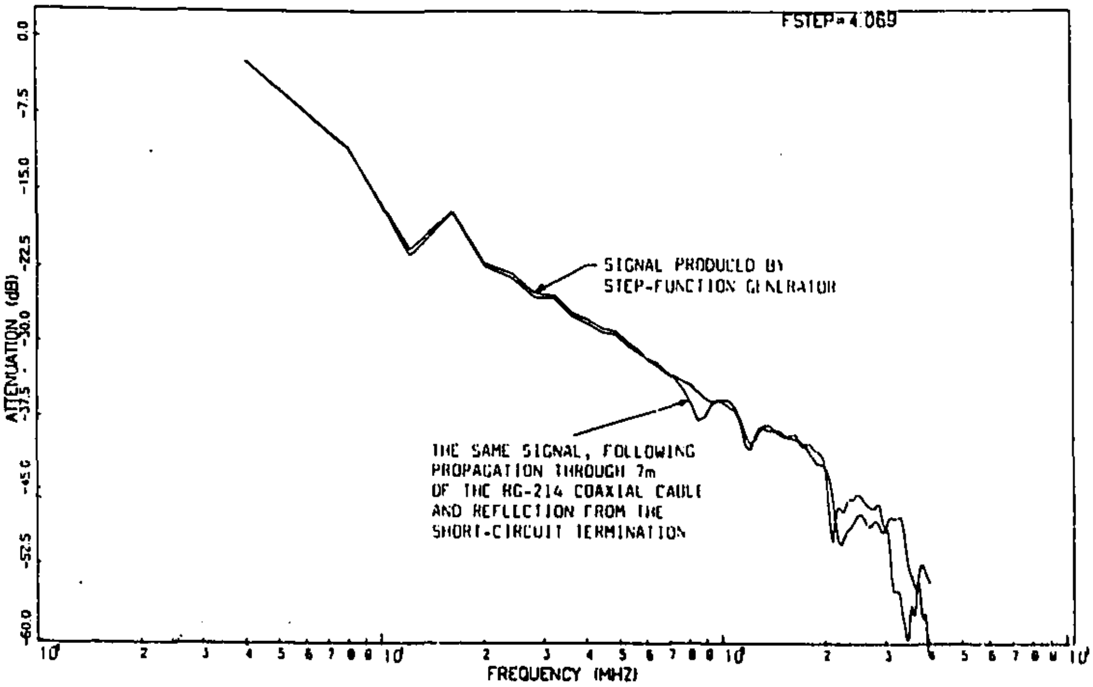

FIG. 5. Effect of pulse propagation through the coaxial cable on the signal attenuation (frequency domain FFT).

TABLE 1. Chemical characteristics of liquids used in experiments

Pollutant	pH	S (mS/m)	Na (ppm)	Ca (ppm)	K (ppm)	Mg (ppm)	Cl^- (meq/L)	CO_3^{2-} (meq/L)	HCO_3^- (meq/L)	SO_4^{2-} (meq/L)	Al^{3+} (ppm)	Cd^{2+} (ppm)	Cr^{2+} (ppm)	Cu^{2+} (ppm)	Fe^{2+} (ppm)	Ni^{2+} (ppm)	Pb^{2+} (ppm)	Zn^{2+} (ppm)
KAH	7.54	23.0	198	54	103	95	15	0	0	0.02	0	0	0	0	0	0	0	0
CEZ	2.73	58.7	0	8	2	148	27	0	1.0	107.0	15	17	0	42	47	0	1	2983
PB	2.11	64.7	340	2	1	0	45	0	2.0	0.10	0	0	0	0	0	0	63	0
H2O	5.24	0.3	1	1	0	0	0	0	3.0	0.16	0	0	0	0	0	0	0	0

NOTES: S, conductivity; KAH, leachate from Kahnawaki landfill site, south of Montréal; CEZ, by-product of zinc production, collected from a factory west of Montréal (diluted to 200 mg/L); PB, laboratory solution of lead chloride; H2O, distilled water. In addition, pure benzene, pure ethanol, and 0.01 N solution of $CaCl_2$ (label: CACL) were used in experiments.

able ion was found to be Ca^{2+} and the cation exchange capacity (CEC) was determined as 71.4 mg/100g. The liquid and plastic limits were 112% and 28% respectively. The crushed granodiorite originated from Cold Springs Quarry in Lac du Bonnet, Manitoba. Its mineralogical composition was found to include quartz (28%), feldspar plagioclase (35%), and microcline (20%).

Experimental results

Time domain

Measurements were performed on contaminants and on soil-contaminant mixtures, prepared 24 h in advance of testing. During the 10 h testing period, no significant scatter in each material's response was observed. Figures 6-8 display the experimental results obtained with a circuit as shown in Fig. 4. Figure 6 shows the wave forms obtained from tests on contaminants themselves, whereas Figs. 7 and 8 portray the wave forms of soils laced with the individual contaminants. Each wave form, sampled at a 40 ps time step, consists of 4220 data points and illustrates the initial voltage step as the impulse reaches the digitizing oscilloscope and a subsequent reflection from the sample material located at the end of the coaxial cable. The time $t = 0$ signifies the triggering point for the wave form acquisition to the digitizer's memory. The negative time range represents pretrigger events. After about 71 ns following the start of incident impulse acquisition, the reflected signal reaches the digitizer. This time lag is governed by the length of cable between the sampling point and the probe.

Data can also be conveniently presented in terms of the load impedance of various dielectric materials. The transformation, based on the relationship between the reflection coefficient and the load impedance ([2]) is shown in Figs. 9-11. These figures portray the time dependence of the load impedance Z_l, departing from the 50 Ω coaxial cable impedance Z_0.

Frequency domain

The relationship between applied signal and observed response is commonly analyzed in the frequency domain. The technique used for processing of time-domain data in this study involves application of a Hanning window to the last 50% of data points. Additional preprocessing of wave forms includes treating data with a smooth, nonrecursive filter, passing the lower one-third of the Nyquist interval (Hamming 1977). Furthermore, 100% zero padding is applied, so that

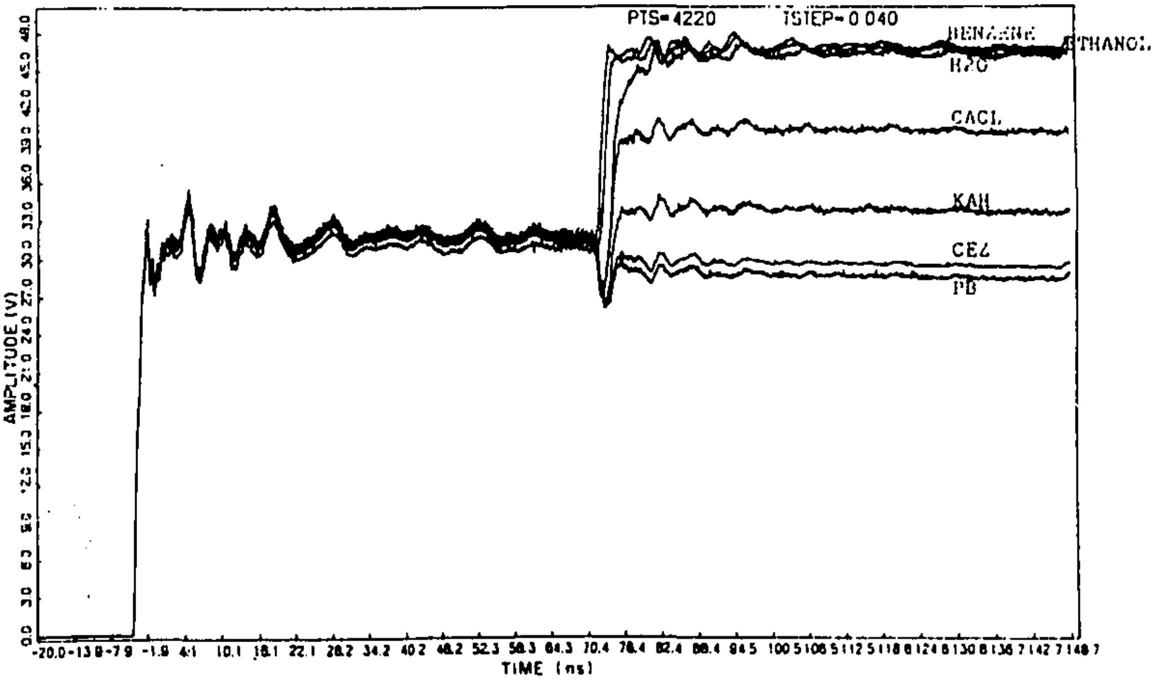

FIG. 6. Time-domain response of various contaminants (time domain).

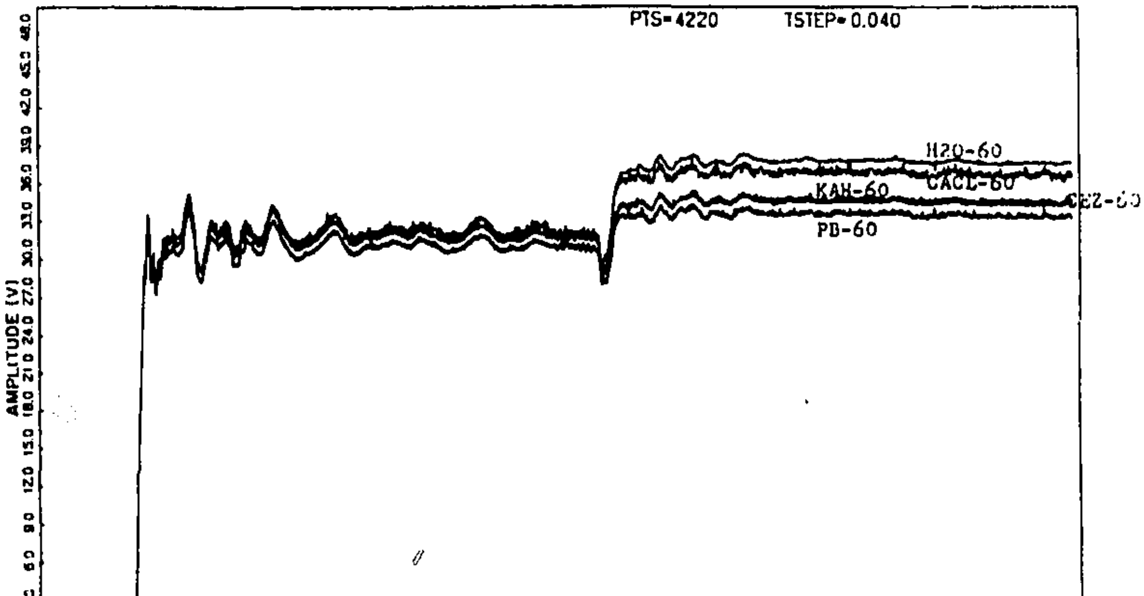

FIG. 7. Time-domain response of soils saturated with contaminants; w = 60%.

the analyzed impulse signal appears to the FFT algorithm as a repetitive wave form. The transfer function or the frequency response, computed by dividing the output wave form by the input in frequency domain, represents the characteristic reflection coefficient for a given dielectric. The spectrum of the input impulse is based on the short-circuit reflection, while the wave form reflected from an analyzed material is taken as an output signal.

Figure 12 illustrates some typical examples of the response to a step-function excitation in a coaxial line terminated by resistance and capacitance. Each time-domain wave form represents a mathematical idealization of the real signal (i.e.,

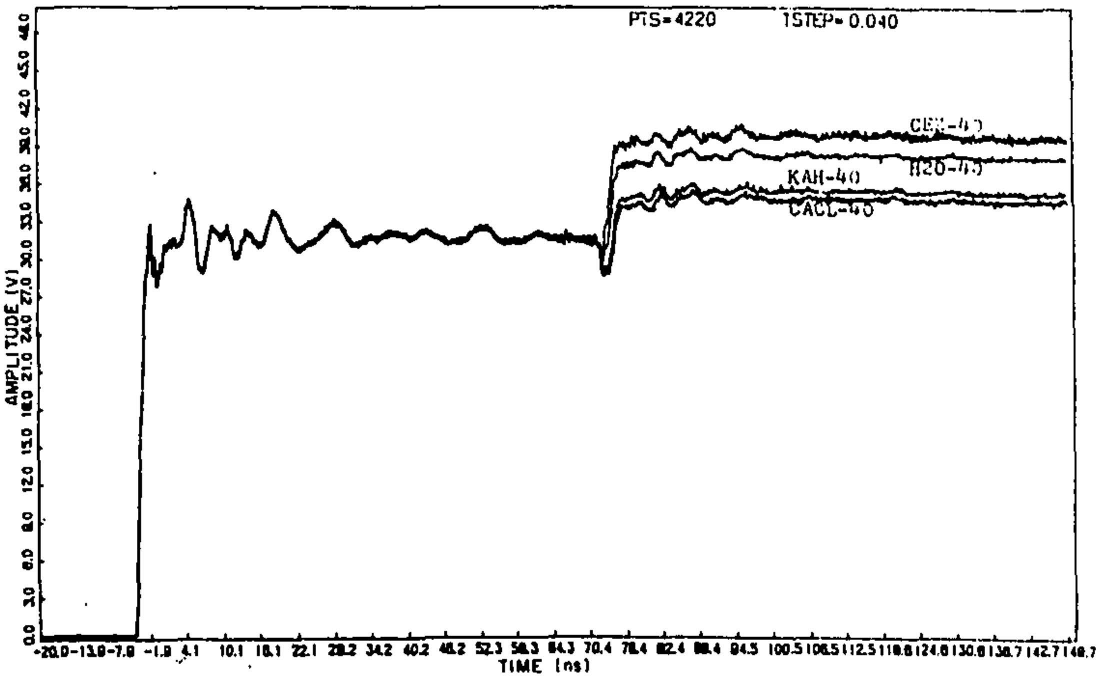

FIG. 8. Time-domain response of soils saturated with contaminants; w = 40%.

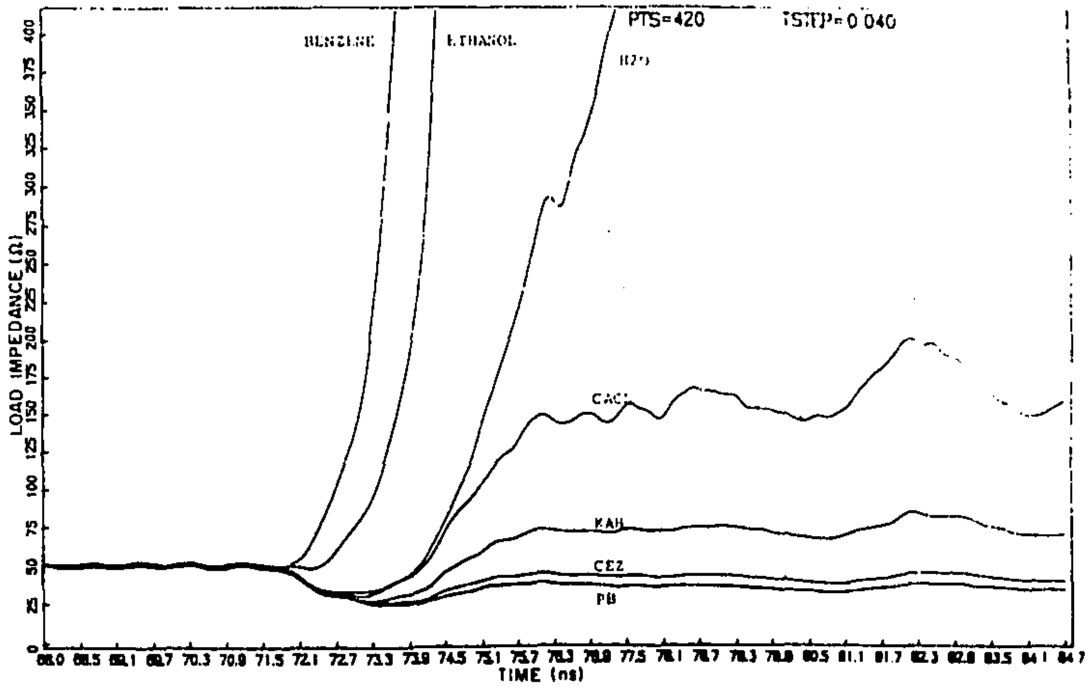

FIG. 9. Load impedance of various contaminants (time domain).

no ripples or distortions), while the corresponding frequency-domain transfer function results from the actual processing technique used in this study. The relationship between the time domain and the frequency domain may be regarded as reciprocal, meaning that at short times the wave form is described by the high-frequency harmonics, while at longer times it is shaped by the low frequencies and a dc component of the impulse. It can be observed that the initial time-domain response of the capacitor corresponds to that of a short circuit ($R = 0$), while in the latter stages it approaches exponentially the behaviour of an open circuit ($R = \infty$). This phenomenon reflects the capacitor's property of con-

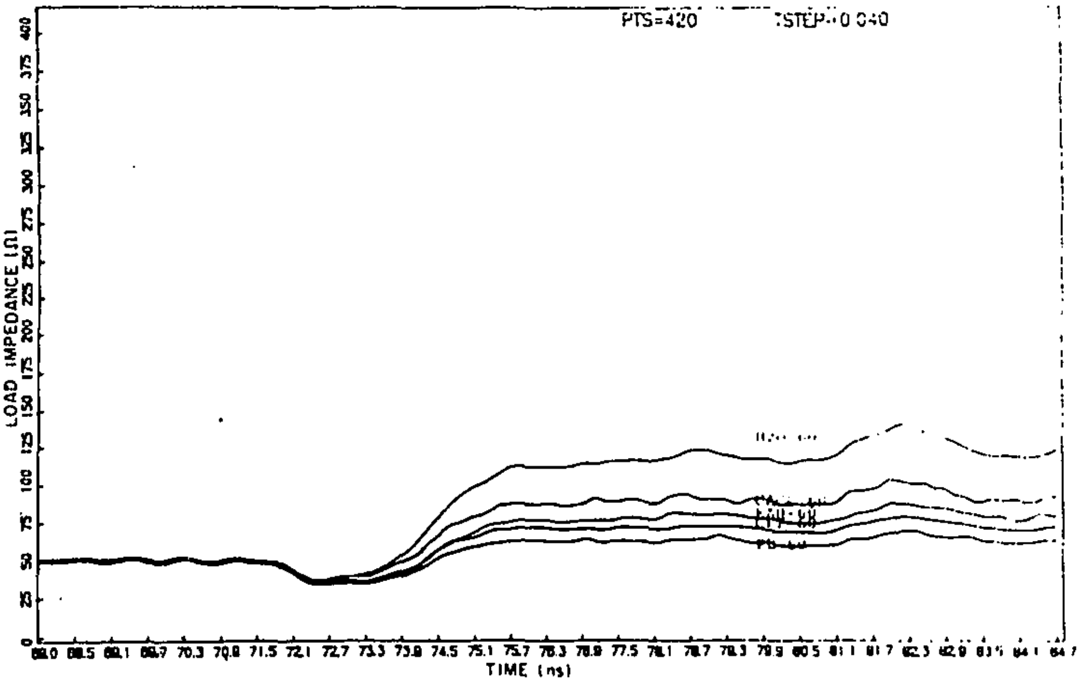

FIG. 10. Load impedance of soils saturated with contaminants (time domain); w = 60%.

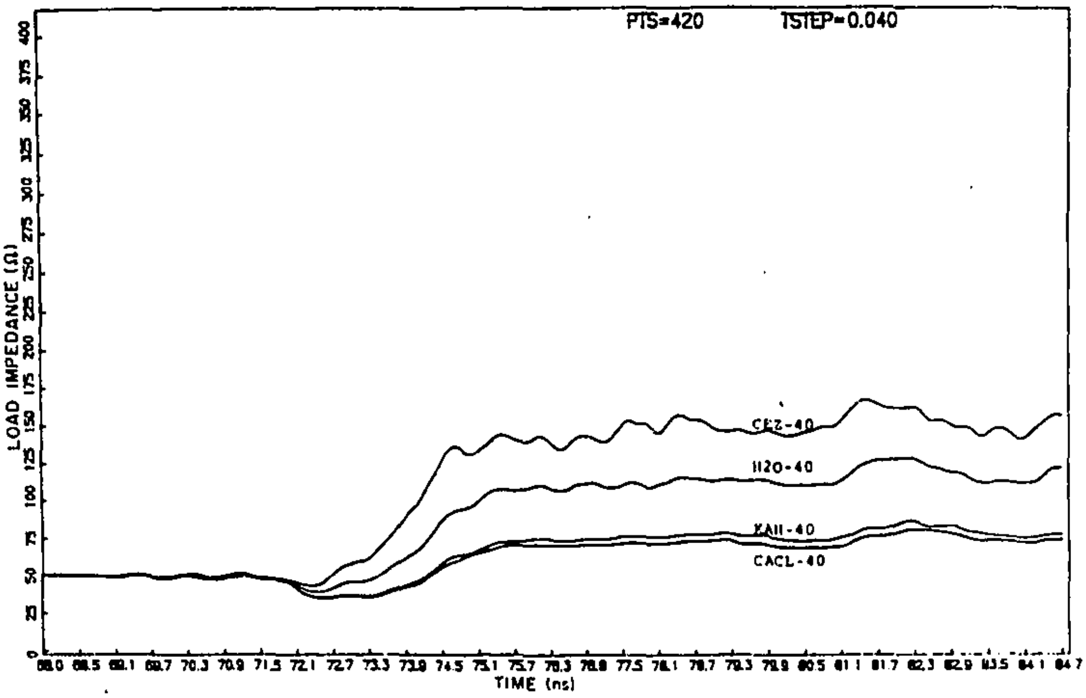

FIG. 11. Load impedance of soils saturated with contaminants (time domain); w = 40%.

ducting at high frequencies while blocking any current at a dc level. Thus, the transfer function of a capacitor indicates a relative phase shift and attenuation of the multitude of frequency components of the applied impulse. By contrast, the resistor transfers all frequencies of the input signal equally, both in magnitude and in phase. In the open-circuit termination (infinite resistance) all frequency components of the output signal appear in phase with the spectrum of the incident signal. In the short-circuit termination (zero resistance) the transfer occurs in antiphase.

A contaminated soil can be viewed as a complex collection of resistors and imperfect capacitors exerting a combined

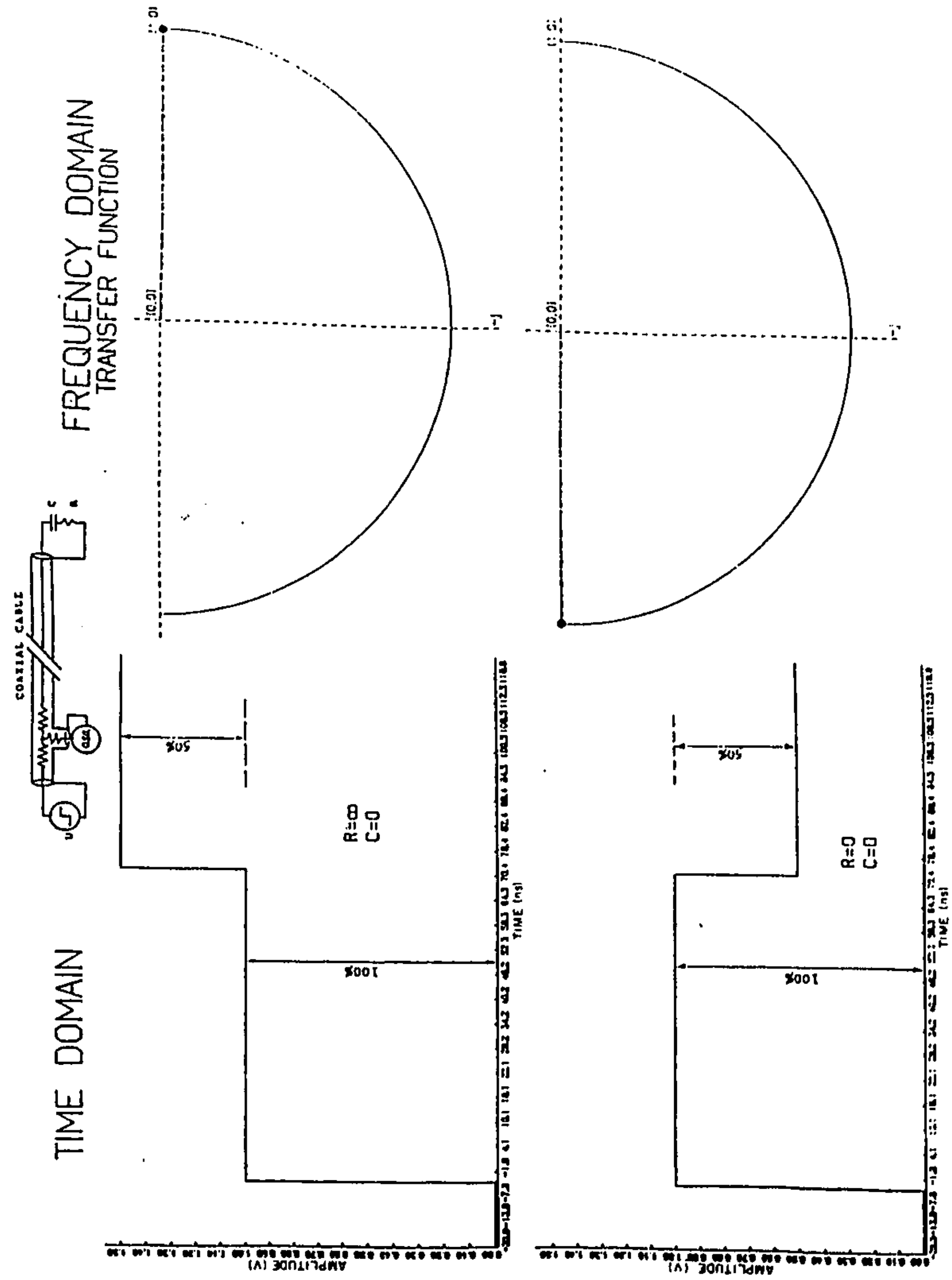

Fig. 12. Examples of the response to a step-function excitation in a circuit consisting of resistance (R) and capacitance (C).

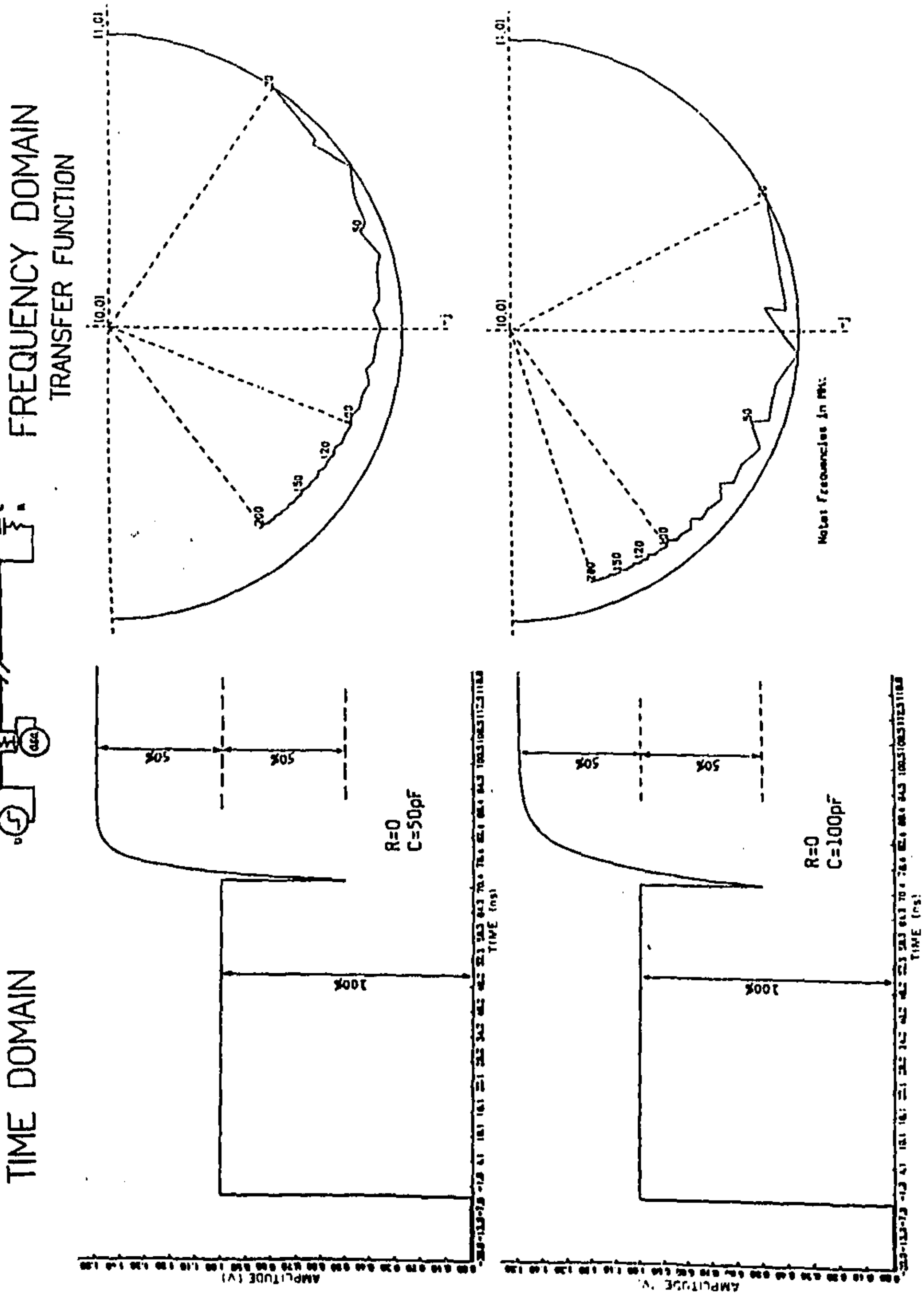

FIG. 12 (*concluded*)

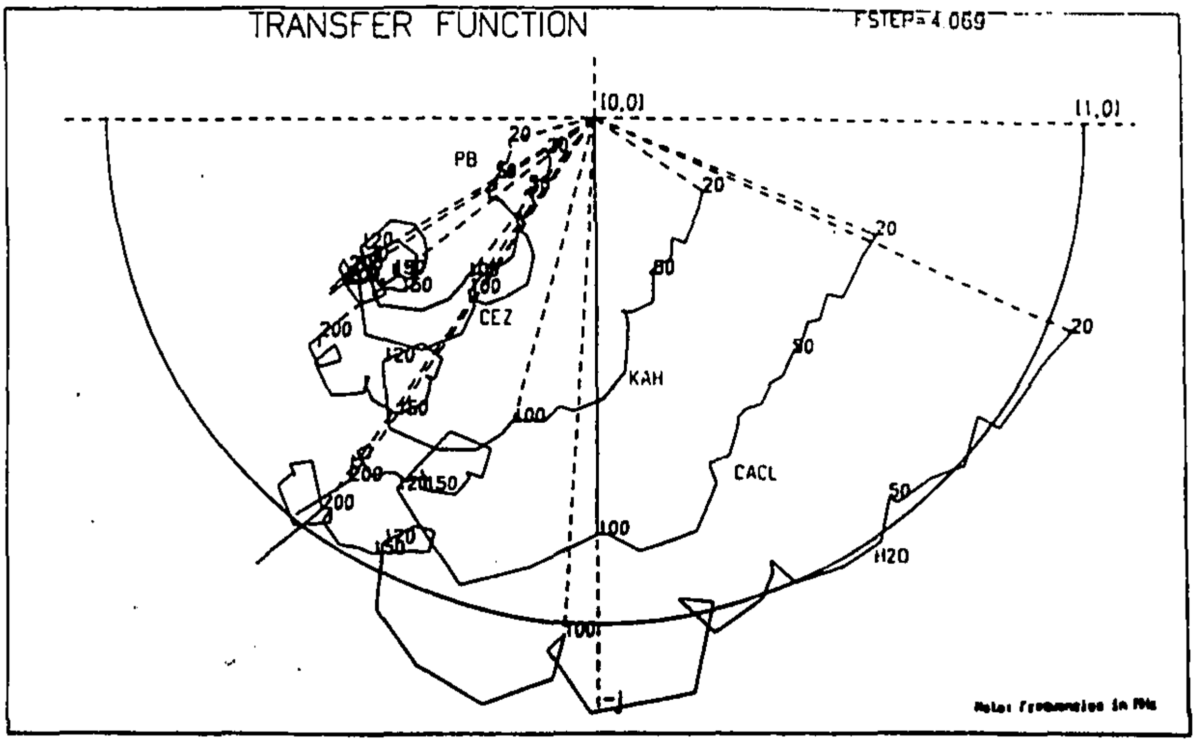

FIG. 13. Frequency response (FFT) of various contaminants.

influence on the overall electrical response. Some representative frequency-domain results are shown in Figs. 13–17. Transfer functions for contaminants and soil–contaminant mixtures are computed in the spectral range of 20–200 MHz, in 4 MHz frequency increments, and are expressed in polar coordinates. The upper limit is governed by the attenuation of the incident impulse in the analyzed material and by the initial spectral composition of the generated signal.

It will be noted that distinct transfer-function signatures can be obtained for the various test cases studied. The exact quantitative determination of individual chemical components cannot be made at this stage; however, it is expected that with a greater variety of test situations, a series of characteristic signatures can be catalogued to permit rapid qualitative analysis.

Discussion

The time-domain relationship, shown in Figs. 6–8, reveals various wave forms as they are acquired by the digitizer. It can be seen that the applied step function is not perfectly rectangular. The initial stage of the incident impulse is affected by ripples, stemming from imperfections in the impulse generator and from unwanted reflections in the measuring circuit. However, the shape of the incident signal, and therefore its spectral composition, remains virtually identical in different tests. The reflected voltage step, commencing at about 71 ns, is characteristic of the material being analyzed. Thus, in nonpolar liquids, such as benzene or ethanol (Fig. 6), the reflected wave form practically mirrors the applied step voltage. A substantial signal attenuation occurs in conductive liquids, such as CEZ or PB (see Table 1 for explanation of terms). The initial dip of the reflected impulse signifies capacitive effects. The latter part of each wave form approaches a steady value, indicative of the DC resistivity. It appears that the transition period between the initial and final amplitude of the reflected signal is not purely exponential, signifying a phenomenon of more complex nature than the charging of an ideal capacitor. This dielectric response is most predominant in the first 4 ns of the reflected wave form.

Graphs displaying the load impedance of various materials (Figs. 9–11) portray differences in the dielectric response of highly conductive fluids, such as CEZ or PB, as compared with virtual insulators, such as benzene. Soil–contaminant mixtures (Figs. 10, 11) produce more attenuated reflections, stemming from the conductivity contribution of soil particles. However, wave forms of a pure contaminant and of a corresponding soil–contaminant mixture indicate some resemblance in the initial stages of the acquisition (i.e., at high frequencies).

Since in the time-domain relationship the shape of the initial stage of each wave form is governed by its high-frequency content, while the final stage relates to a DC term, it is meaningful to look at results in the frequency domain, as displayed in Figs. 13–17. In these figures the attenuation and phase-shift characteristics of individual contaminants and soil–contaminant mixtures are presented as material transfer functions. They are computed by dividing the spectrum of the reflected signal (output FFT) by the spectrum of the incident impulse (input FFT). The results are shown in a polar form, with the modulus being the distance from the point of origin to the particular frequency component of the wave form and the corresponding phase angle measured relative to the positive *x*-axis. With reference to

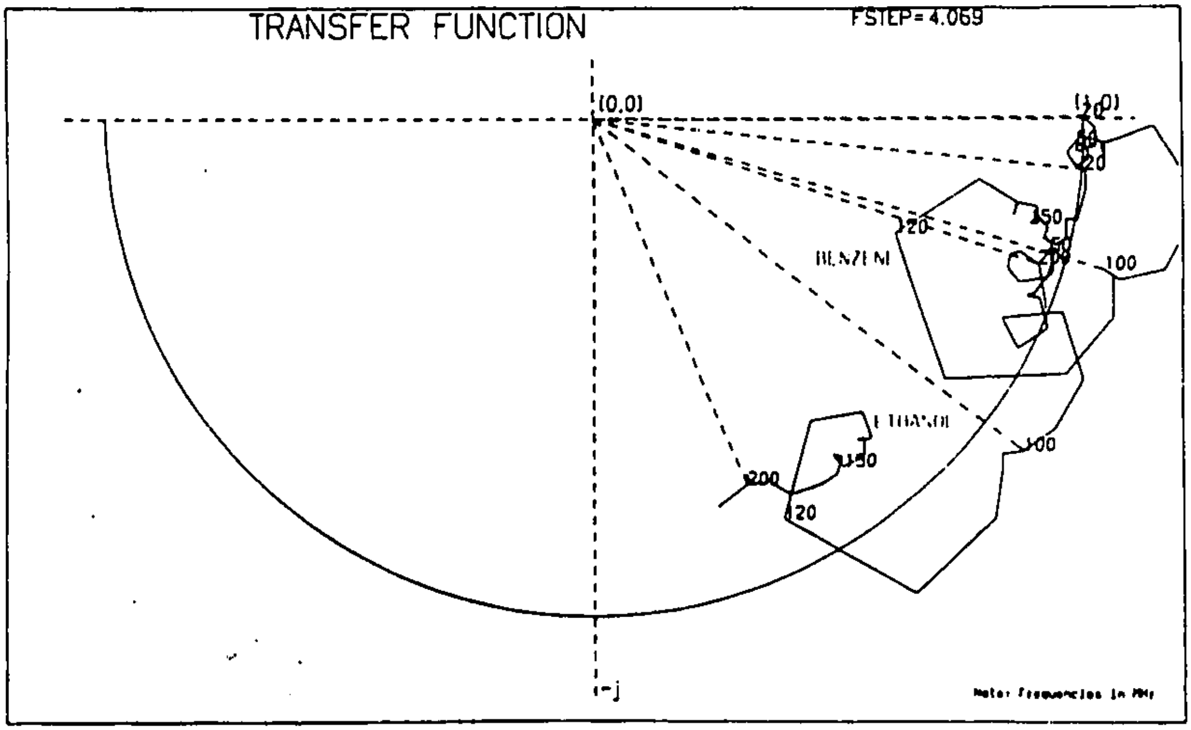

FIG. 14. Frequency response (FFT) of benzene and ethanol.

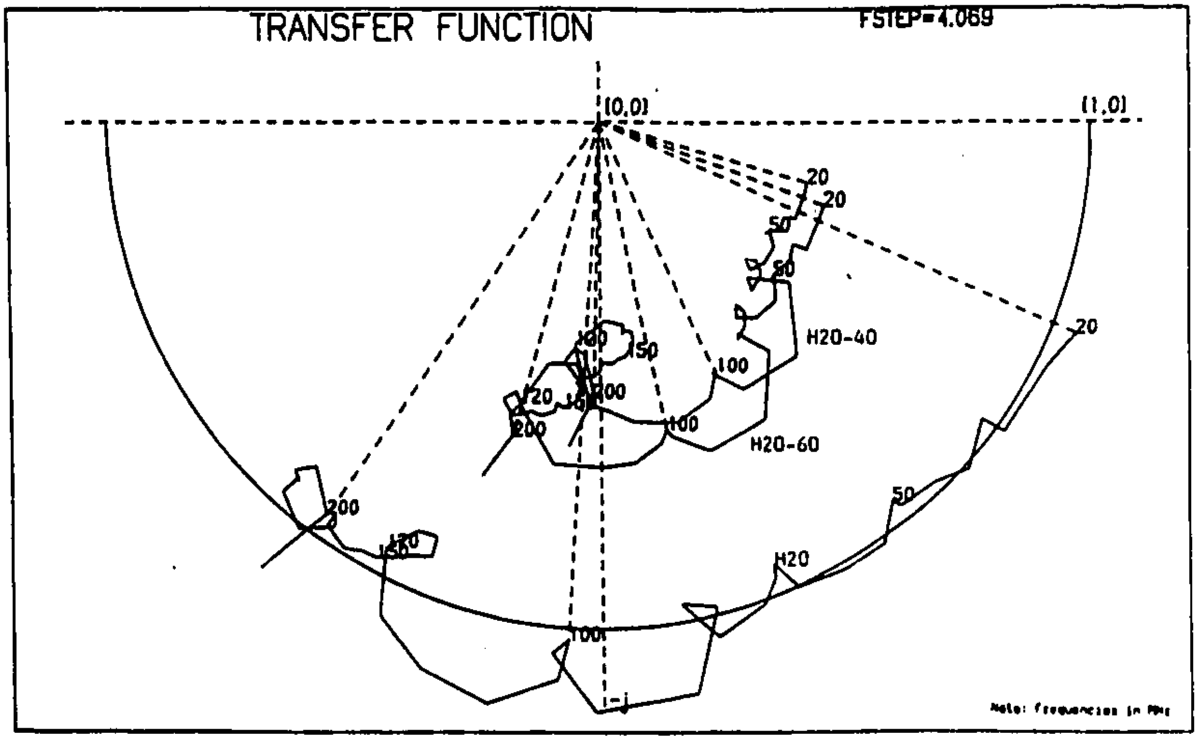

FIG. 15. Frequency response (FFT) of H2O and of soils containing 60 and 40% of H2O.

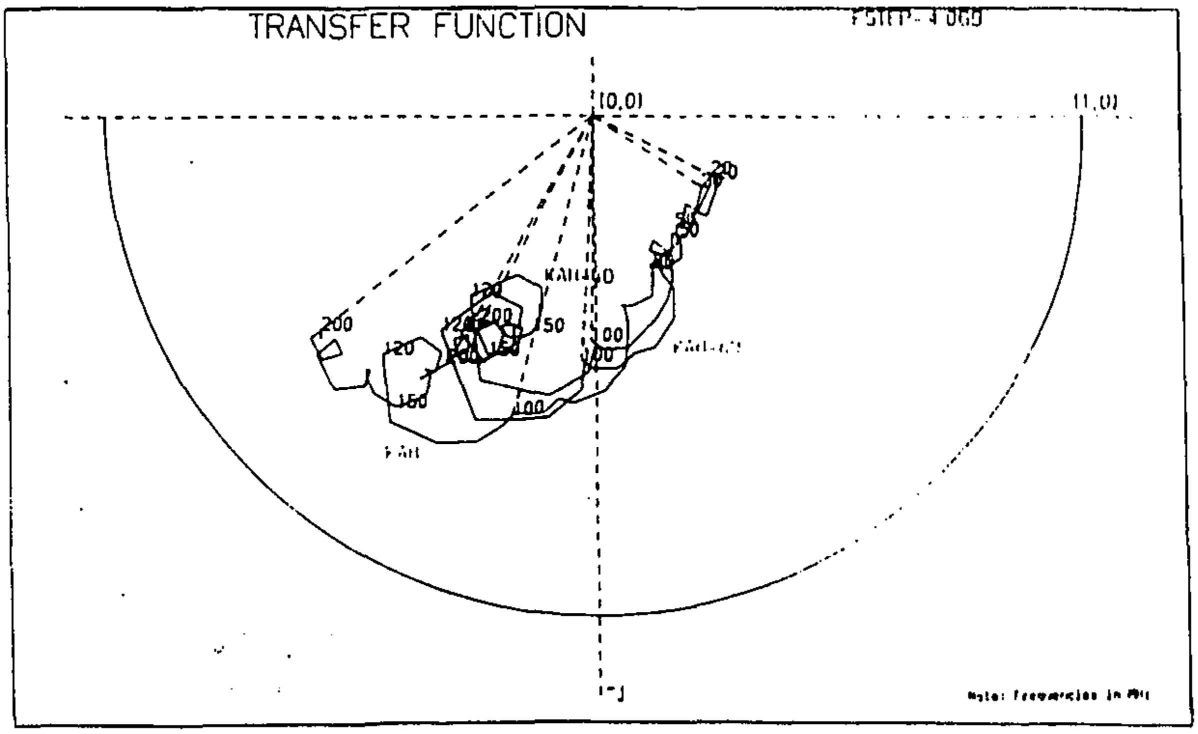

FIG. 16. Frequency response (FFT) of KAH and of soils containing 60 and 40% of KAH.

Fig. 12, while it would appear that the material's resistivity (or conductivity) affects the transfer-function position along the x-axis, and that its dielectric constant causes the relative phase shift of various frequencies, it is likely that the processes contributing to the results shown are more complicated. The real part of the resistivity (or imaginary part of ϵ) would also affect the phase shift.

The transfer-function representation provides a meaningful insight into the material's dielectric behaviour. When the sample material is either conductive or polar, or possibly both, it does not behave like a perfect capacitor (as in Fig. 12), leading to a particular phase shift of various harmonics. If the charges contained in the material are free to move[1] under the influence of an electrical field, the resistance is effectively independent of the frequency of the applied signal, but if these charges are bound, as in oscillating dipoles, the resistance becomes a characteristic function of frequency. This pattern manifests itself readily in Figs. 13-17.

It can be seen that the transfer function exhibits a different signature for different contaminants. In a highly conductive liquid, such as CEZ (Fig. 17), it approaches the response of a short circuit (Fig. 12). In a practically nonpolar material, such as benzene (Fig. 14), the phase shift and attenuation of different frequency components are minimal. The transfer function reflects the combined influence of the dielectric constant and resistivity of a given material, and thus the response of benzene (ϵ = 2.3), ethanol (ϵ = 31.2), and distilled water (ϵ = 80) illustrate the trend of increasing dielectric constant and diminishing resistivity.

In general, the signature of the transfer function of a pure contaminant resembles the corresponding transfer function of a soil–contaminant mixture. It appears that at higher frequencies the transfer function is influenced predominantly by the dielectric properties of a liquid. This phenomenon can be exploited to trace the extent of a subsurface contaminant plume and its approximate concentration.

As stated previously, a greater collection of information from various before and after (contamination) situations would provide one with the basis for establishing a general catalogue of signatures. It is hoped that through systematic amassing of data a qualitative approach can be developed to permit one to deduce the presence of contaminants in soils. Further work also remains to be done on the evaluation of the effects of chemical interaction between the contaminant and the soil vis-a-vis alteration of the dielectric properties of the contaminant fluid (see, for example, Olhoeft 1987). Obviously, other factors that need full consideration include clay type, contaminant species and concentration, multispecies contaminants, etc. The list is endless. However, it is hoped that a demonstration of the ability of the technique presented would spur others to pursue further (added) documentation of signatures.

Conclusions

This study is intended to demonstrate the feasibility of constructing an effective *in situ* contaminant-detection technique based on the phenomenon of electrical polarization. In principle, the proposed approach is similar to the presently utilized geophysical technique of induced polarization. The main difference stems from the necessity of detecting high-frequency polarization phenomena occurring in the

---

[1] Interfacial polarization is from "free" charge movement, and is significant at these frequencies.

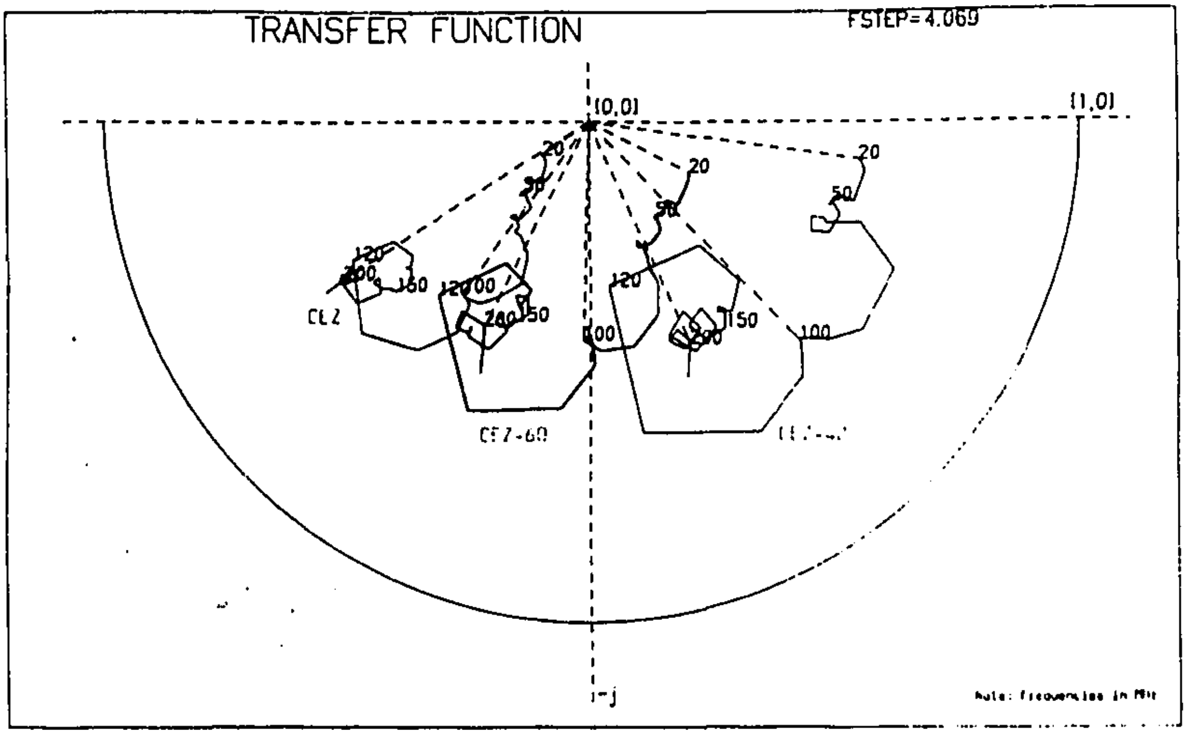

FIG. 17. Frequency response (FFT) of CEZ and of soils containing 60 and 40% of CEZ.

pore fluid, as opposed to low-frequency interfacial polarization indicative of mineral content. Technically, the measuring setup is relatively simple, requiring only one cable to be inserted into the soil. Wave-form acquisition by a digitizer and its processing by a portable computer can be performed directly *in situ*, with the aid of a database of signatures established from more detailed laboratory testing. The extent of an underground contamination can be detected by probing the affected area and analyzing the spectral signature of a subsurface pore fluid for the presence of a contaminant. Presentation of results in terms of a transfer function, expressed in polar coordinates, facilitates the task of contaminant detection and monitoring. This task can be further enhanced if the technique proposed in this study is used in conjunction with other monitoring methods. Thus, an initial site reconnaissance can be rapidly performed with a portable electromagnetic conductivity instrument. The area of interest can be subsequently narrowed down with the aid of the electrical polarization method. Further refinement, if required, can be achieved by a direct drilling and sampling from a monitoring well, which at this stage can be judiciously located. Currently, there is a growing need for a quick and efficient technique to assess the extent of a localized ground contamination and it is envisaged that this study can lead to further work, which would be applied to the development of a mobile contaminant-detection system.

Much work remains to be done to sort out specific effects of contaminant-soil interaction—particularly for situations involving multicomponent contaminants. "Calibration" experiments that seek to identify before and after (contamination) situations are needed for cataloguing of signatures—especially with reference to soil type, contaminant species, and concentration. For the present, the results obtained indicate the usefulness and ability of this technique for detection of contaminant presence.

Acknowledgments

The authors with to express their gratitude to Dr. Ryszard Malewski of the Hydro-Québec Research Institute (IREQ), for his constructive comments and helpful guidance in performing measurements. Furthermore, the technical assistance of Messrs. Jean Douville and Louis Lavallée of IREQ is gratefully acknowledged. Critical comments from Mr. Daniel Tschudi of Asea Brown Boveri are also appreciated. The authors also wish to thank the reviewers for their very constructive inputs for improvement of the paper. This study was supported by grants from the Ministère de l'Éducation du Québec (FCAR/MESST) and the Natural Sciences and Engineering Research Council of Canada (grant No. A-882).

ANDREWS, J.R. 1973. Random sampling oscilloscope for the observation of mercury switch closure transition times. IEEE Transactions on Instrumentation and Measurement, IM-22: 375–381.

BOCKRIS, J.O'M., GILEADI, E., and MÜLLER, K. 1966. Dielectric relaxation in the electric double layer. Journal of Chemical Physics, 44: 1445–1456.

COLE, K.S., and COLE, R.H. 1941. Dispersion and absorption in dielectrics. Journal of Chemical Physics, 9: 341–353.

DANIEL, V.V. 1967. Dielectric relaxation. Academic Press, New York, NY.

DAVIS, J.L., TOPP, G.C., and ANNAN, A.P. 1977. Measuring soil water content *in situ* using time-domain reflectometry techniques. Geological Survey of Canada, Report on Activities, Part B, Paper 77-1B.

Debye, P. 1929. Polar molecules. Chemical Catalogue Company, New York, NY.

Fellner-Feldegg, H. 1969. The measurement of dielectrics in time domain. Journal of Physical Chemistry, 73: 616–623.

Gemant, A. 1933. Liquid dielectrics. John Wiley, New York, NY.

Hamming, R.W. 1977. Digital filters. Prentice-Hall, Englewood Cliffs, NJ.

Harvey, S.C., and Hoekstra, P. 1972. Dielectric relaxation spectra of water adsorbed on lysozyme. Journal of Physical Chemistry, 76: 2987–2994.

Hoekstra, P., and Delaney, A. 1974. Dielectric properties of soils at UHF and microwave frequencies. Journal of Geophysical Research, 79: 1699–1708.

Iskander, M.F., and Stuchly, S.S. 1972. A time domain technique for measurement of the dielectric properties of biological substances. IEEE Transactions on Instrumentation and Measurement, IM-21: 425–429.

Keller, G.V., and Frischknecht, F.C. 1966. Electrical methods in geophysical prospecting. Pergamon Press, Elmsford, NY.

Lorentz, H.A. 1915. The theory of electrons. Dover Publications, New York, NY.

Maxwell, J.C. 1854. Treatise on electricity and magnetism. Vol. 1 Dover Publications, New York, NY, p. 452.

_____ 1987*a*. Ministère dé l'Environnement du Québec. Règlements sur les déchets solides.

_____ 1987*b*. Guide technique pour l'implentation et la gestion de lieu d'enfuissement des sols contaminés.

Olhoeft, G.R. 1986. Direct detection of hydrocarbon and organic chemicals with ground penetrating radar and complex resistivity. Proceedings, National Well Water Association - American Petroleum Institute Conference on Petroleum Hydrocarbons and Organic Chemicals in Groundwater—Prevention, Detection and Restoration, NWWA, pp. 284–305.

_____ 1987. Electrical properties from 10^{-3} to 10^{9}—physics and chemistry. Proceedings, 2nd International Symposium on the Physics and Chemistry of Porous Media, American Institute of Physics Conference, Proceeding 154, pp. 281–298.

Ramirez, R.W. 1985. The FFT fundamentals and concepts. Prentice-Hall, Englewood Cliffs, NJ.

van Gemert, M.J.C. 1973. High frequency time domain methods in dielectric spectroscopy. Philips Research Reports, 28: 530–572.

von Hippel, A.R. 1954. Dielectrics and waves. The M.I.T. Press, Cambridge, MA.

Wagner, K.W. 1913. Annalen der Physik (Leipzig), Series 4, 40: 817–855.

Waldemeyer, J. 1980. Fast Fourier Transform for step-like functions: the synthesis of three apparently different methods. IEEE Transactions on Instrumentation and Measurement, IM-29: 36–39.

Waller, M.J., and Davis, J.L. 1984. Assessment of innovative techniques to detect waste impoundment liner failures. National Technical Information Service, Springfield, VA.

Yong, R.N., Boonsinsuk, P., and Wong, G. 1986. Formulation of backfill material for a nuclear fuel waste disposal vault. Canadian Geotechnical Journal, 23: 216–228.

REFERENCES

Adam, J.A. 1988. Soviets Arrive in Nevada for Blast. *The Institute*, vol. 12, no. 10, pp. 1-4.

Al'pin, L.M., and Berdichevskii, M.N. 1966. *Dipole Methods for Measuring Earth Conductivity*. Consultants Bureau Enterprises, Inc., New York.

Andrews, J.R. 1973. Random Sampling Oscilloscope for the Observation of Mercury Switch Closure Transition Times. *IEEE Transactions on Instrumentation and Measurement*, vol. IM-22, no. 4, pp. 375-381.

Arulanandan, K., and Mitchell, J.K. 1968. Low Frequency Dielectric Dispersion of Clay-Water-Electrolyte Systems. *Clays and Clay Minerals*, vol. 16, pp. 337-351.

Benignus, V.A. 1969. Estimation of Coherence Spectrum and Its Confidence Interval Using the Fast Fourier Transform. *IEEE Transactions on Audio and Electroacoustics*, vol. AU-17, no. 2, pp. 145-150.

Bleil, D.F. 1953. Induced Polarization: A Method of Geophysical Prospecting. *Geophysics*, vol. 18, no. 3, pp. 636-648.

Bockris, J.O'M., Gileadi, E., and Müller, K. 1966. Dielectric Relaxation in the Electric Double Layer. *The Journal of Chemical Physics*, vol. 44, no. 4, pp. 1445-1456.

Boraiko, A.A. 1985. Hazardous Waste. *National Geographic*, vol. 167, no. 3, pp. 319-351.

Bose, T.K., Bottreau, A.M., and Chanine, R. 1986. Development of a Dipole Probe for the Study of Dielectric Properties of Biological Substances in Radiofrequency and Microwave Region with Time-Domain Reflectometry. *IEEE Transactions on Instrumentation and Measurement*, vol. IM-35, no. 1, pp. 56-60.

Bowders, J.J., Jr., Lord, A.E., Jr., and Koerner, R.M. 1982. Sensitivity Study of a Ground Probing Radar. *Geotechnical Testing Journal*, vol. 5, no. 3/4, pp. 96-100.

Brown, J.T.L., and Pollard, C.E. 1947. Mercury Contact Relays. *Electrical Engineering*, vol. 66, pp. 1106-1108.

Carter, G.C. 1972. *Estimation of the Magnitude-Squared Coherence Function (Spectrum)*. Technical Report 4343, Naval Underwater Systems Center, Newport, Rhode Island.

Cole, K.S., and Cole, R.H. 1941. Dispersion and Absorption in Dielectrics. *Journal of Chemical Physics*, vol. 9, pp. 341-353.

Davis, J.L., and Annan, A.P. 1977. Electromagnetic Detection of Soil Moisture: Progress Report I. *Canadian Journal of Remote Sensing*, vol. 3, pp. 76-86.

Debye, P. 1929. *Polar Molecules*. Chemical Catalogue Company, New York.

Dev, S.B., North, A.M., and Pethrick, R.A. 1972. Computational Techniques in the Analysis of Dielectric Relaxation Measurements. *Advanced Molecular Relaxation Processes*, vol. 4, pp. 159-191.

Fellner-Feldegg, H. 1969. The Measurement of Dielectrics in Time Domain. *The Journal of Physical Chemistry*, vol. 73, no. 3, pp. 616-623.

Gajda, B.G., and Stuchly, S.S. 1983. Numerical Analysis of Open-Ended Coaxial Lines. *IEEE Transactions on Microwave Theory and Techniques*, vol. MTT-31, no. 5, pp. 380-384.

van Gemert, M.J.C. 1973. High Frequency Time Domain Methods in Dielectric Spectroscopy. *Philips Research Reports*, vol. 28, pp. 530-572.

Gerlach, A.A. 1980. *Role of the Sectionalized Fourier Transform in High-Speed Coherence Processing.* Technical Report 8438. Naval Research Laboratory, Washington, D.C.

Gonzalez, R.C., and Wintz, P. 1987. *Digital Image Processing.* Addison-Wesley, Reading.

Gooch, D.W., Harrison, C.W., King, R.W.P., and Wu, T.T. 1963. Impedances of Long Antennas in Air and in Dissipative Media. *Journal of Research of National Bureau of Standards*, vol. 67D, pp. 355-360.

Gouy, G. 1910. Sur la Constitution de la Charge Electrique à la Surface d'un Electrolyte. *Ann. Phys.*, Paris, Série, vol. 4, no. 9, pp. 457-468.

Greenhouse, J.P., and Harris, R.D. 1980. *Hydrogeological Studies of a Sandy Acquifer at an Abandoned Landfill, Part 8, DC, VLF and Inductive Resistivity Surveys.* Department of Earth Sciences, University of Waterloo, Waterloo, Ontario.

Halverstadt, I.F., and Kumler, W.D. 1942. *Journal of American Chemical Society*, vol. 64, pp. 2988-3007.

Harvey, S.C., and Hoekstra, P. 1972. Dielectric Relaxation Spectra of Water Adsorbed on Lysozyme. *The Journal of Physical Chemistry*, vol. 76, no. 21, pp. 2987-2994.

Hasted, J.B., Ritson, D.M., and Collie, C.H. 1948. *Journal of Chemical Physics*, vol. 16, pp. 1-14.

Hedestrand, G. 1929. *Z. Physik. Chem.*, vol. 2B, pp. 428-442.

Hoekstra, P., and Delaney, A. 1974. Dielectric Properties of Soils at UHF and Microwave Frequencies. *Journal of Geophysical Research*, vol. 79, no. 3, pp. 1699-1708.

Hoekstra, P., Mills, T., Blohm, M., and Evans, L. 1988. Time Domain Electromagnetic Soundings for Mapping Sea-Water Intrusion in Monterey County, California. *Ground Water*, vol. 26, no. 6, pp. 771-782.

Iskander, M.F., and DuBow, J.B. 1983. Time- and Frequency-Domain Techniques for Measuring Dielectric Properties of Rocks: A Review. *Journal of Microwave Power*, vol. 18, no. 1, pp. 55-73.

Jackson, H.W. 1976. *Introduction to Electric Circuits.* Prentice-Hall, Englewood Cliffs.

Karably, L.S., and Babcock, K.B. 1989. The Effects of Environmental Variables on Soil Gas Surveys. *Hazardous Materials Control*, vol. 2, pp. 36-43.

Keller, G.V., Frischknecht, F.C. 1966. *Electrical Methods in Geophysical Prospecting.* Pergamon Press, Elmsford.

Koerner, R.M., McCabe, W.M., and Lord, A.E. 1981. *State of the Art Lectures: Acoustic Emission Behavior and Monitoring in Soils.* ASTM Symposium on Acoustic Emission in Geotechnical Engineering Practice, Detroit, Michigan.

Lewis, I.A.D., and Wells, F.H. 1954. *Millimicrosecond Pulse Techniques.* McGraw-Hill, New York.

Look, B.G., and Reeves, I.N. 1992. The Application of Time Domain Reflectometry in Geotechnical Instrumentation. *Geotechnical Testing Journal*, vol. 15, no. 3, pp. 277-283.

Maxwell, J.C. 1854. *Treatise on Electricity and Magnetism.* Dover Publications, New York.

Ministère de l'Environnement du Québec, 1987. *Guide technique pour l'implentation et la géstion de lieu d'enfuissement des sols contaminés.*

Ministère de l'Environnement du Québec, 1987. *Règlements sur les déchets solides.*

Okrasinski, T.A., Koerner, R.M., and Lord, A.E. 1978. Dielectric Constant Determination of Soils at L Band Microwave Frequencies. *Geotechnical Testing Journal*, vol. 1, no. 3, pp. 134-140.

Olhoeft, G.R. 1985. Low Frequency Electrical Properties. *Geophysics*, vol. 50, pp. 2492-2503.

Olhoeft, G.R. 1986. Direct Detection of Hydrocarbon and Organic Chemicals with Ground Penetrating Radar and Complex Resistivity. *Proceedings of the NWWA/API Conference on Petroleum Hydrocarbons and Organic Chemicals in Ground Water-Prevention, Detection and Restoration*, National Water Well Association, Dublin.

Olhoeft, G.R. 1987. Electrical Properties from $10^{-}3$ to 10^{9} - Physics and Chemistry. *Proceedings of the 2nd International Symposium on the Physics and Chemistry of Porous Media*, American Institute of Physics Conference Proceedings, pp. 281-298.

Onsanger, L. 1936. *Journal of American Chemical Society*, vol. 58, pp. 1486-1498.

Ramirez, R.W. 1985. *The FFT Fundamentals and Concepts.* Prentice-Hall, Englewood Cliffs.

Ryu, J., Morrison, H.F., and Ward, S.H. 1972. Electromagnetic Depth Sounding Experiment Across Santa Clara Valley. *Geophysics*, vol. 37, pp. 351-374.

Sachs, S.B., and Spiegler, K.S. 1964. Radiofrequency Measurements of Porous Conductive Plugs. *The Journal of Physical Chemistry*, vol. 68, no. 5, pp. 1214-1222.

Saunders, W.R., and Germeroth, R.M. 1986. *Electromagnetic Measurements for Subsurface Hydrocarbon Investigations.* Report to Port Authority of New York and New Jersey by Camp Dresser & McKee Inc.

Schlumberger, C. 1920. *Etude sur la Prospection electrique du sous-sol.* Gauthier-Villars et Cie., Paris.

Sumner, J.S. 1976. *Principles of Induced Polarization for Geophysical Exploration*. Elsevier, Amsterdam.

Tarrer, A.R. 1993. Impacts of Environmental Regulations on Highway Maintenance. *TR News*, no. 167, pp. 11-15.

Topp, G.C., Davis, J.L., and Annan, A.P. 1980. Electromagnetic Determination of Soil Water Content: Measurement in Coaxial Transmission Lines. *Water Resources Research*, vol. 16, no. 3, pp. 574-582.

Ulriksen, P.F. 1982. *Application of Impuse Radar to Civil Engineering*. Lund University, Department of Engineering Geology, Lund.

Wagner, K.W. 1913. *Annalen Phys.*, vol. 40, no. 4, pp. 817-836.

Wait, J.R. 1959. *Overvoltage Research and Geophysical Applications*. Pergamon Press, London.

Wait, J.R., 1971. *Electromagnetic Probing in Geophysics*. The Golem Press, London.

Waldmeyer, J. 1980. Fast Fourier Transform for Step-like Functions: the Synthesis of Three Apparently Different Methods. *IEEE Transactions on Instrumentation and Measurement*, vol. IM-29, no. 1, pp. 36-39.

Waller, M.J., and Davis, J.L. 1984. *Assessment of Innovative Techniques to Detect Waste Impoundment Liner Failures*. NTIS, Springfield.

Winter, T.G. 1973. A Survey of Sound Propagation in Soils. *Acoustical Holography*, vol. 5, pp. 197-216.

Yong, R.N., and Warkentin, B.P. 1975. *Soil Properties and Behaviour*. Elsevier Scientific Publishing Co., Amsterdam.

Yong, R.N., Boonsinsuk, P., and Wong, G. 1986. Formulation of Backfill Material for a Nuclear Fuel Waste Disposal Vault. *Canadian Geotechnical Journal*, vol. 23, no. 2, pp. 216-228.

Yong, R.N., and Hoppe, E.J. 1989. Application of Electric Polarization to Contaminant Detection in Soils. *Canadian Geotechnical Journal*, vol. 26, no. 4, pp. 536-550.

Yong, R.N., Mohamed, A.M.O., and Warkentin, B.P. 1992. *Principles of Contaminant Transport in Soils*. Elsevier Scientific Publishing Co., Amsterdam.

Zonge, K.L., and Hughes, L.J. 1980. *The Complex Resistivity Method*. Zonge Engineering and Research Organization, Inc., Tucson.